DETERMINING THE IMPACT OF RECQL4 MUTATIONS ON NORMAL HOMEOSTASIS, TUMOUR DEVELOPMENT, AND FUNCTIONAL GENETIC INTERACTIONS

WILSON JAVIER CASTILLO TANDAZO, MD

https://orcid.org/0000-0002-3202-8185

Doctor of Philosophy

July 2020

Cancer and RNA Biology Lab,
St Vincent's Institute of Medical Research
&
Department of Medicine, St Vincent's Hospital
Faculty of Medicine, Dentistry and Health Sciences

The University of Melbourne

This thesis is being submitted in total fulfilment of the degree.

Wilson Javier Castillo Tandazo, MD: *Determining the impact of Recql4 mutations on normal homeostasis, tumour development, and functional genetic interactions,* Doctor of Philosophy, © July 2020

SUPERVISORS:
Prof. Carl R Walkley
Dr Monique F Smeets

ABSTRACT

Since mutations in the *RECQL4* gene were identified as causative of Rothmund-Thomson syndrome (RTS) more than twenty years ago, some inroads have been made in the understanding of this disease and its mutations. It has been discovered that the majority of these mutations are nonsense and frameshift mutations resulting in truncating protein products that delete both the helicase and the C-terminal domain. The deletion of these domains results in a dysfunctional RECQL4 protein and the development of the variable clinical spectrum and the increased predisposition to malignancies, typical of RTS.

Several *Recql4*-mutated mice have been generated as a model for RTS. Although these models have contributed to identify some of the functions of RECQL4, they do not accurately reflect the genetic status of RTS, in which patients generally present with hypomorphic, rather than null alleles. On the other hand, these models have not provided sufficient insight into the specific functions and domains of RECQL4; and the effects of RECQL4 mutations on normal homeostasis, tumour development, and functional genetic interactions. This thesis, through its three related components, aims to address all these gaps by using murine models bearing mutations that inactivate specific functions and domains of RECQL4, and that resemble common mutations seen in humans.

In the first component of this thesis, I generated mice carrying an ATP-binding knock-in mutation to assess the physiological requirements and biological functions of the helicase activity, thought to be critical for the overall functions of RECQL4. Through a variety of experiments, I observed that homozygous mice were normal in terms of embryonic development, body weight, haematopoiesis, B and T cell development, and physiological DNA damage repair. Furthermore, to compare the *in vivo* effects of a helicase-inactive versus truncating mutations, I used conditional deletion models and found that only mice carrying truncating mutations developed bone marrow failure. These findings demonstrated that the ATP-dependent helicase activity

of RECQL4 is not essential for its physiological functions, and that truncating mutations are deleterious.

For the second component of this thesis, I assessed mice carrying germline truncating RECQL4 mutations to understand the impact of the deletion of the helicase and C-terminal domains on normal homeostasis and tumour development. I found that truncating mutations affected stability and subcellular localisation of RECQL4, which translated to a homozygous embryonic lethality and a haploinsufficient low bone mass phenotype through defects in early osteoblast progenitors. Additionally, I observed that the severity of the defect was related to the degree of the truncation, suggesting that gene dosage is an important determinant of the bone phenotype. However, these mutations were not sufficient to initiate tumorigenesis in mice, even after exposure to irradiation, which pointed to the possibility that mutations in other genes, besides *Recql4*, might be contributing to this disease.

In the third and final component of this thesis, I performed a genome-wide genetic rescue screen to identify genetic interactions with mutant *Recql4*, an area largely unexplored. Amongst the genes identified, the standout candidate was *Klhdc3*. In subsequent validation assays, I demonstrated that mutation of *Klhdc3* rescued the phenotypes associated with a pathogenic RECQL4 mutation, which is to my knowledge, the first confirmed genetic interaction associated with an improvement of the cellular phenotypes caused by RECQL4 mutations.

Collectively, the work presented in this thesis makes an original contribution to knowledge through the finding that the ATP-dependent helicase activity of RECQL4 is dispensable for its physiological functions, the discovery that truncating mutations cause a haploinsufficient low bone mass phenotype and that gene dosage is an unsuspected regulator of bone mass, and the identification of *Klhdc3* mutation as being capable of rescuing the proliferation defect caused by a truncating RECQL4 mutation.

DECLARATION

This is to certify that:

1. This thesis comprises only my original work towards the degree Doctor of Philosophy except where indicated in the Preface.

2. Due acknowledgement has been made in the text to all other material used.

3. The thesis is fewer than 100,000 words in length, exclusive of tables, figures, bibliographies and appendices.

Melbourne, July 2020

Wilson Javier Castillo
Tandazo, MD
31 July 2020

PREFACE

In accordance with the regulations of The University of Melbourne, the author's contribution to each chapter was as follows:

- Chapter 5: 70%
- Chapter 6: 80%
- Chapter 7: 85%

While the conceptualisation, design, majority of the experiments, data analysis, and all the writing of this thesis was my principal responsibility, in the following list I acknowledge the contributions of data, provided by others in collaboration, which I present in this thesis:

- Dr Monique Smeets (St Vincent's Institute) contributed to the data acquisition and analysis presented in Figure 5.6, 6.1 F-H, 6.5 E-M, 7.4 B, 7.5 and Supp. Figure 5.3, 6.1, 6.6, 6.7.
- Dr Rui Lui (St Vincent's Institute) contributed to the data acquisition and analysis presented in Figure 5.4 F-I.
- Mr Vincent Murphy (St Vincent's Institute) and Dr Charlotte Hodson (St Vincent's Institute) contributed to the data acquisition and analysis presented in Figure 5.1 B, C, E.
- Prof. Natalie Sims (St Vincent's Institute) provided advice for data analysis presented in Figure 6.2 and 6.3.
- Dr Alistair Chalk (St Vincent's Institute) performed the bioinformatic analysis presented in Figure 7.2 and 7.3
- Dr Ann Frazier (Murdoch Children's Research Institute) provided advice for data acquisition presented in Supp. Figure 6.2.

This work was supported by the following grants:

- Office of the Assistant Secretary of Defense for Health Affairs through the Peer Reviewed Cancer Research under Award No. W81XWH-15-1-0315 (to A/Prof. Carl R Walkley).
- National Health and Medical Research Council Australia project grant (NHMRC) (To A/Prof. Carl R Walkley and A/Prof. Andrew Deans).
- Melbourne Research Scholarship through The University of Melbourne (To Wilson Castillo-Tandazo).
- SVI Top-Up Scholarship through St Vincent's Institute (To Wilson Castillo-Tandazo).

None of this work has been submitted for other qualifications.

None of this work was carried out prior to PhD candidature enrolment.

None of this work has received third party editorial assistance.

PUBLICATIONS

PUBLICATIONS ARISING FROM THESIS:

The following publication and submitted manuscript have been generated as a result of work undertaken toward this degree:

Accepted publications:

1. *Castillo-Tandazo W*, Smeets MF*, Murphy V, Liu R, Hodson C, Heierhorst J, Deans A, Walkley CR*. ATP-dependent helicase activity is dispensable for the physiological functions of Recql4. PLoS Genet. 2019;15(7):e1008266.
   DOI: https://doi.org/10.1371/journal.pgen.1008266
   * These authors contributed equally to this work.

Submitted publications:

1. *Wilson Castillo-Tandazo*, Ann E Frazier, Natalie A Sims, Monique F Smeets*, Carl R Walkley*. Rothmund Thompson Syndrome-like RECQL4 truncating mutations cause a haploinsufficient low bone mass phenotype but do not initiate tumorigenesis in mice.
   * These authors contributed equally to this work.

AFFILIATED PUBLISHED WORKS:

The following publications have been generated during this degree but are not directly related to the aims of this thesis:

1. Walia MK**, *Castillo-Tandazo W*, Mutsaers AJ, Martin TJ, Walkley CR. Murine models of osteosarcoma: A piece of the translational puzzle. J Cell Biochem. 2018;119(6):4241-50.
   DOI: https://doi.org/10.1002/jcb.26601
   ** These authors are co-first authors.

2. *Castillo-Tandazo W*, Mutsaers AJ, Walkley CR. Osteosarcoma in the Post Genome Era: Preclinical Models and Approaches to Identify Tractable Therapeutic Targets. Curr Osteoporos Rep. 2019;17(5):343-52
DOI: https://doi.org/10.1007/s11914-019-00534-w

3. Straszkowski L, Jovic T, *Castillo-Tandazo W*, Ritchie DS, Purton LE. Effects of chemotherapy agents used to treat pediatric acute lymphoblastic leukemia patients on bone parameters and longitudinal growth of juvenile mice. Exp Hematol. 2020;82:1-7
DOI: https://doi.org/10.1016/j.exphem.2020.01.010

ACKNOWLEDGMENTS

First and foremost, I would like to express my deepest gratitude to my supervisors. To A/Prof. Carl Walkley, thank you for your invaluable insight and guidance throughout this project. I really appreciate the autonomy and trust you have given me, and also the re-direction and feedback when needed. To Dr Monique Smeets, thank you for your thorough explanations to my everyday questions. The technical skills you have patiently taught me will be useful for the rest of my career. I would also like to thank both of you for your ideas, comments, and suggestions in the manuscripts submitted and in this thesis. I have learnt from every single one of them.

To the knowledgeable and collaborative scientists that I have had the fortune to work with: A/Prof. Andrew Deans, A/Prof. Jörg Heierhorst, Prof. Louise Purton, Dr Alistair Chalk, Dr Ann Frazier, Prof. David Thorburn, Dr Rui Liu, and Mr Vince Murphy; thank you for your invaluable contribution to this project. Special thanks to Prof. Natalie Sims, who besides being a valuable collaborator, was also my advisory committee chair. Thanks for taking the time to attend my progress meetings and to ensure that I have a timely completion. I also wish to thank Ms Lenny Straszkowski, Mrs Emma McGowan, Mrs Narelle McGregor, and Mrs Ingrid Poulton; who kindly trained me in the techniques you are all expert in.

To all past and present members of the Cancer and RNA Biology Lab and the Stem Cell Regulation Unit: Ms Jane Xu, Ms Kelli Schleibs, Ms Diannita Kwang, Mrs Ankita Goradia, Mr Scott Taylor, Dr Gavin Tjin, Dr Jackie Heraud-Farlow, Ms Shannon Mendez, Mr Xining Li, Ms Clea Grace, and Dr Mannu Walia; thank you for your help, advice, and laughs. I truly enjoyed my time working with all of you. I also would like to thank my fellow PhD students: Ms Martha Blank, Dr Winnie Tan, Ms Yao Sun, Dr Tingting Ge, Ms Vanessa Tsui, and Mr Ashley Ovens; thank you for the wonderful times during the student society events, lunches, and the memorable student retreats.

To the University of Melbourne, St Vincent's Institute Foundation, Department of Defense (USA), and National Health and Medical Research Council Australia; thank you for your generous financial support in the form of scholarships or grants for this project. Without you, this thesis would not have been possible.

To my friends outside work: Ms Camila Gonzalez, Ms Teyra Jasso, Mr Luis Ramirez, Mrs Milena Bolaño, Ms Sean Hiller, Mrs Liz Huanuco, Mr Frank Carrera, Mr Julio Carrera, Mr Sebastian Currea, Ms Jacqueline Brown, Ms Dianne Bartelloni, Mr Abhinav Badrinarayanan, and Ms Maria de Winter; thank you for becoming my family in Australia and for bringing me sanity during the hard times.

Finally, to my parents, sister, brother, and partner, Paul; this thesis is dedicated to all of you. Thank you for your unconditional love and encouragement during this journey. Without the support and the sacrifices you all have made, I would not be where I am today, and for that, I am forever grateful.

CONTENTS

Chapter 1

1 INTRODUCTION 3

1.1 Problem statement . . . 3
1.2 Overall aim and scope of the thesis . . . 4
1.3 Overview of the thesis . . . 4

Chapter 2

2 LITERATURE REVIEW 9

2.1 Helicases . . . 9
2.2 RecQ helicases . . . 10
2.2.1 Structure of RecQ helicases . . . 11
2.2.2 RecQ helicases and syndromes associated . . . 12
2.3 Recql4 and human disease . . . 13
2.3.1 RECQL4 associated disorders . . . 14
2.3.2 RECQL4 and cancer predisposition . . . 20
2.3.3 Mutations in the RECQL4 gene . . . 22
2.4 RECQL4 . . . 25
2.4.1 Tissue expression . . . 25
2.4.2 Sub-cellular localisation . . . 26
2.4.3 Physiological functions of RECQL4 . . . 28
2.4.4 Protein interactions of RECQL4 . . . 32
2.4.5 RECQL4 domains . . . 35
2.5 Murine models of RECQL4 mutation . . . 38

Chapter 3

3 AIMS AND HYPOTHESES 47

3.1 Preamble . . . 47
3.2 Study Hypotheses . . . 48
3.3 Aims of the thesis . . . 49

Chapter 4

4 MATERIALS AND METHODS 53

4.1 Materials . . . 53
4.2 Experimental mice . . . 62
4.2.1 Ethics statement . . . 62
4.2.2 Mouse housing . . . 62
4.2.3 Mouse strains . . . 62
4.2.4 DNA isolation . . . 63
4.2.5 Genotyping . . . 63
4.3 Flow cytometry analysis . . . 67
4.3.1 Tissue collection . . . 67
4.3.2 Peripheral blood analysis . . . 67
4.3.3 Bone marrow cell isolation . . . 68
4.3.4 Spleen and cell thymic cell isolation . . . 68
4.3.5 FACS analysis . . . 68
4.3.6 In vitro class switch recombination assay . . . 71
4.4 Micro-computed tomography (Micro-CT) . . . 71
4.5 Cell culture . . . 72
4.5.1 Cell maintenance . . . 72
4.5.2 Freezing and thawing of cells . . . 73
4.5.3 Generation of retrovirus . . . 73
4.5.4 Transduction of Kusa4b10 cells with retroviral constructs 74
4.5.5 Immortalisation of myeloid cells by Hoxb8 retrovirus . 74
4.5.6 Cell proliferation assays . . . 75
4.5.7 Retroviral transduction and complementation assays with human RECQL4 constructs . . . 75
4.5.8 ATP-Lite cell viability assay - *In vitro* DNA damage response assay . . . 76
4.5.9 Seahorse XF24 extracellular flux analyser . . . 76
4.5.10 Live cell imaging and image processing of *RECQL4* fusion proteins . . . 77
4.6 Protein analysis . . . 77
4.6.1 Protein extraction . . . 77
4.6.2 Protein quantification . . . 78
4.6.3 Protein gel electrophoresis and Western blotting . . . 78
4.7 Biochemical helicase assays . . . 79
4.7.1 RECQL4 cloning, expression, and purification . . . 79
4.7.2 RECQL4 helicase assay . . . 79
4.7.3 RECQL4 ATPase assay . . . 80

4.7.4 RECQL4 DNA binding assay 80
4.8 Molecular biology 80
4.8.1 Overexpression construct design and cloning 80
4.8.2 Restriction enzyme digestion 82
4.8.3 Ligation 82
4.8.4 Transformation 82
4.8.5 Plasmid purification 83
4.9 CRISPR/Cas9 screen 83
4.9.1 Generation of lentivirus 83
4.9.2 Generation of murine Cas9-expressing cell lines 83
4.9.3 Assaying Cas9 activity in Cas9 blasticidin cell lines . . 84
4.9.4 Titration of lentivirus containing Brie library 84
4.9.5 CRISPR knockout screen 84
4.9.6 Genomic DNA preparation 85
4.9.7 Library preparation for Illumina sequencing 85
4.9.8 Bioinformatics analysis 89
4.9.9 CRISPR secondary validation screen 89
4.10 Statistical analysis 90

Chapter 5

5 UNDERSTANDING THE PHYSIOLOGICAL REQUIREMENTS OF THE HELICASE DOMAIN OF RECQL4 93
5.1 Introduction 93
5.2 Published manuscript 94
5.2.1 Abstract 94
5.2.2 Introduction 94
5.2.3 Results 96
5.2.4 Discussion 111
5.2.5 Supporting information 116
5.3 Research in context 121

Chapter 6

6 DETERMINING THE IMPACT OF RECQL4 TRUNCATING MUTATIONS IN NORMAL HOMEOSTASIS AND TUMOUR DEVELOPMENT 125
6.1 Introduction 125
6.2 Submitted manuscript 126
6.2.1 Abstract 126
6.2.2 Introduction 126

6.2.3 Results . . . 128
6.2.4 Discussion . . . 147
6.2.5 Supporting information . . . 151
6.3 Research in context . . . 158

CHAPTER 7

7 IDENTIFICATION OF NOVEL GENETIC INTERACTIONS WITH RECQL4 IN A GENOME-WIDE CRISPR/CAS9 RESCUE SCREEN 161
7.1 Introduction . . . 161
7.2 Results . . . 163
7.2.1 Hoxb8 *Recql4* myeloid cells stably express Cas9 . . . 163
7.2.2 Genome-wide CRISPR/Cas9 knockout screen identifies *Klhdc3* as a candidate *Recql4* interacting gene . . . 165
7.2.3 KLHDC3 mutation partially rescues the proliferation defect of cells expressing truncated mutant RECQL4 . 171
7.3 Discussion . . . 175

CHAPTER 8

8 CONCLUDING REMARKS 183

APPENDIX

A PUBLICATIONS ASSOCIATED WITH THIS THESIS 193
B AFFILIATED PUBLISHED WORK 213
C LIST OF AWARDS ARISING DURING THIS CANDIDATURE 241
D LIST OF MEETINGS ATTENDED TO PRESENT RESEARCH ARISING FROM THIS THESIS 243

BIBLIOGRAPHY 245

LIST OF FIGURES

Figure 2.1 Classification of helicases 10
Figure 2.2 Structure and classification of human RecQ helicases 12
Figure 2.3 Venn diagram of the overlapping and unique features of RECQL4 associated disorders 15
Figure 2.4 Clinical symptoms in patients with RTS 18
Figure 2.5 Mutations in the *RECQL4* gene 24
Figure 2.6 Structure of the *RECQL4* gene 25
Figure 2.7 *RECQL4* mRNA tissue expression 26
Figure 4.1 Regions of interest of trabecular and cortical region . 72
Figure 5.1 The $Recql4^{K525A}$ mutation results in a biochemically inactive helicase protein 98
Figure 5.2 Homozygous and heterozygous helicase-dead mice are viable, have normal body weight and composition, and normal long-term survival 100
Figure 5.3 The ATP-dependent helicase function of Recql4 is not required for normal haematopoiesis *in vivo* 103
Figure 5.4 ATP-dependent helicase function of Recql4 is not required for B or T cell development 106
Figure 5.5 *In vitro* sensitivity to DNA damaging agents is not modified by helicase-dead mutation 108
Figure 5.6 Truncating mutations, but not helicase inactivation, result in deleterious effects 111
Figure 6.1 Truncating RECQL4 mutations G522Efs and R347X affect protein expression and localisation differently and are homozygous embryo lethal 133
Figure 6.2 Germline truncating mutants G522Efs and R347X cause low bone mass and narrow bones 137
Figure 6.3 Expression of only the truncating mutations in pre-osteoblasts results in low bone mass 140

Figure 6.4 Compound heterozygous *Recql4* mutants tolerate a sublethal dose of ionising radiation and do not develop OS 143
Figure 6.5 Truncating human RECQL4 mutations C525Afs and R350Gfs fail to rescue *Recql4* deletion and impede proliferation, similar to their murine homologs, while mutations that conserve the protein are better tolerated 146
Figure 7.1 Hoxb8 *Recql4* myeloid cells stably expressing Cas9 . . 165
Figure 7.2 CRISPR Screen design and quality control 168
Figure 7.3 Identification of top genetic hits in the CRISPR/Cas9 knockout screen 170
Figure 7.4 *Klhdc3* sgRNA knockout partially rescues the proliferation defect of RECQL4 mutant cells 172
Figure 7.5 Validation of stable *Recql4* deletion and *Klhdc3* mutation 175

LIST OF TABLES

Table 2.1	Classification of RTS	17
Table 2.2	Proteins interacting with human RECQL4	33
Table 2.3	Murine models of Rothmund-Thomson Syndrome	41
Table 4.1	Reagents and materials, and their suppliers used in this study.	53
Table 4.2	Solutions used in this study.	59
Table 4.3	List of equipment and their manufacturers used in this study	60
Table 4.4	Genotyping PCR cycling conditions	64
Table 4.5	Genotyping oligonucleotide list	65
Table 4.6	Genotyping KASP assay cycling conditions	67
Table 4.7	FACS antibodies (anti-mouse)	69
Table 4.8	P5 primer mix	86
Table 4.9	P7 primers	87
Table 4.10	Thermocycling parameters of PCR	88

LIST OF ABBREVIATIONS

α-MEM – Alpha Minimum Essential Medium
aa – Amino Acids
aBMD – Areal Bone Mineral Density
ANOVA – Analysis Of Variance
AP – Anteroposterior
AURKB – Aurora B Kinase
BER – Base Excision Repair
BGS – Baller-Gerold Syndrome
BM – Bone Marrow
bp – Base Pair
BSA – Bovine Serum Albumin
BV – Bone Volume
CDKs – Cyclin-Dependent Kinases
cDNA – Complementary DNA
CFU-E – Colony Forming Unit-Erythroid
CMPs – Common Myeloid Progenitors
CoFC – Cofractionation
CoIP – Coimmunoprecipitation
CoLC – Colocalisation
Cre – Cre Recombinase
CRISPR – Clustered Regularly Interspaced Short Palindrome Repeats
Ct. Th – Cortical Thickness
DMEM – Dulbecco's Modified Eagle Medium
DMSO – Dimethyl Sulfoxide
DN – Double Negative
DNA – Deoxyribonucleic Acid
DNAse – Deoxyribonuclease
DSBR – Double-Strand Break Repair
DSBs – Double-Strand Breaks
dsDNA – Double-Stranded DNA
DTT – Dithiothreitol

EDTA – Ethylenediaminetetra Acetic Acid
ENU – *N*-ethyl-*N*-nitrosourea
eYFP – Enhanced Yellow Fluorescent Protein
FACS – Flow Activated Cell Sorting
FBS – Foetal Bovine Serum
FC – Fold Change
FCCP – Carbonyl Cyanide 4-(Trifluoromethoxy) Phenylhydrazone
FL – Floxed
FO – Follicular Zone
gDNA – Genomic DNA
GFP – Green Fluorescent Protein
GM-CSF – Granulocyte-Macrophage Colony-Stimulating Factor
GMPs – Granulocyte Macrophage Progenitors
GST-PD – GST Pull-Down Assay
Gy – Gray
HBS – HEPES Buffered Saline
HHBS – Hank's Buffer with HEPES
HR – Homologous Recombination
HRDC – Helicase-And-Ribonuclease D-Like C-Terminal
HSCs – Haematopoietic Stem Cells
Ig – Immunoglobulin
IL – Interleukin
IMDM – Iscove's Modified Dulbecco's Medium
IR – Ionising Radiation
KASP – Competitive Allele-Specific PCR
kDa – Kilo Dalton
KI – Knock-in
KO – Knockout
Lin – Lineage
LPS – Lipopolysaccharide
LT-HSC – Long-Term Haematopoietic Stem Cells
MAP – Microtubule-Associated Protein
MEP – Myelo-Erythroid Progenitor
Micro-CT – Micro-Computed Tomography
MKP – Megakaryocyte Progenitor
ML – Mediolateral
MMR – Mismatch Repair

MOI – Multiplicity Of Infection
MPMI – Mean Polar Moment of Inertia
MPP – Multipotent Progenitor
MS – Mass Spectrometry
MSCF – Recombinant Murine Stem Cell Factor
MZ – Marginal Zone
NER – Nucleotide Excision Repair
NES – Nuclear Export Signals
NFDM – Non-Fat Dry Milk
NHEJ – Non-Homologous End-Joining
NLS – Nuclear Localisation Signal
NoS – Nucleolar Localisation Signal
NTP – Nucleoside Triphosphate
OCR – Oxygen Consumption Rate
ORC – Origin Recognition Complex
OS – Osteosarcoma
Osx – Osterix
PAM – Protospacer Adjacent Motif
PARP – Poly ADP Ribose Polymerase
PB – Peripheral Blood
PBS – Phosphate Buffered Saline
PCA – Principal Component Analysis
PCR – Polymerase Chain Reaction
PCR-RFLP – PCR-Restriction Fragment Length Polymorphism
PFA – Paraformaldehyde
PM – Point Mutant
Pre-RC – Pre-Replicative Complex
Ps. Pm – Periosteal Perimeter
PVDF – Immobilon-P Polyvinylidene Difluoride
R26 – Rosa26 Locus
R4ZBD – Recql4-$Zn2^{+}$-Binding Domain
RBC – Red Blood Cell
RFU – Relative Fluorescence Units
RNAse – Ribonuclease
ROI – Region of Interest
RPA – Replication Protein A
RPM – Revolutions per Minute

RQC – RecQ C-Terminal
RT-PCR – Reverse Transcriptase Polymerase Chain Reaction
RTS – Rothmund-Thomson Syndrome
SEM – Standard Error of the Mean
sgRNA – Single Guide RNA
SSBs – Single-Strand DNA Breaks
ssDNA – Single-Strand DNA
ST-HSC – Short-Term Haematopoietic Stem Cells
Tam – Tamoxifen
Tb. N – Trabecular Number
Tb. Sp – Trabecular Separation
TBS – Tris Buffered Saline
TBST – Tris-Buffered Saline With Tween
TIDE – Tracking of Indels by Decomposition
TV – Trabecular Volume
v/v – Volume/Volume
w/v – Weight/Volume
WT – Wild Type
Y2H – Yeast Two-Hybrid Assay

CHAPTER 1

1

INTRODUCTION

1.1 PROBLEM STATEMENT

Rothmund-Thomson syndrome (RTS, OMIM #268400) is an autosomal recessive disorder first described in 1868 and 1936 by Drs August Rothmund and Sydney Thomson, respectively. They reported patients with skin rash (poikiloderma), cataracts, growth retardation and skeletal dysplasias. Years later, in 1999, Kitao *et al.* cloned and mapped the gene *RECQL4* for the first time, and identified mutations in this gene as causative of RTS.

Since then, some advances have been made in the understanding of this disease and the mutations affecting *RECQL4*. It has been discovered that the skeletal system is affected in the majority of RTS patients and that the worst prognosis is associated with the presence of truncating/hypomorphic mutations. It has also been found that RECQL4 is involved in DNA replication, DNA repair, mitosis and telomere maintenance, and that it interacts with selected proteins in these processes. However, the role of the specific domains of RECQL4; the impact of mutations in processes like protein stability, haematopoiesis, bone development, and tumorigenesis; and the functional genetic interactions of *RECQL4* remain poorly understood.

Several murine models of *Recql4* have been developed to understand its *in vivo* function and to gain greater insight into how its mutation causes the phenotypes seen in RTS patients. Although these models have uncovered some of the functions of RECQL4, they do not accurately reflect the genetic landscape of RTS. Modelling these mutations is therefore critical in order to identify the requirements of the individual domains of RECQL4, the

phenotypes they cause when deleted, and additional genes that might interact with *Recql4*.

1.2 OVERALL AIM AND SCOPE OF THE THESIS

The overall aim of this thesis is to improve understanding of the individual domains and functions of RECQL4 and the impact that different *Recql4* mutations have on normal homeostasis, tumour development, and functional genetic interactions.

1.3 OVERVIEW OF THE THESIS

The work in this thesis has three areas of focus:

(i) Understanding the function(s) of the ATP-dependent helicase activity of RECQL4.

(ii) Determining the impact of truncating mutations affecting the C-terminal and the helicase domain on normal homeostasis and tumour development.

(iii) Identifying functional genetic interactions with *Recql4*.

Chapter 2 contains a review of the current literature. It begins with a brief description of helicases and the RecQ helicases. Subsequently, *RECQL4* associated disorders, cancer predisposition, and its mutations are discussed in detail. This is followed by an in-depth review of RECQL4 in terms of its expression, localisation, functions, interactions, and domains. This chapter finishes with a discussion of previously reported murine models.

Chapter 3 describes the aims and hypotheses of this thesis, which are based on the three areas of focus previously mentioned.

Chapter 4 provides a procedural description of the materials and methods used in this thesis.

Chapter 5 will address whether the ATP-dependent helicase activity of RECQL4 is essential for its physiological functions. For this chapter, I will use mice carrying an ATP-binding-deficient knock-in mutation and will assess the effects of this mutation on embryonic development, body weight,

haematopoiesis, B and T cell development, and physiological DNA damage repair. This will allow me to determine the physiological requirement and biological functions of RECQL4 helicase activity.

Chapter 6 will assess the effects of RECQL4 truncating mutations that affect both the C-terminal and the helicase domain on protein stability, subcellular localisation, bone development, and tumorigenesis. Furthermore, in this chapter, I will utilise murine *Recql4* null cells to evaluate the impact of a wider range of human *RECQL4* mutations using an *in vitro* complementation assay. These data will allow a better understanding of the cellular consequences of common mutations seen in RTS patients.

Chapter 7 will describe a search for novel *Recql4* genetic interactions that may enable an improvement of the phenotypes associated with a pathogenic *Recql4* mutation. For this chapter, I will utilise immortalised haematopoietic cells, generated from one of the truncating mutants, to perform a genome-wide genetic rescue screen using CRISPR/Cas9 technology.

Lastly, Chapter 8 contains the conclusions of this thesis. It will present a summary of the results of each component, an explanation of how these results have addressed the research aims, the implications of the findings, and suggestions for future research.

CHAPTER 2

2

LITERATURE REVIEW

2.1 HELICASES

Helicases are fundamental to life. In order to access genetic information during DNA replication, repair, recombination, or transcription, it is necessary to unwind the chromatin and nucleic acids. A large group of proteins known as helicases are responsible for this process. In eukaryotic organisms, the number of helicases found is strikingly high with ~1% of their genes encoding these proteins [1, 2]. This high number has made their classification very challenging. Initially, helicases were categorised based on structure-function analysis in three superfamilies (SF1, SF2, SF3) and two smaller families [3]. However, with further research and the discovery of additional motifs, this classification has expanded to six -very different- superfamilies (SF1-SF6) [4, 5].

Although different in structure and function, these superfamilies have something in common, the presence of signature "core domains" that form structures similar to RecA (recombination strand exchange enzyme) from *Escherichia coli* [6]. These domains contain conserved residues that participate in the hydrolysis and binding of nucleoside triphosphate (NTP) to the Walker A and B motifs, present in many ATPases [5, 7, 8].

From a structural perspective, SF1 and SF2 helicases are the best characterised. Both contain a conserved helicase core that includes seven characteristic motifs. Each motif contains two RecA-like folds within a single polypeptide chain, and can function as monomers or dimers. In contrast, SF3-SF6 helicases have fewer conserved motifs containing only one Rec-A like fold per monomer, and can function as hexamers forming structures

known as toroidal rings [7, 9] (Figure 2.1). From all the superfamilies of helicases, the SF2 cluster is the largest and most diverse group. It contains ten families including DEAD-box, RecG-like, Ski2-like, Rad3/XPD, type I restriction enzyme, NS3/NPH-II, RIG-I-like, DEAH/RHA, Sri/Snf, and the RecQ family [10]. All these proteins have highly evolutionary-conserved motifs with distinct roles in DNA or RNA metabolism. For this thesis, I will focus on the RecQ family only.

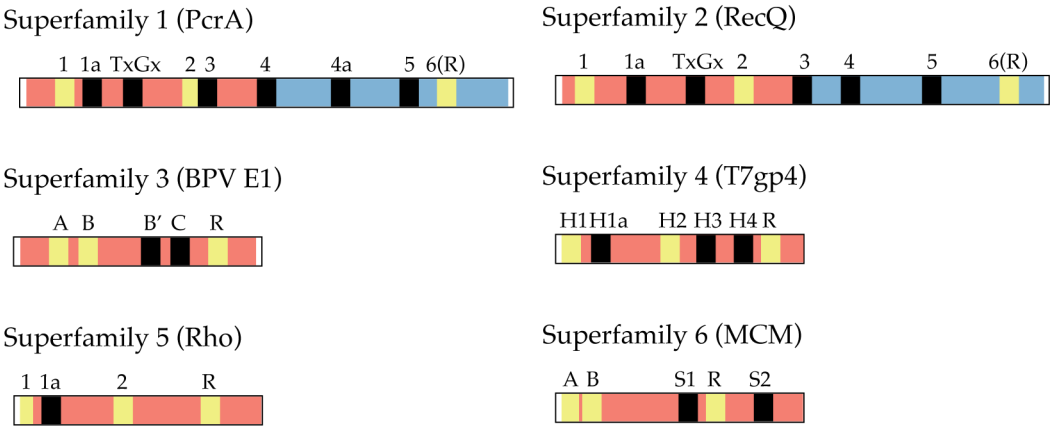

Figure 2.1: *Classification of helicases.* The helicase family consists of six superfamilies. Their structure is detailed in each figure with one example of a member in parentheses. The yellow boxes indicate universal conserved motifs across superfamilies. The red and blue boxes represent RecA or AAA^+ -like domains, interconnected by NTP analogues in black boxes. Figure adapted from Singleton *et al.* [5].

2.2 RECQ HELICASES

From all the families that comprise the SF2 helicases, the RecQ family is particularly important. Its name comes from the RecQ gene, first identified in *E. coli* in 1984 [11]. Subsequent studies showed that this group of proteins has been evolutionarily conserved from bacteria to mammals. Furthermore, they showed that lower eukaryotic species, such as *Schizosaccharomyces pombe* and *Saccharomyces cerevisiae*, contained a single RecQ-like helicase [12–14]; whereas in higher eukaryotic organisms, this number had expanded with most vertebrates having two or more of these proteins [15]. This evolutionary conservation and expansion in more complex organisms highlights the importance of this family.

Five helicases compose the RecQ family in humans: RECQL1, RECQL4, RECQL5, BLM, and WRN. Although all of them share important core motifs,

each has individual domains with unique features and functions. These will be discussed in the following section.

2.2.1 *Structure of RecQ helicases*

RecQ helicases contain three important domains: "The helicase domain, the RecQ C-terminal (RQC) domain, and the helicase-and-ribonuclease D-like C-terminal (HRDC) domain" [16]. The only conserved domain in the entire family is the helicase domain, whereas the RQC and the HRDC domains differ depending on the protein. The variation seen in these domains gives these proteins a variety of extra functions and a wide range of protein sizes going from 649 aa for RECQ1 to 1,432 aa for WRN [17, 18].

The core helicase domain is the most prominent feature of the RecQ helicases. It contains ~400 aa and its main function is to use energy of NTP hydrolysis into the unwinding of nucleic acids [5, 19]. It contains two important motifs: Walker A and B. The Walker A motif contains a conserved lysine residue important for ATP hydrolysis [8]. On the other hand, the Walker B motif contains aspartate and glutamate residues that coordinate magnesium ions and ATP hydrolysis [20]. The second domain of the RecQ helicases is the RQC domain, which features two regions: A Winged-Helix domain and a Zinc-binding domain. Both domains enable double-stranded DNA (dsDNA) binding [21] and contribute to protein stability [22]. This domain is present in all the RecQ helicases except RECQL4, which has the RecQ4-Zn^{2+} -binding domain (R4ZBD) instead [23]. The third domain is the HRDC domain, only found in BLM and WRN. In BLM, this domain has been reported to be critical for the unwinding of Holliday junctions [24]; whereas in WRN, it is thought to have an important role in protein-to-protein interaction networks [25] (Figure 2.2). The variability of these domains supports the argument that, even though they are part of the same family, their functions have separated during evolution.

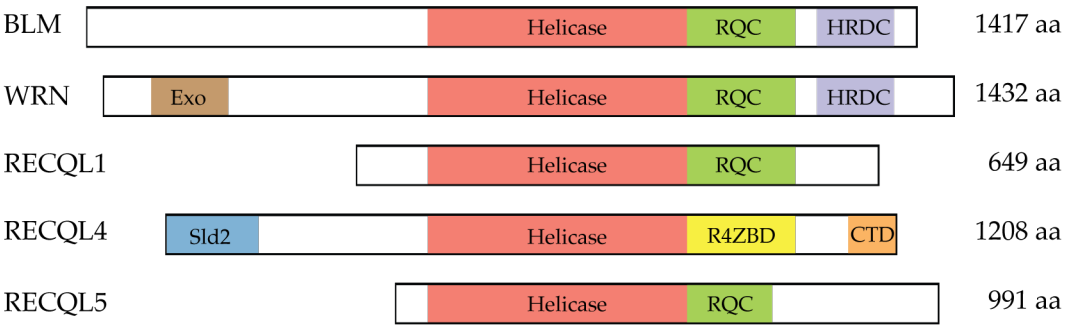

Figure 2.2: *Structure and classification of human RecQ helicases.* Structural comparison of RecQ helicases. The figure shows the helicase domain, highly conserved across RecQ helicases; followed by the RQC domain, which is present in all except for RECQL4, which has the R4ZBD domain instead. The HRDC domain is the least conserved domain amongst this group and is present in BLM and WRN only. Colour code: Helicase-red, RQC-green, HRDC-purple, R4ZBD-yellow, CTD-orange, Exonuclease-brown, Sld2-like-blue. Figure adapted from Kaiser and Larsen *et al.* [23, 26].

2.2.2 *RecQ helicases and syndromes associated*

The discovery that the highly conserved RecQ helicases have a tumour-suppressor role has created great interest in their study. In humans, mutations in three of them (WRN, BLM, and RECQL4) are linked to specific hereditary cancer syndromes, while the remaining two (RECQL1 and RECQL5) are associated with increased cancer predisposition. Given the structural similarity of these proteins, it is possible that some functional redundancy may exist. In fact, one study found that BLM physically and functionally interacted with RECQL4 [27]. Similarly, another study reported that WRN interacted with RECQL4 at telomeres [28]. However, the fact that the knockout of one RecQ helicase cannot be rescued by the remaining other family members suggests that there are non-overlapping functions for each. In the following section, I will provide a brief description of the roles and syndromes associated with RecQ helicases in humans, before getting into a more detailed discussion of the diseases associated with my helicase of interest, RECQL4.

The *BLM* gene is located on chromosome 15. As a helicase, it has roles not only in the unwinding of simple dsDNA structures, but also in complex structures like double Holliday junctions, D-loop, and G-quadruplexes [29]. Bi-allelic mutations in *BLM* result in Bloom syndrome, which is characterised by skin photosensitivity, short stature, reduced fertility, immunodeficiency, and increased cancer predisposition [30]. These mutations also produce a

10-fold increase in sister chromatid exchange between homologous chromosomes [31], which constitutes a hallmark of its molecular diagnosis.

Regarding the *WRN* gene, it is located on chromosome 8 and its mutation causes Werner syndrome. Patients affected by this disease appear normal until adolescence, at which time they fail to undergo a growth spurt. Subsequently, they develop a premature ageing phenotype that includes cataracts, greying of hair, skin atrophy, atherosclerosis, diabetes mellitus and malignancies [32]. The majority of these mutations generate truncated products of the WRN protein [33], which result in a high frequency of telomere dysfunction and chromosomal instability [34, 35]. Additionally, WRN-deficient cells have high levels of double-strand breaks (DSBs) after exposure to replication stress [36], which suggests a role in DNA repair.

Although no specific genetic syndromes have currently been associated with mutations in *RECQL1* or *RECQL5*, research has shown that these two genes may be involved in certain types of cancer. For instance, in pancreatic cancer, polymorphisms in *RECQL1* are associated with low survival [37]. Similarly, in breast cancer, low levels of RECQL1 are associated with larger tumour size and higher pleomorphism [38]. Regarding RECQL5, increased activity of this protein in patients with breast cancer and urothelial carcinoma of the bladder has also been linked to poor prognosis [39, 40]. While the specific role of these proteins in cancer pathogenesis is still unknown, several studies have discovered some of their basic functions. At a molecular level, it has been found that RECQL1 binds and unwinds simple and complex DNA structures during DNA replication and repair [41, 42]; while RECQL5 has roles at the intersection of transcription and replication preventing transition conflicts [43, 44]. However, more studies are required to further understand the association of these proteins with cancer prognosis.

2.3 RECQL4 AND HUMAN DISEASE

RECQL4 mutations have been reported in three clinical syndromes: RAPADILINO Syndrome, Baller-Gerold Syndrome (BGS) and RTS. In this section, I will start with a description of these diseases, followed by the cancer predisposition and mutation spectrum they present with special emphasis on my disease of interest, RTS.

2.3.1 *RECQL4 associated disorders*

2.3.1.1 *RAPADILINO syndrome*

RAPADILINO syndrome (OMIM #266280) is an autosomal recessive disease originally reported by Kääriäinen *et al.* in 1989 [45]. It is most prevalent in Finland, with fifteen reported cases in this population. The acronym stands for the features of the syndrome: "RA for RAdial hypoplasia, PA for both absent/hypoplastic PAtellae and cleft/high arched PAlate, DI for DIarrhoea as well as DIslocated joints, LI for LIttle size and LImb malformations, and NO for long, slender NOse and NOrmal intelligence" [45].

The most frequent mutation amongst patients with RAPIDILINO syndrome is the c.1390+delT (p.Ala420-Ala463del), which results in an in-frame deletion of exon seven [46]. Interestingly, while the clinical features between RAPIDILINO and RTS usually overlap, some features are unique to RAPADILINO. For example, RAPADILINO patients generally do not develop the characteristic ectodermal symptoms of RTS. On the other hand, joint dislocations and patella hypo/aplasia are not seen in RTS but are common in female RAPADILINO patients [47]. Lastly, around 7% of RAPADILINO patients develop tumours, mainly lymphomas and osteosarcoma (OS) [47]. Although significant compared to the general population, this is significantly lower than the rates of tumour development seen in RTS (Figure 2.3).

2.3.1.2 *Baller-Gerold syndrome*

BGS (OMIM #218600) is a very rare autosomal recessive disease with less than 40 cases reported. It was first described by Baller [48] and Gerold [49] in patients that presented both bilateral radial aplasia and craniosynostosis (premature closure of sutures in the skull). These two skeletal defects can be found separately in a variety of syndromes. For instance, bilateral radial ray hypoplasia/aplasia are found in SALL4-related syndromes, Robert SC phocomelia, Fanconi Anaemia, Holt-Oram syndrome, thrombocytopaenia-absent radius syndrome, and RTS [50]. On the other hand, craniosynostosis can be present in at least fifty genetically distinct syndromes (summarised in [51]). This genetic heterogeneity and partial clinical overlap have made the diagnosis of BGS very challenging.

The fact that both BGS and RTS have radial hypoplasia/aplasia amongst their manifestations, led to the discovery that BGS patients also have mutations in *RECQL4*. However, some non-overlapping features such as the lack of OS and premature ageing in BGS; and the absence of craniosynostosis in RTS, allow differentiation between them (Figure 2.3).

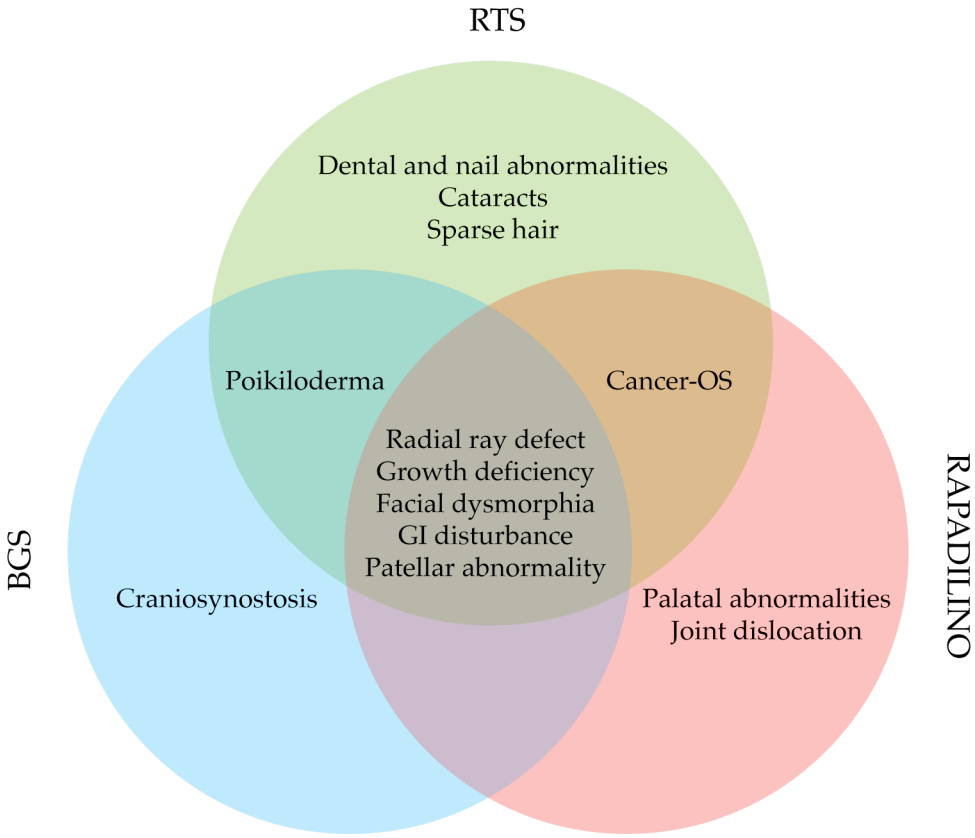

Figure 2.3: *Venn diagram of the overlapping and unique features of RECQL4 associated disorders.* Image adapted from Van Maldergem *et al.* [52].

2.3.1.3 *Rothmund-Thomson Syndrome*

RTS (OMIM #268400) is an autosomal recessive and heterogeneous disease initially reported in 1868 by the ophthalmologist August Von Rothmund. He described ten children with poikiloderma, juvenile cataracts and growth retardation in a small village in the southeast of Germany [53]. In 1936, the dermatologist Sydney Thomson described three subjects with similar symptoms, but no cataracts [54]. These two entities were combined in 1957 by Dr William Taylor [55], who described several patients with the previously mentioned symptoms and created the eponym Rothmund-Thomson syndrome.

RTS is a rare disease with ~400 cases reported in the literature. Due to its variable clinical spectrum, patients that present with borderline clinical symptoms may be overlooked or not diagnosed. Thereby, its incidence may be higher. Consistent with its autosomal recessive mode of inheritance, most cases are isolated. However, cases from small communities and consanguineous relatives have been reported. Most RTS patients present with compound bi-allelic heterozygous mutations of the *RECQL4* gene [56], which result in truncated protein products deleting the majority of the helicase and the C-terminal domain. Regarding life expectancy, although published follow-up data is limited, the lifespan of RTS patients is considered normal, unless they develop cancer [57].

RTS Subtypes

Based on the clinical features and *RECQL4* mutation status, two types of RTS have been categorised: RTS type 1 and type 2. For the sake of brevity, throughout this thesis, the term RTS will be used to refer to RTS type 2. RTS type 1 will not be covered in detail in this thesis and will only be described in the following paragraphs.

RTS TYPE 1 is characterised by poikiloderma and extracutaneous manifestations such as dental abnormalities, skeletal defects and juvenile cataracts [58]. The aetiology of this subtype was linked to mutations in the *ANAPC1* gene in a recent study [59]. This study performed whole-exome sequencing in ten clinically-diagnosed RTS type 1 patients and found splicing mutations in the *ANAPC1* gene. This mutation was homozygous in half of the patients, and coincided with other mutations in the rest [59]. *ANAPC1* encodes the APC1 protein, whose levels were decreased in this group of patients. Furthermore, APC1 is part of the anaphase-promoting complex/cyclosome (APC/C), an E3 ubiquitin ligase with important roles in protein degradation, cell cycle transition, cellular senescence, DNA replication and DNA repair [60, 61].

Since most of the patients that present with juvenile cataracts are diagnosed with RTS type 1, it is more likely that they harbour *ANAPC1* mutations. In fact, studies in zebrafish have shown that defects in the APC protein lead to defects in cell proliferation and differentiation in the lens [62]. Furthermore, heterozygous mice carrying a knockout mutation of the *ANAPC1* gene

showed an increased incidence of lens opacities [63]. This may explain why these cataracts are more common in this suptype of RTS.

RTS type 2 is characterised by poikiloderma, ectodermal dysplasias, skeletal defects, OS predisposition, and the presence of biallelic mutations in *RECQL4*. A detailed description of the features of *RECQL4* mutant disease is provided in the next section. Given the clinical overlap between the RTS subtypes (Table 2.1) and the fact that mutations in *ANAPC1* and *RECQL4* lead to defects in DNA replication and DNA repair, it is possible that both genes converge on a common pathway. Future studies should focus on the discovery of other constituents of this pathway, which might eventually contribute to the full understanding of the pathogenesis of RTS.

Table 2.1: *Classification of RTS*

CLINICAL FEATURES / MUTATION STATUS	RTS TYPE 1	RTS TYPE 2
Poikiloderma and extracutaneous symptoms	Yes	Yes
Dental abnormalities	Yes	Yes
Skeletal defects	Yes	Yes
Juvenile cataracts	Yes	No
Mutations in *RECQL4*	No (*ANAPC1*)	Yes
Osteosarcoma	No	Yes

Clinical Features

The clinical hallmark of RTS is cutaneous poikiloderma. It is defined as skin atrophy with mixed areas of hypo/hyperpigmentation and telangiectasia (small widened vessels in the skin). It generally appears at around three to six months of age as a skin rash with erythema, oedema, and blisters in the cheeks. Subsequently, it spreads to the buttocks and the upper and lower limbs sparing the abdomen and trunk [64]. Histologically, the lesions are characterised by epidermal thinning, perivascular lymphocytic infiltrate, and telangiectasia [65, 66]. The rash can be worsened by sun exposure, and thereby, strict photo-protection is an integral part of its management (Figure 2.4 A-E).

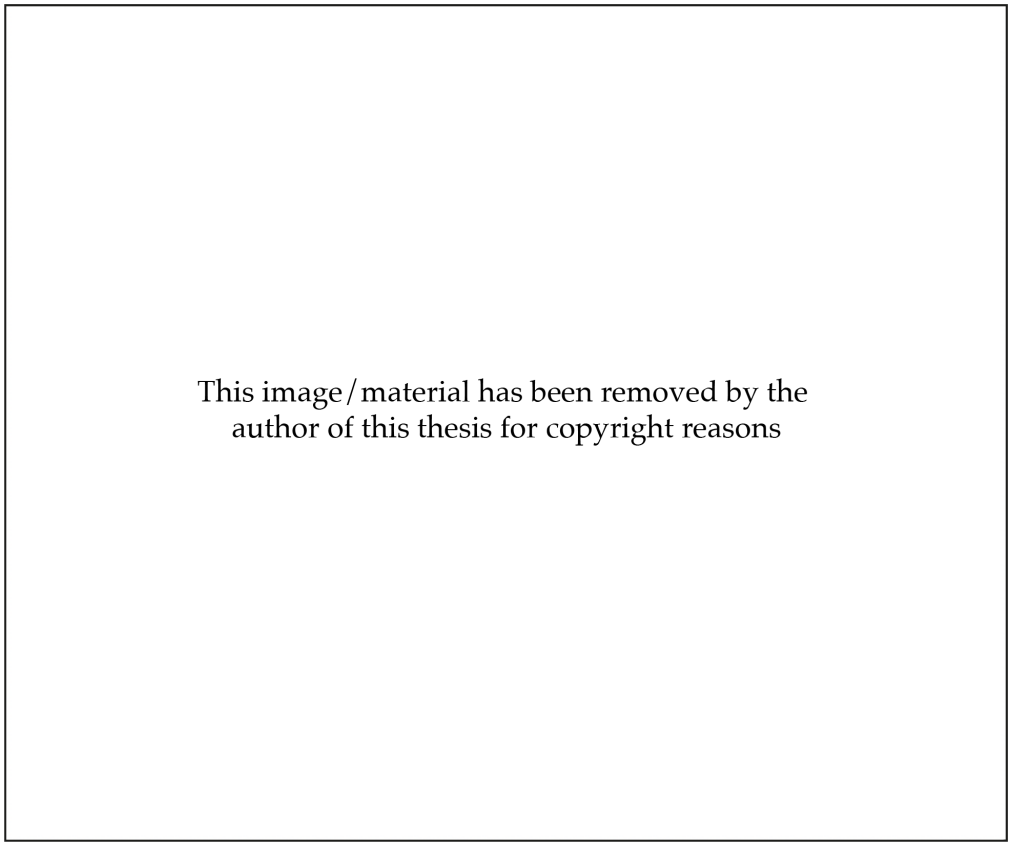

Figure 2.4: *Clinical symptoms in patients with RTS.* (A) Poikiloderma in the cheeks. (B) Poikiloderma with partial alopecia. (C) Poikiloderma. (D) Poikiloderma in the face and upper limbs (trunk is spared). (E) Poikiloderma and knee valgus. (F) Thumb aplasia. (G) Cystic lesion of the distal epiphysis of the humerus. Image derived from Larizza *et al.* [64].

Ectodermal dysplasias are common in RTS. These include hair, nails and dental abnormalities. A cohort of 41 patients found that 73% had sparse eyebrows and eyelashes, while 50% developed sparse scalp hair [67]. Dystrophic brittle nails can also be found amongst RTS patients [64]. Regarding dental abnormalities, case reports have described microdontia, delayed eruption, hypoplastic, supernumerary or congenitally missing teeth, malocclusion, and increased incidence of caries [68–72].

The skeletal system is affected in the majority of RTS patients. An early review of the literature found that 68% of patients presented skeletal abnormalities that include osteopaenia, frontal bossing, saddle nose, syndactyly, and hypoplasia/agenesis of bones [73]. General medical examinations do not detect some of these anomalies, thereby radiographic tests are required. Wang *et al.* reported that 75% of RTS patients that underwent radiographic skeletal surveys, presented some type of skeletal abnormalities. The same

study reported that two-thirds of subjects presented small stature without asymmetry, and in most of the cases, with normal growth hormone levels [67]. These findings are consistent with those of Mehollin-Ray *et al.*, who analysed twenty-eight RTS patients and found that 75% of them presented at least one skeletal abnormality that included osteopaenia, abnormal metaphyseal trabeculation, radial aplasia/hypoplasia, brachymesophalangy, and patellae ossification defects [74]. The exact mechanism of why the skeletal system is more frequently affected than other organs remains unknown.

Low bone mass and increased bone fragility are also features of RTS. A study that investigated twenty-nine RTS patients found a significantly increased number of individuals with low bone mass, which was defined as areal bone mineral density (aBMD) Z-score lower than -2.0 [75]. This change was considerably greater than the general population (Z-score=0) [76], which suggests that mutations in RECQL4 may be causally related to this phenotype. These changes in bone mass can predispose RTS patients to pathological fractures. Cao *et al.* found that 45% of children and 67% of adults diagnosed with RTS reported at least one previous fracture. They also found that the presence of a RECQL4 mutation increased the probability of having a fracture by five-fold [75]. This has been confirmed by several additional studies that have reported pathological fractures in RTS patients. One study reported an adult patient with multiple tibial fractures, lower extremity osteopaenia, and normal calcium levels [77]. Similarly, another study described a patient with multiple episodes of long bone fractures and significant delayed healing [78]. The latter was also reported in a young patient with a delayed union of the fifth metatarsal following a fracture [79]. Recently, a patient with poor growth and recurrent fractures was also reported [80]. Since a large proportion of RTS patients are predisposed to OS, which could debut as a pathological fracture, investigation for this malignancy might be necessary in RTS patients with fractures.

Other manifestations in RTS involve the ocular and gastrointestinal system. Amongst ocular symptoms, juvenile cataracts are the most common. As previously mentioned, these are associated with RTS type 1 and their prevalence is highly variable. An early literature review reported a prevalence of 49% [73], whereas a later cohort stated it to be as low as 10% [67]. This explains why cataracts are not a definitive symptom in the diagnosis of RTS and also highlights the variable penetrance of many of the clinical features of RTS.

Regarding the gastrointestinal system, some children present with symptoms such as chronic emesis, diarrhoea, and some form of stenosis, atresia, or fistula in the gastrointestinal tract [67, 81, 82]. These symptoms appear to be rare and resolve spontaneously during early childhood.

Lastly, although haematological disorders are not amongst the classical features of RTS, several studies have reported defects in the blood system, particularly within the leukocyte lineage. In fact, several studies have reported RTS patients with immunological abnormalities. Two studies reported patients with recurrent sinus and pulmonary infections [83] and severe herpes encephalitis [84]. Both presented low levels of Immunoglobulin G. A subsequent study reported a patient with mutations in *RECQL4* and agammaglobulinemia, who presented complete immune reconstitution after an allogeneic cord blood stem cell transplant [85]. Later, a study reported an RTS patient with skin granulomas following Varicella Zoster infection. This patient presented hypogammaglobulinemia with low levels of T CD8, NK CD16, NK CD56, and class-switched B cells, [86]. A recent study described an RTS patient with respiratory infections and lymphopaenia, thrombocytopaenia, and hypogammaglobulinemia [87]. Finally, although the pathophysiology of immunological abnormalities in RTS has not been completely understood, my group reported the first association of acute loss of *Recql4* and bone marrow failure. They found that RECQL4 was essential for B cells, T cells, and myeloid progenitor development [88]. However, further research is needed to establish the specific role of RECQL4 in haematopoiesis.

2.3.2 *RECQL4 and cancer predisposition*

Cancer is a complex and heterogeneous disease. It arises when cells acquire proliferation and survival advantages from mutations, which are the result of inherited genetic changes and environmental factors [89]. Some paediatric cancers are caused by genetic mutations linked to cancer predisposition syndromes [90]. One of them is RTS. Children with RTS have higher rates of malignancies when compared to healthy children. Amongst the most common malignancies reported in RTS patients are OS, epithelial tumours, and haematological neoplasias [56, 64, 67].

OS is the most frequent primary bone tumour found in children and adolescents. It is mainly located in the growth plates of long bones and its

prognosis is variable [91]. Patients with sporadic OS have a 60-70% 5-year survival rate, which drastically reduces to 20-30% when metastases develop [92]. Amongst patients with RTS, OS is the most common type of cancer. In a clinical cohort study that evaluated 41 RTS patients, 32% developed OS at a median age of 11.5 years [67]. This is significantly younger than the median age of sporadic OS, which is 16 years [93]. Therefore, the diagnosis of OS at a younger age should raise suspicion of RTS. Despite the high OS predisposition in RTS, only a few studies have investigated the role of *RECQL4* in OS. An early study that evaluated 23 RTS patients found that truncating *RECQL4* mutations increased the risk of developing OS [58]. A second independent study that analysed OS tumours in RTS patients reported that the histology, clinical characteristics, and prognosis of these tumours were very similar to those seen in sporadic OS [94]. With regards to its mutation spectrum, a study found that the majority of RTS patients that develop OS carry compound heterozygous mutations [56].

At a molecular level, studies have shown different results. An early study that analysed 9 OS cell lines and 26 OS tissue samples found no abnormalities in the *RECQL4* gene [95]. Similarly, a study that performed whole-genome DNA sequencing in 20 sporadic OS tumour samples did not find any *RECQL4* mutations. Instead, mutations in other genes associated with OS including *TP53*, *RB1*, *ATRX*, and *DLG2* were reported [96]. Although these studies did not find *RECQL4* mutations amongst the samples analysed, other studies have. A study that analysed 123 OS samples found *RECQL4* as one of the 14 OS driver genes [97]. Similarly, a study that performed whole-exome or targeted sequencing of the DNA of 1,244 OS patients, also found pathogenic variants of *RECQL4* [98]. In addition to these focused OS studies, a recent study that analysed germline sequence data from 5,562 paediatric cancer patients found a significant enrichment of heterozygous *RECQL4* mutations in patients with OS [99]. The differences between these studies might be explained by the much smaller cohorts of tumours analysed in the earlier studies. Therefore, is it possible that the association of *RECQL4* with sporadic OS could have been missed. These findings, together with the high predisposition to OS that RTS patients have, illustrate that *RECQL4* is one of the genes contributing to OS development. However, its specific role in tumorigenesis remains unknown.

In contrast to OS, epithelial tumours are more frequent in adult RTS patients (median age=34.4) [100]. These include basal cell carcinoma, squamous cell carcinoma, and melanoma [100–102]. A study reported cutaneous squamous cell carcinoma in three siblings with RTS, who were between 35 and 38 years old [103]. Interestingly, this cancer was found in non-sun exposed areas, suggesting that other mechanisms besides direct UV damage may underlie its pathogenesis.

Although less frequent, haematological malignancies have also been reported in RTS. These relate to both myeloid and lymphoid lineages and include myelodysplastic syndrome, acute myeloid leukaemia and non-Hodgkin's lymphoma [104–109]. The mechanism of how RECQL4 mutations cause haematological malignancies is unknown and require further studies.

2.3.3 *Mutations in the RECQL4 gene*

The most common mutations affecting the *RECQL4* gene are nonsense and frameshift mutations (Figure 2.5) [56]. In nonsense mutations, changes in DNA base pairs lead to the substitution of an amino acid codon by an early stop codon. In frameshift mutations, the addition or removal of DNA bases change a gene's reading frame leading to a modification of the amino acid code, usually resulting in a shortened non-functional protein. Therefore, both mutations lead to the same result: a truncated protein product.

Over half of the mutations that create truncated products are within the helicase domain [56]. This domain is encoded by exons 8-14 and has been considered essential for the functioning of RECQL4. The prevailing theory in the field is that inactivation of the helicase causes the phenotypes seen in RTS. This theory leaves out the C-terminal domain, which is often lost as a result of the truncating mutations, and of which deletion alone has also shown to produce an RTS phenotype [110]. In fact, a recent study reported two RTS patients carrying the homozygous mutations c.3054A>G in exon 17 and c.3236G>T in exon 18 [110]. Both patients had an intact helicase domain and yet still developed the canonical, albeit milder features of RTS, which highlights the contribution of this domain to the RTS phenotypes.

Most RTS patients present with compound heterozygous mutations. A study evaluating 33 RTS patients found that 90% of them presented a mu-

tation in both alleles [58]. This distribution makes the study of genotype-phenotype correlation extra challenging since different domains might be affected in the same individual. A possible solution could be the use of murine models with mutations in different domains that resemble those seen in patients. This would be an efficient way to study the effects of these mutations *in vivo*, and thereby, the role of the domains affected by them.

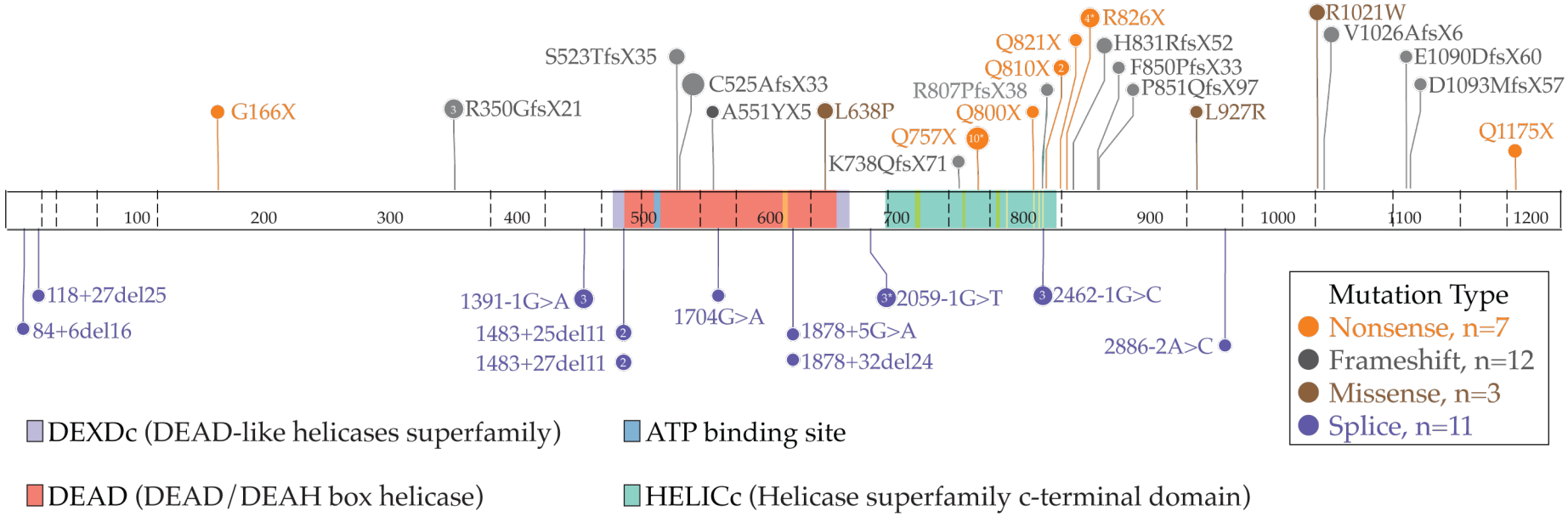

Figure 2.5: *Mutations in the RECQL4 gene.* Schematic illustration of *RECQL4* somatic mutations in RTS patients. The selected mutations were published by Siitonen *et al.* [56]. As illustrated, the majority of mutations are nonsense or frameshift affecting the helicase or C-terminal domain and creating truncating protein products. Image generated using Protein painter (Pecan portal St Jude's).

2.4 RECQL4

Given the clinical heterogeneity of the phenotypes of RTS, it is clear that *RECQL4* has functions in multiple cell types. In this section, I will describe these functions in detail, in addition to the domains, tissue expression, and cellular localisation of the RECQL4 protein.

The human *RECQL4* gene was first cloned and mapped by Kitao *et al.* in 1999 [111]. The gene is located on the long arm of chromosome eight (8q24.3) and is relatively condensed (6.5 Kb). It contains 21 exons with a full-length transcript of 3,627 bp and 13 introns of less than 100 bp in length [111, 112]. Deletions within these small introns can make them too small for efficient splicing leading to an unusual mechanism that generates truncating or loss-of-function mutations (Figure 2.6) [112]. The human *RECQL4* gene encodes a protein by the same name, which contains 1,208 aa with a molecular weight of 133 kDa.

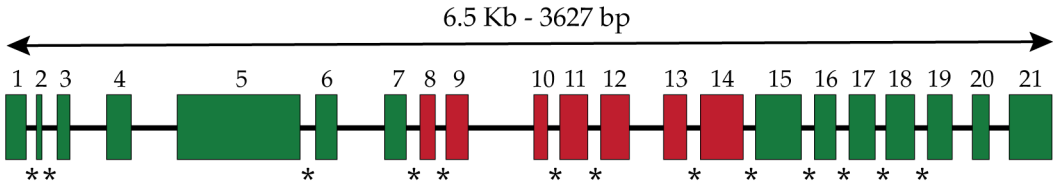

Figure 2.6: *Structure of the RECQL4 gene.* Red boxes identify the exons that encode the helicase domain. Introns are represented by interconnecting lines. Asterisks represent introns of less than 100 bp in length. Image adapted from Wang *et al.* [112].

2.4.1 *Tissue expression*

Regarding tissue expression, *RECQL4* mRNA is expressed highly in bone marrow, thymus and testis; and low in the placenta, brain, heart, pancreas, small intestine, and colon (Figure 2.7) [113]. Furthermore, its expression is cell cycle phase and tissue-specific. In fact, studies have shown its highest expression during the transition from G1 to S-phase of the cell cycle [114, 115].

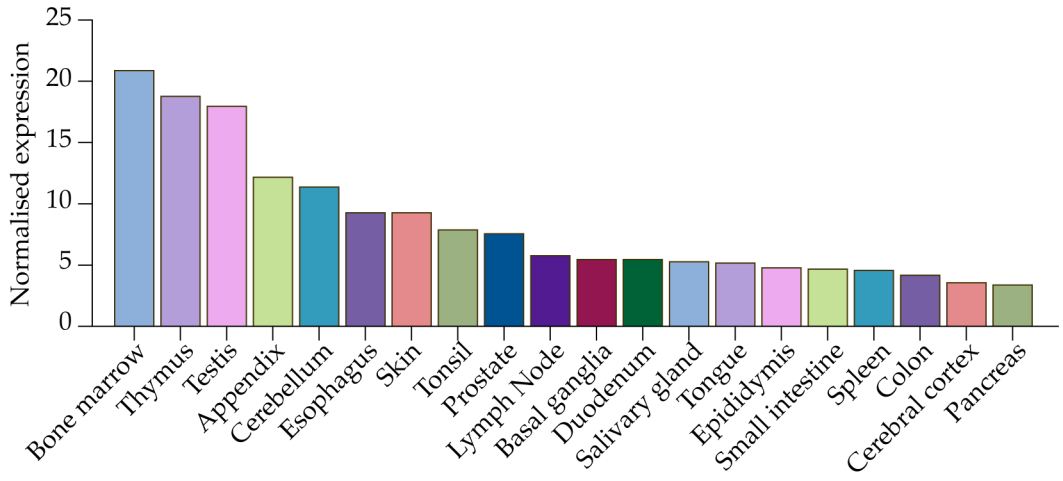

Figure 2.7: *RECQL4 mRNA tissue expression.* As illustrated, the expression of *RECQL4* is particularly high in bone marrow, thymus, and testis. This figure contains data of human tissue expression from the Consensus Normalised Expression dataset, created by combining three transcriptomics datasets (HPA, GTEx, and FANTOM5). It was obtained from the Human Protein Atlas page https://www.proteinatlas.org/ENSG00000160957-RECQL4/tissue [116].

RECQL4 has different expression levels in disease. Recent studies have reported overexpression of *RECQL4* in breast, gastric, and metastatic prostate cancer tissues [117–119]. Interestingly, when authors reduced *RECQL4* expression using small interfering RNA (siRNA) in prostate cancer cells, they observed a dramatic reduction of tumorigenicity *in vivo* and cell invasiveness *in vitro* [119]. This finding potentially implicated *RECQL4* as a prognostic marker for prostatic carcinoma. Furthermore, it allowed the authors to suggest that based on its prominent role in DNA replication initiation, *RECQL4* overexpression may reflect rapidly dividing cells in the context of a tumour. Furthermore, they suggested that the DNA repair role of RECQL4 may provide an advantage to tumour cells by protecting them from endogenous and exogenous DNA damage [119]. However, more studies are required to confirm these hypotheses.

2.4.2 *Sub-cellular localisation*

Several studies have identified RECQL4 in both the nucleus and the cytoplasm. The first study to assess its localisation used overexpression of Flag-tagged RECQL4 in HeLa cells and found that RECQL4 was localised in the nucleus spreading across the nucleoplasm [120]. In contrast, a second study that analysed endogenous RECQL4 in HeLa, MCF7, and Jurkat cells

found a predominantly cytoplasmic localisation. However, when the same study analysed untransformed fibroblasts (WI-38), the authors described that RECQL4 was mostly nuclear [121]. In contrast, another study that used HeLa, WI38/VA13 and primary skin fibroblasts found a punctuate nuclear staining of RECQL4 [122]. These contradictory findings led to several studies that aimed to determine the specific localisation of RECQL4. Using HeLa, WI38/VA13, and U2OS cells, authors reported that RECQL4 was in the nucleus of 87% of cells, in the cytoplasm of 4%, and in both compartments in 9% of cells [123]. Similarly, another study using HeLa cells found that RECQL4 was localised primarily in the nucleus of 70% of cells, followed by both nucleus and cytoplasm in 22%, and only in the cytoplasm in 8% of cells [124]. The same study also found that the N-terminal domain of RECQL4 interacted with the histone acetyltransferase p300. Acetylation by p300 led to an inability to import acetylated RECQL4 into the nucleus causing accumulation of RECQL4 in the cytoplasm [124]. Together, these findings suggest that RECQL4 localisation is cell type-specific and may vary with its modification. However, its reported localisation depends on the methods used to detect it.

Since RECQL4 has been found in both the nucleus and the cytoplasm, several studies aimed to identify the sequences responsible for its intracellular trafficking. Two nuclear localisation signals (NLS) within the N-terminal domain (NTS1 and NTS2) have been reported. NTS1 is located between residues 37 and 66 and has a weak nuclear import function; whereas NTS2 is located between residues 363 and 492 and has shown to be the primary nuclear localisation signal [123]. Furthermore, two nuclear export signals (NES) have been described within the C-terminal domain: pNES2 and pNES3. pNES2 is located within residues 1,187-1,198 and is considered the most potent amongst the two [125].

Regarding specific organelle localisation, RECQL4 was reported to localise to the nucleoli of HeLa cells. This localisation was further enriched after exposure to oxidative stress agents. The same study also identified a nucleolar localisation signal (NoLS) between residues 376 and 386 [126]. Within the cytoplasm, several studies have found RECQL4 colocalised with mitochondria [125, 127]. However, this finding has not been consistent across studies.

2.4.3 *Physiological functions of RECQL4*

2.4.3.1 *DNA Replication*

DNA replication is a complex process in eukaryotic cells. Due to its large genome, replication happens simultaneously in multiple genomic sites called replication origins [128]. The activation of these sites is the first step of a multistep process. It happens during G1 phase and requires the recruitment of several proteins to generate the pre-replicative complex (pre-RC) [129]. This complex includes the origin recognition complex (ORC), CDT1, and CDC6, which further recruits MCM2-7 [130]. As the cell transitions from G1 to S phase, it recruits two kinases; S-phase Cyclin-dependent kinase (CDK) and DBF4-dependent CDC7 kinase (DDK). The phosphorylation by these kinases triggers the binding of the initiation factor CDC45 in the presence of TOPBP1, MCM10, and the GINS complex forming a stable complex with MCM2-7 [131–133]. This complex works as a DNA unwinding machine and, with the assistance of other replication factors and DNA polymerases, leads to the assembly of the replisome, which finally starts DNA replication.

There is compelling evidence that RECQL4 is a core component of the mammalian DNA replication machinery. First, the Sld2-like region located in the first 54 aa of the N-terminal domain was shown to interact with TOPBP1 [134], an important protein for the formation of the replication complex. RECQL4 has also been shown to interact with other replication factors within this complex, including MCM10, MCM2-7, CDC45, and GINS [115, 135]. In HeLa cells, a recent study fused RECQL4 with ORC4, a component of the ORC, and found that the forced attachment of RECQL4 to the pre-RC resulted in increased recruitment of essential initiation factors and increased DNA synthesis during early S phase [136]. In line with these findings, nascent-DNA assays demonstrated that RECQL4-depleted T98G cells had lower amounts of newly synthesised DNA [114]; while in another study, replication timing was found to be significantly altered in RTS fibroblasts [137]. Lastly, the helicase activity of RECQL4 was stimulated by the addition of Replication protein A (RPA), which also colocalised in the nucleus of HeLa cells [138]. All these findings corroborate an essential role for RECQL4 in DNA replication. Furthermore, they align with the fact that full knockout

murine models of RECQL4 are not viable [139] and that mutations in RTS patients result in truncated, rather than null alleles [56].

2.4.3.2 *DNA Repair*

Cells are regularly exposed to internal or external stressors causing DNA damage. As a result, multiple DNA repair pathways are activated. The main four DNA repair pathways in the cell are: "Base excision repair (BER), nucleotide excision repair (NER), mismatch repair (MMR), and double-strand break (DSB) repair (DSBR)" [140]. A description of the role of RECQL4 in the different DNA repair pathways follows. It is necessary to mention, however, that in this section I have not included studies that assess the response of RTS-derived cells to DNA damaging agents given the variable results due to different cell types and techniques utilised.

BASE EXCISION REPAIR (BER) corrects damage caused by single-strand DNA (ssDNA) breaks (SSBs), ionising radiation (IR), alkylation, and oxidation. One of the proteins involved in this pathway is APE1. This enzyme cleaves apurinic/apyrimidinic (AP) sites, creating a SSB intermediate [141]. RECQL4 was reported to colocalise with APE1 after oxidative DNA damage caused by hydrogen peroxide [142]. Recently, a study revealed that RECQL4 interacts with OGG1 in the repair of 8-oxoguanine, another lesion caused by oxidative DNA damage [143]. Furthermore, RECQL4 has also been shown to interact with FEN1 [142] and Poly ADP Ribose Polymerase (PARP) 1 protein [126], which are important proteins in this pathway.

NUCLEOTIDE EXCISION REPAIR (NER) corrects helix-distorting bulky lesions, such as those caused by UV-induced pyrimidine dimers. It has been shown that RECQL4 directly interacts with a critical NER protein called xeroderma pigmentosum group A (XPA) and that this interaction was accelerated by UV exposure [144].

MISMATCH REPAIR (MMR) corrects small nucleotide repeats and single-base mismatches. Although BLM, WRN, and RECQL1 are associated with MMR proteins [145], no studies that I could assess have reported RECQL4 to be involved with any of the proteins associated with this pathway.

DOUBLE-STRAND BREAK REPAIR (DSBR) involves the repair of the most severe form of DNA damage using homologous recombination (HR) or non-homologous end-joining (NHEJ). RECQL4 was reported to be implicated in this pathway through its interaction with vital proteins. After the induction of DNA DSBs in human cells, RECQL4 was found to colocalise with RAD51 [122], a key component of HR. While a previous study showed that RECQL4 physically interacted with MRN (MRE11-RAD50-NBS1) [146], a more recent study showed that depletion of MRE11 or NBS1 did not affect the binding of RECQL4 to DSB sites. This study suggested that the binding of RECQL4 to these sites occurs without the participation of the MRN complex, and that the interaction of RECQL4 with this complex only takes place during the repair of the DSBs [147]. Regarding a potential function in NHEJ repair, the N-terminal domain of RECQL4 co-immunoprecipitated with the Ku70/80 heterodimer, an essential component of this pathway. Furthermore, the same study also described decreased NHEJ activity in RECQL4-depleted human cells [148].

The findings reported in this section and the observations that cells from RTS patients have chromosomal instabilities and increased sensitivity to DNA damaging agents [149–152], support the theory that RECQL4 can play a crucial role in DNA repair. However, more studies are required to elucidate the specific pathways and mechanisms in which RECQL4 is involved.

2.4.3.3 *Telomere maintenance*

One of the hallmark features of RTS is genomic instability. When the DNA repair machinery fails to correct DSBs or repairs them improperly, DSBs can lead to cell death or chromosomal translocations. These lead to genomic instability, and therefore, to an increased frequency of malignancies. Since the terminal ends of linear chromosomes simulate DSBs, an attempted repair of this region could result in aberrant chromosome fusions and must be prevented. Particular nucleotide sequences called telomeres protect these ends and their shortening or instability are associated with ageing and oxidative stress [153]. In RTS, studies using cells derived from patients have shown highly unstable telomeric ends [28]. Furthermore, following RECQL4 depletion, human cells have exhibited an accumulation of fragile sites, DSBs, and exchanges between sister chromosomes at telomeric sites [28].

Human RECQL4 was shown to localise to telomeres and to coimmunoprecipitate with TRF1 and TRF2 [28]. These, along with POT1, are specialised shelterin proteins that bind short tandem repeat DNA sequences in the telomeres, contributing to their stability [154]. It has been demonstrated that these proteins could stimulate the helicase activity of RECQL4 and that RECQL4 could interact with another helicase, WRN, to resolve telomeric D-loops [28]. This process has been considered essential for the progression of replication within telomeres [155]. Furthermore, it has been reported that RECQL4 preferentially unwinds telomeric D-loops containing thymine glycol [156], structures considered harmful to human cells [157]. While only limited studies from a small number of laboratories have investigated the role of RECQL4 in telomere maintenance, it is unclear whether RECQL4 mutations would directly disrupt these structures. This requires further investigation.

2.4.3.4 *Mitosis*

Several factors including continuous DNA damage, extended growth arrest, inhibition of CDKs, and disruption of mitotic spindles can affect mitosis [158]. Recent studies have highlighted a potential role for RECQL4 in mitosis. Using *Recql4*-deficient mouse embryonic fibroblasts, a significant increase in the frequency of premature centromere separation was observed [159]. These defects predispose cells to abnormal mitosis and chromosome mis-segregation with aneuploidy as a result.

In addition, other studies have suggested that RECQL4 can participate in mitotic spindle formation through two mechanisms. First, through the stabilisation of microtubules, which are considered essential for the assembly of the mitotic spindle. A recent study found that RECQL4 acts as a microtubule-associated protein (MAP) and that contributes to the stability of these structures during metaphase [160]. If the function of RECQL4 is affected, this critical step will not be adequately conducted, leading to defects in cell division and chromosome segregation [161], which can result in chromosome instability and aneuploidy, key features of cancer cells. The second mechanism is through its interaction with Aurora B Kinase (AURKB). It was reported that RECQL4, particularly its N-terminal region, interacts with this protein and that depletion of RECQL4 resulted in a measurable reduction of AURKB expression as a result of increased ubiquitination [162]. AURKB

is one of the proteins involved in the formation of the mitotic spindle and its role is crucial for error-free chromosome segregation [163]. Therefore, a reduction of AURKB expression will affect the formation of this structure, leading to the accumulation of mitotic defects that result in apoptosis. On the other hand, since RECQL4 overexpression has also been implicated in some types of cancer [118, 119], it would be tempting to speculate that it is through upregulation of AURKB, which could protect cancer cells from mitotic irregularities conferring them a survival advantage. However, more research is required to confirm this hypothesis.

2.4.4 *Protein interactions of RECQL4*

Thus far, I have described several proteins that can interact with RECQL4. To better understand this information, I have consolidated the current literature with a previously published table from Croteau *et al.* [164] into Table 2.2. This table summarises the protein interactions of human RECQL4, in addition to a description of the cell lines in which the experiments were done, the detection methods used, the domain of RECQL4 that interacts with, and the function of this interaction.

Table 2.2: *Proteins interacting with human RECQL4*

PROTEIN	CELL LINE	INTERACTION DOMAIN OF RECQL4	DETECTION METHODS	FUNCTION/PATHWAY	REFERENCE
APE1	HeLa	Unknown	CoLC	DNA repair (BER)	[142]
AURKB	293T	N-terminal	CoIP, MS	Mitotic spindle formation	[162]
BLM	HeLa	N-terminal (361-478 aa)	CoIP, Y2H	BLM helicase stimulation	[27]
FEN1	HeLa	Unknown	CoLC	DNA repair (BER)	[142]
Ku70/80	HeLa	N-terminal	CoIP	DNA repair (NHEJ)	[148]
MCM10	293T	N-terminal (1-200 aa)	CoIP	DNA replication	[115, 135]
MRN complex	293T	N-terminal	CoIP	DNA repair (HR)	[146]
OGG1	U2OS	N-terminal	CoIP	DNA repair (BER)	[143]
ORC4	HeLa	N-terminal	CoIP	DNA replication	[136]
P300	293T	N-terminal	CoIP	Regulation of RECQL4 subcellular trafficking	[124]
P53	NHF	N-terminal (270-400)	GST-PD, CoLC	Masking of NLS of RECQL4 and P53	[165]
PARP1	293T	C-terminal	PDS, CoIP	DNA repair (BER)	[126]
RAD51	HeLa	Unknown	CoIP, CoLC	DNA repair (HR)	[122]

TABLE 2.2 – CONTINUED FROM PREVIOUS PAGE

PROTEIN	CELL LINE	INTERACTION DOMAIN OF RECQL4	DETECTION METHODS	FUNCTION/PATHWAY	REFERENCE
RPA	HeLa	Unknown	CoLC	RECQL4 helicase stimulation	[138]
TOPBP1	293T	N-terminal (1-54 aa)	GST-PD, CoIP	DNA replication	[134]
TRF1	U2OS	Unknown	CoIP	Telomere maintenance, helicase stimulation	[28]
TRF2	U2OS	Unknown	CoIP	Telomere maintenance, helicase stimulation	[28]
UBR1/2	HeLa	Unknown	CoIP, CoFC, MS	Chromosome stability (N-end rule pathway)	[121]
WRN	U2OS	Unknown	CoIP	Resolution of telomeric D-loops	[155]
XPA	293T	Unknown	CoIP, GST-PD, CoLC.	DNA repair (NER)	[144]

Abbreviations used in this table: BER, Base excision repair; CoFC, Cofractionation; CoIP, Coimmunoprecipitation; CoLC, Colocalisation; GST-PD, GST pull-down assay; HR, Homologous recombination; MS, mass spectrometry; NHEJ, Non-homologous end joining; NLS, Nuclear localisation signal; Y2H, yeast two-hybrid assay. Table adapted from Croteau *et al.* [164]

The limited number of studies with little or no replication or independent validation addressing interacting proteins with RECQL4 has made the identification of pathways, in which RECQL4 is involved, challenging. As a consequence, the molecular landscape of Rothmund-Thomson syndrome remains incomplete. Future research should focus on the inclusion of novel technologies like functional genetic screens using CRISPR/Cas9, which could reveal pathways and indirect interactions and are not limited to physically interacting proteins.

2.4.5 *RECQL4 domains*

Up until now, I have described the diseases associated with defects in RECQL4 with special emphasis on my disease of interest, Rothmund-Thomson syndrome. I have also described the mutations associated with this disease, in addition to a description of the physiological roles of this protein. In this section, I will focus in detail on the three well-establish functional domains of RECQL4.

2.4.5.1 *Helicase domain*

The helicase domain is present in all RecQ helicases from bacteria to humans. This high degree of evolutionary conservation suggests an essential role in organisms, however, its function is still not fully understood. The first study that biochemically characterised human RECQL4 showed ATPase activity and ssDNA annealing but failed to detect DNA helicase activity [166]. A possible explanation was that the strong annealing activity caused re-association of the ssDNA products masking the unwinding activity of RECQL4. To avoid this problem, a following study added a third strand of ssDNA and reported for the first time ATP-dependent helicase activity [167]. Subsequently, a study found helicase activity without adding extra ssDNA. This study proposed that the failure of previous attempts to detect helicase activity was due to insufficient ATP and magnesium ions in the reaction [168]. These findings were further validated by another study that generated a point mutation (PM) within the helicase domain. This mutation (K508M) altered the conserved lysine residue within the Walker A motif, required for ATP hydrolysis, which led to an inability to hydrolyse ATP and a failure in DNA unwinding [138]. Although this study confirmed that the helicase domain is

responsible for DNA unwinding, it is still not clear whether this function is responsible for the phenotypes associated with *RECQL4* mutations.

In vitro experiments have indicated that the ATP-dependent helicase function of RECQL4 is not essential. A study in DT40 chicken cell lines showed that expression of an ATP-binding deficient RECQL4 (GFP-RECQL4 K508A) could restore the viability of RECQL4-depleted cells [169]. My laboratory also reported a similar finding using the same variant (K508A). They reported that the helicase-dead mutation could rescue RECQL4 deficiency in primary murine haematopoietic cells in culture [88]. Taken together, these findings indicate that the ATP-dependent helicase function of RECQL4 was not essential for cell viability, at least *in vitro*. However, the effects of its absence *in vivo* remain unknown.

2.4.5.2 *N-terminal domain*

The N-terminal domain of RECQL4 is unique amongst the RecQ helicases. It contains a sequence similar to the yeast replication initiation factor *Sld2*, making it the only protein in human and other mammals with this homology [170]. This sequence is found in the first 400 aa of RECQL4 and is most enriched in its first 54 [134]. In yeast, *Sld2* is essential for viability. It constitutes a substrate of CDKs, and once phosphorylated, it interacts with DPB11 and other proteins forming an essential complex for initiation of DNA replication [171, 172]. In humans, the SLD2 homology region of RECQL4 is putatively as important as in its yeast counterparts. Consistent with this notion is that most of the mutations reported in RTS patients affect the helicase or the C-terminal domain, leaving the N-terminal region intact [56]. Furthermore, expression of just the N-terminal domain was able to restore viability in RECQL4-depleted DT40 chicken cells [169], suggesting this may be a key functional domain of RECQL4. These findings underscore the uniqueness and importance of the N-terminal domain of RECQL4, once considered a largely uncharacterised region.

With more research, more functions have been ascribed to this domain. Firstly, this region was shown to have strong DNA annealing activity [173], a function also attributed to the helicase domain [167, 168, 174]. Additionally, this region was revealed to be the home of multiple DNA binding sites. A

study found three independent DNA-binding domains between residues 1-54, 55-170, and 251-388 aa. All of them bound to several DNA structures, including ssDNA, dsDNA, and Y-DNA [173]. The N-terminal region was also shown to be essential for DNA replication. It was reported that within the first 200 aa of RECQL4, there were domains that interacted with proteins involved in DNA replication such as MCM2-7, MCM10, GINS, and CDC45 [115]. This finding was further corroborated by a recent study that found that CDK phosphorylation within the N-terminal region was critical for activation of some of these replication factors [136]. In the context of DNA repair, as previously described, the N-terminal region interacts with several proteins involved in these pathways. Finally, the N-terminal domain contains the previously described nuclear targeting signals, essential for subcellular localisation, and a combined NLS/microtubule-binding region in *Xenopus*, required for chromosome alignment [160]. Collectively, the N-terminal region is one of the most critical regions for RECQL4 intracellular localisation and functioning, with roles in DNA replication, DNA repair and genomic stability.

2.4.5.3 *C-terminal domain*

The C-terminal region is mutated and deleted in the majority of RTS patients [56], who most commonly present with compound heterozygous mutations predicted to generate truncated products. However, despite its association with disease, the C-terminal domain remains the least studied region of RECQL4.

Recently, studies have identified novel domains within this region. Through bioinformatic analysis, a study found a putative RQC domain [175], which contained a winged-helix domain and a zinc-binding domain and was responsible for nucleic acid interaction [176]. This finding was quickly followed by an independent study, which identified an entirely new domain within this region, the R4ZBD domain, bearing only little resemblance to the RQC domain. This new domain features two winged-helix domains and a zinc-binding site and could be responsible for interaction with more complex DNA metabolism intermediate structures, as well as facilitate protein-to-protein interactions [23]. The same study found the CTD domain, located in the last 92 aa of the C-terminal region and with functions in dsDNA unwinding through translocation [23].

The extended C-terminal domain has other important functions. Using C-terminal sequences of RECQL4 in a T7 phage display system, PARP1 was identified as an interacting protein with this region [126]. This protein is an important DNA damage sensor that modulates cell sensitivity to γ-irradiation [164]. Additionally, the C-terminal region also contains two nuclear export signals, which I previously described. Considering this evidence, it seems that the C-terminal domain has roles in DNA repair and cellular localisation. However, this domain remains relatively unknown. Future research should focus on the discovery of interacting pathways that are affected when this region is deleted, as it happens in the majority of RTS patients.

2.5 MURINE MODELS OF RECQL4 MUTATION

To understand the relationships between *RECQL4* mutations and the phenotypes they cause, several murine models of *Recql4* mutation have been described (Table 2.3). The first reported model was developed by Ichikawa *et al.* and deleted exons 5-8 within the N-terminal region. This led to a short-truncated protein lacking half of the N-terminal region and the entire helicase and C-terminal region, which resulted in very early embryonic lethality between days 3 and 7 of gestation [139]. The lethality reported in this model is clear evidence that the N-terminal region of RECQL4 is essential for mammalian viability and development.

A second model replaced the last helicase coding exon with a neomycin cassette. Results showed that, when homozygous, 95% of animals died within two weeks of birth [177]. This seemed surprising in light of the viability of RTS patients. However, further analysis demonstrated that the targeted allele also gave rise to a significant number of shortened transcripts covering exon 1 to 12, which could encode truncated protein products potentially contributing to the high mortality seen in this study.

A third non-conditional model deleted exons 9-13, which includes the conserved helicase domain. Homozygous animals were viable, however, 16% of them died within 24 hours of birth [159]. The surviving mutant mice presented with hypo/hyper-pigmented skin on their tails, skeletal defects (polydactyly, limb hypoplasia, and palatal defects) and genomic instability. Furthermore, 5 out of 100 mice developed tumours (2 OS and 3 lymphomas).

The engineered mutation was predicted to result in a 480 aa truncated product with an absence of the helicase and C-terminal domain. The same model was described in another study, which reported sparse tail hair and haematopoietic defects consistent with increased senescence [178].

Based on the high embryonic lethality seen in the previous murine models, my host laboratory generated the first conditional knockout model of *Recql4* by inserting loxP sites to flank either exons 9 and 10. This resulted in a frameshift mutation and a null allele. The germline deletion of exons 9 and 10 demonstrated that RECQL4 was essential for embryonic development [88], consistent with earlier reports from Ichikawa *et al.* [139]. They additionally showed that RECQL4 was essential for haematopoiesis given that acute somatic loss of *Recql4* in adult mice using *Rosa26*-CreER^{T2} and tamoxifen treatment caused death as a result of a fully penetrant bone marrow failure. This involved defects across the lymphoid, myeloid, and erythroid lineages. When *Recql4* was deleted specifically in haematopoietic stem cells (HSCs) using *hScl*-CreER^{T}, there was a loss of all fully deleted cells and the mice recovered with a stable population of *Recql4* heterozygous cells. This demonstrated that *Recql4* was required to sustain haematopoiesis from HSCs onwards. In contrast, when erythroid lineage-specific deletion using *Epor*-Cre was assessed, there was no phenotype. This was thought to reflect the late-stage deletion and subsequent enucleation that occurs in erythroid cells, relieving the requirement for both DNA replication and further cell division. Furthermore, by retroviral complementation of RECQL4-null cells, they found that the ATP-dependent helicase activity of RECQL4 was not essential for its role in haematopoiesis *in vitro* [88]. It is important to consider that although the results of this study advanced the knowledge in the field, these mouse models did not accurately reflect the genetic status of RTS patients, who rather than having null alleles, carry compound heterozygous bi-allelic mutations [56]. Furthermore, RTS patients present with chronically reduced levels of RECQL4, rather than acute. Therefore, it is crucial to assess the role of haematopoiesis in compound heterozygous germline models, which may model the disease more accurately.

In a separate study, my host laboratory also evaluated the requirement of RECQL4 in normal osteoblast function. This was achieved by generating a mouse model that genetically lacked *Recql4* within the multiple populations of the osteoblast lineage. They used the Osterix promoter-driven Cre recom-

binase (*Osx1*-Cre *Recql4*$^{fl/fl}$) to target the early osteoblast progenitors [179], and the *Dmp1*-Cre to target mature osteoblasts [180]. *Osx*-Cre *Recql4*$^{fl/fl}$ mice had shortened bones with decreased trabecular bone and defects in osteoblast proliferation and maturation [181]. Strikingly, when *Recql4* was deleted in mature osteoblasts (*Dmp1*-Cre) the skeletal phenotype did not occur, identifying a function for RECQL4 in the proliferative immature osteoblast populations only [181]. These findings were confirmed by another group that used a similar model utilising *Prx1*-Cre to induce deletion of *Recql4* in multipotent skeletal progenitor cells of the limb buds [182, 183]. In addition to the limb abnormalities and craniosynostosis seen in these mice, this study reported a similar phenotype to the osteoblast restricted deletion with a decrease in bone mass in the knockout mice [183]. Furthermore, this study used *Col2α1*-Cre to delete *Recql4* in chondrocytes. The majority of mice died after birth showing severe defects in the rib cage and vertebrae [183]. Together, these findings demonstrated a crucial role of RECQL4 within osteoblast and skeletal development. However, as they utilised full null alleles, they lack the context of RTS, where patients generally present with compound heterozygous truncating mutations. Therefore, the unresolved question that remains is what the effects of common RECQL4 mutations in bone development are.

Table 2.3: *Murine models of Rothmund-Thomson Syndrome*

MODEL	CELL LINEAGE	LETHALITY	PHENOTYPES	MALIGNANCIES	REFERENCES
Recql4$^{-/-}$ Exons 5-8 deletion (5-6 in humans)	Germline	High embryonic lethality	–	–	[139]
Recql4$^{-/-}$ Exon 13 deletion (13 in humans)	Germline	High embryonic lethality	Skin, skeletal, and immunological abnormalities	No	[177]
Recql4$^{-/-}$ Exons 9-13 deletion (10-13 in humans)	Germline	Low embryonic lethality	Sparse tail hair, skeletal abnormalities, genomic instability, and haematological defects	5/100 mice (2 OS, 3 lymphoma)	[159, 178]
Recql4$^{-/-}$ Exons 9-10 deletion (10 in humans)	Germline	Embryonic lethal	–	–	[88]
R26-CreER^{T2} *Recql4*$^{fl/fl}$ Exons 9-10 deletion (10 in humans)	Conditional knockout	Mice were viable and fertile	Somatic deletion of *Recql4* caused rapid bone marrow failure	No	[88]

TABLE 2.3 – CONTINUED FROM PREVIOUS PAGE

MODEL	CELL LINEAGE	LETHALITY	PHENOTYPES	MALIGNANCIES	REFERENCES
Epor-Cre *R26*-eYFP$^{ki/ki}$ *Recql4*$^{fl/fl}$	Erythroid progenitors-restricted deletion	Mice were viable and fertile	No	No	[88]
hScl-CreER^{T} *R26*-eYFP $^{ki/ki}$ *Recql4*$^{fl/fl}$	HSCs and primitive progenitors-restricted deletion	Mice were viable and fertile	No	No	[88]
Osx-Cre *R26*-eYFP$^{ki/ki}$ *Recql4*$^{fl/fl}$ Exons 9-10 deletion (10 in humans)	Early osteoblast-restricted deletion	Mice were viable and fertile	Reduced skeletal growth, reduced bone volume, and defects in osteoblast proliferation and maturation	No	[181]
Dmp1-Cre *R26*-eYFP$^{ki/ki}$ *Recql4*$^{fl/fl}$ Exons 9-10 deletion (10 in humans)	Mature and osteoblasts-restricted deletion	Mice were viable and fertile	No	No	[181]

TABLE 2.3 – CONTINUED FROM PREVIOUS PAGE

MODEL	CELL LINEAGE	LETHALITY	PHENOTYPES	MALIGNANCIES	REFERENCES
Col2α1-Cre+ *Recql4*$^{fl/fl}$ Exons 5-8 deletion (5-6 in humans)	Chondrocytes-restricted deletion	Perinatal lethality	Severe rib cage and vertebral defects	–	[183]
Prx1-Cre+ *Recql4*$^{fl/fl}$ Exons 5-8 deletion (5-6 in humans)	Skeletal progenitors-restricted deletion	Mice were viable and fertile	Limb abnormalities, craniosynostosis, reduced bone volume.	No	[183]

* The human equivalent sequences have been added in brackets under each mouse model name.

Although these murine models have helped to understand some of the functions of RECQL4, they do not accurately reflect the genetic basis of RTS. Therefore, it is essential to model the mutation spectrum seen in these patients. The study of these mutations will not only reveal information about the requirements of the individual domains of RECQL4 but will also contribute to the understanding and prediction of the impact that these mutations may have in RTS patients.

CHAPTER 3

3

AIMS AND HYPOTHESES

3.1 PREAMBLE

Although important discoveries have been made regarding the clinical features and genetics of RTS, there are still gaps in the existing knowledge that make our understanding of this disease incomplete.

Firstly, data regarding the functions of individual domains of RECQL4 is limited. A current theory in the field is that the majority of RTS phenotypes are caused by defects in the helicase domain. This theory stems from an evolutionary point of view, given that the helicase domain is conserved across species, and also from the observation that the majority of mutations seen in patients are localised in this domain. However, this theory does not consider potential functions of the C-terminal domain, which is also affected by truncating mutations present in the majority of RTS patients. Therefore, it is important to assess the effects of mutations that affect different domains to improve our understanding of their functions.

Secondly, although several murine models have been useful to understand some of the functions of RECQL4, they do not accurately reflect the mutation spectrum seen in RTS patients, which are most often affected by truncating/hypomorphic mutations rather than null alleles. Modelling these patient-centred mutations is therefore critical, in order to understand their impact on protein stability, and on processes such as bone homeostasis, haematopoiesis and tumorigenesis.

Finally, the literature regarding the molecular and genetic interactions of RECQL4 is sparse. Since the majority of the protein interactions have been

identified by immunoprecipitation studies, only a selected few have been looked at in detail in terms of their functional interactions. Furthermore, nothing is known about other genes that either positively or negatively contribute to the phenotypes of RTS. Thereby, it is important to identify additional interactors of RECQL4, in order to identify potential therapeutic targets.

All these gaps in knowledge have led to the overall aim of this thesis, which is to improve understanding of the individual domains and functions of RECQL4; and the impact that different *Recql4* mutations have in normal homeostasis, tumour development, and genetic interactions. The specific hypotheses and aims for the three components of this thesis will be covered in the following section.

3.2 STUDY HYPOTHESES

3.2.1 Understanding the physiological requirements of the helicase domain of RECQL4.

- A mutation that abolishes the ATP-dependent helicase activity will not affect the physiological functions of RECQL4.

3.2.2 Determining the impact of RECQL4 truncating mutations in normal homeostasis and tumour development.

- Truncating mutations of RECQL4 will have deleterious effects on protein stability, cellular localisation, and bone homeostasis.
- Tumour development will be initiated by RECQL4 truncating mutations and accelerated by ionising radiation.

3.2.3 Identification of novel genetic interactions with RECQL4 in a genome-wide CRISPR/Cas9 rescue screen.

- A genome-wide rescue screen will identify additional genes that interact with *Recql4* to create the phenotypes of RTS.

3.3 AIMS OF THE THESIS

3.3.1 Understanding the physiological requirements of the helicase domain of RECQL4.

3.3.1.1 Primary Aim

1. To assess the physiological requirements of the ATP-dependent helicase function of RECQL4 in a mouse model containing a knock-in point mutation that abolishes its ATP-dependent helicase activity.

3.3.1.2 Secondary Aims

1. To biochemically characterise the ATPase deficient mutation in murine *Recql4*.
2. To determine the role of the ATP-dependent helicase activity of RECQL4 in haematopoiesis and T and B cell development *in vivo*.
3. To examine the requirement of the ATP-dependent helicase activity in response to DNA damaging agents *in vitro*.
4. To compare the effects of a helicase-inactive *Recql4* mutation to truncating/hypomorphic mutations *in vivo*.

3.3.2 Determining the impact of RECQL4 truncating mutations in normal homeostasis and tumour development.

3.3.2.1 Primary Aim

1. To determine the impact of the deletion of the C-terminal and helicase domains in normal homeostasis and tumour development by using mice carrying *Recql4* truncating mutations that resemble those seen in humans.

3.3.2.2 Secondary Aims

1. To assess if truncated RECQL4 proteins have altered cellular localisation and protein stability.
2. To examine the bone mass of truncating mutations in germline and osteoblast-restricted *RECQL4* murine models.
3. To determine whether ionising radiation initiates tumour development in compound heterozygous mutant mice.
4. To assess the impact of different human RECQL4 mutations using *in vitro* complementation assays.

3.3.3 Identification of novel genetic interactions with RECQL4 using a genome-wide loss-of-function rescue screen.

3.3.3.1 Primary Aim

1. To identify novel genetic interactions with *Recql4* that contribute to the improvement of the phenotypes associated with pathogenic *Recql4* mutations using a genome-wide loss-of-function genetic rescue screen.

3.3.3.2 Secondary Aims

1. To generate cell lines with a conditionally expressed truncating RECQL4 mutation that can be used in a genome-wide CRISPR/Cas9 mediated loss-of-function rescue screen.
2. To identify genes that, when deleted, rescue the phenotypes associated with a truncating RECQL4 mutation.
3. To validate the results of the rescue screen.

CHAPTER 4

4

MATERIALS AND METHODS

4.1 MATERIALS

All reagents and materials, solutions, and equipment used throughout this study are listed in Table 4.1, Table 4.2, and Table 4.3, respectively. Solutions were prepared using Elix or Milli-Q^{TM} ultra-pure water (Thermo Fisher Scientific; Waltham, MA, USA). Unless stated otherwise, experiments were performed at room temperature.

Table 4.1: *Reagents and materials, and their suppliers used in this study.* Abbreviations given in brackets.

REAGENT	SUPPLIER
4-Hydroxy tamoxifen	Merck Millipore (Billerica, MA, USA)
Agarose tablets	Bioline (London, UK)
Alpha Minimum Essential Medium (α-MEM)	Sigma-Aldrich (St Louis, MO, USA)
AMPure XP magnetic beads	Beckman Coulter (Brea, CA, USA)
Anti-Flag M2–Affinity Gel	Sigma-Aldrich (St Louis, MO, USA)
Antimycin A	Sigma-Aldrich (St Louis, MO, USA)
ATPlite Luminescence Assay System	Perkin Elmer (Waltham, MA, USA)
B Cell Isolation Kit, mouse	Miltenyi Biotec (Bergisch Gladbach, Germany)
BD microtainer K2E tubes	BD Biosciences (San Jose, CA, USA)
BD vacutainer capillary tubes	BD Biosciences (San Jose, CA, USA)

TABLE 4.1 – CONTINUED FROM PREVIOUS PAGE

REAGENT	SUPPLIER
Benzonase® nuclease	Sigma-Aldrich (St Louis, MO, USA)
Blasticidin	Sigma-Aldrich (St Louis, MO, USA)
Bovine serum albumin (BSA)	Sigma-Aldrich (St Louis, MO, USA)
Calcium chloride	Sigma-Aldrich (St Louis, MO, USA)
Carbonyl cyanide 4-(trifluoromethoxy) phenylhydrazone (FCCP)	Sigma-Aldrich (St Louis, MO, USA)
Cell counter chamber slide (Countess)	Thermo Fisher Scientific (Waltham, MA, USA)
Cell strainer (40 μm)	Corning (Tewksbury, MA, USA)
CellTrace^{TM} Violet Cell Proliferation Kit	Thermo Fisher Scientific (Waltham, MA, USA)
Cryotube vials	Thermo Fisher Scientific (Waltham, MA, USA)
CutSmart buffer	New England Biolabs (Ipswich, MA, USA)
Cyquant cell proliferation assay	Thermo Fisher Scientific (Waltham, MA, USA)
Dimethyl sulfoxide (DMSO)	Sigma-Aldrich (St Louis, MO, USA)
Disposable Pipettes (5, 10, 25 mL)	Corning (Tewksbury, MA, USA)
Disposable scalpel	Swann Morton (Sheffield, England)
Dithiothreitol (DTT)	Sigma-Aldrich (St Louis, MO, USA)
Dulbecco's Modified Eagle Medium (DMEM)	Sigma-Aldrich (St Louis, MO, USA)
DNA molecular weight marker 50 bp (HyperLadder)	Bioline (London, UK)
Dneasy Blood & Tissue Kit	Qiagen (Hilden, Germany)
Doxorubicin	St Vincent's Hospital Pharmacy (Melbourne, VIC, Australia)

TABLE 4.1 – CONTINUED FROM PREVIOUS PAGE

REAGENT	SUPPLIER
Dulbecco's Phosphate Buffered Saline (PBS)	Sigma-Aldrich (St Louis, MO, USA)
ECL Western blotting detection reagent	GE Healthcare (Buckinghamshire, UK)
Eppendorf tubes	Corning (Tewksbury, MA, USA)
Ethanol (EtOH)	Thermo Fisher Scientific Australia Pty Ltd (Scoresby, VIC, Australia)
Ethylenediaminetetra acetic acid (EDTA)	Astral Scientific (Taren Point, NSW, Australia)
Falcon centrifuge tubes (5, 10, 50 mL)	Thermo Fisher Scientific (Waltham, MA, USA)
Ficoll-paque premium	GE Healthcare (Buckinghamshire, UK)
Flat 8 Cap Strips	Thermo Fisher Scientific (Waltham, MA, USA)
Foetal bovine serum (FBS)	Assay Matrix (Melbourne, VIC, Australia)
Gel Loading Dye	New England Biolabs (Ipswich, MA, USA)
Gentra Puregene Cell Kit	Qiagen (Hilden, Germany)
Glycerol	Merck (Darmstadt, Germany)
HRP-conjugated goat anti-mouse	Thermo Fisher Scientific (Waltham, MA, USA)
HRP-conjugated goat anti-rat	Thermo Fisher Scientific (Waltham, MA, USA)
Hydroxyurea	Selleck chemicals (Houston, TX, USA)
Immobilon-P Polyvinylidene Difluoride (PVDF) membrane	Merck Millipore (Billerica, MA, USA)
Iscove's Modified Dulbecco's Medium (IMDM)	Sigma-Aldrich (St Louis, MO, USA)
Isolate II PCR and Gel kit	Bioline (London, UK)
Isolate II Plasmid Mini kit	Bioline (London, UK)

TABLE 4.1 – CONTINUED FROM PREVIOUS PAGE

REAGENT	SUPPLIER
Isopropanol	Merck Pty Ltd (NSW, Australia)
KASP MasterMix	Biosearch Technologies (Novato, California, United States)
L-Alanyl-L-Glutamine	Sigma-Aldrich (St Louis, MO, USA)
LPS-EB Ultrapure	Invivogen (San Diego, CA, USA)
Magnesium chloride ($MgCl_2$)	Sigma-Aldrich (St Louis, MO, USA)
Methanol (MeOH)	Thermo Fisher Scientific Australia Pty Ltd (Scoresby, VIC, Australia)
Microscope slides and coverslips	Thermo Fisher Scientific Australia Pty Ltd (Scoresby, VIC, Australia)
Mitochondrial staining reagent (Blue-Cytopainter, ab219940)	Abcam (Cambridge, UK)
Mouse Anti-actin antibody	Sigma-Aldrich (St Louis, MO, USA)
Mr Frosty^{TM} Freezing Container	Thermo Fisher Scientific (Waltham, MA, USA)
MyTaq HS DNA polymerase	Bioline (London, UK)
MyTaq Red Reaction Buffer	Bioline (London, UK)
Nitroquinoline	Sigma-Aldrich (St Louis, MO, USA)
Nunc^{TM} EasYFlask^{TM} Cell Culture T75 Flasks	Thermo Fisher Scientific (Waltham, MA, USA)
NuPAGE LDS Sample Buffer (4x)	Life Technologies (Carlsbad, CA, USA)
NuPAGE Sample Reducing Agent (10x)	Life Technologies (Carlsbad, CA, USA)
NuPAGE BOLT Transfer Buffer 20X	Life Technologies (Carlsbad, CA, USA)
NuPAGE MOPS SDS running buffer (20X)	Life Technologies (Carlsbad, CA, USA)
NuPAGE BOLT 8% bis-tris gel	Life Technologies (Carlsbad, CA, USA)
Oligomycin	Sigma-Aldrich (St Louis, MO, USA)

TABLE 4.1 – CONTINUED FROM PREVIOUS PAGE

REAGENT	SUPPLIER
Oligonucleotides PCR Primers	Integrated DNA Technologies (IDT; Coralville, Iowa, USA)
Paraffin	Bemis (Neenah, WI, USA)
Paraformaldehyde (PFA) aqueous solution (16%)	Proscitech (QLD, Australia)
Paraformaldehyde (PFA) powder (95%)	Sigma-Aldrich (St Louis, MO, USA)
PCR 8-strip Tubes with flat-caps	SSIbio (Lodi, CA, USA)
Penicillin/Streptomycin	Sigma-Aldrich (St Louis, MO, USA)
Phos-Stop tablets	Roche Applied Sciences (Mannheim, Germany)
PiColorLock^{TM} phosphate detection reagent	Expedeon (Cambridge, UK)
Pierce BCA protein assay reagent	Thermo Fisher Scientific (Waltham, MA, USA)
Polybrene (Hexadimethrine bromide)	Sigma-Aldrich (St Louis, MO, USA)
Potassium chloride (KCl)	Sigma-Aldrich (St Louis, MO, USA)
Protease Inhibitor cocktail tablets	Roche Applied Sciences (Mannheim, Germany)
Puromycin Dihydrochloride	Merck (Darmstadt, Germany)
QIAprep Miniprep kit	Qiagen (Hilden, Germany)
qPCR Master Mix	Agilent Technologies (Santa Clara, CA, USA)
Rat monoclonal anti-mouse	WEHI Antibody Services (Melbourne, VIC, USA)
RECQL4 antibody	
Recombinant human IL-6	Amgen (Thousand Oaks, CA, USA)
Recombinant murine IL-3	Peprotech (Rocky Hill, NJ, USA)
Recombinant murine IL-4	Peprotech (Rocky Hill, NJ, USA)

TABLE 4.1 – CONTINUED FROM PREVIOUS PAGE

REAGENT	SUPPLIER
Recombinant murine stem cell factor (mSCF)	Peprotech (Rocky Hill, NJ, USA)
Restriction enzymes (various)	New England Biolabs (NEB, Ipswich, Massachusetts, USA)
Retronectin	Takara Bio (Kusatsu, Shiga, Japan)
RNase A solution	Qiagen (Hilden, Germany)
Rotenone	Sigma-Aldrich (St Louis, MO, USA)
RPMI medium	Sigma-Aldrich (St Louis, MO, USA)
Seahorse XF medium	Seahorse Bioscience (Billerica, MA, USA)
SeeBlue Plus2 Pre-stained Protein Standard	Life Technologies (Carlsbad, CA, USA)
Skim milk powder	Devondale (VIC, Australia)
Sodium chloride (NaCl)	Sigma-Aldrich (St Louis, MO, USA)
Sodium hydroxide (NaOH) tablets	Merck (Darmstadt, Germany)
Sodium pyruvate	Sigma-Aldrich (St Louis, MO, USA)
SuperSignal chemiluminescent substrate	GE Healthcare (Buckinghamshire, UK)
SYBR Safe^{TM} DNA gel stain	Thermo Fisher Scientific (Waltham, MA, USA)
TE Buffer	Invitrogen (Carlsbad, CA, USA)
Tetraethylammonium (TEA)	Sigma-Aldrich (St Louis, MO, USA)
Tissue culture 10 cm dishes	Corning (Tewksbury, MA, USA)
Tissue culture flask (T25, T75, T175)	Corning (Tewksbury, MA, USA)
Tissue culture plates (6, 12, 24, 48, 96 wells)	Corning (Tewksbury, MA, USA)
Topotecan	Sigma-Aldrich (St Louis, MO, USA)
Tris-hydrochloride (Tris HCl)	Astral Scientific (Taren Point, NSW, Australia)

TABLE 4.1 – CONTINUED FROM PREVIOUS PAGE

REAGENT	SUPPLIER
Trypan blue solution (0.4%)	NanoEnTek (Seoul, South Korea)
Trypsin (0.025% in PBS-EDTA)	St Vincent's Institute (prepared by Dr Jacki Heraud-Farlow)
Tween-20	Sigma-Aldrich (St Louis, MO, USA)
UltraPure DNAse/RNAse-free water	Life Technologies (Carlsbad, CA, USA)
Whatman filter papers	GE Healthcare (Buckinghamshire, UK)
X-ray film	Fujifilm (Minato, Japan)
β-mercaptoethanol	Sigma-Aldrich (St Louis, MO, USA)

Table 4.2: *Solutions used in this study.* Abbreviation in brackets.

SOLUTIONS	COMPOSITION
Agarose gel 3%	3 g agarose tablets in 100 mL TBE 1x
Cell Culture Medium Supplements	10% (v/v) FSB, 1% (v/v) Penicillin-Streptomycin, 1% (v/v) Glutamine, 1% (v/v) GM-CSF; GM-CSF conditioned media collected from BHK-HM5 cells (Gift from Prof Steve Collins; Fred Hutchinson Cancer Research Centre)
FACS buffer	2% FBS (v/v) in PBS
Fixing solution (for tissues)	2% in PBS from 16x PFA in distilled water (v/v) or PFA powder (v/w)
Cell freezing medium	90% (v/v) FBS, 10% (v/v) DMSO
Hank's Buffer with HEPES (HHBS)	Hank's Balanced Salt solution, 20 mM HEPES buffer
HEPES buffered saline (HBS)	HBS, pH 7.05; 140 mM NaCl, 1.5 mM Na_2HPO_4, $2H_2O$, 50 mM HEPES
Complete αMEM	Minimum essential eagle medium-α medium (αMEM), 10% (v/v) FBS, 1% (v/v) Penicillin-Streptomycin, 1% (v/v) Glutamine

TABLE 4.2 – CONTINUED FROM PREVIOUS PAGE

SOLUTIONS	COMPOSITION
Red blood cell (RBC) lysis buffer	150 mM NH_4Cl, 10 mM $KHCO_3$, 0.1 mM Na_2 EDTA, pH 7.3
RIPA buffer	20 mM Tris-Cl, 150 mM NaCl, 1 mM EDTA, 1 mM EGTA, 1% (v/v) Triton-X, 1% (w/v) Sodium deoxycholate
Seahorse medium	Non-buffered DMEM base media (Seahorse XF medium) containing 25 mM glucose, 1 mM sodium pyruvate, glutamine, pH 7.4
SOC medium	2% tryptone, 0.5% yeast extract, 10 mM NaCl, 2.5 mM KCl, 10 mM $MgCl_2$, 10 mM $MgSO4$, 20 mM glucose
TNG Buffer	20 mM TEA pH 7.5, 150 mM NaCl, 10% glycerol, 1 mM DTT
Tris buffered saline (TBS) 10x	15 g Tris, 40 g Sodium chloride, 1 g Potassium chloride, pH 7.5
Tris-buffered saline with tween 20 (TBST) buffer	0.1% (v/v) Tween-20 in 1x TBS
Western blocking solution	5% (w/v) Skim milk in TBST

Table 4.3: *List of equipment and their manufacturers used in this study*

EQUIPMENT	MANUFACTURER
Automatic Pipette S1 (with filter)	Thermo Fisher Scientific (Waltham, MA, USA)
BD LSR II Fortessa	BD Biosciences (San Jose, CA, USA)
CO_2 Incubator HeraCell 240i	Thermo Fisher Scientific (Waltham, MA, USA)
Countess II cell counter	Thermo Fisher Scientific (Waltham, MA, USA)
Enspire plate reader	PerkinElmer (Melbourne, VIC, Australia)

TABLE 4.3 – CONTINUED FROM PREVIOUS PAGE

EQUIPMENT	MANUFACTURER
EPSON Perfection V700 photo scanner	EPSON (Suwa, Nagano, Japan)
Freezer (-80°C)	Thermo Fisher Scientific (Waltham, MA, USA)
Gelaire Class II Biological Safety Cabinet	Gelaire Pty Ltd (Sydney, NSW, Australia)
Heraeus Multifuge 3SR+ Centrifuge	Thermo Fisher Scientific (Waltham, MA, USA)
Heraeus Pico 17 Centrifuge	Thermo Fisher Scientific (Waltham, MA, USA)
Mastercycler Pro PCR machine	Eppendorf (Hamburg, Germany)
Medium Orbital Shaker	Ratek (Boronia, VIC, Australia)
Milli-Q^{TM} ultra-pure water	Thermo Fisher Scientific (Waltham, MA, USA)
Olympus CKX31 inverted microscope	Olympus Corporation (Tokyo, Japan)
Olympus IX81 fluorescent microscope	Olympus Corporation (Tokyo, Japan)
PowerEase 90 W	Life Technologies (Carlsbad, CA, USA)
Powerpac Electrophoresis System	Bio-Rad Laboratories (Hercules, CA, USA)
Retiga-EXi 12 Bit CCD camera	QImaging (Tucson, AZ, USA)
Rotary Tube Mixer with Disc	Ratek (Boronia, VIC, Australia)
Seahorse XF24-3 Flux Analyser	Seahorse Bioscience (Billerica, MA, USA)
Skyscan 1076 system	Bruker MicroCT (Kontich, Belgium)
Spectrophotometer ND – 1000 (Nanodrop)	Thermo Fisher Scientific (Waltham, MA, USA)
Stratagene Mx3000P qPCR machine	Agilent Technologies (Santa Clara, Ca, USA)

TABLE 4.3 – CONTINUED FROM PREVIOUS PAGE

EQUIPMENT	MANUFACTURER
Sysmex KX21 Haematology Analyser	Sysmex Corporation (Kobe, Hyogo, Japan)
T3000 Thermocycler	Biometra (Göttingen, Germany)
Ultra Basic pH Meter	Denver Instrument (Bohemia, NY, USA)
VersaDoc Imaging System	Bio-Rad Laboratories (Hercules, CA, USA)
Vortemp 56 Shaking Incubator	Labnet International Inc. (Edison, NJ, USA)
Vortex Mixer SA8	Stuart Equipment (Staffordshire, UK)
Water bath WB7	Ratek (Boronia, VIC, Australia)

4.2 EXPERIMENTAL MICE

4.2.1 *Ethics statement*

All animal experiments were performed according to the National Health and Medical Research Council Act 1992 and the Australian Code for the Care and Use of Animals for Scientific Purposes (2013). The procedures were approved by the Animal Ethics Committee, St Vincent's Hospital, Melbourne, Australia (#034/13, 007/14, 011/15, and 015/17).

4.2.2 *Mouse housing*

All animals were housed at the Bioresources Centre (BRC) located at St Vincent's Hospital. Mice were maintained and bred in microisolators under specific pathogen-free conditions with autoclaved food and acidified water provided *ad libitum*.

4.2.3 *Mouse strains*

The *Osx*-Cre, *Rosa26*-eYFP, and *Recql4*$^{fl/fl}$ mice (C57BL/6-*Recql4*^{tm2272Arte}) have been previously described [88, 179, 181]. *Rosa26*-CreER^{T2} mice were

originally purchased from The Jackson Laboratory (B6.129-Gt(ROSA)26 Sor$^{tm1(cre/ERT2)Tyj}$/J, Stock Number: 008463) and have also been previously described [88]. Mice carrying the *Recql4* p.Lys525Ala (K525A) and p.Gly522 GlufsTer43 (G522Efs) mutations were generated using CRISPR/Cas9 methods by the Mouse Engineering at Garvan/ABR (MEGA) services (Garvan Institute, Darlinghurst, Australia). Lysine 525 was mutated to Alanine (AAG>GCA) in single-cell embryos via sgRNA-directed gene targeting and homologous recombination with a single-stranded DNA oligonucleotide substrate. Viable pups were screened by DNA sequencing and one C57BL/6 male carrying the K525A mutation on one allele and a 2 bp insertion (GA) after the T521 codon (G522Efs) on the other allele was identified as a founder. The chemically *N*-ethyl-*N*-nitrosourea (ENU) induced *Recql4* p.Met789Lys (M789K) and p.Arg347* (R347X) mutations were obtained from the Australian Phenomics Facility (APF, Canberra, Australia: IGL01381 and IGL01809). All mutant lines were backcrossed into the C57BL/6 background. ENU mutants were outcrossed at least six times and assessed across multiple generations to eliminate the effects of any additional mutations. Tamoxifen containing diet was prepared at 400 mg/kg tamoxifen citrate in standard mouse chow (Specialty Feeds, Western Australia) and then irradiated. When used, tamoxifen containing chow was fed *ad libitum* for the duration of treatment.

4.2.4 *DNA isolation*

For colony genotyping, genomic DNA (gDNA) was isolated from toe clips. Tissues were collected in 1.5 mL microcentrifuge tubes, spun for 5 seconds, and digested in 300 μL 50 mM NaOH for 25 minutes at 95°C and 120 revolutions per minute (rpm) using a Vortemp 56 Shaking incubator. Next, 100 μL of 1 M Tris-HCl (pH 8.0) was added, and tubes were vortexed for 5 seconds. This was followed by spinning at 13000 rpm for 5 minutes using a Heraeus Multifuge 3SR+ Centrifuge. Soluble gDNA was then used for genotyping. For experimental adult mice, gDNA was extracted from ear tissue using the DNeasy Blood & Tissue Kit following the manufacturer's instructions.

4.2.5 *Genotyping*

Genotyping of all mouse strains was performed by PCR using oligonucleotides ordered from IDT. For the K525A and G522Efs alleles, the same

primer pair was used as the mutations are located close to each other in the same region. gDNA for all reactions (except *Osx*-Cre) was used after a 1:5 dilution in nuclease-free water. Reactions were set up in PCR tubes as follows: 2 μL MyTaq red reaction buffer (5x), 1 μL pooled oligonucleotides (10 μM), 0.1 μL MyTaq HS DNA polymerase, 5.9 μL nuclease-free water and 1 μL of (diluted) gDNA. All genotyping reactions (except R347X) were performed using the same PCR conditions (Table 4.4) on a Mastercycler Pro PCR machine. PCR products from K525A, G522Efs, and M789K strains were further digested for restriction fragment length polymorphism (RFLP) analysis by adding a mix containing 2 μL CutSmart buffer, 0.25 μL *Msl*I (NEB) restriction enzyme, and 7.75 μL of nuclease-free water to the 10 μL PCR reaction, followed by incubation at 37°C for one hour. Details of the digested PCR products for the wild type (WT) and the PM alleles are described in Table 4.5. PCR products, including after digestion, and a standard DNA 50 bp Hyperladder, were loaded into 3% agarose gels containing SYBR DNA gel stain (1:20,000) and run by electrophoresis using a Powerpac Electrophoresis system at 120 V for 50 minutes. Subsequently, the gel was visualised using a VersaDoc imaging system. For the R347X mutation, genotyping was determined by KASP (competitive allele-specific PCR) technology (LGC). In 96-well PCR plates, 2 μL of gDNA was added to a mix containing 5 μL KASP master mix, 0.14 μL of oligonucleotide primer (Table 4.5), and 2.86 μL of nuclease-free water. The plate containing the mix was centrifuged using an Allegra X-12 Centrifuge at 1300 rpm for 3 minutes and cycled on the Stratagene Mx3000P qPCR machine following the KASP cycling protocol described in Table 4.6.

Table 4.4: *Genotyping PCR cycling conditions*

TEMPERATURE	DURATION	CYCLE NUMBER
95°C	5 minutes	x1
95°C	20 seconds	x35
60°C	30 seconds	
72°C	45 seconds	
72°C	3 minutes	x1
20°C	Hold	-

Table 4.5: *Genotyping oligonucleotide list*

GENOTYPING ALLELE	OLIGONUCLEOTIDE SEQUENCE (5′-3′)	DETECTED ALLELE	PRODUCT SIZE (BP)
Osx-Cre	GCCAGGCAGGTGCCTGGACAT CTCTTCATGAGGAGGACCCT	Transgenic	450
Rosa26-eYFP	AAAGTCGCTCTGAGTTGTTAT	WT	500
	GCGAAGAGTTTGTCCTCAACC	KI	250
	GGAGCGGGAGAAATGGATATG		
Rosa26-CreER^{T2}	CCTGATCCTGGCAATTTCG	KI	825
	GGAGCGGGAGAAATGGATATG	WT	650
	AAAGTCGCTCTGAGTTGTTAT		
Recql4$^{fl/fl}$	CACTCTAGAAGAGGGAGTCAGATGG	Floxed	325
	CGCGCGAAAGCTGAGGAGTT	Excised	256
	ACAGCAACAGAACAGCAACTACG	WT	165
Recql4^{K525A}	TAGACCTTATGAAACCTCAAAGCC	*Msl*I RFLP	
	AGAACATTGGGCATTCGGC	WT: 416+175 bp PM: 361+175+55 bp	591

TABLE 4.5 – CONTINUED FROM PREVIOUS PAGE

GENOTYPING ALLELE	OLIGONUCLEOTIDE SEQUENCE (5′-3′)	DETECTED ALLELE	PRODUCT SIZE (BP)
Recql4^{G522Efs}	TAGACCTTATGAAACCTCAAAGCC AGAACATTGGGCATTCGGC	*Msl*I RFLP WT: 416+175 bp PM: 347+175+71 bp	591
Recql4^{M789K}	AATAGGTGGCAATGGGCAGG GCACTCGGCGAAAGGATACA	*Msl*I RFLP WT: 277+143 bp PM: 420 bp	420
Recql4^{R347X}	GAAGGTGACCAAGTTCATGCTAAAGCGTTTGTTTTTCATGTTGAGTCG GAAGGTCGGAGTCAACGGATTCAAAGCGTTTGTTTTTCATGTTGAGTCA GCTTCCCTAGACAGAGGGAACTATA	WT PM	HEX FAM

WT, wild type; KI, knock-in; PM, point mutant.

Table 4.6: *Genotyping KASP assay cycling conditions*

TEMPERATURE	DURATION	CYCLE NUMBER
30°C	1 minute	x1 Pre-read
94°C	15 minutes	x1
94°C 61°C	20 seconds 1 minute	x10 (-0.6°C/cycle)
94°C 55°C	20 seconds 1 minute	x26
30°C	1 minute	x1 Post-read

4.3 FLOW CYTOMETRY ANALYSIS

4.3.1 *Tissue collection*

Peripheral blood (PB) samples (~200 μL) were obtained by retro-orbital eye-bleeding using BD microtainer K2E tubes and BD vacutainer capillary tubes. A/Prof. Carl Walkley performed this procedure. Mice were then euthanised by CO_2 asphyxiation or cervical dislocation. The ear tissue was kept in 1.5 mL microcentrifuge tubes and stored in a -80°C freezer for re-genotyping if needed. Tissues including spleen, thymus, femurs, tibiae, iliac crests and sternum were collected and either processed to obtain single-cell suspensions or fixed with 2% PFA overnight and then washed with PBS and stored in 70% ethanol the following day. The muscle/flesh was removed from bones using sterile scalpels.

4.3.2 *Peripheral blood analysis*

PB was diluted 1:4 with PBS and analysed on a Sysmex KX21 haematological analyser to obtain whole blood cell counts. For flow cytometric analysis, the remaining PB was depleted of red blood cells (RBCs) by mixing with 1 mL RBC lysis buffer and spinning at 400 g for 5 minutes. The supernatant was discarded, and the process repeated. After one wash with 1 mL PBS, the

remaining pellet of cells was then resuspended in 150 μL of FACS buffer and stored on ice until cell staining.

4.3.3 *Bone marrow cell isolation*

For flow cytometry analysis, the two femurs were flushed in 2 mL of FACS buffer using a 1 mL syringe with a 23-gauge needle. Flushing was repeated twice to remove all the haematopoietic cells leaving the bone white. The cell suspension was filtered using a 40 μm cell strainer, and 100 μL was transferred to a 1.5 mL microcentrifuge tube for cell counts using the Sysmex KX21 haematological analyser. The remaining cells were stored on ice until cell staining.

4.3.4 *Spleen and cell thymic cell isolation*

Spleens and thymi were cleaned of any adipose or connective tissue, weighed, and stored in FACS buffer. Each organ was then crushed using the back of a 3 mL syringe plunger against a 40 μm cell strainer and collected into 5 mL or 2 mL of FACS buffer respectively. 100 μL of the suspension was transferred to a 1.5 mL microcentrifuge tube for cell counts using the Sysmex KX21 haematological analyser. The remaining cells were stored on ice until cell staining.

4.3.5 *FACS analysis*

The antibodies and their conjugates, dilutions, catalogue numbers and suppliers are listed in Table 4.7 [88, 184, 185]. All antibody cocktails were freshly prepared in FACS buffer at the optimum concentration determined previously by antibody titration. 25 μL of primary antibodies were mixed with 1 million cells in 96-well round-bottom plates and incubated on ice for 25 minutes. Cells were then washed with 200 μL of FACS buffer. When biotinylated antibodies were used, cells were incubated in 25 μL of streptavidin-conjugated with Brilliant Violet-605 for ten additional minutes. After a final wash, cells were resuspended in 70-200 μL of FACS buffer and samples were analysed on a BD LSR II Fortessa. Compensation and data acquisition were performed using the Cell Diva software version 8.1 (BD Biosciences, San Jose, CA, USA) and analysis using FlowJo software version 9.0 or 10.0 (Treestar).

Table 4.7: *FACS Antibodies (anti-mouse)*

ANTIBODY (CLONE)	CONJUGATE	DILUTION	CATALOGUE #	SUPPLIER
B220/CD45R (RA3-6B2)	APC	1:200	17-0452-83	Life Technologies Australia Pty Ltd/Thermo Fisher
c-Kit/CD117 (2B8)	APC-eFluor-780	1:200	47-1171-82	Life Technologies Australia Pty Ltd/Thermo Fisher
CD105 (MJ7/18)	PE-Cy7	1:400	120409	Biolegend
CD135/Flk2/Flt3 (A2F10)	PE	1:100	12-1351-82	Life Technologies Australia Pty Ltd/Thermo Fisher
CD150 (TC15-12F12.2)	PE	1:100	115904	Biolegend
CD19 (1D3)	PerCP-Cy5.5	1:150	45-0193-82	Life Technologies Australia Pty Ltd/Thermo Fisher
CD25 (PC61.5)	PE	1:400	12-0251-83	Life Technologies Australia Pty Ltd/Thermo Fisher
CD34 (RAM34)	eFluor-660	1:25	50-0341-82	Life Technologies Australia Pty Ltd/Thermo Fisher
CD4 (RM4-5)	eFluor-450	1:400	48-0042-82	Life Technologies Australia Pty Ltd/Thermo Fisher
CD41 (MWReg30)	eFluor-450	1:200	48-0411-82	Life Technologies Australia Pty Ltd/Thermo Fisher
CD43 (S7)	PE	1:200	553271	BD Pharmingen
CD44 (IM7)	APC	1:400	17-0441-83	Life Technologies Australia Pty Ltd/Thermo Fisher
CD44	PECy7	1:400	25-0441-82	eBioscience

TABLE 4.7 – CONTINUED FROM PREVIOUS PAGE

ANTIBODY (CLONE)	CONJUGATE	DILUTION	CATALOGUE #	SUPPLIER
CD71 (RI7 217.1.4)	APC	1:400	17-0711-82	Life Technologies Australia Pty Ltd/Thermo Fisher
CD8a/Ly-2 (53-6.7)	APC-eFluor 780	1:400	47-0081-82	Life Technologies Australia Pty Ltd/Thermo Fisher
F4/80 (BM8.1)	APC	1:250	20-4801-U100	Tonbo Biosciences
FcγRII/CD16/32 (93)	PerCP-Cy5.5	1:300	45-0161-82	Life Technologies Australia Pty Ltd/Thermo Fisher
Gr-1/Ly6G (RB6-8C5)	PE-Cy7	1:1000	25-5931-82	Life Technologies Australia Pty Ltd/Thermo Fisher
IgM (II/41)	Biotin	1:400	13-5790-82	Life Technologies Australia Pty Ltd/Thermo Fisher
Mac1/CD11b (M1/70)	PE	1:400	12-0112-83	Life Technologies Australia Pty Ltd/Thermo Fisher
Rat anti-mouse IgG1-APC	APC	1:100	550874	BD Pharmingen
Sca-1 (D7)	APC	1:100	17-5981-82	Life Technologies Australia Pty Ltd/Thermo Fisher
Streptavidin	BV 605	1:400	563260	BD Pharmingen
TCRβ (H57-597)	PE	1:400	12-5961-83	Life Technologies Australia Pty Ltd/Thermo Fisher
Ter119 (TER-119)	PE	1:400	12-5921-83	Life Technologies Australia Pty Ltd/Thermo Fisher

4.3.6 *In vitro class switch recombination assay*

B cells were purified from single-cell spleen suspensions using a B Cell Isolation kit. One million cells per well were cultured in 6-well plates for four days in RPMI medium supplemented with 10% FBS, 100 U/mL penicillin, 100 ng/mL streptomycin, 2 mM L-glutamine, 1 x MEM non-essential amino acids, 1 mM sodium pyruvate, 50 μM β-mercaptoethanol, 15 μg/mL LPS (tlrl-3pelps) and 10 ng/mL recombinant murine IL-4. Cells were stained with CellTrace Violet and rat anti-mouse IgG1-APC [186]. Stained cells were assessed using a BD LSR II Fortessa, and data was collected using the Cell Diva software version 8.1 (BD Biosciences, San Jose, CA, USA) and analysed using FlowJo software version 9.0 or 10.0 (Treestar).

4.4 MICRO-COMPUTED TOMOGRAPHY (MICRO-CT)

Tibiae were collected from mutant mice and their littermate controls and fixed in 2% PFA overnight. The next day, tibiae were washed twice with PBS and then stored in 70% ethanol. Before analysis, the attached soft tissue was carefully removed. Tibia morphology and microarchitecture was analysed by *ex-vivo* micro-CT using a Skyscan 1076 system. The tibiae were wrapped in 70% ethanol-soaked gauze within a cryovial to prevent drying during imaging. Images were acquired at 9 μm pixel size, 0.5 mm aluminium filter, 44 kV voltage, 220 μA current, 2,300 ms exposure time, 0.5° rotation, 1 frame averaging. Image slices were reconstructed by NRecon (Bruker, version 1.6.10.2) using the following settings: 36% beam-hardening correction, 6 ring artefact correction, 1 smoothing, and no defect pixel masking. The reconstructed images were analysed with software programs Dataviewer (Bruker, version 1.4.4), CTan (Bruker, version 1.15.4.0), and CTVox (Bruker, version 2.4.0). The trabecular and cortical region of interest (ROI) were determined by identifying the start of the mineralised zone of the proximal growth plate and calculating a distance equal to 3.5% (trabecular) and 40% (cortical) of the total tibial length, respectively. From that point, a further 5% of the total tibial length was analysed as the secondary spongiosa trabecular ROI and a 5% as the cortical ROI. Analysis of bone structure was completed by adaptative thresholding in CTan, which was determined by performing automatic thresholding on three samples from each experimental group resulting in threshold values of 50-255 for trabecular bone and 90-255 for

cortical bone. Representative 3D images of reconstructed trabecular and cortical bone, with colour-coded quantitative mineralisation, were made of the specimen whose value was closest to the group mean using the trabecular bone volume and cortical thickness parameters.

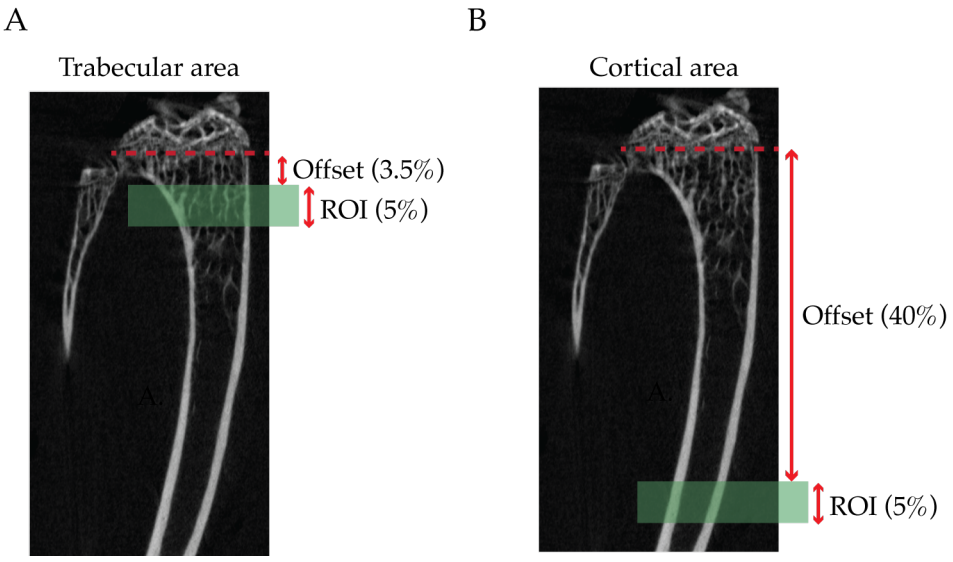

Figure 4.1: *Regions of interest of trabecular and cortical region*

4.5 CELL CULTURE

All cell culture experiments were conducted in a Gelaire class II biological safety cabinet. To reduce the risk of contamination, materials were sprayed with 70% ethanol. Solutions were maintained at 4°C for storage and were pre-heated in a WB7 water bath at 37°C before use. Cells were incubated in a CO_2 HeraCell 240i incubator at 5% CO_2 and 37°C.

4.5.1 *Cell maintenance*

Cells were maintained in tissue culture treated 6-well multi-well plates, 25 cm^2 flasks or 10 cm dishes with complete medium and passaged before reaching 80-90% confluency. For passaging, adherent cells were treated with trypsin (0.025% in PBS-EDTA) and incubated for 3-5 mins at 37°C. The flask/dish was tapped gently to dislodge the cells, and PBS was added to neutralise the trypsin. The mix was then spun at 400 g for 5 minutes, the supernatant discarded, and cells were counted and re-seeded at the desired cell density in pre-warmed medium. This process was repeated every two to three days. Regarding suspension cells, these were mixed properly before

a sample was taken for counting and then split every two to three days to reach concentrations no higher than 2x10^6 cells/mL.

To seed cells at a specific density, cells were counted by mixing 10 μL of cells with 10 μL trypan blue, loading 10 μL of the sample into the chamber of a sample slide and counting them using a Countess II cell counter.

4.5.2 *Freezing and thawing of cells*

When cells reached 80% confluency, they were collected for cryopreservation. Approximately 5x10^6 cells were either harvested by trypsinisation or taken straight from the suspension culture and spun at 400 g for 5 minutes. The supernatant was then discarded, and the cell pellet resuspended in 1 mL of freezing medium (Table 4.2). The suspension was next transferred into cryotube vials and allowed to freeze slowly in a Mr Frosty^{TM} Freezing Container in the -80°C freezer. After 24 hours, the tubes were taken out of the freezing container and put into boxes in -80°C freezer for short-term storage or in liquid nitrogen for long-term storage.

To thaw the cells, they were placed in a water bath at 37°C for 2 minutes. Cells were then resuspended in 10 mL of PBS and centrifuged at 400 g for 5 minutes. The supernatant was discarded, and cells resuspended in the appropriate medium.

4.5.3 *Generation of retrovirus*

Retrovirus was produced using transient transfection of HEK293T cells, which were seeded in 10 cm tissue culture dishes in 10 mL complete DMEM at a density of 8x10^6 cells to reach 70% confluency in 24 hours. Plasmid DNA was then introduced by calcium-phosphate-mediated transfection as follows: To a solution containing 10 μg EcoPac packaging construct, 10 μg retroviral plasmid construct of interest (MSCV-*Recql4* plasmids), 61 μL 2 M Calcium Chloride and nuclease-free water up to 500 μL. 500 μL of 2x HBS were added dropwise while vortexing. This solution was added immediately drop by drop to the HEK293T cells, and dishes were returned to the incubator for 7-10 hours. Alternatively, small-scale transfections in 6-well plates were spun at 1,000 g for 30 minutes at 25°C, before returning them to the incubator. The transfection medium was gently replaced by fresh medium at the end

of the day, and cells were incubated for a further 48 hours. Virus containing supernatant was collected at 48 and 72 hours in 1 mL aliquots and stored at -80°C.

4.5.4 *Transduction of Kusa4b10 cells with retroviral constructs*

The day before spin-infection, 12,500 Kusa4b10 cells were seeded in 6-well plates containing 2 mL of DMEM medium. Twenty-four hours later, 0.5 mL was removed and replaced with 0.5 mL of retrovirus. Additionally, 2 μL of polybrene (8 mg/mL) was added. The mix was spun at 1,100 g for 1 hour 30 minutes at 25°C and then kept in a 37°C CO_2 incubator. The following day the transduction medium was replaced by fresh medium.

4.5.5 *Immortalisation of myeloid cells by Hoxb8 retrovirus*

For immortalisation of myeloid cells with Hoxb8 [187], femurs, tibiae, and iliac crest were cut into small fragments and put in a small mortar. Bones were crushed gently with a pestle, and bone marrow (BM) was aspirated after the addition of 5 mL of FACS buffer. The cell suspension was then filtered using a 40 μm cell strainer. The process was repeated until bones were light pink. The cell suspension was then spun at 400 g for 5 minutes using the Heraeus Multi-age 3SR+ centrifuge. The supernatant was discarded, and cells were resuspended in 4 mL FACS buffer. In a 15 mL Falcon tube, 3 mL of Ficoll-Paque was carefully overlaid with this cell suspension and centrifuged for 10 minutes at 400 g without braking. Next, 1-2 mL of mononuclear cells were collected from the interphase and transferred to a new 15 mL Falcon tube. Subsequently, 13 mL of pre-heated PBS was added, and the mix was spun for 5 minutes at 400 g. The supernatant was removed, and cells were resuspended at 1-2x10^6 cells/mL in complete IMDM + SCF (100 ng/mL), IL-3 (10 ng/mL) and IL-6 (20 ng/mL) for 48 hours to stimulate cells to enter the cell cycle. In a 12-well plate, 1.0 million cells in 1 mL of IMDM medium were then mixed with 1 mL of Hoxb8 retrovirus (prepared by Ms Ankita Goradia). Extra cytokines (SCF, IL-3, and IL-6) were added to the mix, as well as polybrene (8 μg/mL). The cells were then spin-infected for 1 hour at 1,100 g and 25°C and then returned to the incubator. After 24 hours, the supernatant was replaced by fresh medium and cytokines, and 24 hours later, cells were transferred to T25 flasks with extra IMDM medium plus cytokines. Three days later, cells were diluted with medium

containing 10% FBS (non-heat inactivated) and 1% Granulocyte-Macrophage Colony-Stimulating Factor (GM-CSF) conditioned media plus SCF, IL-3 and IL-6, and then passaged and transferred to new flasks every 2-3 days with IMDM/10% FBS + 1% GM-CSF only. This was maintained for three to four weeks until cells were fully immortalised.

4.5.6 *Cell proliferation assays*

Low-passage Hoxb8 immortalised [187] *R26*-CreER^{T2} *Recql4*$^{fl/+}$, *R26*-CreER^{T2} *Recql4*$^{fl/G522Efs}$, and *R26*-CreER^{T2} *Recql4*$^{fl/R347X}$ cells were counted and seeded at a density of 200,000 cells/mL in 5 mL of IMDM/10% FBS + 1% GM-CSF in T25 flasks. On day 0, 400 nM/mL of 4-hydroxy tamoxifen was added, and cells were kept in a 37°C CO_2 incubator. Every two to three days, cells were counted, and the corresponding volume for the number of cells needed to re-seed 2 or 1x10^5 cells/mL was spun at 400 g for 5 mins. The supernatant was discarded, and the remaining cell pellet was resuspended in 5 mL fresh tamoxifen containing medium. Cells were treated for 14 days, and at each time point, cell pellets were collected for DNA recombination/*Recql4* deletion analysis. As a control, untreated cells were kept in parallel and seeded at the same concentration.

4.5.7 *Retroviral transduction and complementation assays with human RECQL4 constructs*

Hoxb8 immortalised *R26*-CreER^{T2} *Recql4*$^{fl/fl}$ cells were maintained in IMDM + 1% GM-CSF. Exponentially growing Hoxb8 *R26*-CreER^{T2} *Recql4*$^{fl/fl}$ cells (100,000 cells/mL) were spin-infected with MSCV-puro EGFP-hRECQL4 retrovirus containing human mutations (described in section 4.5.3) in a 1:1 ratio at 1,100 g for 90 minutes with 8 μg/mL polybrene. Two days after infection, cells were selected with puromycin (0.25 μg/mL) for four days and then expanded. Cells were then treated with 400 nM 4-hydroxy tamoxifen and counted and split every two-three days for 14 days as described for the cell proliferation assays. At each time point, cell pellets were collected for DNA recombination/*Recql4* deletion analysis.

4.5.8 *ATP-Lite cell viability assay - In vitro DNA damage response assay*

Hoxb8 immortalised *R26*-CreER^{T2} *Recql4*$^{fl/+}$ (control), and *R26*-CreER^{T2} *Recql4*$^{fl/K525A}$ cells were maintained in IMDM + 1% GM-CSF. The cells were treated with 400 nM 4-hydroxy tamoxifen for four days and then analysed to confirm complete recombination. Cells were then plated at 10,000 cells in 50 μL/well in 96-well plates and incubated for 48 hours with the indicated concentration of drugs in triplicates per dose (dose range Doxorubicin: 0-0.5 μM, Hydroxyurea: 0-0.5 mM, 4-Nitroquinoline: 0-2 μM and Topotecan: 0-0.5 mM). Cell viability was measured using the ATP-Lite Luminescence Assay System. Briefly, 50 μL of ATP-Lite mammalian cell lysis solution was added per well, and plates were shaken at 700 rpm for 5 minutes using a Medium Orbital Shaker. Next, 50 μL of ATP standard solution was added per well, and the plates were shaken again for 5 minutes at 700 rpm. The plates were left in the dark for 10 minutes before luminescence was measured using an Enspire plate reader.

4.5.9 *Seahorse XF24 extracellular flux analyser*

Hoxb8 immortalised [187] *R26*-CreER^{T2} *Recql4*$^{fl/+}$ (control), *R26*-CreER^{T2} *Recql4*$^{fl/K525A}$, *R26*-CreER^{T2} *Recql4*$^{fl/G522Efs}$, and *R26*-CreER^{T2} *Recql4*$^{fl/R347X}$ myeloid cells were maintained in IMDM, 10% FBS (non-heat inactivated) and 1% GM-CSF containing media. The cells were treated for four days with 400 nM 4-hydroxy tamoxifen and then genotyped to confirm complete recombination. To adhere myeloid (suspension) cells to the XF24 cell culture plate, wells were first coated with 100 μL of Retronectin solution (32 μg/mL in PBS), incubated for 2 hours at room temperature, blocked with 200 μL of 2% BSA in PBS, and washed with PBS. Cells were then seeded at 120,000 cells/well and spun at 1,100 g for 20 seconds. Cell culture media was replaced with non-buffered DMEM base media containing 25 mM glucose, 1 mM sodium pyruvate, glutamine at pH 7.4, and incubated for 1 hour at 37°C in a non-CO_2 incubator. The oxygen consumption rate (OCR) was measured in a Seahorse XF24-3 Flux Analyser. Cells were assayed with a 2-min mix/2-min wait/5-min measurement cycle for three baseline measurements followed by three cycles after each injection of four compounds affecting bioenergetics: 0.5 μM oligomycin (Complex V inhibitor), 0.7 μM carbonyl cyanide 4-(trifluoromethoxy)phenylhydrazone (FCCP; $\Delta\,\Psi$m uncoupler), 3.6

μM antimycin A (Complex III inhibitor), and 6 μM rotenone (Complex I inhibitor). After completion of the analysis, Cyquant cell proliferation assay was used to normalise measurements to cell number in the corresponding wells according to the manufacturer's instructions. Finally, data were analysed using Wave version 2.4 (Agilent Technologies).

4.5.10 *Live cell imaging and image processing of RECQL4 fusion proteins*

Transduced osteoblast-like Kusa4b10 cells were plated on 10 cm dishes, selected with puromycin, and grown to sub-confluency. Single plane images were acquired on an inverted fluorescent microscope (Olympus IX81) with a 40X objective (LUCPLFLN 40X) and were recorded with a Retiga-EXi 12 Bit CCD camera. Image processing and analysis were done using MetaMorph version 7.8.6 (Molecular Devices) and Adobe Photoshop version 21.1.2. Non-adherent HoxB8 immortalised myeloid cells were concentrated by centrifugation and 5 μL of cell suspension dispensed on a slide before image acquisition with a 60X objective (UPLANAPO 60X water immersion). For live mitochondrial staining, 250 μL of Mitochondrial Staining Solution (CytoPainter MitoBlue Indicator Reagent (ab219940), 1:500 diluted in HHBS) was added to Kusa4b10 cells grown on coverslips in 250 μL DMEM in a 24-well multi-well plate and incubated for 30 minutes to 2 hours in a 37°C/5% CO_2 incubator. Coverslips were washed twice with HHBS, and live cells were then imaged as described above.

4.6 PROTEIN ANALYSIS

4.6.1 *Protein extraction*

Lysates from thymocytes and Kusa4b10 cells transduced with MSCV puro EGFP-hRECQL4 retrovirus (WT, K508A, R807Pfs, Q757X, L638P, C525Afs, and R350Gfs) were prepared in 100 μL RIPA buffer (Table 4.2) plus Complete protease inhibitor and PhosStop tablets. Cell suspensions were incubated on wet ice for 15 minutes and then spun at 16,000 g for 20 minutes at 4°C to sediment cell debris. The soluble protein fraction was then transferred to a 1.5 mL microcentrifuge tube and kept on ice for quantification prior to SDS gel electrophoresis or storage at -80°C. Lysates from 2 million HoxB8 immortalised myeloid cells (*R26*-CreER^{T2} *Recql4*$^{fl/G522Efs}$, *R26*-CreER^{T2} *Recql4*$^{fl/R347X}$ and *R26*-CreER^{T2} *Recql4*$^{+/+}$ transduced with MSCV puro 3xFlag-RECQL4) were

prepared directly in 100 μL NuPAGE LDS sample buffer (1x in RIPA buffer plus NuPAGE Reducing Agent and Protease and Phosphatase inhibitors), heated at 70°C for 10 minutes, and stored at -80°C.

4.6.2 *Protein quantification*

The protein concentration of thymocyte and Kusa4b10 lysates was determined using the Pierce BCA protein assay kit. For each sample, 5 μL of protein extracts was added to 200 μL of A:B solution (ratio 50:1) in 96-well plates. BSA (2 mg/mL) was used as protein concentration reference standards (final concentration: 0-200 μg/mL). The plates were then incubated at 37°C for 30 minutes, and colour change was measured at Abs_{562nm} using the Enspire plate reader. 50 μg of total protein from thymocyte or Kusa4b10 extracts were mixed with 12.5 μL 4x NuPAGE LDS Sample Buffer, 5 μL 10x NuPAGE Reducing Agent, and RIPA buffer to make up a final volume of 50 μL. Samples were heat-denatured at 70°C for 10 minutes before loading into the gel.

4.6.3 *Protein gel electrophoresis and Western blotting*

50 μg of whole protein extracts from thymocytes or Kusa4b10 cells or 50 μL from myeloid cells were loaded into pre-cast NuPAGE^{TM} BOLT 8% Bis-Tris polyacrylamide gels with 10 μL of SeeBlue Plus2 Protein as a marker. Proteins were separated by electrophoresis at 165 V for 50 minutes in 1x NuPAGE® MOPS SDS running buffer using the PowerEase 90 W Electrophoresis system. Following denaturing gel electrophoresis, proteins were transferred onto pre-charged Immobilon-P PVDF membranes in 1x BOLT transfer buffer at 40 V for 1 hour and 15 minutes. Membranes were stained with Ponceau S to confirm proper transfer and then blocked with 5% Non-Fat Dry Milk (NFDM) powder in Tris-buffered saline with tween (TBST) for 1-2 hours at room temperature. After blocking, membranes were sealed in a polyethylene bag with 5 mL of the following antibodies diluted in 5% NFDM in TBST: rat monoclonal anti-RECQL4 (clone 3B10 at 1:750 for detection of mouse RECQL4 or endogenous mouse protein; and clone 3B1 at 1:500 for detection of human RECQL4; antibodies made by WEHI Antibody facility, Dr Monique Smeets, and Vince Murphy at St Vincent's Institute), mouse anti-Actin (1:5,000) or mouse anti-Flag (1:7,000); and incubated at 4°C overnight on a rotary wheel. Unbound antibody was removed in 3x washes for 5 minutes with TBST

using an orbital shaker. Membranes were then probed with HRP-conjugated goat anti-rat or goat anti-mouse secondary antibodies (1:10,000 in 5% NFDM in TBST) for 1 hour at room temperature and washed 3x with TBST for 5 minutes and 1x with TBS for 5 minutes. Protein bands were visualised after incubation with ECL Prime Reagent for chemiluminescent detection and exposure to Fuji X-ray film.

4.7 BIOCHEMICAL HELICASE ASSAYS

4.7.1 *RECQL4 cloning, expression, and purification*

The full-length WT and K525A mutant codon-optimised cDNA sequence of the mouse *Recql4* containing 3xFlag tag at the C-terminus was generated by gene-synthesis (IDT) and cloned into vector pFL-EGFP and transferred to the Multibac expression system to generate baculovirus [188]. Baculovirus-infected High Five cells were resuspended in TNG buffer supplemented with 1 mM EDTA and 1x mammalian protease inhibitors. Mixtures were sonicated three times for 30 seconds on ice. Lysates were clarified by centrifugation at 50,000 g for 30 minutes. Anti-Flag M2–Affinity Gel resin was added and incubated for 60 minutes. The resin was extensively washed with TNG (without protease inhibitors or EDTA), then washed overnight in TNG containing Benzonase® nuclease. Further washes were performed to remove the nuclease. Subsequently, RECQL4 was eluted with 100 μg/mL Flag peptide in TNG.

4.7.2 *RECQL4 helicase assay*

Helicase assays were performed according to Kaiser *et al.* [23]. 80 μl reactions containing 0.5 μM protein and 50 nM of a 15 nt 3'-overhang (OH) DNA substrate in assay buffer (20 mM HEPES pH 8.0, 5% Glycerol, 10 mM NaCl, 0.5 mM TCEP, 1 mM $MgCl_2$) were assayed in an EnSpire 2300 microplate reader at 25°C. The DNA substrate (T3-Cy3 annealed to B1-Dab) contained a 3'-15 nt polyT single-stranded DNA (ssDNA) loading site and a 15 nt dsDNA part with a generic sequence. After measuring baseline fluorescence levels for 60 seconds (Excitation 530 nm/Emission 580 nm), ATP was added to a final concentration of 1.25 nM to start the helicase reaction, and the increased Cy-3 fluorescence levels were recorded for 5 minutes as the quencher-labelled strand was separated from the Cy3-labelled strand. Measurements using

H_2O instead of ATP and buffer instead of protein served as blanks and were subtracted from the ATP-data.

4.7.3 *RECQL4 ATPase assay*

PiColorLock^{TM} phosphate detection reagent was used to measure the presence of inorganic phosphate (Pi) released from ATP as a measure *Recql4* ATPase activity. The proteins were assayed at 115 nM in the presence of 1 mM ATP and DNA in assay buffer (20 mM HEPES pH 8.0, 5% Glycerol, 10 mM NaCl, 0.5 mM TCEP, 1 mM $MgCl_2$). Colour change was measured at Abs_{650nm} in an EnSpire 2300 microplate reader at 25°C.

4.7.4 *RECQL4 DNA binding assay*

Electrophoretic-mobility shift assay was used to measure the relative binding of WT versus K525A mutant *Recql4* to DNA binding. Protein was serially diluted from 300 nM to 19 nM and bound to 25 nM single-stranded DNA oligo XOm1 conjugated to IRDye680. Bound Protein-DNA complex was separated on a 6% TBE/Acrylamide gel. The gel was directly imaged on a Li-Cor Odyssey CLx near-infrared fluorescence imaging system.

4.8 MOLECULAR BIOLOGY

4.8.1 *Overexpression construct design and cloning*

Human EGFP-RECQL4 and EGFP-RECQL4 K508A (provided by T. Enomoto, Musashino University, Tokyo, Japan; [169]) were cloned into MSCV puro. All other human mutations were created by gBlock (IDT; synthesised dsDNA fragments) replacement of the wild type sequence of RECQL4 in MSCV puro with the appropriate mutation containing DNA fragment. For assembly of R350GfsX21, a 1.5 kb EcoRI-BamHI fragment from MSCV puro EGFP-RECQL4 WT was cloned into pUC19 ΔEcoRI-BamH1. A 539 bp KpnI-BamHI R350Gfs gBlock was then cloned into pUC19 ΔKpnI-BamHI, followed by a 3-part ligation of 1.5 kb EcoRI-BamHI R350Gfs from pUC19 plus 2.2 kb BamHI-SalI WT RECQL4 plus 6.7 kb SalI-EcoRI WT-MSCV puro backbone. For R807PfsX38, a 2.2 kb BamHI-SalI fragment from MSCV puro EGFP-RECQL4 WT was introduced into pUC19 ΔBamH1-SalI. A 1,368 bp SfiI-XhoI R807Pfs gBlock was then cloned into pUC19 ΔSfiI-XhoI. For L638P and Q755X, 613

bp PmlI-SfiI L638P and Q757X gBlocks were cloned into PmlI-SfiI digested pUC19 containing the same 2.2 kb BamHI-SalI WT RECQL4 fragment. MSCV puro EGFP-RECQL4^{R807Pfs}, EGFP-RECQL4^{L638P} and EGFP-RECQL4^{Q757X} were then assembled in a 3-part ligation of 1.5 kb EcoRI-BamHI WT RECQL4 plus 2.2 kb BamHI-SalI R807Pfs, L638P or Q757X from pUC19 plus 6.7 kb SalI-EcoRI WT-MSCV puro backbone. MSCV puro EGFP-RECQL4^{C525Afs} was created by replacing a 250 bp BamHI-PmlI fragment from MSCV puro EGFP-RECQL4 WT with a 250 bp BamHI-PmlI C525AfsX33 (ΔT) IDT gBlock.

Mouse mCherry-RECQL4 was assembled from a codon optimised synthetic murine *Recql4* cDNA (GeneArt, Life Technologies), placed behind a mCherry cDNA (gBlock, IDT) in MSCV puro (759 bp BglII-EcoRI mCherry gBlock into ΔBglII-EcoRI MSCV puro, then 3.66 kb BamHI-EcoRI m*Recql4* from 11AASYJC in pMA into 6.88 kb ΔBamHI-EcoRI MSCV puro mCherry). Mouse mutations were created by gBlock (IDT) replacement of a fragment of *Recql4*. K525A and R347X G-blocks were cloned into StrataClone Blunt. 0.86 kb HincII-PmlI K525A and R347X fragments were then cloned into 5.2 kb ΔHincII-PmlI 11AASYJC in pMA. 3.6 kb BamHI-EcoRI full-length murine *Recql4*^{K525A} and *mRecql4*^{R347X} cDNA from 11AASYJC were then cloned into 6.6 kb ΔBamHI-EcoRI MSCV puro mCherry. A 1.1 kb NdeI-NheI M789K gBlock and a 0.876 kb HincII-PmlI G522EfsX43 gBlock were cloned into 4.9 kb ΔNdeI-NheI and 5.2 kb ΔHincII-PmlI 11AASYJC in pMA respectively. 3.6 kb BamHI-EcoRI full-length *mRecql4*^{M789K} and *mRecql4*^{G522Efs} from 11AASYJC were then cloned into 6.6 kb ΔBamHI-EcoRI MSCV puro mCherry.

Mouse 3xFlag-RECQL4^{R347X} was created as follows: a 98 bp PCR product was created with primers XhoI-BamHI-3xFlag-F and BglII-3xFLAG-R using pKA mRecql4-3xFlag (11AASYKC in pMK-RQ) as a template. The XhoI-BglII digested product (81 bp) was cloned into ΔXhoI-BamHI MSCV puro mCherry *Recql4*^{R347X}. Mouse 3xFlag-RECQL4^{G522Efs} was assembled from a 2.753 kb HincII fragment from MSCV puro mCherry *Recql4*^{G522Efs} cloned into ΔHincII MSCV puro 3xFlag-Recql4^{R347X}.

All constructs contained full-length ORFs including those coding for truncating mutations. All constructs and mutations were confirmed by Sanger sequencing.

4.8.2 *Restriction enzyme digestion*

Digestion of gBlock gene fragments and plasmids was performed by combining the following: 100 ng of gBlock DNA or 1 μg of plasmid DNA, 3 μL of 10x CutSmart buffer, 1 μL each of restriction enzymes BamHI-HF and PmlI, and nuclease-free water to a total volume of 30 μL. The digestion mix was then incubated at 37°C for 3 hours. Following digestion, the 5′ and 3′ ends of the vector DNA were dephosphorylated by the addition of 1 μL (1U) recombinant Shrimp Alkaline Phosphatase (NEB) and a 30-minute incubation at 37°C. Vector samples were then mixed with 6 μL of 6x Purple Gel loading dye (NEB) and loaded in a combined 1% (top) and 3% (bottom) agarose gel and run at 120 V for a total of 1 hour and 15 minutes. The desired DNA fragment was excised from the gel with a razor blade, and vector and insert DNA was then purified using the Bioline Isolate II PCR and Gel kit according to the manufacturer's instructions. The amount of DNA recovered was quantified using the Nanodrop spectrophotometer.

4.8.3 *Ligation*

Vector and insert/gBlock DNA were ligated in a 1:5 (or 1:3) molar ratio with a total of 25-50 ng. Typically, for a 10.1 kb vector and a 250 bp insert, the following were combined in a PCR tube: 2.25 μL or 25 ng vector DNA, 0.5 μL or 3 ng insert DNA, 0.25 μL 10X Ligase Buffer, 0.25 μL T4 DNA Ligase and 1.25 μL nuclease-free water. A control reaction was included without insert DNA. The ligation mix was incubated for 2 hours at room temperature or overnight at 16°C.

4.8.4 *Transformation*

Competent bacterial host cells (Stbl3) were thawed on ice for 15 minutes, and 50 μL of cells were then carefully added to 2 μL of ligation product in a 1.5 mL tube. This mix was incubated on wet ice for 30 minutes, followed by a 45-second heat shock at 42°C and a 2-minute incubation on ice. 250 μL of SOC medium was added, and the transformed cells were incubated at 37°C for 1 hour with agitation. 50 μL and 250 μL of the transformed cells were then spread onto agar plates containing Carbenicillin and incubated at 35°C overnight. If no or few colonies had grown on the no-insert control plates and more than 200 and 1,000 colonies on the real ligation plates, 2-5

colonies were picked and grown in 1.5 mL LB plus Carbenicillin overnight at 35°C for subsequent plasmid DNA miniprep extraction and restriction digest analysis. Plasmids with the correct restriction pattern were sent for Sanger sequencing to confirm accurate cloning and the corresponding clones were further amplified and cryopreserved.

4.8.5 *Plasmid purification*

Plasmid DNA was purified using the Bioline Isolate II Plasmid Mini kit according to the manufacturer's instructions. DNA was quantified using the Nanodrop Spectrophotometer equipment and verified by restriction enzyme digestion as described above.

4.9 CRISPR/CAS9 SCREEN

4.9.1 *Generation of lentivirus*

The lentiviral Cas9 blasticidin (LentiCas9-Blast) plasmid was provided by A/Prof. Kaylene Simpson (Victorian Centre for Functional Genomics (VCFG), Peter MacCallum Cancer Centre) from stock purchased from Addgene (#52962; http://n2t.net/addgene:52962;RRID:Addgene_52962) [189]. The plasmid was co-transfected into sub-confluent (70%) HEK293T cells with packaging plasmid psPAX2 (Addgene) and MSCV-VSVg (Addgene) by calcium-phosphate transfection as described in section 4.5.3.

4.9.2 *Generation of murine Cas9-expressing cell lines*

For the generation of Cas9-expressing cells, 2x10^5 Hoxb8 *R26*-CreER^{T2} *Recql4*$^{fl/+}$ and *R26*-CreER^{T2} *Recql4*$^{fl/R347X}$ myeloid cells were transduced with 1 mL of lentiCas9-blasticidin virus as described in section 4.5.4. This cell type was chosen given the previously reported requirement of RECQL4 for maintenance of this cell population *in vivo* [88]; and because they are grown in suspension (non-adherent), which made cell culture significantly easier. Additionally, these cells divide rapidly, and therefore, can be obtained in sufficient numbers for screening at a suitable copy number per sgRNA. Next, to positively select cells expressing Cas9, blasticidin (3 μg/mL) was added 48 hours after infection and maintained for 14 days with regular splits every 2 to 3 days.

4.9.3 *Assaying Cas9 activity in Cas9 blasticidin cell lines*

To check the target editing efficiency of the Cas9 Hoxb8 *R26*-CreER^{T2} *Recql4*$^{fl/+}$ and *R26*-CreER^{T2} *Recql4*$^{fl/R347X}$ cell lines, stable Cas9 cells were transduced with pLentiGuide (VCFG, from Addgene) expressing sgRNA targeting CD44, a cell surface marker highly expressed on all immortalised Hoxb8 cells. Forty-eight hours after infection, puromycin (0.25 μg/mL) was added to select for pLentiGuide sg*Cd44* expression. Four days later, 0.5-1x10^6 cells were stained with a PE-Cy7 conjugated anti-CD44 antibody (1:400) and analysed by flow cytometry using the FACS BD LSR II Fortessa system.

4.9.4 *Titration of lentivirus containing Brie library*

Aliquots of concentrated Brie sgRNA library were made by the VCFG. To determine the optimal concentration of the pooled lentiviral genome-wide Brie sgRNA library, which contains four sgRNA per mouse gene [190], 1.25 million cells in 1 mL of medium were seeded in 12-well plates, and spin-infected with different amounts of concentrated virus (0, 2.5, 5, 7.5, 10, 12.5, 20 μL). After 4-6 hours, the mix was topped up with 1 mL of medium, and 24 hours later, all medium was replaced by 2 mL fresh medium. Forty-eight hours after spin-infection, puromycin (0.25 μg/mL) was added, and 72 hours later, cell viability was assessed by trypan blue with the Countess II cell counter to determine the viral concentration that results in ~30% of cell survival, which corresponds to a multiplicity of infection (MOI) of 0.3. An MOI of 0.3 was used to ensure cells only received a single sgRNA integrant.

4.9.5 *CRISPR knockout screen*

On day 1 of the CRISPR knockout screen, 20 million cells from Cas9 Hoxb8 *R26*-CreER^{T2} *Recql4*$^{fl/+}$ and *R26*-CreER^{T2} *Recql4*$^{fl/R347X}$ in 20 mL of medium were mixed with 120 μL of lentivirus containing the genome-wide Brie sgRNA library and 20 μL of polybrene in Nunc^{TM} cell culture T75 flasks. The transfection mix was spun at 1,100 g and 25°C for 1.5 hours and then returned to the 37°C incubator. At the end of the day, each flask was topped up with 30 mL of pre-heated medium. On day 3, cells were counted and expanded to T175 flasks containing 125 mL of medium at a concentration of 1x10^6 cells/mL. Puromycin was added at a dose of 0.25 μg/mL. On day 4, cells were further diluted to reach a concentration of 3.3x10^5 cells/mL

of medium plus puromycin. On day 7, puromycin was removed from the medium and cells were re-seeded at the standard concentration of $2x10^5$ cells/mL in tamoxifen containing medium (400 nM/mL) to induce Cre-mediated recombination. During the next 14 days, cells were passaged every two or three days at a density to maintain at least 500 cells per sgRNA in the presence of tamoxifen, which corresponded to 2 T175 flasks per cell line with 250 mL at a concentration of 1 or $2x10^5$ cells/mL. Additionally, at each timepoint, pellets of 2 and 25 million cells were kept for DNA recombination analysis and gDNA isolation for library sequencing, respectively.

4.9.6 *Genomic DNA preparation*

Extraction of gDNA was performed using the Gentra Puregene kit following the manufacturer's instructions. Cell pellets were thawed and vortexed to resuspend them. Next, 3 mL of cell lysis solution was added, and tubes were vortexed at high speed for 15 seconds. This was followed by incubation at 37°C for 5 minutes, the addition of 1 mL of protein precipitation solution and an extra high-speed 25 seconds vortex. The tubes were spun at 2,000 g for 10 minutes, and the supernatant was transferred to a 15 mL Falcon tube containing 3 mL isopropanol. After gentle mixing, the tubes were spun at 2,000 g for 3 minutes and the supernatant was discarded. 3 mL of 70% ethanol was added to wash the DNA pellet and another spin at 2,000 g for 1 minute was performed. The supernatant was removed, and the DNA pellet briefly dried before resuspending in 400 μL of DNA hydration solution and incubation at 65°C for 1 hour to dissolve the DNA. Next, the DNA was quantified using the Nanodrop spectrophotometer, and 1 μg was analysed on a 0.8% agarose gel. Gel images were captured using the VersaDoc imaging system.

4.9.7 *Library preparation for Illumina sequencing*

Sequencing libraries were generated based on the PCR amplification of the integrated sgRNA constructs containing a barcode sequence for Illumina sequencing (protocol from Broad Institute; https://portals.broadinstitute.org/gpp/public/resources/protocols). Three time points (Day 0, 4, and 9) of the two cell lines (fl/+ and fl/R347) were selected. To utilise the full amount of gDNA recovered from each 20 million-cell pellet, between 18 and 28 PCR reactions were performed. Each 100 μL PCR reaction contained 10 μg

of gDNA, 10 μL 10x ExTaq reaction buffer, 8 μL 2.5 mM dNTP mixture, 0.75 μL ExTaq polymerase, 0.5 μL P5 primer mix (100 μM; Table 4.8), and, for each of the six samples, 10 μL of a unique P7 index primer (5 μM; Table 4.9) in nuclease-free water. The thermocycling parameters of the PCR are described in Table 4.10. The PCR products were pooled together, and 5 μL of each sample was loaded in a 3% agarose gel and run for 45 minutes at 120 V to confirm the size of the band and check for the presence of contamination or degradation products. Pooled PCR products were then purified using AMPure XP magnetic beads to remove gDNA and PCR contaminants. In brief, 100 μL of pooled PCR was mixed with 100 μL of magnetic beads and incubated at room temperature for 5 minutes. Next, the tubes were placed on a magnetic plate for 5 minutes and the supernatant discarded. The beads were washed twice with 70% ethanol and the DNA eluted in 50 μL TE buffer. The purified pooled library was then quantified with Nanodrop spectrophotometer system, and 2 μL of product was mixed with 2 μL of nuclease-free water and 1.25 μL of loading buffer and run on a 3% agarose gel for a last quality check. Finally, 50 μL of the purified pooled library containing at least 3 ng/μL of DNA was sent for sequencing by HiSeq-PE150 (Illumina) at NovogeneAIT Genomics Singapore Pte Ltd.

Table 4.8: *P5 primer mix*

NAME	SEQUENCE
P5 0 nt stagger	AATGATACGGCGACCACCGAGATCTACACTCTTTCCCTAC ACGACGCTCTTCCGATCTTTGTGGAAAGGACGAAA-CACCG
P5 1 nt stagger	AATGATACGGCGACCACCGAGATCTACACTCTTTCCCTAC ACGACGCTCTTCCGATCTCTTGTGGAAAGGACGAAA-CACCG
P5 2 nt stagger	AATGATACGGCGACCACCGAGATCTACACTCTTTCCCTAC ACGACGCTCTTCCGATCTGCTTGTGGAAAGGACGAAA-CACCG
P5 3 nt stagger	AATGATACGGCGACCACCGAGATCTACACTCTTTCCCTAC ACGACGCTCTTCCGATCTAGCTTGTGGAAAGGAC-GAAACACCG
P5 4 nt stagger	AATGATACGGCGACCACCGAGATCTACACTCTTTCCCTAC ACGACGCTCTTCCGATCTCAACTTGTGGAAAGGAC-GAAACACCG

TABLE 4.8 – CONTINUED FROM PREVIOUS PAGE

NAME	SEQUENCE
P5 6 nt stagger	AATGATACGGCGACCACCGAGATCTACACTCTTTCCCTAC ACGACGCTCTTCCGATCTTGCACCTTGTGGAAAGGAC- GAAACACCG
P5 7 nt stagger	AATGATACGGCGACCACCGAGATCTACACTCTTTCCCTAC ACGACGCTCTTCCGATCTACGCAACTTGTGGAAAG- GACGAAACACCG
P5 8 nt stagger	AATGATACGGCGACCACCGAGATCTACACTCTTTCCCTAC ACGACGCTCTTCCGATCTGAAGACCCTTGTGGAAAG- GACGAAACACCG

Table 4.9: *P7 primers*

NAME	SEQUENCE IN P7 PRIMER 5′-3′	INDEX READ (REV COMP SEQUENCE)	FULL SEQUENCE
P7 index 05 lentiGuide	ATACTCAA	TTGAGTAT	CAAGCAGAAGACGGCA TACGAGATATACTCAA GTGACTGGAGTTCAGA CGTGTGCTCTTCCGAT CTTCTACTATTCTTTC CCCTGCACT*G*T
P7 index 06 lentiGuide	GCTGAGAA	TTCTCAGC	CAAGCAGAAGACGGCA TACGAGATGCTGAGAA GTGACTGGAGTTCAGA CGTGTGCTCTTCCGAT CTTCTACTATTCTTTC CCCTGCACT*G*T
P7 index 07 lentiGuide	ATTGGAGG	CCTCCAAT	CAAGCAGAAGACGGCA TACGAGATATTGGAGG GTGACTGGAGTTCAGA CGTGTGCTCTTCCGAT CTTCTACTATTCTTTC CCCTGCACT*G*T

TABLE 4.9 – CONTINUED FROM PREVIOUS PAGE

NAME	SEQUENCE IN P7 PRIMER 5′-3′	INDEX READ (REV COMP SEQUENCE)	FULL SEQUENCE
P7 index 08 lentiGuide	TAGTCTAA	TTAGACTA	CAAGCAGAAGACGGCA TACGAGATTAGTCTAA GTGACTGGAGTTCAGA CGTGTGCTCTTCCGAT CTTCTACTATTCTTTC CCCTGCACT*G*T
P7 index 09 lentiGuide	CGGTGACC	GGTCACCG	CAAGCAGAAGACGGCA TACGAGATCGGTGACC GTGACTGGAGTTCAGA CGTGTGCTCTTCCGAT CTTCTACTATTCTTTC CCCTGCACT*G*T
P7 index 10 lentiGuide	TACAGAGG	CCTCTGTA	CAAGCAGAAGACGGCA TACGAGATTACAGAGG GTGACTGGAGTTCAGA CGTGTGCTCTTCCGAT CTTCTACTATTCTTTC CCCTGCACT*G*T

Table 4.10: *Thermocycling parameters of PCR*

TEMPERATURE	DURATION	CYCLE NUMBER
95°C	Hot plate start	
95°C	1 minute	x1
95°C	30 seconds	x28
53°C	30 seconds	
72°C	30 seconds	
72°C	10 minutes	x1
4°C	Forever	

4.9.8 *Bioinformatics analysis*

CRISPR screen analysis was performed using CRISPR-Beta-Binomial package by Dr Alistair Chalk (St Vincent's Institute) (CB^2) (v 1.3.0) [191]. To measure differences in sgRNA levels, CB^2 combines a beta-binomial model with a modified Student's t-test. Next, to estimate gene-level significance, a Fisher's combined probability test was conducted. Briefly, raw reads were mapped to the `broadgpp_brie_crispr` library with `run_sgrna_quant()` and read counts were normalised with `get_CPM()`. Gene level statistics were calculated using `measure_gene_stats()`. Annotation with ENSEMBL was performed with biomaRt [192]. Plots were generated using ggplot2 [193]. Core essential genes version 2 (CEG2) was obtained from CEG2 supplemental table 2 "List of the human core essential gene set version 2" [194].

4.9.9 *CRISPR secondary validation screen*

Four individual sgRNAs targeting *Klhdc3* were chosen for cloning into the pLentiGuide vector. Forward (F) and reverse (R)-strand oligos were purchased from IDT. The oligos were phosphorylated and annealed as follows: 1 μL of each F and R oligo (100 μM), 1 μL 10x T4 ligation buffer, 0.5 μL T4 polynucleotide kinase (PNK, NEB) and 6.5 μL nuclease-free water were combined in a PCR tube. Phosphorylation and annealing were achieved in the T3000 thermocycler by using the following thermocycling parameters: 37°C for 30 minutes, 95°C for 5 minutes, then 95°C down to 22°C in 73 cycles of -1°C/15 second cycle and hold at 22°C. Annealed oligos were diluted 1:200 with nuclease-free water, and 0.25 μL of this dilution was added to a ligation mix containing 0.25 μL T4 ligation buffer, 0.25 μL T4 ligase, 0.5 μL BsmB1 digested and dephosphorylated pLentiGuide vector and 1.25 μL H_2O. The ligation mix was incubated at room temperature for 4.5 hours, and then 2 μL was transformed into 30 μL competent Stbl3 bacteria as described above (section 4.8.4). Plasmid DNA was purified using the Bioline Isolate II Plasmid Mini kit and quantified using the Nanodrop spectrophotometer system for use in viral production and subsequent cell proliferation assays.

The sgRNA plasmids targeting *Klhdc3* were individually transfected into HEK293T cells and transduced in Hoxb8 *R26*-CreER^{T2} *Recql4*$^{fl/R347X}$ cells, as described in section 4.9.1 and 4.5.4, respectively. Three days after transduction, puromycin was added at a dose of 0.25 μg/mL and kept for four days for

positive selection. After generating cells expressing lentivirus containing sgRNAs targeting the *Klhdc3* gene, cells received tamoxifen (400 nM/mL) for 14 days in a cell proliferation assay, as previously described in section 4.5.6.

4.10 STATISTICAL ANALYSIS

To determine statistical significance, Kaplan-Meier survival plots, Student's t-tests, ordinary one-way ANOVA, and chi-squared test were conducted in Prism software version 7 and 8 (GraphPad; San Diego, CA, USA).

Throughout this thesis, significance is indicated using the following convention: *P<0.05; **P<0.01; ***P<0.001; ****P<0.0001, and data is presented as mean ± S.E.M. Furthermore, the number of samples used for each experiment is described in the corresponding figure legends.

CHAPTER 5

5

UNDERSTANDING THE PHYSIOLOGICAL REQUIREMENTS OF THE HELICASE DOMAIN OF RECQL4

5.1 INTRODUCTION

The physiological role of the ATP-dependent helicase activity of RECQL4 is unclear. While some studies support the theory that this domain is essential for the functions of RECQL4, others, including ours, have demonstrated *in vitro* that the expression of an ATP-binding deficient RECQL4 could restore the viability of RECQL4-depleted cells [88, 169]. However, the assessment of the physiological requirements of this domain has not been completed *in vivo*.

To address this gap, a murine model with a knock-in point mutation that abolishes its ATP-dependent helicase activity ($Recql4^{K525A}$) was generated. After confirming that the mutation resulted in a helicase-inactive but full-length RECQL4 protein, mice with this mutation were utilised in a variety of experiments to determine their embryonic development, body weight, haematopoiesis, B and T cell development, and physiological DNA damage repair. Furthermore, they were compared to other mutations that produced truncating/hypomorphic alleles. The data in this chapter have been published in *PLoS Genetics* 2019, 15(7), e1008266. The manuscript can be found in the following section and in final published format in Appendix A, except for the Materials and Methods section, which has been consolidated in Chapter 4 to avoid repetition. For consistency, the abbreviations, references, figure numbering, and the spelling have been adapted from the published paper to match the rest of this thesis.

5.2 PUBLISHED MANUSCRIPT

Castillo-Tandazo W, Smeets MF*, Murphy V, Liu R, Hodson C, Heierhorst J, Deans A, Walkley CR*. ATP-dependent helicase activity is dispensable for the physiological functions of Recql4. PLoS Genet. 2019;15(7):e1008266.
DOI: https://doi.org/10.1371/journal.pgen.1008266
* These authors contributed equally to this work.

5.2.1 *Abstract*

RTS is a rare autosomal recessive disorder characterised by skin rash (poikiloderma), skeletal dysplasia, small stature, juvenile cataracts, sparse or absent hair, and predisposition to specific malignancies such as OS and haematological neoplasms. RTS is caused by germline mutations in *RECQL4*, a RecQ helicase family member. *In vitro* studies have identified functions for the ATP-dependent helicase of RECQL4. However, its specific role *in vivo* remains unclear. To determine the physiological requirement and the biological functions of RECQL4 helicase activity, we generated mice with an ATP-binding-deficient knock-in mutation (*Recql4*^{K525A}). *Recql4*$^{K525A/K525A}$ mice were strikingly normal in terms of embryonic development, body weight, haematopoiesis, B and T cell development, and physiological DNA damage repair. However, mice bearing two distinct truncating mutations *Recql4*^{G522Efs} and *Recql4*^{R347X}, that abolished not only the helicase but also the C-terminal domain, developed a profound BM failure and decrease in survival similar to a *Recql4* null allele. These results demonstrate that the ATP-dependent helicase activity of RECQL4 is not essential for its physiological functions and that other domains might contribute to this phenotype. Future studies need to be performed to elucidate the complex interactions of RECQL4 domains and their contribution to the development of RTS.

5.2.2 *Introduction*

RTS (OMIM #268400) is a rare autosomal recessive disorder characterised by skin rash (poikiloderma), skeletal dysplasia, small stature, sparse or absent hair, gastrointestinal complications, and a high predisposition to specific malignancies such as OS and haematological neoplasms [64, 67]. RTS and the related RAPADILINO and BGS are associated with damaging germline mutations in *RECQL4* [46, 52, 111]. The majority of *RECQL4* mutations are

located in its helicase domain, yet the physiological role of this domain remains unclear [56].

Helicases are enzymes that unwind double-stranded or more complex DNA and RNA structures using energy from ATP hydrolysis. The unwinding of dsDNA is necessary to allow access to the DNA during replication, repair, recombination and transcription [195]. In humans, five members of the RecQ helicase family have been identified: *RECQL1*, *RECQL4*, *RECQL5*, *BLM* and *WRN*. Mutations in three are associated with syndromes that present with premature ageing and cancer-predisposition: *WRN* in Werner syndrome, *BLM* in Bloom syndrome, and *RECQL4* in RTS [26, 196]. RecQ-family helicases contain three highly conserved protein domains: an archetypal helicase domain, which contains seven conserved motifs that couple ATP hydrolysis to dsDNA strand separation [26, 196]; the RQC domain, which features a beta-hairpin motif, a winged-helix domain and a zinc-binding motif, for intervention in the binding of G quadruplex DNA and stabilisation of DNA structures [197]; and the HRDC domain, which promotes stable DNA binding [198]. RECQL4 differs from the other family members as it has no HRDC domain and lacks a structurally conserved RQC domain. Instead, it contains the structurally unique domain called R4ZBD and, importantly, an N-terminal region of homology with the *S. cerevisiae* DNA replication initiation factor Sld2 [170, 175]. Sld2 is an essential protein required for activation of replication origins in yeast [199], and RECQL4 is the putative mammalian homologue.

The human *RECQL4* gene is located at the long arm of chromosome eight (8q24.3) and consists of 21 exons and 13 relatively short introns (<100 bp in length), yielding a full-length transcript of 3,627 bp [111]. Mutations in the *RECQL4* gene have been found in the majority of RTS patients, and also in the related RAPADILINO and BGS [56, 64]. Most mutations are either nonsense or frameshift mutations and are predicted to create truncated proteins [56]. Over half of these impact the reading frame at exons 8-14 causing abnormal translation and or truncation of the RECQL4 protein with the presumed loss of DNA helicase function [56]. Very few mutations are located in the N-terminal Sld2 region, and those that are reported are primarily silent or missense [56]. This finding has led to the hypothesis that the N-terminal domain is critical for organismal viability, and that inactivation of the helicase function is a critical effect of the mutation spectrum that is found in RTS.

RECQL4 has been well characterised biochemically in terms of its ssDNA binding, ATP hydrolysis and DNA unwinding ability [138, 167, 168]. *In vitro*, RECQL4 ATPase and helicase activity are completely abolished by point mutations in the canonical Walker A and B motifs [23]. However, helicase-dead mutants can rescue cellular lethality in RECQL4-deficient DT40 chicken cells and murine haematopoietic cells *in vitro* [88, 169]. In addition, mutations that affect the helicase domain not only affect its activity but can also lead to protein truncation or unstable proteins, which does not allow the specific assessment of the physiological requirement of the ATP-dependent helicase RECQL4 in isolation. To understand the biological functions of RECQL4 helicase activity in a whole animal context, we generated a mouse model with a knock-in point mutation that specifically abolishes its ATP-dependent helicase activity ($Recql4^{K525A}$) and compared this to two different truncating mutations $Recql4^{G522Efs}$ and $Recql4^{R347X}$. Here we show that mice with a specific deficiency in *Recql4* helicase activity are strikingly normal, in contrast to pathogenic effects of truncating mutations that remove the entire helicase domain and downstream part of the protein.

5.2.3 *Results*

5.2.3.1 *The $Recql4^{K525A}$ mutation lacks ATP-dependent helicase activity*

To determine the specific effects of the ATP-dependent helicase to the functions of full-length RECQL4 protein, we generated the K525A point mutation, along with a full-length wild type mouse RECQL4 protein. The alanine substitution in the K525A mutation replaced a critical lysine, evolutionarily conserved and present in all Walker A motif-containing ATPases, that is necessary for ATP hydrolysis and corresponds to a previously analysed human RECQL4 K508A mutation that lacks ATP-dependent helicase activity (Figure 5.1 A) [8, 138]. To biochemically characterise an ATPase deficient mutation in murine *Recql4*, we established *in vitro* assays for *Recql4* function. Both WT and K525A proteins had equivalent affinity for ssDNA binding, using an Electrophoretic-mobility shift assay (Figure 5.1 B). In ATPase assays, the WT protein hydrolysed ATP in a DNA-dependent manner whereas $Recql4^{K525A}$ showed no activity above background levels (Figure 5.1 C). Finally, we tested the ability of these recombinant proteins to unwind DNA, using a dsDNA substrate with an ssDNA loading site. If ATP-dependent helicase activity

is present, the fluorophore-labelled strand is released from the quencher-labelled complementary strand providing a real-time fluorescent readout of unwinding activity (Figure 5.1 D). Robust ATP-dependent unwinding of the substrate was observed when using WT-RECQL4 protein, whereas no change in fluorescence was observed using the *Recql4*^{K525A} mutant consistent with an inability to unwind DNA (Figure 5.1 E). Together, our results demonstrate that the *Recql4*^{K525A} protein is helicase and ATPase dead, despite equivalent protein stability and DNA binding properties.

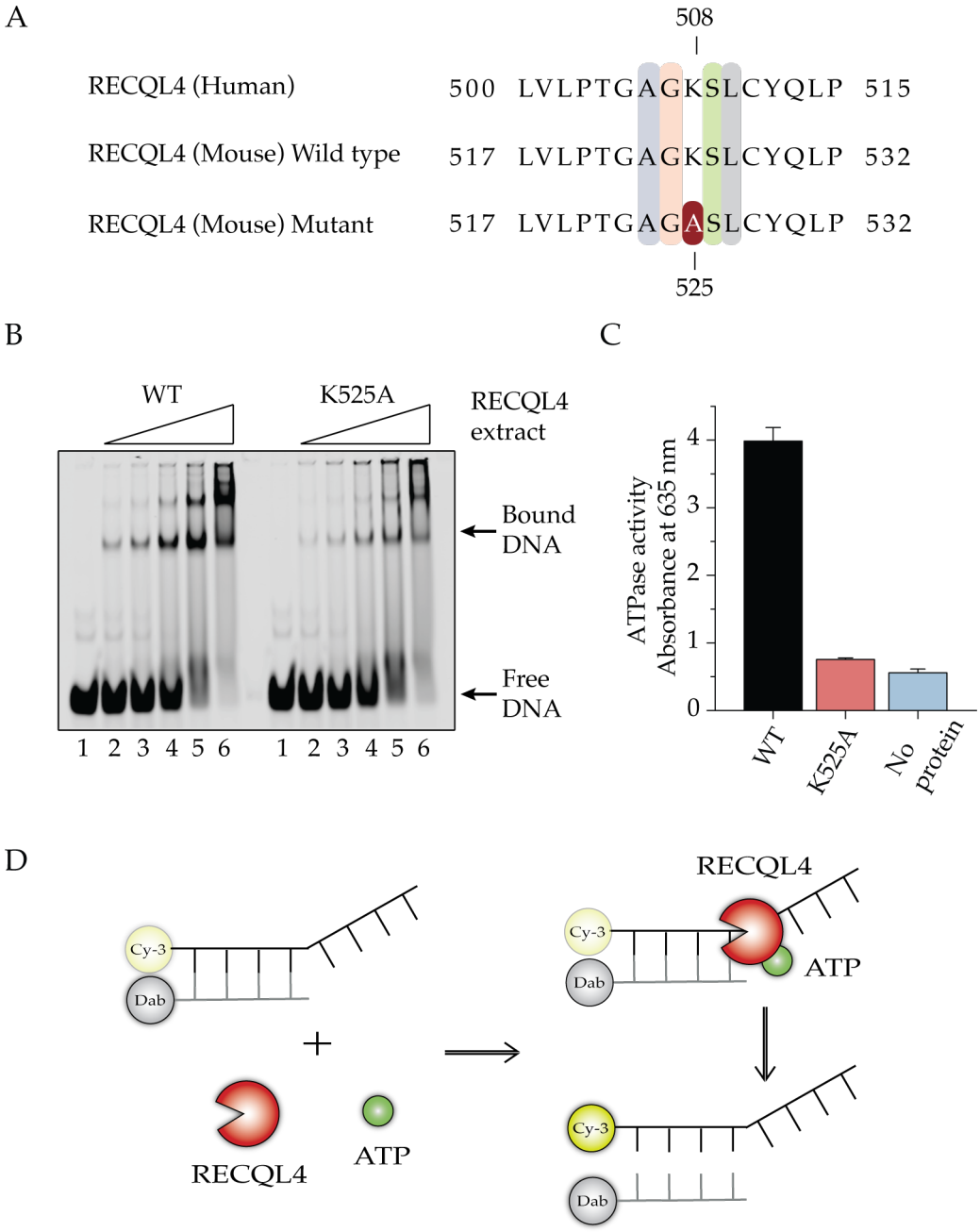

E

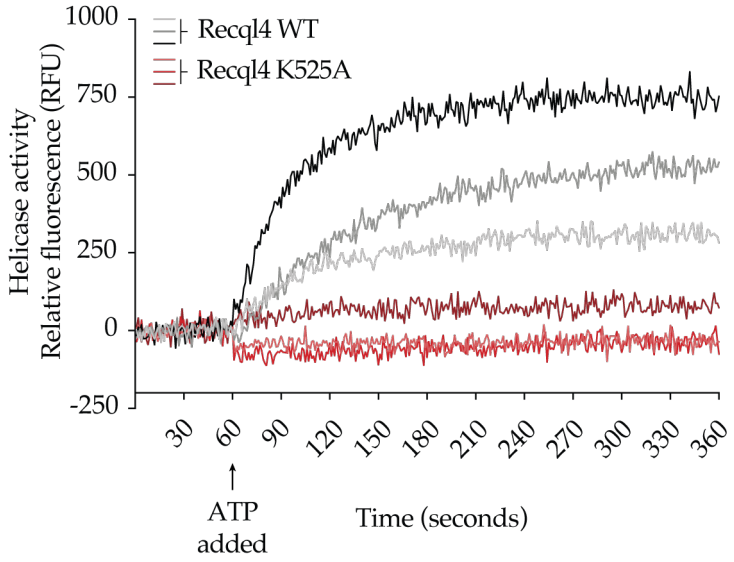

Figure 5.1: *The Recql4^{K525A} mutation results in a biochemically inactive helicase protein.* (A) Sequence homology between human and mouse RECQL4 showing the highly conserved amino acids between species. The helicase-dead mutation was achieved by replacing lysine by alanine in the 525 position in the mouse (508 in humans). (B) Electrophoretic-mobility shift assay comparing the DNA binding of WT versus K525A mutant *Recql4*. Lanes 1-6 show serial dilutions of RECQL4 protein ranging from 19 nM to 300 nM bound to 25 nM ssDNA oligo XOm1 conjugated to IRDye680. (C) *In vitro* ATPase assay of WT versus K525A mutant was obtained by measuring the absorbance at 635 nm. Proteins were assayed at 115 nM in the presence of 1 mM ATP and DNA in assay buffer. (D) Schematic representation of the fluorescence-based helicase assay. The dsDNA substrate with a ssDNA loading site is attached to a fluorescent donor (Cy-3) and a quencher acceptor (Dab). In the presence of ATP, the helicase (RECQL4) is activated and separates the two complementary strands releasing the fluorescent probe. (E) Helicase assay of WT versus K525A mutant. After recording baseline fluorescence for 60 seconds, ATP was added, and helicase activity was measured in relative fluorescence units (RFU) for three different concentrations of RECQL4 protein.

5.2.3.2 *Generation and validation of Recql4 helicase-dead mutant mice*

To understand the contribution of *Recql4* helicase activity in the phenotypes of RTS, we generated an *in vivo* knock-in model of the K525A mutation. Sequencing of the *Recql4* locus in targeted mice confirmed the change in nucleotides encoding lysine (AAG) to alanine (GCA), and the resultant introduction of a unique *Msl*I restriction enzyme site in the mutant allele (Figure 5.2 A). PCR amplification over the mutation site produced a 416 bp fragment in the wild type that was cleaved to 361 bp (+55 bp) by *Msl*I when

the mutation was present (Figure 5.2 B). Finally, to determine the expression and stability of the mutant protein *in vivo* we generated a rat monoclonal antibody against the first 200 aa from the N-terminal of murine *Recql4* (clone 3B10). The K525A mutant protein has the same predicted molecular mass (~133 kDa) as wild type RECQL4 and neither size nor abundance of the protein were affected by the mutation when assessed in thymocyte derived protein samples (Figure 5.2 C). Taken together, these results demonstrate that the loss of helicase activity does not affect the expression or stability of the RECQL4 protein *in vivo*.

5.2.3.3 *Recql4 helicase-dead mice are viable, have normal body weight and composition and normal long-term survival*

We observed a slightly sub-Mendelian ratio of homozygous $Recql4^{K525A/K525A}$ animals at weaning from heterozygous breeding pairs, although this was not statistically significant by chi-squared test (p=0.6255) (Figure 5.2 D). Heterozygous and homozygous mice for the K525A mutation were viable and outwardly normal (Figure 5.2 E). Furthermore, we observed no difference across genotypes or sexes in 10-week old animals assessed for body weight and body composition (Figure 5.2 F, G). Both male and female $Recql4^{K525A/K525A}$ animals were fertile and able to breed, and there was no difference in the survival when comparing the $Recql4^{K525A/K525A}$ and control genotypes using Kaplan Meier survival analysis (Figure 5.2 H). Collectively, these results show that unlike the embryonic lethality of *Recql4* null alleles [88, 139], the $Recql4^{K525A}$ protein supports normal development and adult homeostasis.

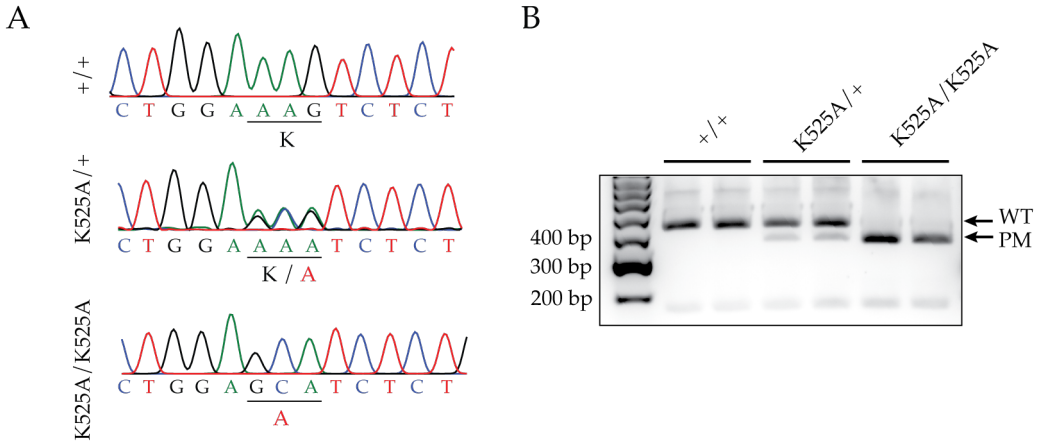

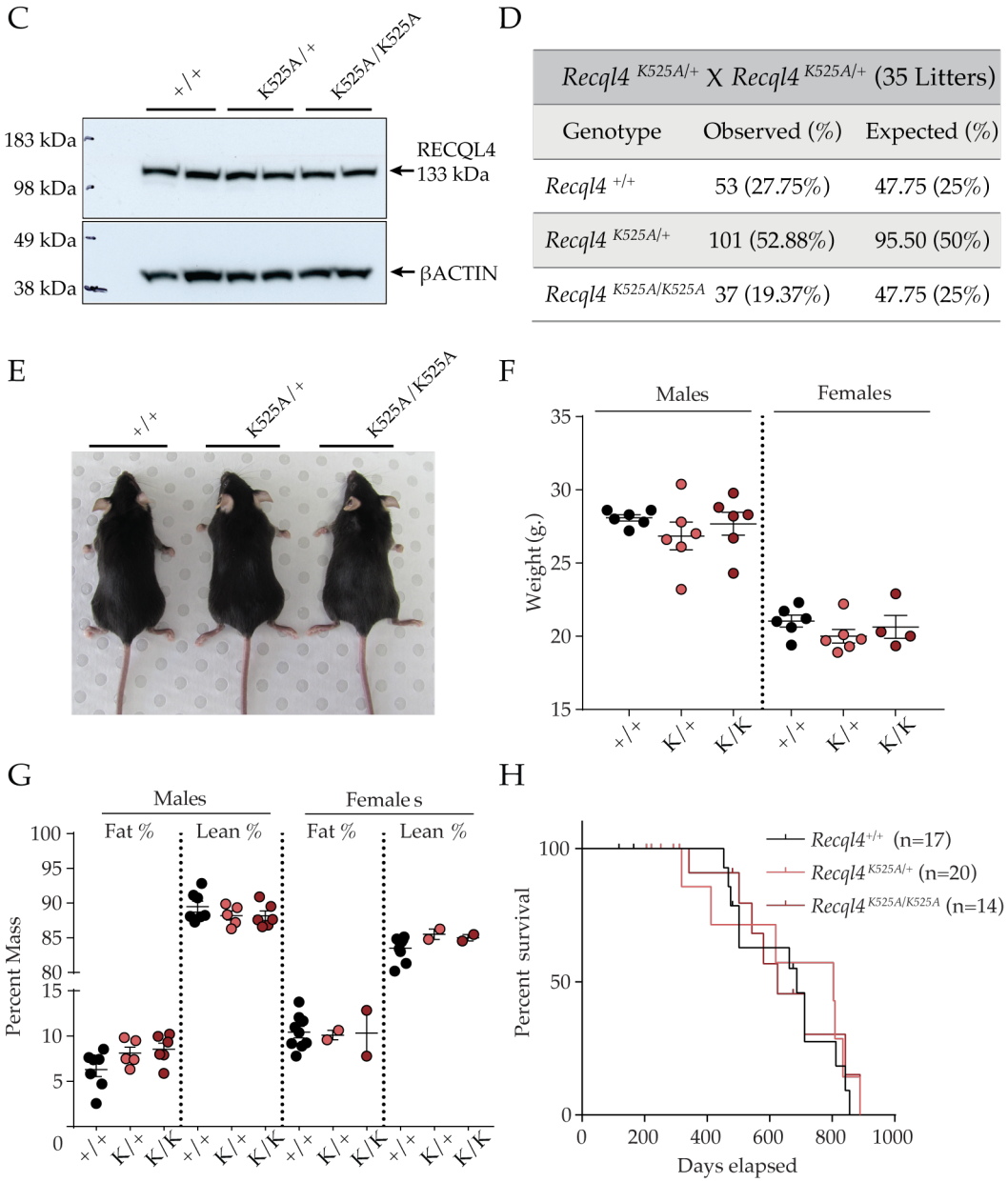

Recql4 $^{K525A/+}$ X *Recql4* $^{K525A/+}$ (35 Litters)		
Genotype	Observed (%)	Expected (%)
Recql4 $^{+/+}$	53 (27.75%)	47.75 (25%)
Recql4 $^{K525A/+}$	101 (52.88%)	95.50 (50%)
Recql4 $^{K525A/K525A}$	37 (19.37%)	47.75 (25%)

Figure 5.2: *Homozygous and heterozygous helicase-dead mice are viable, have normal body weight and composition, and normal long-term survival.*(A) Sequencing traces of the WT, heterozygous and homozygous K525A mutation. Altered nucleotide and amino acid changes are indicated above the sequence trace. (B) Genomic DNA PCR of $Recql4^{+/+}$, $Recql4^{K525A/+}$, $Recql4^{K525A/K525A}$. 2 different mice per genotype. (C) Western blot of thymocyte lysates from $Recql4^{+/+}$, $Recql4^{K525A/+}$, $Recql4^{K525A/K525A}$ 10 weeks old mice probed with anti-RECQL4 (clone 3B10; top). The same blot re-probed with anti-β-Actin (bottom). (D) Breeding data from 35 litters of $Recql4^{K525A/+}$ intercrosses. Observed and expected Mendelian rates of the indicated genotypes are shown. No statistical significance was achieved. (E) Representative photograph of male $Recql4^{+/+}$, $Recql4^{K525A/+}$, $Recql4^{K525A/K525A}$ mice. (F) Gross body weights of 10-week old male and female $Recql4^{+/+}$, $Recql4^{K525A/+}$, $Recql4^{K525A/K525A}$ mice. (G) Echo-MRI analysis of fat and lean percentage at 10 weeks of age from male and female $Recql4^{+/+}$, $Recql4^{K525A/+}$, $Recql4^{K525A/K525A}$ mice. (H) Kaplan-Meier survival plots of the indicated genotypes. K=K525A.

5.2.3.4 *RECQL4 helicase activity is not required for normal haematopoiesis*

We previously reported that somatic deletion of *Recql4* resulted in fully penetrant BM failure [88]. To determine the role of helicase activity in haematopoiesis, we assessed cohorts of adult wild type, *Recql4*$^{K525A/+}$ and *Recql4*$^{K525A/K525A}$ mice. Analysis of the PB revealed no changes in leukocyte or platelet numbers (Figure 5.3 A, B). The absolute RBC counts were subtly increased in both the K525A/+ and K525A/K525A mutants, however, the haemoglobin levels were not changed compared to the WT (Figure 5.3 C, D). Further analysis of the individual leukocyte subsets in the PB including granulocytes, macrophages, B lymphocytes, and $CD4^+$ and $CD8^+$ T lymphocytes revealed no significant differences in the proportions or absolute numbers of these populations (Figure 5.3 E).

Within the BM, the total numbers of leukocytes were comparable across genotypes (Figure 5.3 F). Similarly, granulocyte and macrophage numbers were similar (Figure 5.3 G). Within the B-lymphoid populations ($B220^+IgM^-$), the Pre-B, Pro-B, and Pre-Pro-B subpopulations were all unaltered in *Recql4*$^{K525A/+}$ and *Recql4*$^{K525A/K525A}$ compared to WT littermates (Figure 5.3 H), as were the erythroid subpopulations (Figure 5.3 I). The frequencies and absolute numbers of the primitive haematopoietic stem cells (HSCs) and progenitors were also assessed. There were no major differences in the numbers of phenotypic long-term HSCs (LT-HSC), short-term HSCs (ST-HSC) or multipotent progenitor (MPP; Lin^- c-kit^+ Sca-1^+ CD34/Flt3) fractions, nor in their myeloid committed subpopulations (Figure 5.3 J-L). There was an elevation of the phenotypic myelo-erythroid progenitor (MEP; Lin^- c-kit^+ Sca-1^- CD34/FcγRII) and colony-forming unit-erythroid (CFU-E; Lin^- LKS^- $CD41^-$ Fc$\gamma$$RII^-$ $CD150^-$ $CD105^+$) in the *Recql4*$^{K525A/+}$ animals, however, the absolute change was very small and not statistically significant in the *Recql4*$^{K525A/K525A}$ mice. The basis for this mild elevation in RBC counts and committed erythroid progenitors is currently undefined. In summary, unlike for complete deletion of RECQL4, the abrogation of RECQL4 helicase activity does not substantively perturb haematopoiesis *in vivo*.

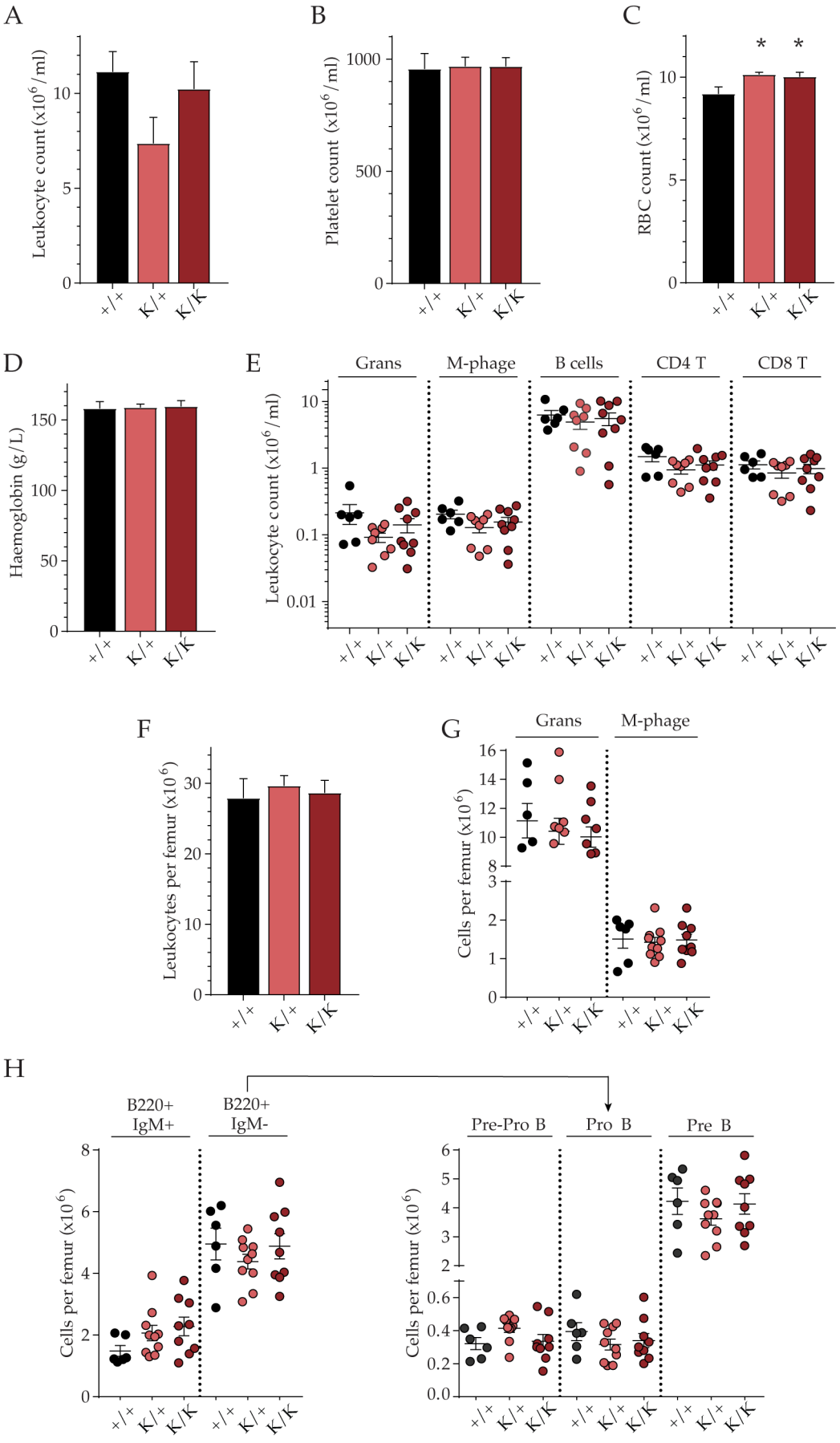
A
Leukocyte count (x10^6/ml)
B
Platelet count (x10^6/ml)
C
RBC count (x10^6/ml)
D
Haemoglobin (g/L)
E
Grans
M-phage
B cells
CD4 T
CD8 T
Leukocyte count (x10^6/ml)
F
Leukocytes per femur (x10^6)
G
Grans
M-phage
Cells per femur (x10^6)
H
B220+ IgM+
B220+ IgM-
Pre-Pro B
Pro B
Pre B
Cells per femur (x10^6)
+/+
K/+
K/K

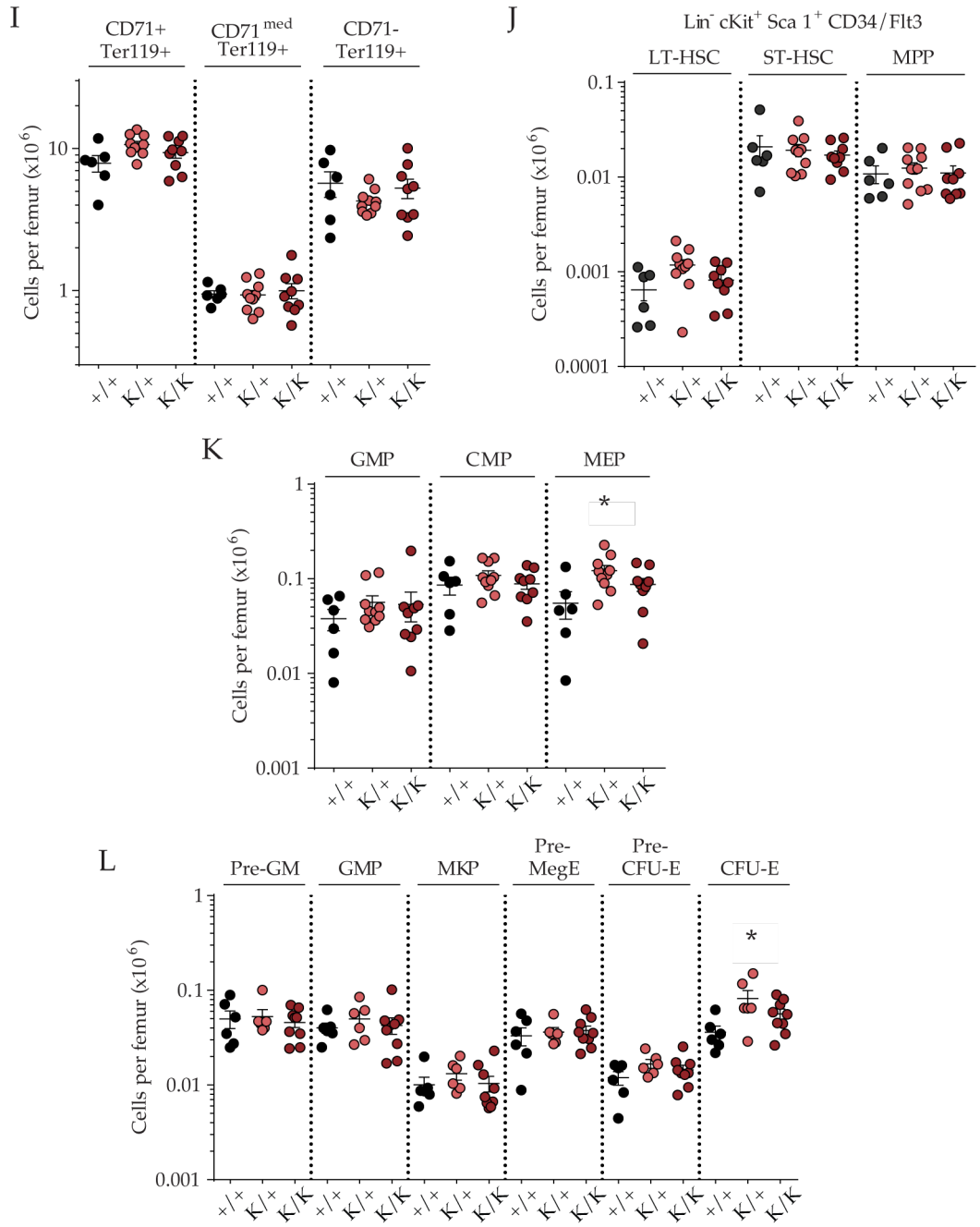

Figure 5.3: *The ATP-dependent helicase function of Recql4 is not required for normal haematopoiesis in vivo.* (A) Leukocyte counts in the PB of *Recql4*$^{+/+}$, *Recql4*$^{K525A/+}$, *Recql4*$^{K525A/K525A}$ 10-week old mice. (B) Platelet count. (C) RBC count. (D) Haemoglobin. (E) Numbers of granulocytes, macrophages, B cells, CD4 T cells, and CD8 T cells in PB. (F) Leukocyte counts in BM. (G) Absolute numbers of granulocytes and macrophages in BM. (H) Mature (B220^{+} IgM^{+}), immature (B220^{+} IgM^{-}) B lymphocytes, and subsets of immature B lymphocytes per femur. (I) Erythroid fractions based on CD71/Ter119 staining per femur. (J) HSC and primitive progenitors based on Lin^{-} c-kit^{+} Sca-1^{+} CD34/Flt3 staining per femur. (K) Myeloid progenitor subpopulations in the BM. (L) Myeloid, erythroid and megakaryocyte progenitor frequency per femur. Data expressed as mean ± SEM, Student's t test. *P<0.05; n≥6 per genotype. Experiments were independently executed on separate cohorts, with results pooled for presentation. K=K525A.

5.2.3.5 *ATP-dependent helicase function is not required for B and T cell development*

Our previous work demonstrated that the human helicase dead RECQL4 (K508A) was able to rescue *in vitro* B and T cell development from murine *Recql4*$^{\Delta/\Delta}$ haematopoietic cells [88]. To determine if this was also the case *in vivo*, T and B cell development was assessed from thymocytes and splenocytes respectively in 10-week-old mutant and WT mice. There was no difference in thymus cellularity or in the numbers of double-positive CD4^{+}/CD8^{+} nor the mature single positive CD4^{+} and CD8^{+} cells (Figure 5.4 A, B). Analysis of early intra-thymic progenitor cells (double negative DN1-4) found no difference in the *Recql4*$^{K525A/K525A}$ compared to the WT littermates (Figure 5.4 C). In the spleen, there was no significant difference in the cellularity or number of mature B cells (Figure 5.4 D, E). To determine the proportion of B cells in the follicular (FO) and marginal zone (MZ) of the white pulp of the spleen, we divided splenic cells with high expression of B220 and CD19 followed by analysis of CD21/CD23 expression (FO B cells: CD21^{low} CD23^{high}; MZ B cells: CD21^{high} CD23^{low}). No shift of B cells in the follicular or marginal zone compartments was apparent (Figure 5.4 F). Therefore, consistent with the prior retroviral rescue data *in vitro*, the ATP-dependent helicase function of RECQL4 is not required for B or T cell development and homeostasis in adult mice.

Given the role of RecQ helicases in repair of DNA damage [198], we sought to determine if there was a function for the ATP-dependent helicase activity of RECQL4 during physiologically induced DNA damage occurring following B cell stimulation. We isolated mature B cells from WT, *Recql4*$^{K525A/+}$ and *Recql4*$^{K525A/K525A}$ spleens and stimulated them *in vitro* using bacterial lipopolysaccharide (LPS) and rmIL-4 to induce proliferation and immunoglobulin gene (*Ig*) class switch recombination. The proliferation of the cells in response to LPS was the same irrespective of RECQL4 helicase status as measured by cell-trace violet dilution kinetics (Figure 5.4 G, H). Additionally, the *Recql4*$^{K525A/K525A}$ cells underwent normal class switching to IgG1 (Figure 5.4 I). Therefore, maturation, physiological activation,a induced proliferation, DNA damage, and immunoglobulin rearrangement of B cells do not require the helicase activity of RECQL4.

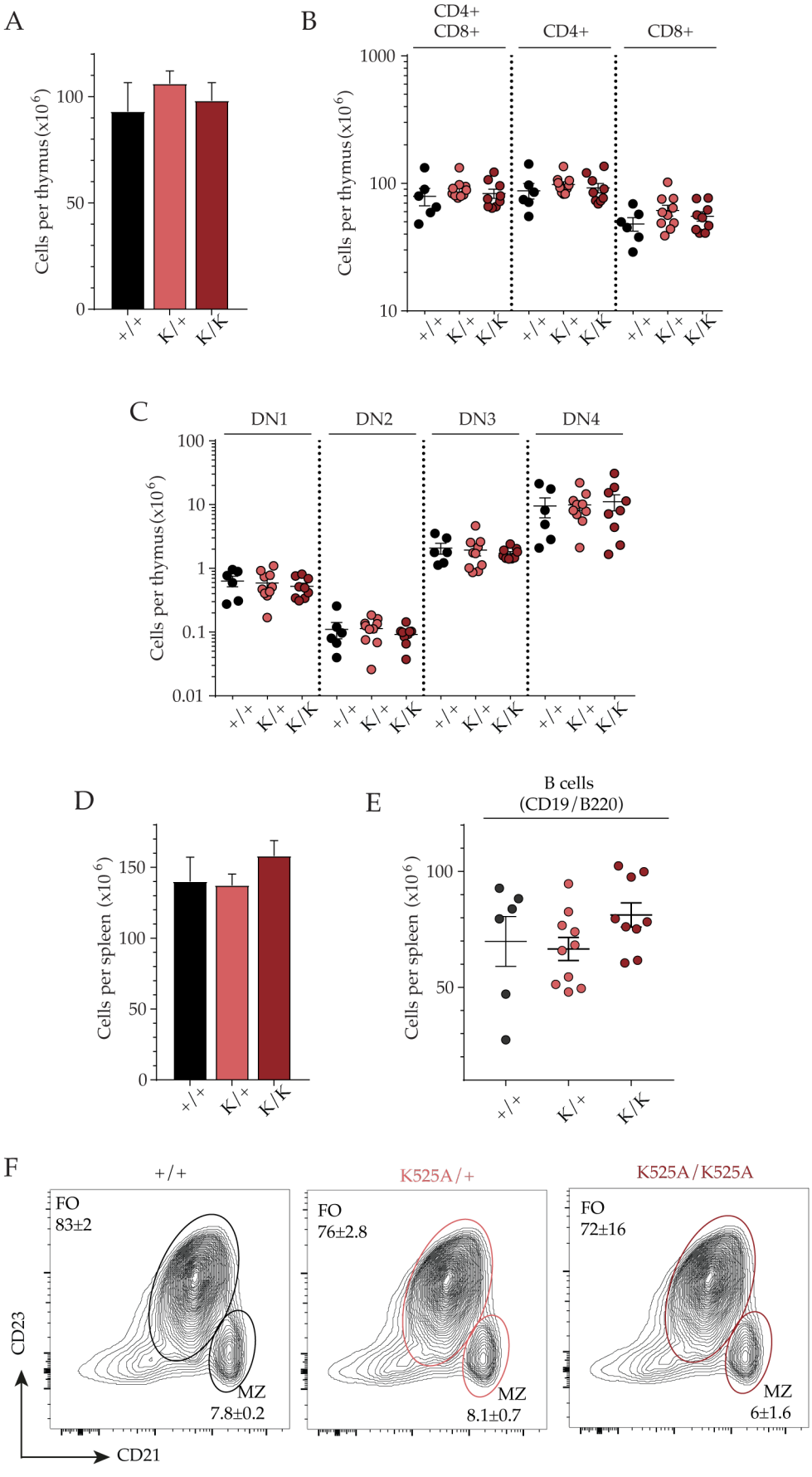
A
Cells per thymus (x10^6)
100
50
0
+/+
K/+
K/K
B
CD4+
CD8+
CD4+
CD8+
Cells per thymus (x10^6)
1000
100
10
C
DN1
DN2
DN3
DN4
Cells per thymus (x10^6)
100
10
1
0.1
0.01
D
Cells per spleen (x10^6)
150
100
50
0
E
B cells
(CD19/B220)
Cells per spleen (x10^6)
100
50
F
+/+
K525A/+
K525A/K525A
FO
83±2
MZ
7.8±0.2
FO
76±2.8
MZ
8.1±0.7
FO
72±16
MZ
6±1.6
CD23
CD21

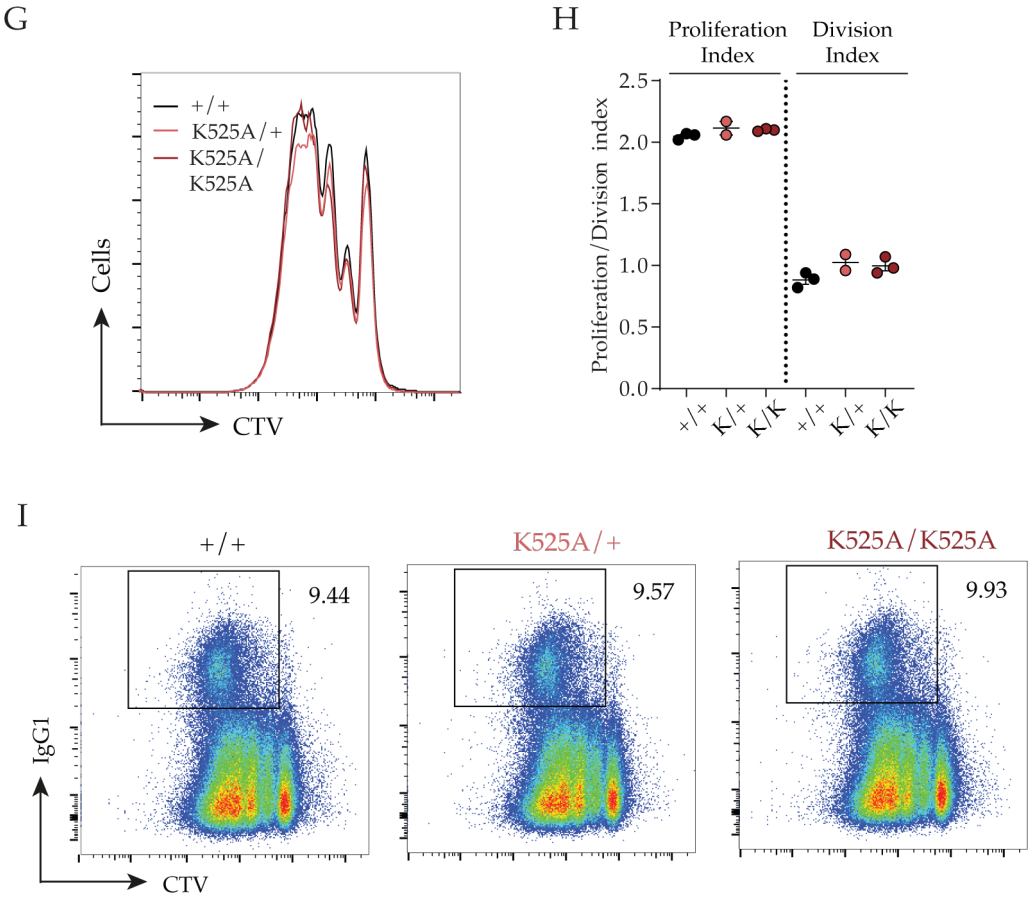

Figure 5.4: *ATP-dependent helicase function of Recql4 is not required for B or T cell development.* (A) Leukocyte counts in thymus. (B) Absolute numbers of double positive CD4/CD8, $CD4^+$, and $CD8^+$ T lymphocytes in thymus. (C) T cell progenitor populations (DN1-DN4). (D) Leukocyte counts in spleen. (E) B lymphocytes in spleen. (F) Representative (n=2 mice per genotype) FACS plots of $B220^+$ $CD19^+$ gated splenocytes stained for follicular (FO, $CD23^{high}$ $CD21^{low}$) and marginal zone (MZ, $CD21^{high}$ $CD23^{low}$) B cells. Numbers indicate cells $x10^6$ per spleen. (G) CellTrace Violet (CTV) dilution in purified B cells treated for 96 hours with 15 μg/ml LPS + 10 ng/ml IL4. Representative examples of n=3 mice per genotype. (H) Quantification of cell division (average division per cell in culture) and proliferation (average division/per dividing cell in culture) indices. n=3 mice per genotype. (I) In vitro class-switch recombination to IgG1 in purified B cells treated as in panel B. Representative examples of n=2 mice per genotype. Data expressed as mean $\pm$ SEM, Student's t test (A-E). Experiments were independently executed on separate cohorts, with results pooled for presentation. K=K525A.

5.2.3.6 *The K525A mutation does not alter sensitivity to DNA damaging agents in vitro*

To further test the requirement for RecQ helicase activity we compared the response to DNA damaging agents *in vitro*. For these studies, we established GM-CSF dependent myeloid progenitor cell lines from *R26*-CreER^{T2} *Recql4*$^{fl/K525A}$ and *R26*-CreER^{T2} *Recql4*$^{fl/+}$ (control genotype) by immortalisation with HoxB8 [187]. To allow analysis of the requirement for RecQ helicase activity, the cells were treated with tamoxifen for 4 days to activate Cre-mediated deletion of the loxP flanked wild type *Recql4* (Recql4^{fl}) allele. This resulted in the cells either becoming *Recql4* heterozygous (*Recql4*$^{\Delta/+}$) or expressing only the K525A mutant allele (*Recql4*$^{\Delta/K525A}$). Isogenic cells from each genotype (pre-treated with tamoxifen for 4 days or untreated) were seeded in 96-well plates and the response to four different genotoxic agents was assessed: doxorubicin (topoisomerase II inhibitor), hydroxyurea (ribonucleotide reductase inhibitor), 4-nitroquinoline (oxidative DNA damage) and topotecan (topoisomerase I inhibitor). Cell viability was measured after 48 hours using the CellTiter-Glo Luminescent assay. As shown in Figure 5.5 A-D, *R26*-CreER^{T2} *Recql4*$^{\Delta/K525A}$ had a comparable IC^{50} to Doxorubicin, Hydroxyurea, 4-Nitroquinoline, and Topotecan as the non-tamoxifen treated isogenic controls (Figure 5.5 A-D and Supp. Figure 5.1). Additionally, *R26*-CreER^{T2} *Recql4*$^{\Delta/+}$ showed a similar IC^{50} to Doxorubicin, Hydroxyurea, and Topotecan, except for 4-Nitroquinoline, which exhibited a mildly increased resistance in the tamoxifen-treated cells in comparison to the non-tamoxifen treated controls. These results indicate that the role of RECQL4 in non-physiological, pharmacologically induced DNA repair does not depend on its helicase activity.

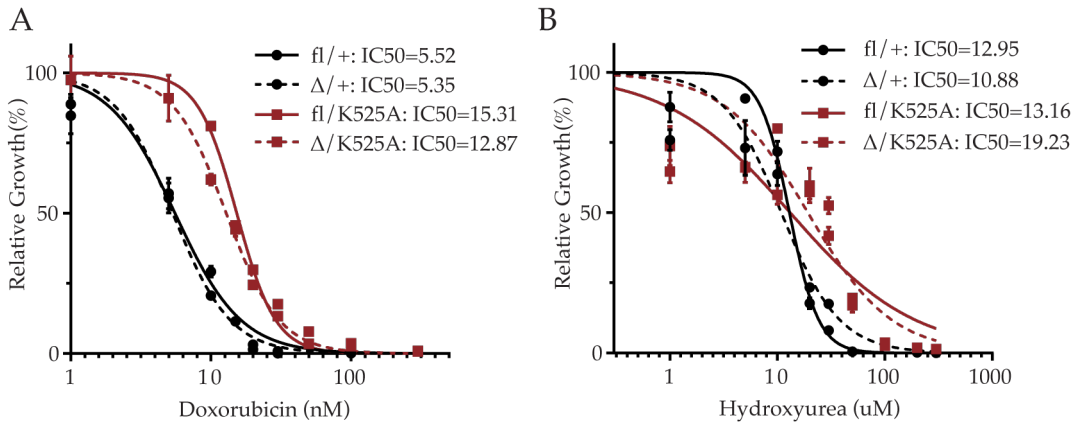

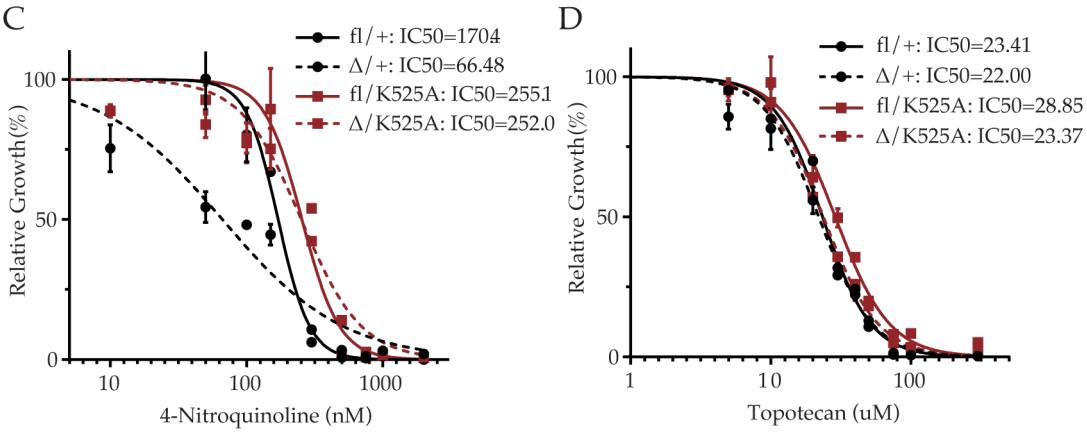

Figure 5.5: *In vitro sensitivity to DNA damaging agents is not modified by helicase-dead mutation.* Dose-response curves for relative growth rate of HoxB8 immortalised *R26*-CreER^{T2} *Recql4*$^{fl/K525A}$ (red) and *R26*-CreER^{T2} *Recql4*$^{fl/+}$ (black). Dotted lines represent cells expressing the K525 mutant only after the floxed allele was excised by tamoxifen addition. Cells were incubated for 48 hours with the following drugs: (A) Doxorubicin. (B) Hydroxyurea. (C) 4-Nitroquinoline. (D) Topotecan. The calculated IC^{50} values are stated for each genotype/treatment.

5.2.3.7 *Truncating mutations, but not helicase inactivation, of RECQL4 are pathogenic*

The results so far establish that the ATP-dependent helicase activity of RECQL4 is not essential *in vivo*. To directly compare the effects of having a protein truncating/hypomorphic allele compared to a helicase-dead full-length RECQL4 protein, we established three additional point mutant alleles (Figure 5.6 A). The G522EfsX43 truncated mutation was generated as a co-incidental mutation during the CRISPR/Cas9 mediate generation of the K525A allele and maps closely to the relatively common RTS associated mutations in human *RECQL4*, S523TfsX35 and C525AfsX33 [56]. We also identified an ENU mutagenesis induced truncated mutation R347X (R355 in humans). Three RTS patients have been reported with p.Arg350GlyfsX21 mutations, mapping closely to this allele (Supp. Figure 5.2) [56]. A second ENU induced mutation, M789K mutation (V767 in human), was identified and used as a control for mutations within the *Recql4* locus as this mutation was predicted to be benign. We crossed all the individual point mutant alleles (M789K, K525A, G522Efs and R347X) to the *R26*-CreER^{T2} *Recql4*$^{fl/fl}$ line that we previously described and assessed the *R26*-CreER^{T2} Recql4$^{fl/PM}$ in parallel with the *R26*-CreER^{T2} *Recql4*$^{fl/+}$ and *R26*-CreER^{T2} *Recql4*$^{fl/fl}$

allele [88]. At 8-10 weeks of age, mice were fed tamoxifen containing chow for 30 days to activate the Cre mediated deletion of the wild type *Recql4* floxed allele broadly throughout the body. Using this experimental design, the tamoxifen-treated *R26*-CreER^{T2} *Recql4*$^{fl/fl}$ animals (completely RECQL4 deficient) developed fully penetrant BM failure [88]. The efficiency of *Recql4* deletion was confirmed by PCR for genomic recombination (Supp. Figure 5.3).

Analysis of PB (Figure 5.6 B, C) showed an approximately 50% reduction in leukocytes and erythrocytes in mice expressing the truncating mutations G522Efs and R347X, very similar to mice rendered null for RECQL4 protein expression (*Recql4*$^{\Delta/\Delta}$). The K525A and M789K mutation, as well as the heterozygous (*Recql4*$^{fl/+}$) control, did not show any significant changes in leukocyte or erythroid indices. In addition, analysis of individual lineages within the PB showed a similar pattern across granulocytes, B lymphocytes, and CD4$^+$ and CD8$^+$ T lymphocytes in the truncating and null mutant (Figure 5.6 D). When the BM was analysed, leukocytes and erythroid precursors (CD71$^+$ Ter119$^+$) from *R26*-CreER$^{ki/+}$ *Recql4*$^{\Delta/G522Efs}$ and *Recql4*$^{\Delta/R347X}$ mice showed a dramatic decrease, consistent with the BM failure phenotype we had previously described in *Recql4*$^{\Delta/\Delta}$ (Figure 5.6 E, F). The *Recql4*$^{\Delta/+}$ and K525A and M789K only expressing animals did not develop any phenotype after 30 days of treatment with tamoxifen and, whilst developing a pan-cytopenia in PB and BM, seven of eight G522Efs mice were still alive at the end of the treatment. In contrast, mice expressing the most severely truncating R347X allele developed a profound BM failure and three of five required euthanasia prior to 30 days of treatment, a phenotype similar to complete loss of RECQL4 protein (Figure 5.6 G). Collectively, these analyses establish that the ATP-dependent helicase is not required for the physiological functions of RECQL4 *in vivo*, however, mutations resulting in truncated protein products are deleterious.

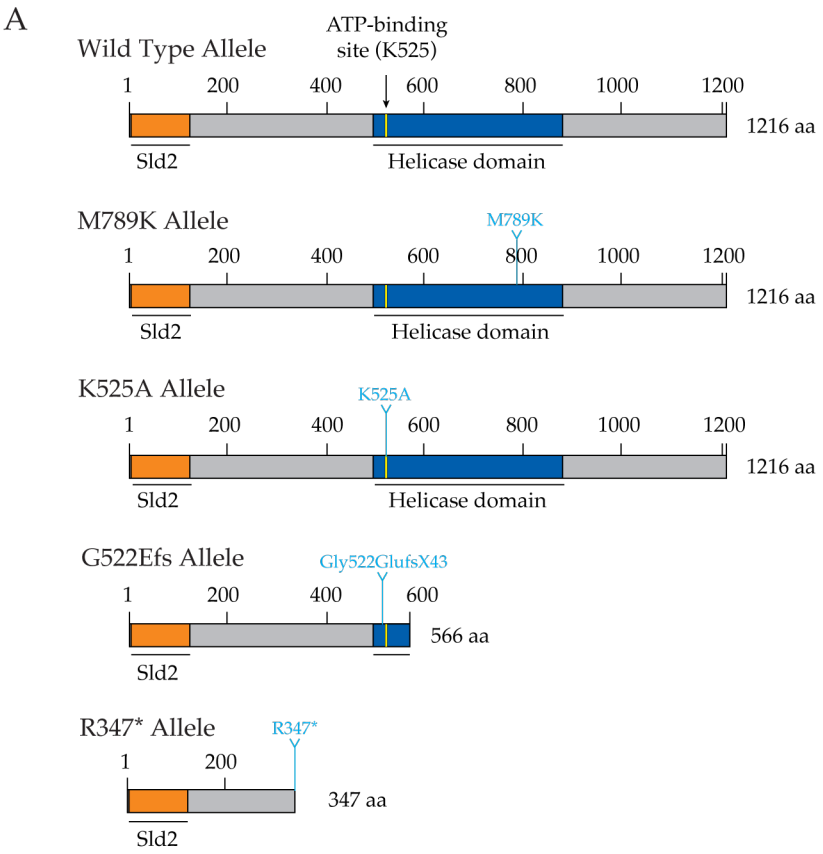
A
Wild Type Allele
ATP-binding site (K525)
1 200 400 600 800 1000 1200
1216 aa
Sld2
Helicase domain
M789K Allele
M789K
1 200 400 600 800 1000 1200
1216 aa
Sld2
Helicase domain
K525A Allele
K525A
1 200 400 600 800 1000 1200
1216 aa
Sld2
Helicase domain
G522Efs Allele
Gly522GlufsX43
1 200 400 600
566 aa
Sld2
R347* Allele
R347*
1 200
347 aa
Sld2

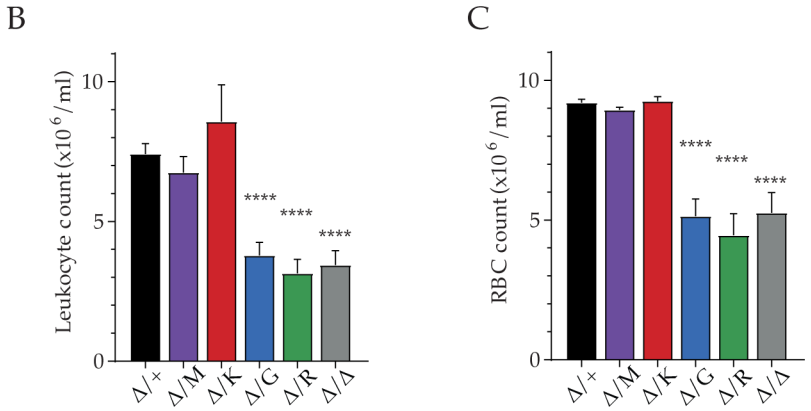
B
Leukocyte count (x10 6 /ml)
10
5
0
****
****
****
Δ/+ Δ/M Δ/K Δ/G Δ/R Δ/Δ
C
RBC count (x10 6 /ml)
10
5
0
****
****
****
Δ/+ Δ/M Δ/K Δ/G Δ/R Δ/Δ

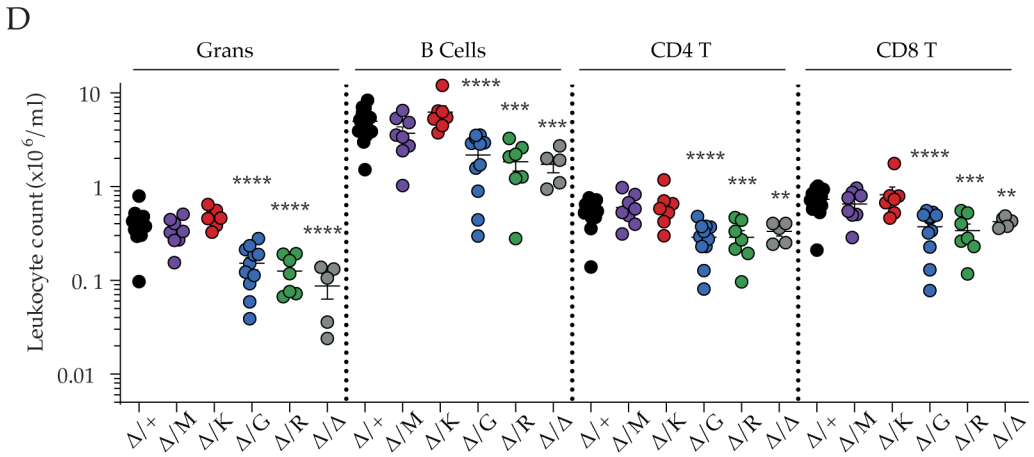
D
Grans
B Cells
CD4 T
CD8 T
Leukocyte count (x10 6 /ml)
10
1
0. 1
0.01
Δ/+ Δ/M Δ/K Δ/G Δ/R Δ/Δ

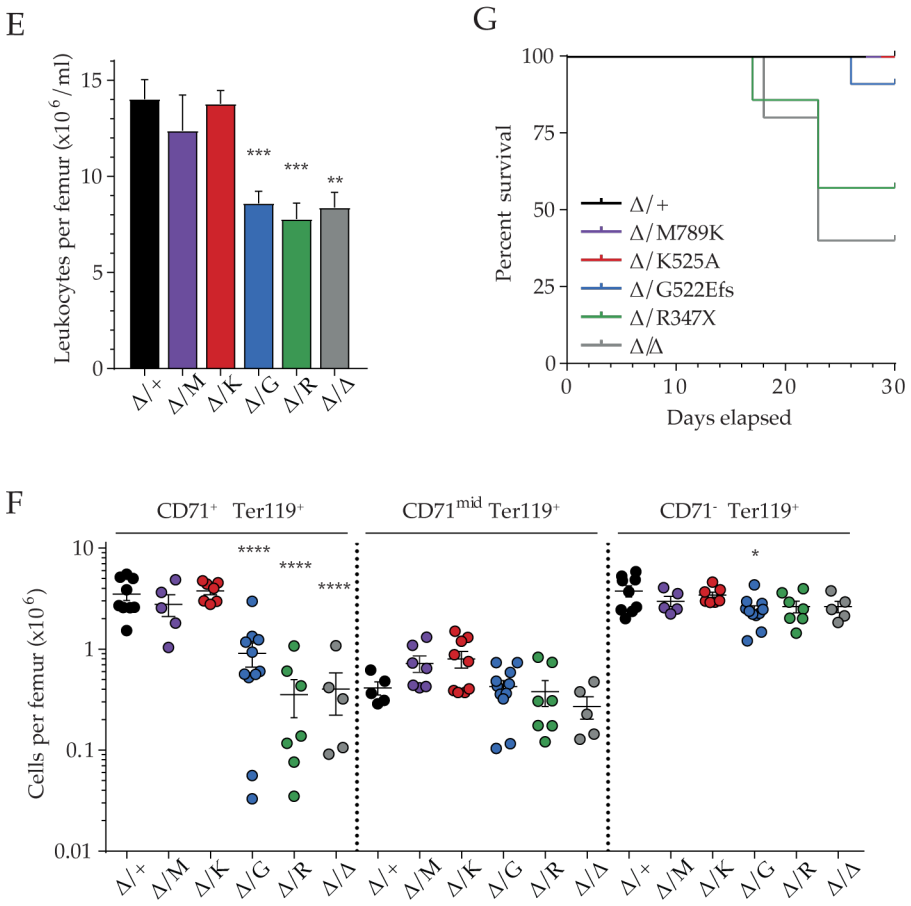

Figure 5.6: *Truncating mutations, but not helicase inactivation, result in deleterious effects.* (A) Schematic representation of the *R26*-CreER^{T2} Recql4$^{fl/PM}$ murine alleles used in this study. (B) Leukocyte counts in PB. (C) RBC counts in PB. (D) Absolute numbers of leukocyte subsets in PB. (E) Leukocyte counts in BM. (F) Erythroid fractions based on CD71/Ter119 staining per femur. (G) Kaplan-Meier survival plots of the indicated genotypes in days on Tamoxifen food. All data are from day of sacrifice and expressed as mean ± SEM, Student's t test. *P<0.05; **P<0.01; ***P<0.001; ****P<0.0001; n≥6 per genotype (B-F). Experiments were independently executed on separate cohorts, with results pooled for presentation. M=M789K; K=K525A; G=G522Efs; R=R347X.

5.2.4 *Discussion*

The N-terminal Sld2-domain of RECQL4 protein is unique amongst RecQ family members and has been shown to be critical for the initiation of DNA replication in chicken, *Drosophila*, *Xenopus* and human cells [114, 167, 169, 170, 200], mostly likely through Sld2-domain dependent recruitment of the MCM10 and CTF4 factors to origins of replication [201]. The importance of the Sld2-domain to cell viability is reflected in the mutation spectrum detected in RTS patients – it is rarely mutated and always intact in at least

one allele [56]. These findings implied that RTS and related disorders were caused by the loss of activity of the canonical ATP-dependent helicase domain, whose role in the replication initiation function is less clear. While initial *in vitro* studies using purified full-length human RECQL4 protein did not detect any unwinding potential on long DNA substrates [166], it was later shown that RECQL4 could unwind shorter duplex regions if a single strand-loading region was provided [23, 168]. This activity, together with the single-stranded DNA dependent ATP hydrolysing activity, was lost in human Walker motif mutants RECQL4^{K508A} and ^{D605A}. We now demonstrate that the murine *Recql4*^{K525A} mutant protein is able to bind DNA but cannot hydrolyse ATP nor unwind DNA substrates, confirming that the mutant is helicase-dead and the homologue of human RECQL4^{K508A}. Unexpectedly, however, we found that this protein behaved comparably to wild type RECQL4 in supporting viability, fertility and normal physiological development of mice. No phenotypes or symptoms consistent with RTS were observed. Perhaps more surprising, was the normal response of *Recql4*$^{K525A/K525A}$ cells in replication, and in their response to both physiologically or exogenously induced DNA damage.

The most highly conserved domain of the RecQ helicases is the ATPase core. By analogy to multiple other DNA helicases (reviewed in ref. [202]), it was assumed that the ATP-dependent helicase activity of RECQL4 is essential for normal cellular DNA metabolism. Several studies have reported findings consistent with this interpretation. Complementation experiments in *Drosophila* showed that the helicase-dead K898N mutant could not rescue the viability of RecQ4 null mutants [174]. Similarly, a helicase-inactive human D605A mutant could not restore replication of x*Recql4* depleted cells in *Xenopus* egg extracts [170]. Murine studies to date have only assessed complete nulls or severe hypomorphic alleles. The deletion of the exons that precede the helicase domain (exons 5-8) resulted in embryonic lethality by day 3-6 and a significantly truncated protein with no helicase or C-terminal domain [139]. When the entire helicase domain was deleted (exons 9-13; in-frame deletion), mice were viable but showed high rates of perinatal lethality [159] and a truncated protein product of 480 aa was predicted. With the aim to maintain an intact protein, a study replaced the last helicase coding exon (13) with a neomycin cassette. 95% of animals died within 2 weeks after birth and a substantial number of short transcripts covering exon 1 to 12 were re-

ported, encoding potentially truncated products [177]. Since all these models effectively create proteins that lack the helicase and C-terminal domain, it is unclear if the observed phenotype could be attributed to the absence of the helicase domain only. Our study demonstrates that mice carrying the K525A helicase-dead mutation, with a stable full-length RECQL4 protein, were viable and fertile with no apparent phenotype.

A range of prior *in vitro* studies have pointed to the importance of the N-terminal Sld2-like region. Lethality of RECQL4-depleted chicken cells was rescued by expression of the N-terminal region only [169]. In addition, the N-terminal domain of RECQL4 was shown to physically interact with several proteins involved in DNA replication in *Xenopus laevis* and human cell extracts [115, 203]. In our *in vivo* experiments however, we have shown that one copy of the N-terminal region alone (R347X or G522Efs) is insufficient for viability, indicating that a certain level of expression or localisation of full-length RECQL4 protein is required even if it has no ATP-ase or unwinding capacity.

The high frequency of chromosome abnormalities found in cells from RTS patients and the increased cancer incidence rates suggest that RECQL4 may have a role in maintaining genome stability through DNA repair [67]. Prior studies have attributed several DNA repair functions of RECQL4 to its ATP-dependent helicase region, but they also have noted participation of the N-terminal region. Lu *et al.* found that a helicase-dead K508M could not rescue the loss of DNA end resection and HR repair after RECQL4 siRNA knockdown, suggesting that the ATP-dependent helicase function of RECQL4 is involved in HR [146]. However, they also showed that it is the N-terminus of RECQL4 that physically interacts with MRN and CtIP [204]. In a similar fashion, a role for RECQL4 in NHEJ was linked to its interaction with the Ku70-80 by the N-terminal domain [148]. RECQL4 deficiency has been associated with modulation of core proteins involved in BER such as POLB, FEN1, and APE1. The latter has shown to specifically interact with the N-terminal region of RECQL4 [142]. Herein, we observed no differences in the sensitivity of helicase-dead mutant cells compared to WT cells in response to various kinds of DNA damage (NHEJ, MMEJ, and HR for doxorubicin, BER for hydroxyurea, NER and BER for 4-nitroquinoline, and BER/SSBR for topotecan). Taken together, there was no evidence for a role of the ATP-

dependent function of RECQL4 in the repair of pathological environmentally induced DNA damage.

A recent study showed that RECQL4-depleted U2OS cells were also deficient in ATM-dependent checkpoint activation in response to drug-induced DNA DSBs. Complementation assays using helicase-inactive point mutants in Walker A (K508G) or Walker B motif (D605A and E606A) further indicated that this was the result of a lack of helicase activity [147]. The ATM pathway plays an equally important role in the physiological processes of DSB repair and recombination, such as V(D)J recombination in T cell development and class switch recombination in B cell activation [205–207]. In our *in vivo* analysis we did not detect any defect in T cell maturation at the $CD4^+/CD8^+$ double-positive to $CD4^+$ and $CD8^+$ single-positive transition or any earlier stage, nor did the mice develop any T cell lymphomas as a result of chromosomal anomalies. In addition, *in vitro* B cell activation and class switch recombination in helicase-dead splenic B lymphocytes was indistinguishable from that in WT cells, arguing that the helicase activity is not required for either physiological checkpoint activation or DNA damage repair.

RTS patients, however, usually present with compound heterozygous mutations. It was reported that in 46% of RTS patients compound heterozygous mutations were present in the *RECQL4* gene [56]. The majority of these mutations affect the helicase and C-terminal region and are predicted to create truncated proteins caused by an early stop codon, frameshift, or missplicing [56]. The phenotypes in RTS patients, although grossly similar, can vary widely in severity. The relatively common C525AfsX33 (12 alleles) for example, has been found in all three syndromes (RTS, RAPADILINO and BGS) and no single mutation has been assigned to a specific set of clinical features. In our study, we demonstrate that mice carrying a sole truncating mutation (G522Efs and R347X) presented with a BM failure reminiscent of the *Recql4* null. This was not seen in the helicase-dead K525A, the M789K or the WT heterozygous null mice. Furthermore, when we assessed BM, PB, thymus, and spleen from heterozygous and homozygous K525A helicase-dead mutants, we did not find any significant change. A similar observation was made for the human WRN helicase. A naturally occurring single nucleotide polymorphism (R834C) was shown to have less than 10% of the WT helicase activity, but normal exonuclease activity. None of the heterozygous or homozygous carriers of this mutation developed Werner Syndrome (as defined

by the clinical phenotype), clearly separating the WRN helicase function from other WRN functions [208]. Our findings demonstrate that the helicase activity of RECQL4 is also not required *in vivo* in mammals.

Although the *in vivo* studies reported herein support a conclusion that the ATP-dependent helicase activity of RECQL4 is not essential for replication or viability, this study has some limitations. First, it is possible that other RecQ helicase members increase their expression in an attempt to compensate for the loss of RECQL4 helicase activity. The expression levels of other RecQ helicases have not been measured in this study. Second, it is also possible that other proteins, outside of the RecQ family, are rescuing the phenotypes caused by the ATP-dependent helicase inactive mutation. However, given our limited understanding of the molecular basis of RTS, this remains unknown.

Collectively, this study has demonstrated the ATP-dependent helicase activity of RECQL4 is not physiologically essential for murine embryonic development or adult homeostasis, cellular replication and physiological DNA damage repair. However, mutations that create truncating proteins are not tolerated. Further studies will have to be performed to elucidate the complex interactions of *Recql4* mutations, their role in RTS and the contribution of the individual RECQL4 domains to its normal physiological function.

5.2.5 *Supporting information*

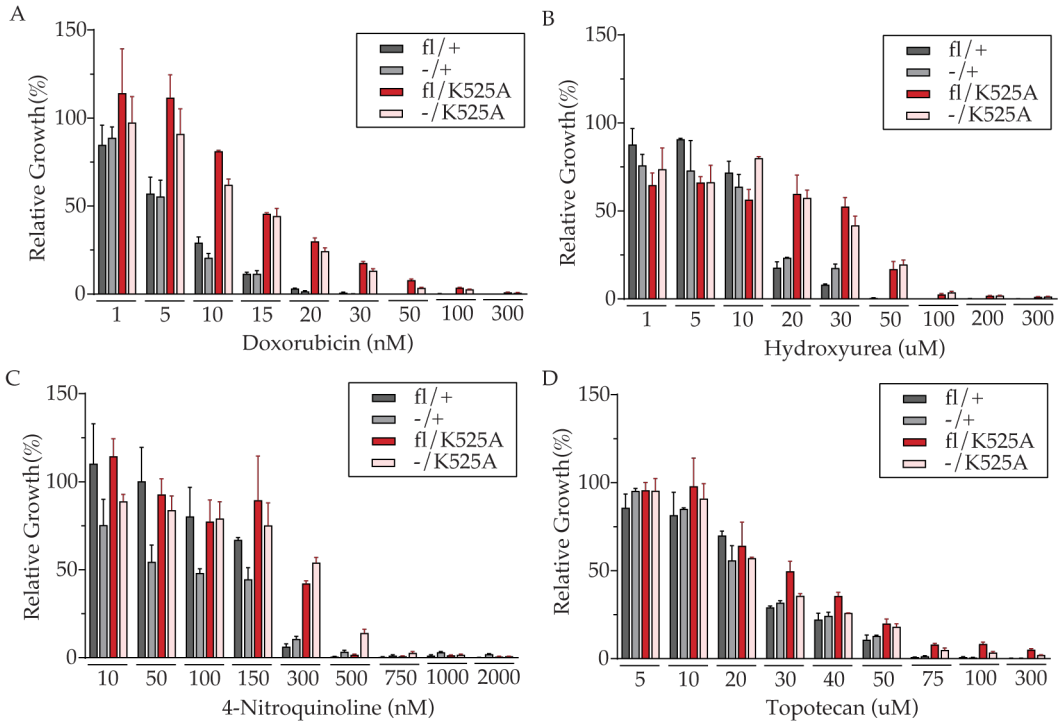

Supp. Figure 5.1. Drug Assays - Individual Doses Dataset. Data showing the response to each individual drug dose used to calculate the IC^{50} values in Figure 5.5 from *R26*-CreER^{T2} *Recql4*$^{\Delta/K525A}$ and *R26*-CreER^{T2} *Recql4*$^{\Delta/+}$ with the non-tamoxifen treated isogenic controls. The X axis shows the individual drug doses of (A) Doxorubicin, (B) Hydroxyurea, (C) 4-Nitroquinoline, (D) Topotecan.

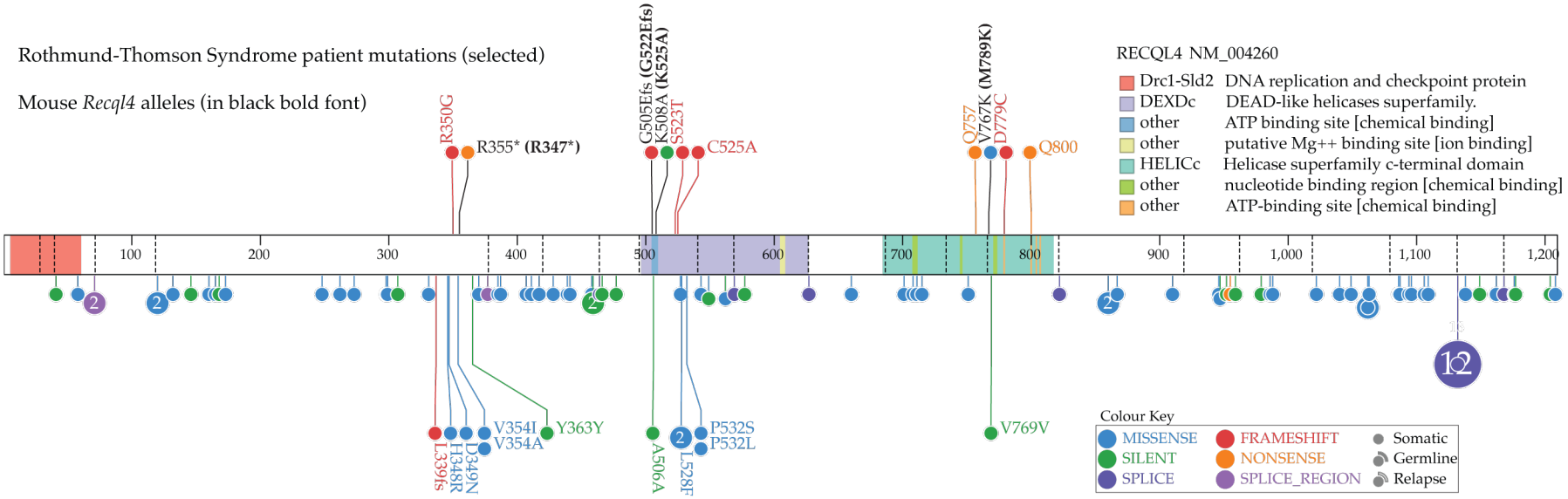

Supp. Figure 5.2. RECQL4 mutations in COSMIC database (110 mutations; somatic mutations). Data from COSMIC database. Image generated using Protein painter (Pecan portal St Jude's).

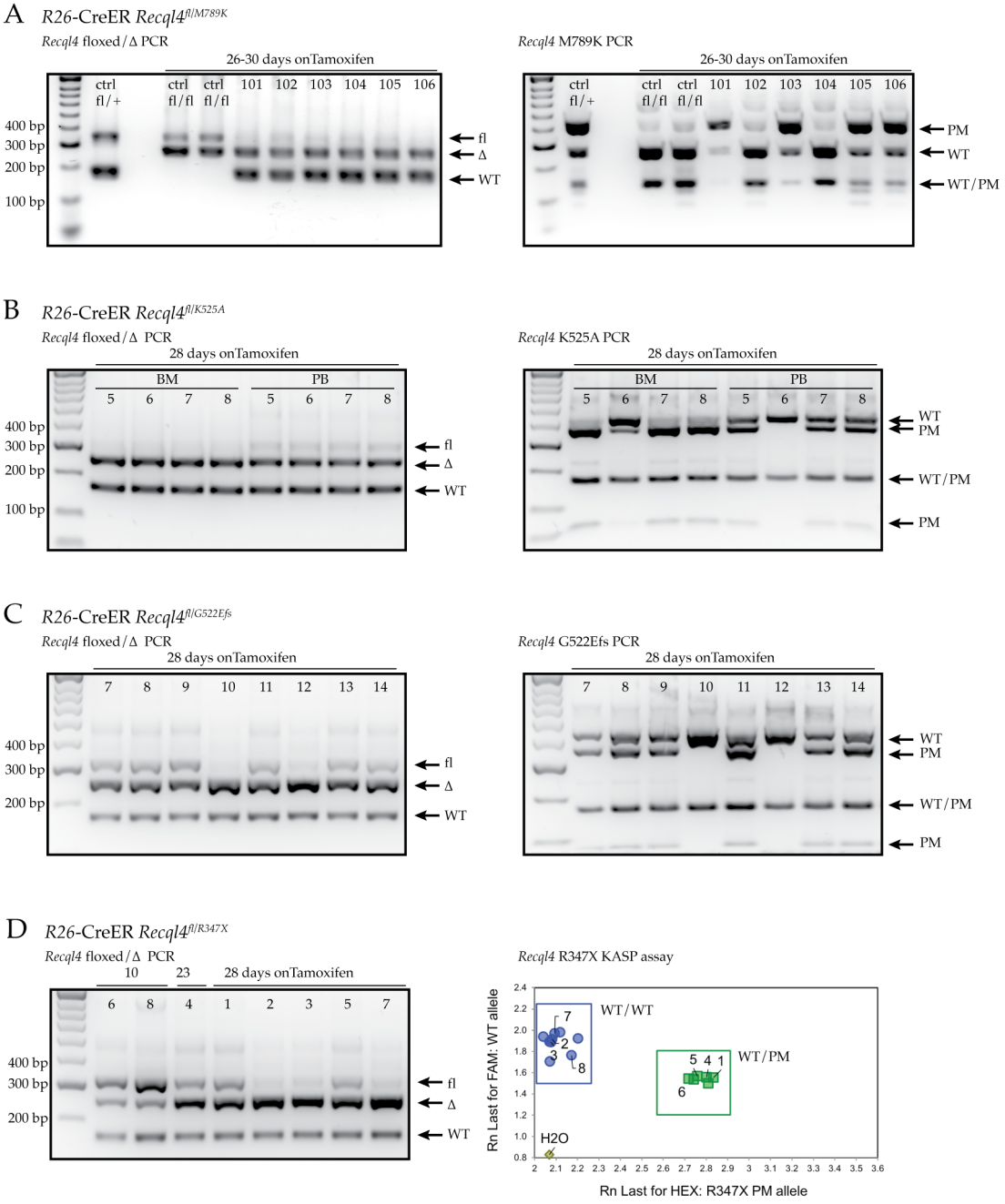

Supp. Figure 5.3. Analysis of recombination and genotyping of point mutant alleles. Genomic PCR showing recombination of the floxed allele to produce the excised product of the expected size (left) and genotyping PCRs of the point mutants (right) of the following alleles: (A) M789K, (B) K525A, (C) G522Efs, (D) R347X.

Supp. Table 5.1: FACS Antibodies (anti-mouse). List of antibodies used for flow cytometry in this study.

ANTIBODY (CLONE)	CONJUGATE	CATALOGUE #	COMPANY
Ter119 (TER-119)	PE	12-5921-83	Life Technologies Australia Pty Ltd/Thermo Fisher
CD71 (RI7 217.1.4)	APC	17-0711-82	Life Technologies Australia Pty Ltd/Thermo Fisher
B220/CD45R (RA3-6B2)	APC	17-0452-83	Life Technologies Australia Pty Ltd/Thermo Fisher
IgM (II/41)	Biotin	13-5790-82	Life Technologies Australia Pty Ltd/Thermo Fisher
CD43 (S7)	PE	553271	BD Pharmingen
CD19 (1D3)	PerCP-Cy5.5	45-0193-82	Life Technologies Australia Pty Ltd/Thermo Fisher
Mac1/CD11b (M1/70)	PE	12-0112-83	Life Technologies Australia Pty Ltd/Thermo Fisher
Gr-1/Ly6G (RB6-8C5)	PE-Cy7	25-5931-82	Life Technologies Australia Pty Ltd/Thermo Fisher
F4/80 (BM8.1)	APC	20-4801-U100	Tonbo Biosciences
CD4 (RM4-5)	eFluor-450	48-0042-82	Life Technologies Australia Pty Ltd/Thermo Fisher
CD8a/Ly-2 (53-6.7)	APC-eFluor 780	47-0081-82	Life Technologies Australia Pty Ltd/Thermo Fisher
TCRβ (H57-597)	PE	12-5961-83	Life Technologies Australia Pty Ltd/Thermo Fisher
CD25 (PC61.5)	PE	12-0251-83	Life Technologies Australia Pty Ltd/Thermo Fisher
CD44 (IM7)	APC	17-0441-83	Life Technologies Australia Pty Ltd/Thermo Fisher
Sca-1 (D7)	APC	17-5981-82	Life Technologies Australia Pty Ltd/Thermo Fisher

TABLE 5.1 – CONTINUED FROM PREVIOUS PAGE

ANTIBODY (CLONE)	CONJUGATE	CATALOGUE #	COMPANY
c-Kit/CD117 (2B8)	APC-eFluor-780	47-1171-82	Life Technologies Australia Pty Ltd/Thermo Fisher
CD34 (RAM34)	eFluor-660	50-0341-82	Life Technologies Australia Pty Ltd/Thermo Fisher
CD135/Flk2/Flt3 (A2F10)	PE	12-1351-82	Life Technologies Australia Pty Ltd/Thermo Fisher
FcgR/CD16/32 (93)	PerCP-Cy5.5	45-0161-82	Life Technologies Australia Pty Ltd/Thermo Fisher
CD41 (MWReg30)	eFluor-450	48-0411-82	Life Technologies Australia Pty Ltd/Thermo Fisher
CD105 (MJ7/18)	PE-Cy7	120409	Biolegend
CD150 (TC15-12F12.2)	PE	115904	Biolegend
CD23	Biotin*	553137	BD Pharmingen
CD21	PE	123410	Biolegend
Streptavidin	BV 605	563260	BD Pharmingen
Streptavidin (used with CD23)	BV 605	405229	Biolegend

5.3 RESEARCH IN CONTEXT

Although the ATP-dependent helicase activity was presumed to be critical for the function of RECQL4, *in vivo* studies were lacking. The results presented in this chapter evaluated the specific role of the ATP-dependent helicase of RECQL4. From these experiments, I was able to demonstrate that the ATP-dependent helicase function of RECQL4 was not required for physiological processes such as embryonic development, haematopoiesis, B and T cell development, and DNA damage repair. This confirms my hypothesis that the ATP-dependent helicase activity of RECQL4 is not essential for the physiological functions evaluated and aligns with previous *in vitro* studies that demonstrated that a similar mutation could restore viability of RECQL4-deficient cells [88, 169]. Surprisingly, the ATP-dependent helicase activity was not needed for response to induced DNA damage, whether physiological in the case of B cell receptor rearrangements or in response to chemotherapy.

In addition to clearly defining that the helicase activity of RECQL4 was non-essential to physiological functions, this study also provided initial evidence regarding truncating mutations, which are seen in the majority of RTS patients [56]. Results showed that after tamoxifen deletion of a wild type floxed allele, mice carrying truncating mutations developed a BM failure phenotype similar to having a complete null allele. In contrast, the helicase-inactive mutants did not show any phenotype, similar to the wild type control and a benign mutation. These findings confirmed in a different context, that the ATP-dependent helicase function was dispensable for the functions of RECQL4, however, mutations resulting in truncated protein products with deletion of both the helicase and the C-terminal domain were deleterious. The assessment of mice carrying these truncating mutations will be discussed in greater detail in the following chapter.

CHAPTER 6

6

DETERMINING THE IMPACT OF RECQL4 TRUNCATING MUTATIONS IN NORMAL HOMEOSTASIS AND TUMOUR DEVELOPMENT

6.1 INTRODUCTION

In Chapter 5, my results demonstrated that mice carrying truncating mutations of RECQL4 developed BM failure after somatic deletion of a wild type floxed allele (see Figure 5.6). Although these results enabled a direct comparison of the effects of a helicase-inactive mutation to truncating mutations, they do not reflect what happens in RTS, in which the deficiency of RECQL4 is chronic and sustained, instead of an acute somatic expression of the mutation after deletion of the floxed allele. Furthermore, the effects of truncating mutations in other physiological processes could not be readily explored using this model.

To address this gap, the long-term consequences of two truncating mutations that resemble common mutations seen in RTS patients were assessed. I performed several experiments in these mice to determine the impact of these mutations on protein stability, cellular localisation, bone homeostasis, haematopoiesis, and tumorigenesis. Furthermore, to further understand the effects of these mutations, their human homologues, and other common human mutations, I performed *in vitro* complementation assays. The results of this chapter have been submitted as a whole for publication. The submitted manuscript and associated data can be found in the following section, except for the Materials and Methods section, which has been consolidated in Chapter 4 to avoid repetition. For consistency across my thesis, I have adapted the abbreviations, references and figure numbering and corrected the spelling to Australian English.

6.2 SUBMITTED MANUSCRIPT

6.2.1 *Abstract*

RTS is an autosomal recessive disorder characterised by poikiloderma, sparse or absent hair, and defects in the skeletal system such as bone hypoplasia, short stature, low bone mass, and OS. RTS type 2 patients typically present with germline compound bi-allelic protein-truncating mutations of *RECQL4*. As existing murine models predominantly employ *Recql4* null alleles, we have here attempted to more accurately model the mutational spectrum of RTS by generating mice with patient-mimicking truncating *Recql4* mutations. We found that truncating mutations impaired stability and subcellular localisation of RECQL4, and homozygosity was developmentally lethal. Surprisingly, *Recql4* truncating mutations led to haploinsufficient reduced trabecular bone mass and cortical bone thickness. Combination of a truncating mutation with a conditional null allele that deletes *Recql4* at the osteoblastic progenitor stage of differentiation resulted in a similar phenotype, suggesting that these defects were intrinsic to the osteoblast lineage. However, the truncating mutations did not promote OS or tumorigenesis, even after exposure to irradiation. We also utilised murine *Recql4* null cells to assess the impact of a wider range of human *RECQL4* mutations in *in vitro* complementation assays. We found differential effects of distinct RECQL4 mutations. While some created unstable protein products, others altered subcellular localisation of the protein. Interestingly, the severity of the phenotypes correlated with the extent of protein truncation. Collectively, our results identify RECQL4 gene dosage as an unsuspected regulator of bone mass and suggest that additional mutations may synergise with *RECQL4* to initiate tumorigenesis in RTS patients.

6.2.2 *Introduction*

RTS (OMIM #268400) is a rare autosomal recessive disorder that presents with skin rash (poikiloderma), sparse or absent hair, juvenile cataracts, gastrointestinal and skeletal complications [64, 67]. Approximately 75% of patients have skeletal abnormalities, including bone hypoplasia, short stature, polydactyly, and low bone mass [74]. Furthermore, OS, along with epithelial and haematological cancers, is a malignancy frequently associated with this

syndrome [56, 58, 64, 67]. RTS is classified into two forms: RTS type 1, where patients present with juvenile cataracts, have frequent mutations in *ANAPC1* but do not have increased incidence of OS [59]; and RTS type 2, where patients harbour mainly biallelic mutations in *RECQL4* and have a significantly increased incidence of OS [67].

RECQL4 is located on the long arm of chromosome eight (8q24.3) [111]. The reported mutational spectrum includes the introduction of early stop codons, frameshift mutations, as well as deletions within numerous short introns (<100 bp) that can impair RNA splicing, resulting in protein truncations and loss-of-function alleles [112]. The *RECQL4* gene encodes a protein of 1,208 aa that has three well-characterised domains: The N-terminal region shares sequence homology to the essential yeast DNA replication factor Sld2. In higher eukaryotes, this Sld2-like homology domain is unique to RECQL4 [134, 209]. Studies have shown that this region has roles in DNA replication and DNA repair, and it is critical for viability [115, 148, 173]. The highly conserved central RecQ helicase domain has an ATPase core with seven motifs that contribute to the coupling between ATP hydrolysis and strand separation of dsDNA [210]. ATP dependent helicase activity was thought to be vital for the function of RECQL4. However, we recently reported that mice homozygous for a helicase-inactivating point mutation (K525A) had no overt phenotypes [211]. Finally, the C-terminal region harbours both the R4ZBD domain, in place of an RQC domain seen in other RecQ helicases, and at the very end (1,117-1,208 aa), the small CTD domain, associated with DNA-binding affinity [23]. RECQL4 is primarily localised in the nucleus but has also been reported in the cytoplasm [122, 126]. However, its distribution within these compartments depends on the cell type assessed and the cell cycle phase [122].

RTS Type 2 patients have a high incidence of skeletal abnormalities and OS. In a cohort study of 41 patients, 32% developed this cancer [67]. Furthermore, an independent cohort reported that the median age at diagnosis in RTS patients was ten years of age, significantly younger than the median age for sporadic OS, which peaks in adolescence [94, 99, 212]. We and others have previously reported that in mice the deletion of *Recql4* in pre-osteoblasts or limb bud progenitors caused shortened bones and decreased bone volume [181, 183]. However, neither model developed OS, even in combination with *Tp53* deficiency [181]. In contrast to the described murine models of

Recql4 mutation that generated null alleles, RTS patients predominantly have compound heterozygous *RECQL4* mutations that are predicted to generate truncated protein products [56]. More than half of these truncate the protein before or within the helicase domain and result in a substantially increased risk of developing OS compared to non-truncating mutations [58].

To more faithfully model the RTS-relevant *RECQL4* mutation spectrum beyond existing null alleles, we have generated mice bearing truncating *Recql4* mutations. Here we show that these truncating mutations affected stability and subcellular localisation of RECQL4, which resulted in homozygous developmental lethality and a haploinsufficient low bone mass phenotype. However, these mutations did not cause an increased incidence of OS or a more general cancer predisposition, even after a sub-lethal dose of ionising radiation. This suggests that mutations in RECQL4 alone are not sufficient to initiate malignant transformation in the mouse and that additional molecular and cellular changes are required for the full spectrum of RTS phenotypes to develop.

6.2.3 *Results*

6.2.3.1 *Truncating mutations of RECQL4 affect protein expression levels and cause developmental lethality in homozygotes*

To understand the *in vivo* impact of truncating RECQL4 mutations, we generated two novel mouse *Recql4* alleles [211]. These new mutations were similar to common mutations seen in RTS type 2 patients (Figure 6.1 A). The p.Gly522GlufsTer43 (G522Efs) mutation, closely related to the human p.Cys525 AlafsX33 (C525Afs) mutation, was created by a two-base pair insertion (c.1646_1647insGA). This frameshift caused a premature stop codon 44 aa downstream, resulting in a predicted truncated protein of 566 aa, that lacks the majority of the helicase domain and all of the C-terminal domain. The second allele was a p.Arg347* (R347X) mutation, a nonsense mutation (c.1122C>T) identified from an ENU mutagenesis collection, similar to p.Arg350GlyfsX21 (R350Gfs) in RTS patients. This mutation yielded a predicted 347 aa protein lacking both the helicase and C-terminal domains entirely (Figure 6.1 B). To confirm the genetic status of these mice, we used PCR-restriction fragment length polymorphism (PCR-RFLP) for the G522Efs

allele (Figure 6.1 C), and KASP assay for the R347X allele (Figure 6.1 D), both of which confirmed the correct genotype.

The heterozygous *Recql4*$^{R347X/+}$ and *Recql4*$^{G522Efs/+}$ mice were viable and fertile. To determine if individual homozygous truncating mutants were viable, the respective heterozygous mice were inbred. We did not recover any *Recql4*$^{R347X/R347X}$ or *Recql4*$^{G522Efs/G522Efs}$ pups at genotyping (day 7-10 after birth), indicating that the homozygous mutants were developmentally lethal (Figure 6.1 E). We have not established the time point in development at which the respective mutants are no longer viable.

Next, we investigated the *in vivo* expression of the predicted truncated proteins. We prepared lysates from the thymus of germline heterozygous mutants of each respective allele and probed them with a monoclonal antibody raised against the first 200 aa of murine RECQL4 by Western blot [211]. We found a truncated protein product of the predicted size for the R347X mutant in thymocyte extracts, though at a much lower intensity than the WT band (Figure 6.1 F). In contrast, the G522Efs mutant protein could not be detected (Figure 6.1 F), and even when ectopically overexpressed as a cDNA with an N-terminal 3xFlag tag, its expression was significantly lower than the R347X (Figure 6.1 G). To assess whether the truncated proteins had altered cellular localisation, we generated N-terminal mCherry-tagged mouse RECQL4 fusion constructs. These were retrovirally infected into the murine osteoblastic Kusa4b10 cell line. Protein localisation was analysed by fluorescence microscopy. The full-length WT (control) murine RECQL4 protein was predominantly localised in the nucleus as expected, with an apparent enrichment in the nucleolus. The ATP-binding point mutant p.Lys525Ala (K525A) mutation had a similar localisation to WT RECQL4 (Figure 6.1 H). In contrast, the R347X protein, while also localised to the nucleus, was poorly incorporated in the nucleoli (Figure 6.1 H). Interestingly, consistent with the weak protein expression *in vivo* (Figure 6.1 F), the G522Efs protein was poorly expressed and difficult to detect robustly. We further assessed if the cellular localisation patterns were shared in the human RTS mutations most similar to those used in this study. For this purpose, we utilised a human N-terminal EGFP-tagged WT and K508A mutant RECQL4 (provided by T. Enomoto, Musashino University, Tokyo, Japan) and created the C525Afs and R350Gfs mutations. These constitute the human equivalents of, or map closely to, the murine mutations K525A (human p.Lys508Ala (K508A)), G522Efs, and

R347X, respectively. Comparable localisation results to the murine proteins were obtained for the human RECQL4 proteins (Figure 6.1 1).

Finally, it has been suggested that RECQL4 could localise to the mitochondria [125, 127]. Using the fluorescent fusion proteins, we could not detect mouse or human RECQL4 (WT or mutant) in the cytoplasm nor overlapping with the mitochondria (Supp. Figure 6.1). To evaluate this result functionally, we assessed mitochondrial function based on the Seahorse bioenergetic assay. To enable comparison of the different point mutations in isolation, we used HoxB8 immortalised myeloid progenitor cells [187] derived from *R26*-CreER^{T2} *Recql4*$^{fl/+}$, *R26*-CreER^{T2} *Recql4*$^{fl/K525A}$, *R26*-CreER^{T2} *Recql4*$^{fl/R347X}$, and *R26*-CreER^{T2} *Recql4*$^{fl/G522Efs}$ and exposed them to tamoxifen for four days to delete the wild type *Recql4* floxed allele. We found no difference in either basal or maximal oxygen consumption rate between the non-tamoxifen and tamoxifen-treated groups (Supp. Figure 6.2), demonstrating that mutations in RECQL4 that significantly impact protein stability and function do not measurably affect mitochondrial respiration. Taken together, our results demonstrate that the murine RECQL4 mutants behave similarly to their human counterparts; and while the specific mutations differentially impact their level of expression and subcellular localisation, they do not measurably affect mitochondrial respiration.

A

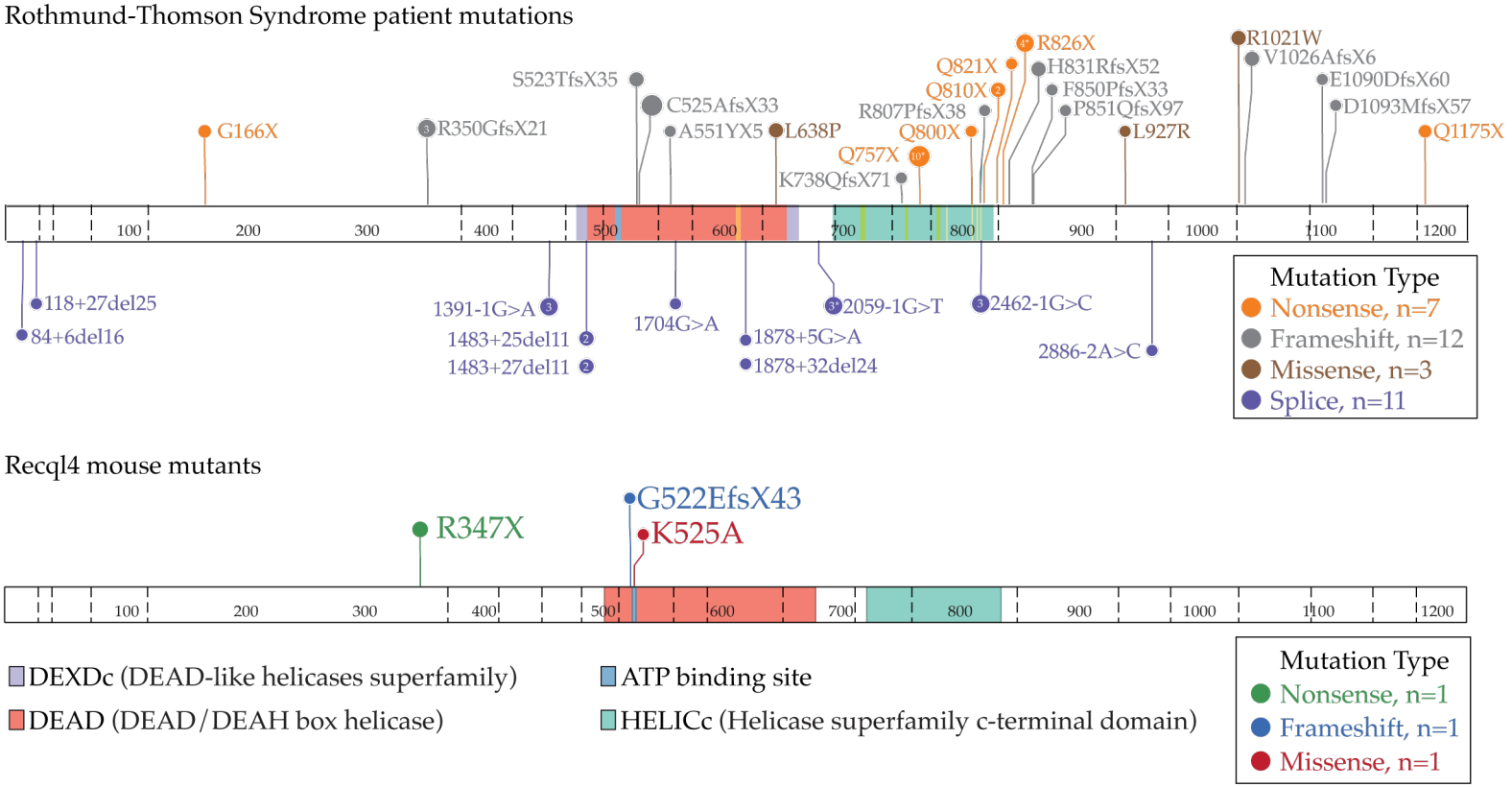
Rothmund-Thomson Syndrome patient mutations
G166X
R350GfsX21
S523TfsX35
C525AfsX33
A551YX5
L638P
K738QfsX71
Q757X
R807PfsX38
Q800X
Q821X
Q810X
R826X
H831RfsX52
F850PfsX33
P851QfsX97
L927R
R1021W
V1026AfsX6
E1090DfsX60
D1093MfsX57
Q1175X
100
200
300
400
500
600
700
800
900
1000
1100
1200
118+27del25
84+6del16
1391-1G>A
1483+25del11
1483+27del11
1704G>A
1878+5G>A
1878+32del24
2059-1G>T
2462-1G>C
2886-2A>C
Mutation Type
Nonsense, n=7
Frameshift, n=12
Missense, n=3
Splice, n=11
Recql4 mouse mutants
R347X
G522EfsX43
K525A
100
200
300
400
500
600
700
800
900
1000
1100
1200
DEXDc (DEAD-like helicases superfamily)
DEAD (DEAD/DEAH box helicase)
ATP binding site
HELICc (Helicase superfamily c-terminal domain)
Mutation Type
Nonsense, n=1
Frameshift, n=1
Missense, n=1

B

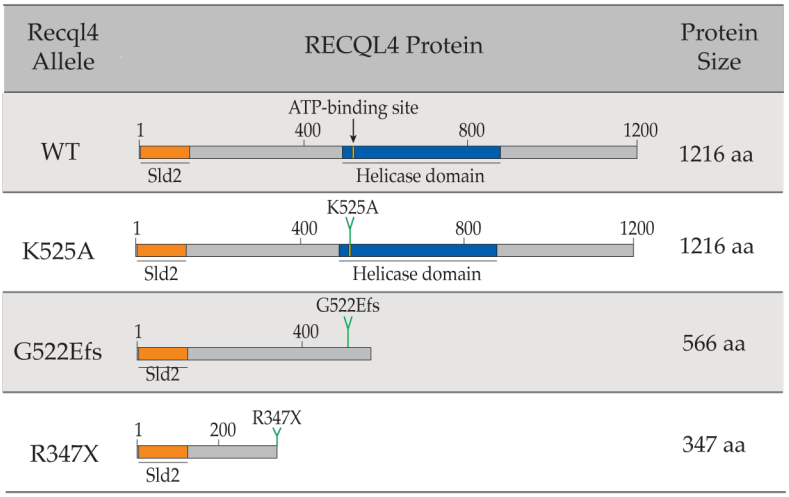

C

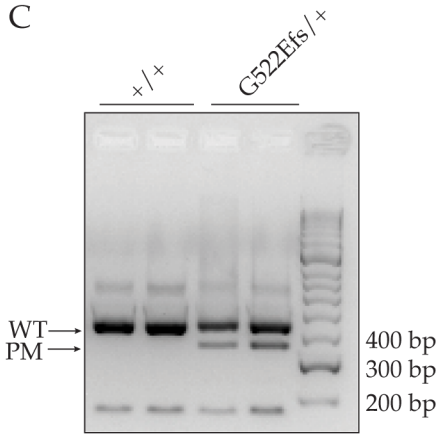

D

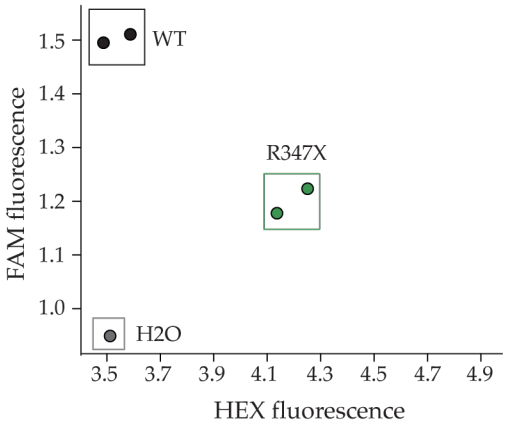

E

Line	Genotype	Observed (%)	Expected (%)
Recql4 G522Efs (From heterozygous intercrosses) 49 Litters	*Recql4* $^{+/+}$	75 (33.8%)	55.5 (25%)
	Recql4 $^{G522Efs/+}$	147 (66.2%)	111 (50%)
	Recql4 $^{G522Efs\ /\ G522Efs}$	0 (0%)	55.5 (25%)
Recql4 R347X (From heterozygous intercrosses) 24 Litters	*Recql4* $^{+/+}$	36 (34%)	26.75 (25%)
	Recql4 $^{R347X/+}$	71 (66 %)	53.5 (50%)
	Recql4 $^{R347X/R347X}$	0 (0 %)	26.75 (25%)

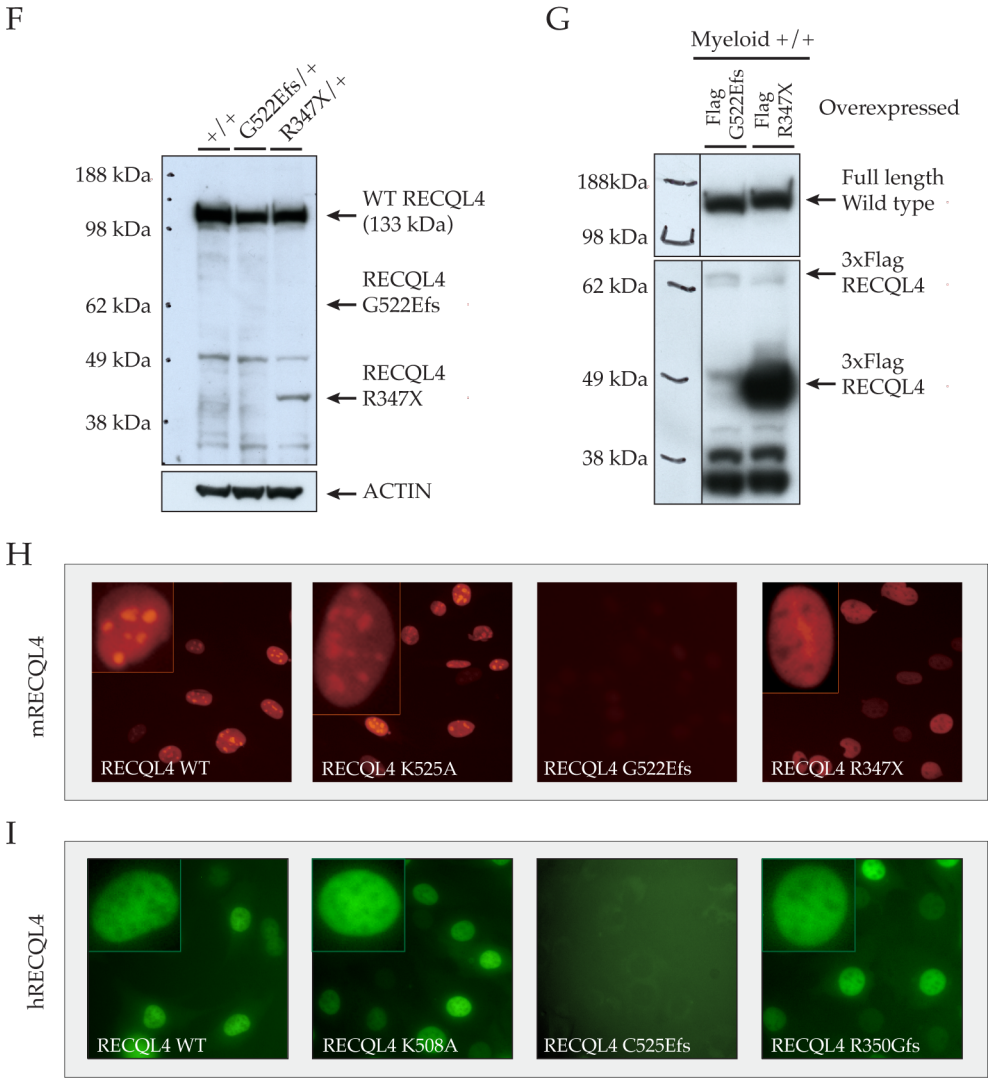

Figure 6.1: *Truncating RECQL4 mutations G522Efs and R347X affect protein expression and localisation differently and are homozygous embryo lethal.* (A) Schematic illustration of RECQL4 mutations reported in RTS patients and murine mutations used in this study. Image generated using Protein Painter (PeCan portal, St Jude's). (B) *Recql4* mutations and their corresponding predicted protein products. (C) Genomic DNA PCR plus *Msl*I digest of $Recql4^{+/+}$ and $Recql4^{G522Efs/+}$. Two independent mice per genotype. (D) KASP genotyping of $Recql4^{+/+}$ and $Recql4^{R347X/+}$. HEX positive represents the R347X allele; FAM positive represents wild type allele. Two independent mice per genotype. (E) Breeding data from 49 litters of $Recql4^{G522Efs/+}$ and 24 litters of $Recql4^{R347X/+}$ intercrosses. Observed and expected Mendelian frequencies of the indicated genotypes are shown. No statistical significance was achieved. (F) Western blot of thymocyte lysates from $Recql4^{+/+}$, $Recql4^{G522Efs/+}$, and $Recql4^{R347X/+}$ probed with anti-mouse RECQL4 (clone 3B10; top). The same blot re-probed with anti-Actin (bottom). (G) Western blot of lysates from HoxB8 immortalised *R26*-CreER^{T2} $Recql4^{+/+}$ infected with MSCV puro 3xFlag RECQL4 and probed with anti-RECQL4 (clone 3B10; top) and M2 anti-Flag antibody (bottom). (H) Fluorescent microscopy of RECQL4 expression in Kusa 4b10 cells with murine mCherry fused WT, K525A, G522Efs, and R347X and (I) human EGFP fused WT, K508A, C525Efs, and R350Gfs mutations.

6.2.3.2 *Recql4*$^{R347X/+}$ *and Recql4*$^{G522Efs/+}$ *heterozygosity lead to reduced bone mass phenotype*

Based on our previous finding of bone defects in conditional *Recql4* null mice [181] and the skeletal/bone phenotypes associated with RTS Type 2, we assessed skeletal growth in the two heterozygous mutants. We could not assess homozygous mutants for either allele due to the developmental lethality previously described. These germline heterozygous animals are, therefore, most similar to the parents of RTS patients. Ten-week old male mice were assessed for all genotypes to avoid the effects of asynchronous oestrous in cohorts of female mice. Results showed that heterozygous *Recql4*$^{R347X/+}$ mice were significantly smaller, while heterozygous *Recql4*$^{G522Efs/+}$ mice had a reduced body weight that did not reach statistical significance within the cohort assessed (p=0.076) (Figure 6.2 A). We utilised Echo-MRI to investigate if the lower body weight was associated with a change in fat/lean mass proportion and found no differences, suggesting that the reduced mass was not likely to stem from changes in adiposity (Supp. Figure 6.3). We then evaluated the tibial length of 10-week old males by micro-CT. Overall tibial length in both *Recql4*$^{R347X/+}$ and *Recql4*$^{G522Efs/+}$ mutants did not reach statistically significant differences compared to either wild type (littermate) controls or K525A homozygous males (Figure 6.2 B). However, the mediolateral and anteroposterior widths measured by micro-CT in the midshaft tibia were significantly lower in both *Recql4*$^{R347X/+}$ and *Recql4*$^{G522Efs/+}$ mutants, indicating narrower tibiae in both genotypes (Figure 6.2 C, D). For comparison, tibiae from the helicase-inactive K525A homozygous mice did not show differences in any of these parameters when compared to the WT controls.

We further looked at possible bone changes in trabecular microarchitecture and cortical morphology of WT and mutant 10-week old male mice. For trabecular analysis, we selected a region corresponding to the secondary spongiosa in the proximal metaphysis of the tibia (Figure 6.2 E). The trabecular bone volume of *Recql4*$^{R347X/+}$ and *Recql4*$^{G522Efs/+}$ mice was significantly lower by 24% and 26%, respectively (Figure 6.2 F). The trabecular number was also lower by 25% in the *Recql4*$^{R347X/+}$ and 20% in the *Recql4*$^{G522Efs/+}$ mice (Figure 6.2 G). The trabecular separation was 25% greater in the *Recql4*$^{R347X/+}$ mice but not different in the *Recql4*$^{G522Efs/+}$ mice (Figure 6.2 H). For cortical analysis, we assessed a region corresponding to the mid-diaphysis of the

tibia (Figure 6.2 J). Cortical thickness was 10% lower in the *Recql4*$^{R347X/+}$ mutants, whereas there was a slight (7%) but non-significant decrease in the *Recql4*$^{G522Efs/+}$ mice, compared to controls (Figure 6.2 K). For both the *Recql4*$^{R347X/+}$ and *Recql4*$^{G522Efs/+}$, the periosteal perimeter showed a reduction of 14% and 7%, respectively, when compared with littermate controls (Figure 6.2 L), which was reflected in a lower moment of inertia for both groups (Figure 6.2 M). This suggested a lower torsional rigidity and increased fracture risk in the germline heterozygous truncating mutant mice. In contrast, the non-truncating but ATP-binding helicase-inactive *Recql4*$^{K525A/K525A}$ mutants did not show any change in any trabecular or cortical parameter when compared to the WT control (Figure 6.2 E-H, J-M). All morphological changes could be visualised in the colour-coded 3D reconstructed images (Figure 6.2 I, N). Collectively, these results demonstrate that truncating mutations of RECQL4 resulted in haploinsufficient narrow bones and skeletal dysplasia phenotype in mice.

Given that the changes in skeletal parameters can impact haematopoiesis, we assessed if these affected the haematopoietic system in the germline heterozygous mutant mice. We observed a decrease in the cell hierarchy involved in myeloid development, which did not affect mature granulocytes or macrophages (Supp. Figure 6.4). The remaining parameters assessed were normal. Therefore, a single copy of a truncating mutation in the presence of a retained WT allele is not sufficient to cause marked changes in haematopoiesis and is consistent with the reports from RTS patients and the apparent normality of haematopoiesis in their heterozygous parents. Taken together, these observations suggest that heterozygous truncating RECQL4 mutations cause a haploinsufficient low bone mass phenotype through defects in trabecular and cortical bone. Interestingly, the expression of a single copy of a full-length wild type is sufficient to maintain haematopoiesis, which indicates cellular differences between osteoblast lineage cells and blood-forming cells in sensitivity to RECQL4 dosage.

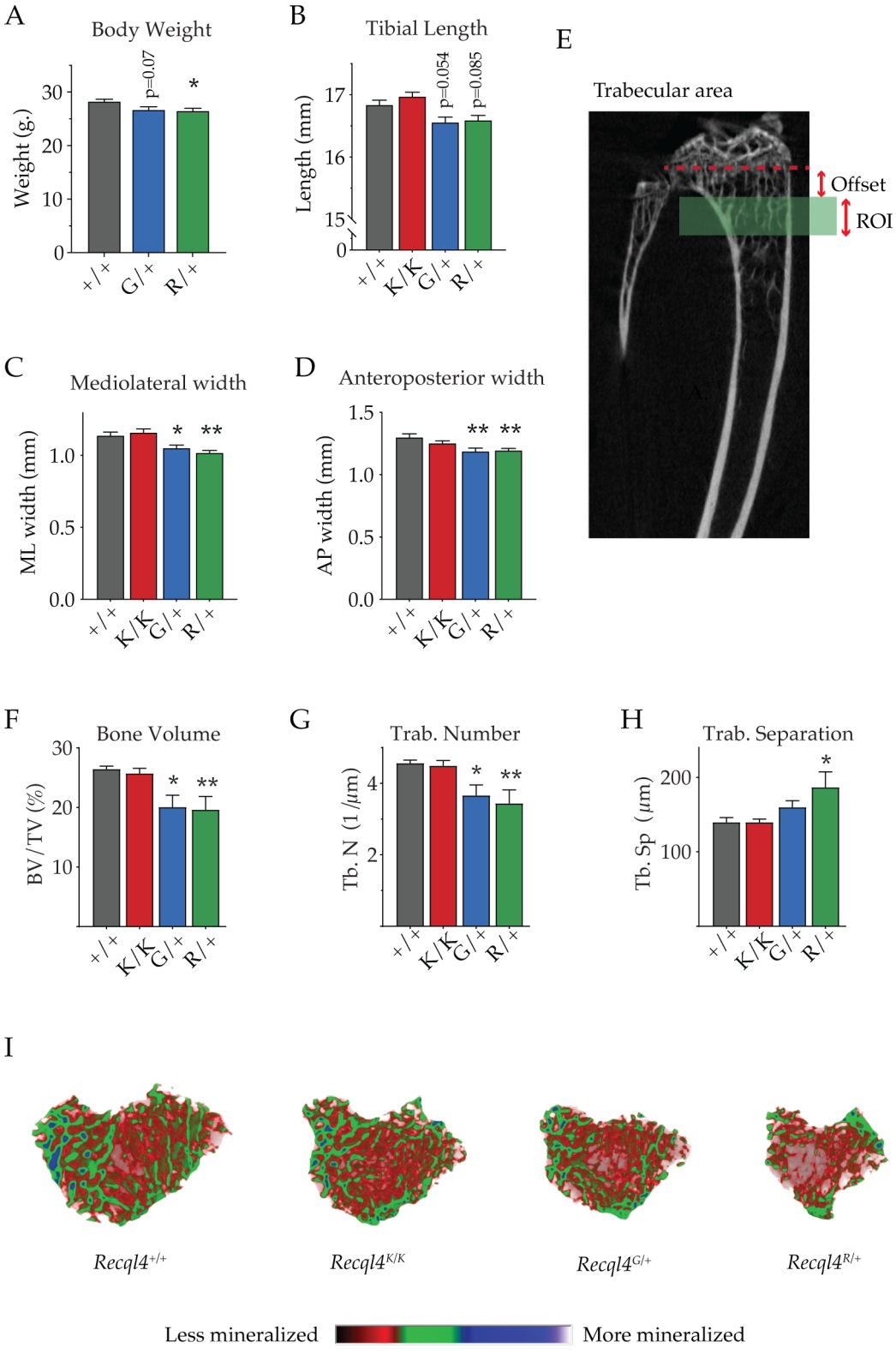
A
Body Weight
Weight (g.)
30
20
10
0
p=0.07
*
+/+
G/+
R/+
B
Tibial Length
Length (mm)
17
16
15
0
p=0.054
p=0.085
+/+
K/K
G/+
R/+
E
Trabecular area
Offset
ROI
C
Mediolateral width
ML width (mm)
1.0
0.5
0.0
*
**
+/+
K/K
G/+
R/+
D
Anteroposterior width
AP width (mm)
1.5
1.0
0.5
0.0
**
**
+/+
K/K
G/+
R/+
F
Bone Volume
BV/TV (%)
30
20
10
*
**
+/+
K/K
G/+
R/+
G
Trab. Number
Tb. N (1/μm)
4
2
*
**
+/+
K/K
G/+
R/+
H
Trab. Separation
Tb. Sp (μm)
200
100
*
+/+
K/K
G/+
R/+
I
Recql4+/+
Recql4K/K
Recql4G/+
Recql4R/+
Less mineralized
More mineralized

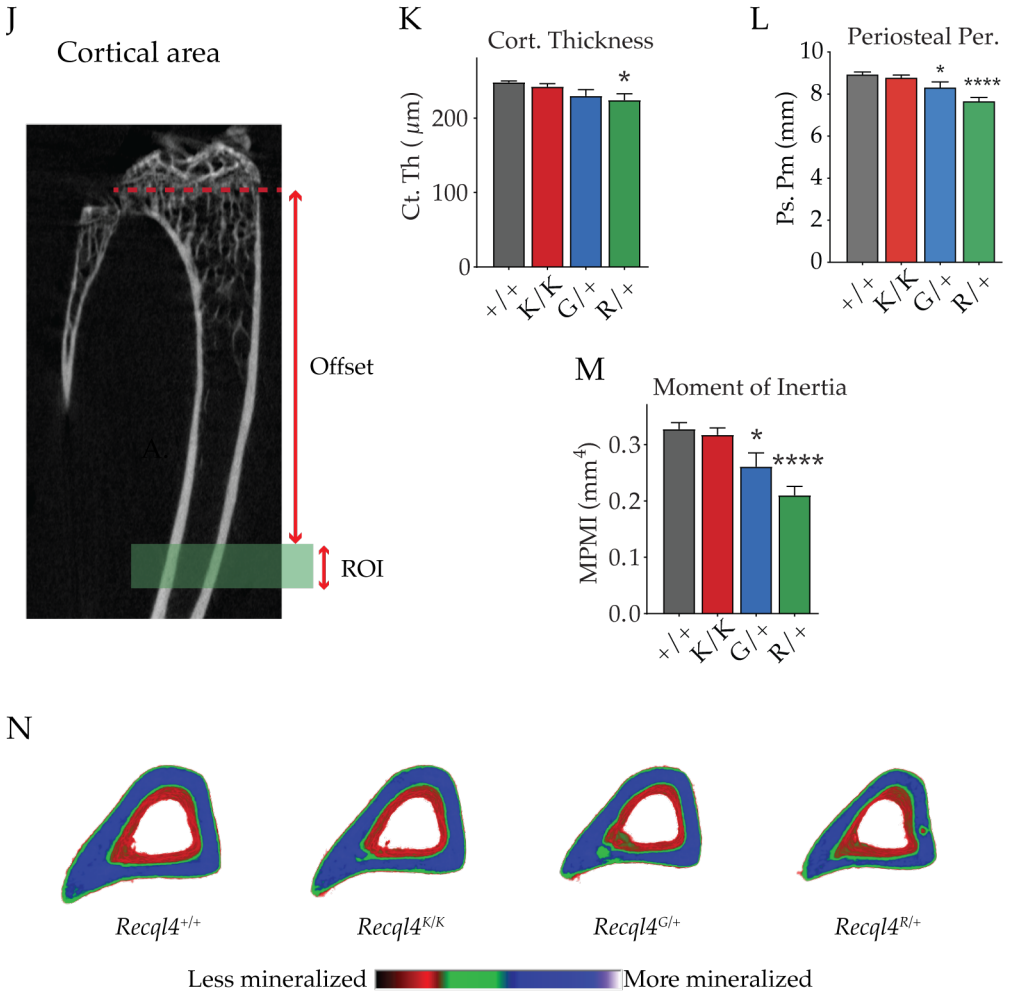

Figure 6.2: *Germline truncating mutants G522Efs and R347X cause low bone mass and narrow bones.* (A) Gross body weights of 10-week old males *Recql4*$^{+/+}$, *Recql4*$^{G522Efs/+}$, and *Recql4*$^{R347X/+}$ mice. Micro-CT measurements of (B) Tibial length, (C) Mediolateral width, and (D) Anteroposterior width from 10-week old males *Recql4*$^{+/+}$, *Recql4*$^{K525A/K525A}$, *Recql4*$^{G522Efs/+}$, and *Recql4*$^{R347X/+}$ mice. (E) Trabecular region of interest beginning at 3.5% (Offset) distal to the growth plate and extending for 5% (ROI) of the total tibia length. (F) Trabecular bone volume. (G) Trabecular number. (H) Trabecular separation. (I) Representative images (Axial plane) of reconstructed trabecular bone with colour-coded quantitative mineralisation from germline *Recql4* mutants. (J) Cortical region of interest beginning at 40% (Offset) distal to the growth plate and extending for 5% (ROI) of the total tibia length. (K) Cortical thickness. (L) Periosteal perimeter. (M) Moment of inertia. (N) Representative images (Axial plane) of reconstructed cortical bone with colour-coded quantitative mineralisation from germline *Recql4* mutants. Data expressed as mean ± SEM, Ordinary one-way ANOVA. *P<0.05; **P<0.01; ***P<0.001; ****P<0.0001; n≥6 per genotype. Experiments were independently executed on separate cohorts, with results pooled for presentation. K=K525A; G=G522Efs; R=R347X.

6.2.3.3 *Intrinsic defects in osteoblast lineage cells cause the low bone mass phenotype of RECQL4 truncating mutants*

The low bone volume and impaired skeletal growth in the germline heterozygous truncating mutants are similar to the phenotype of the conditional full *Recql4* deletion in the osteoblast lineage [181]. We, therefore, crossed the $Recql4^{R347X/+}$ and $Recql4^{G522Efs/+}$ to the *Osx*-Cre $Recql4^{fl/fl}$ mice [179, 181] to enable deletion of the wild type *Recql4* allele, leaving only a truncated protein expressed in osteoblastic cells. The osteoblast restricted point mutant mice were compared to *Osx*-Cre+ $Recql4^{fl/+}$ mice to control for the known effects of the *Osx*-Cre transgene on bone [213, 214]. This approach also allowed bypassing the lethality of homozygous mutant mice and the assessment of cells only expressing truncated proteins in adult mice. The analysis showed that only the *Osx*-Cre $Recql4^{\Delta/R347X}$ mice had a lower body weight and tibial length compared with *Osx*-Cre $Recql4^{\Delta/+}$ littermates (Figure 6.3 A, B). The *Osx*-Cre $Recql4^{\Delta/G522Efs}$ mice had a reduction in body weight, but it did not reach statistical significance (p=0.09) (Figure 6.3 A). Trabecular analysis showed lower trabecular bone volumes by 13% for *Osx*-Cre $Recql4^{\Delta/G522Efs}$ and 25% for *Osx*-Cre $Recql4^{\Delta/R347X}$ (Figure 6.3 C). Correspondingly, there was a 12% and 23% reduction in trabecular number, respectively, compared to controls (Figure 6.3 D). Trabecular separation was 17% greater in the *Osx*-Cre $Recql4^{\Delta/R347X}$ mice only (Figure 6.3 E).

For cortical bone parameters, only mice carrying the R347X mutation showed an 8% lower periosteal perimeter and 25% lower mean polar moment of inertia consistent with an 8% reduction in mediolateral width and no change in anteroposterior width when compared to controls (Figure 6.3 G-K). Again, the K525A mutant mice did not show any detectable cortical phenotype when compared to the controls (Figure 6.3 G-K). All morphological changes are illustrated in the 3D reconstruction images (Figure 6.3 F, L). In summary, these data demonstrate that truncating mutations of RECQL4 disrupt bone microstructure through defects intrinsic to the osteoblast lineage with the more severe phenotype seen in mice expressing the shortest truncated protein (R347X).

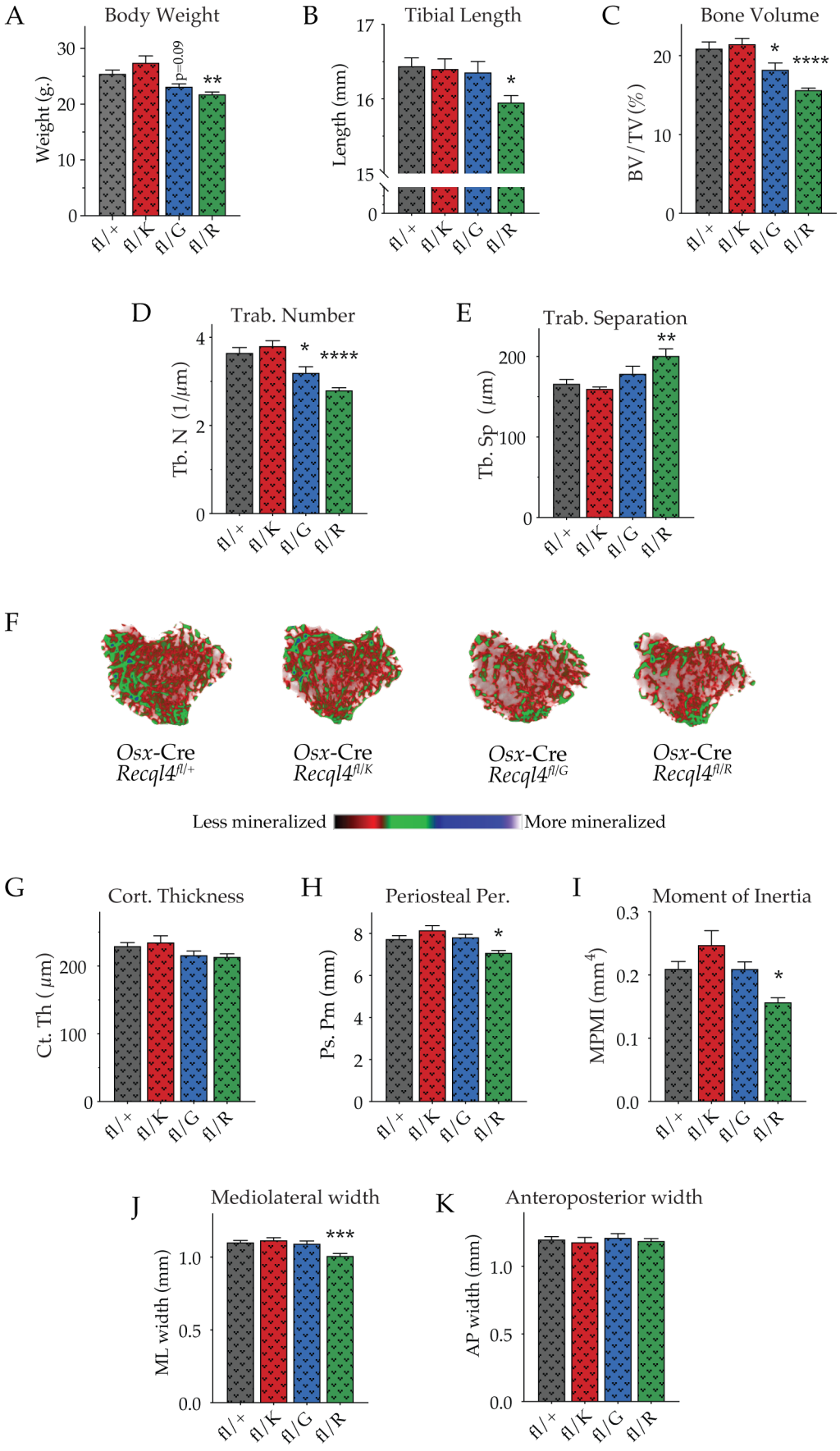
A
Body Weight
Weight (g.)
30
20
10
0
p=0.09
**
fl/+
fl/K
fl/G
fl/R
B
Tibial Length
Length (mm)
17
16
15
0
*
C
Bone Volume
BV/TV (%)
20
10
0
*
****
D
Trab. Number
Tb. N (1/μm)
4
2
0
*
****
E
Trab. Separation
Tb. Sp (μm)
200
100
0
**
F
Osx-Cre
Recql4fl/+
Osx-Cre
Recql4fl/K
Osx-Cre
Recql4fl/G
Osx-Cre
Recql4fl/R
Less mineralized
More mineralized
G
Cort. Thickness
Ct. Th (μm)
200
100
0
H
Periosteal Per.
Ps. Pm (mm)
8
6
4
2
0
*
I
Moment of Inertia
MPMI (mm4)
0.3
0.2
0.1
0.0
*
J
Mediolateral width
ML width (mm)
1.0
0.5
0.0
***
K
Anteroposterior width
AP width (mm)
1.0
0.5
0.0

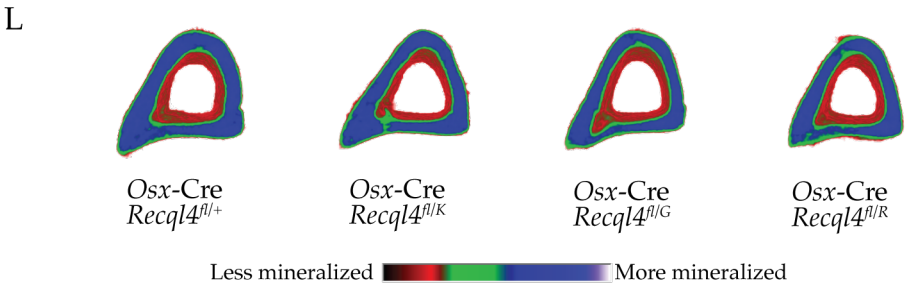

Figure 6.3: *Expression of only the truncating mutations in pre-osteoblasts results in low bone mass.* (A) Gross body weights of 10-week old males *Osx*-Cre $Recql4^{fl/+}$, *Osx*-Cre $Recql4^{fl/K525A}$, *Osx*-Cre $Recql4^{fl/G522Efs}$, and *Osx*-Cre $Recql4^{fl/R347X}$ mice. (B) Tibial length. (C) Trabecular bone volume. (D) Trabecular number. (E) Trabecular separation. (F) Representative images (Axial plane) of reconstructed trabecular bone with colour-coded quantitative mineralisation from *Osx*-Cre *Recql4* mutants. (G) Cortical thickness. (H) Periosteal perimeter (I) Moment of inertia. (J) Mediolateral width. (K) Anteroposterior width. (L) Representative images (Axial plane) of reconstructed cortical bone with colour-coded quantitative mineralisation from *Osx*-Cre *Recql4* mutants. Data expressed as mean ± SEM, Ordinary one-way ANOVA. *P<0.05; **P<0.01; ***P<0.001; ****P<0.0001; n≥6 per genotype. Experiments were independently executed on separate cohorts, with results pooled for presentation. fl=Floxed; K=K525A; G=G522Efs; R=R347X.

6.2.3.4 *Compound heterozygous Recql4 mutants tolerate ionising radiation and do not develop OS*

Based on previous studies that show that RTS patients have compound heterozygous mutations with one allele more severely truncated than the other [56, 58], we generated compound heterozygous mouse lines combining the G522Efs or R347X mutations with the K525A. Although this approach does not fully mimic RTS, it allowed us to determine the *in vivo* effects of a truncated allele and a helicase-inactive allele. Surprisingly, the compound heterozygous $Recql4^{G522Efs/K525A}$ and $Recql4^{R347X/K525A}$ mice were viable, and pups were born at the expected Mendelian ratio (Figure 6.4 A). Moreover, long-term survival cohorts demonstrated that $Recql4^{G522Efs/K525A}$ and $Recql4^{R347X/K525A}$ mice had normal longevity compared to WT mice without an increased tumour incidence (Figure 6.4 B). Although all genotypes developed a small number of spontaneous tumours affecting the liver, spleen, thymus, and intestine, no OS was detected in compound heterozygotes (Supp. Table 6.1).

Previous studies have reported increased sensitivity of RECQL4 mutant cell lines to ionising radiation [150, 215]. To assess the *in vivo* response of

compound heterozygous mutant mice and whether this increased susceptibility to cancer formation of any kind, we treated a small cohort of mice with whole-body ionising radiation. A single sub-lethal dose of 5 Gy total body γ-irradiation was administered to 9-week old *Recql4*$^{G522Efs/K525A}$, *Recql4*$^{R347X/K525A}$ and *Recql4*$^{K525A/+}$ mice as controls. We monitored the cohorts for one year, assessing PB parameters at several time points to evaluate haematologic recovery (Figure 6.4 C). The efficiency of the radiation was demonstrated by a similar transient reduction in blood cell populations across all genotypes (Figure 6.4 D-I). After one year, all mice were euthanised and autopsies performed. We found an intestinal tumour in a *Recql4*$^{G522Efs/K525A}$ mouse, while the remaining genotypes did not show any tumours (Figure 6.4 J). Collectively, these results demonstrate that a full-length, even helicase dead allele, is sufficient to rescue the truncating mutant viability. They further demonstrate that these compound heterozygous *Recql4* mutations are not sufficient to accelerate or sensitise murine models to cancer initiation.

A

Line	Genotype	Observed (%)	Expected (%)
Recql4 G522Efs /K525A (From hom K525A and het G522 Efs) 26 Litters	*Recql4* $^{K525A/+}$	80 (51%)	78 (50%)
	Recql4 $^{G522Efs/K525A}$	76 (49%)	78 (50%)
Recql4 R347X /K525A (From hom K525A and het R347X) 25 Litters	*Recql4* $^{K525A/+}$	67 (52.3%)	64 (50%)
	Recql4 $^{R347X/K525A}$	61 (47.7%)	64 (50%)

B

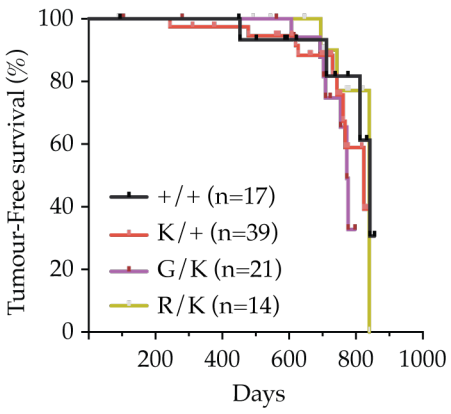

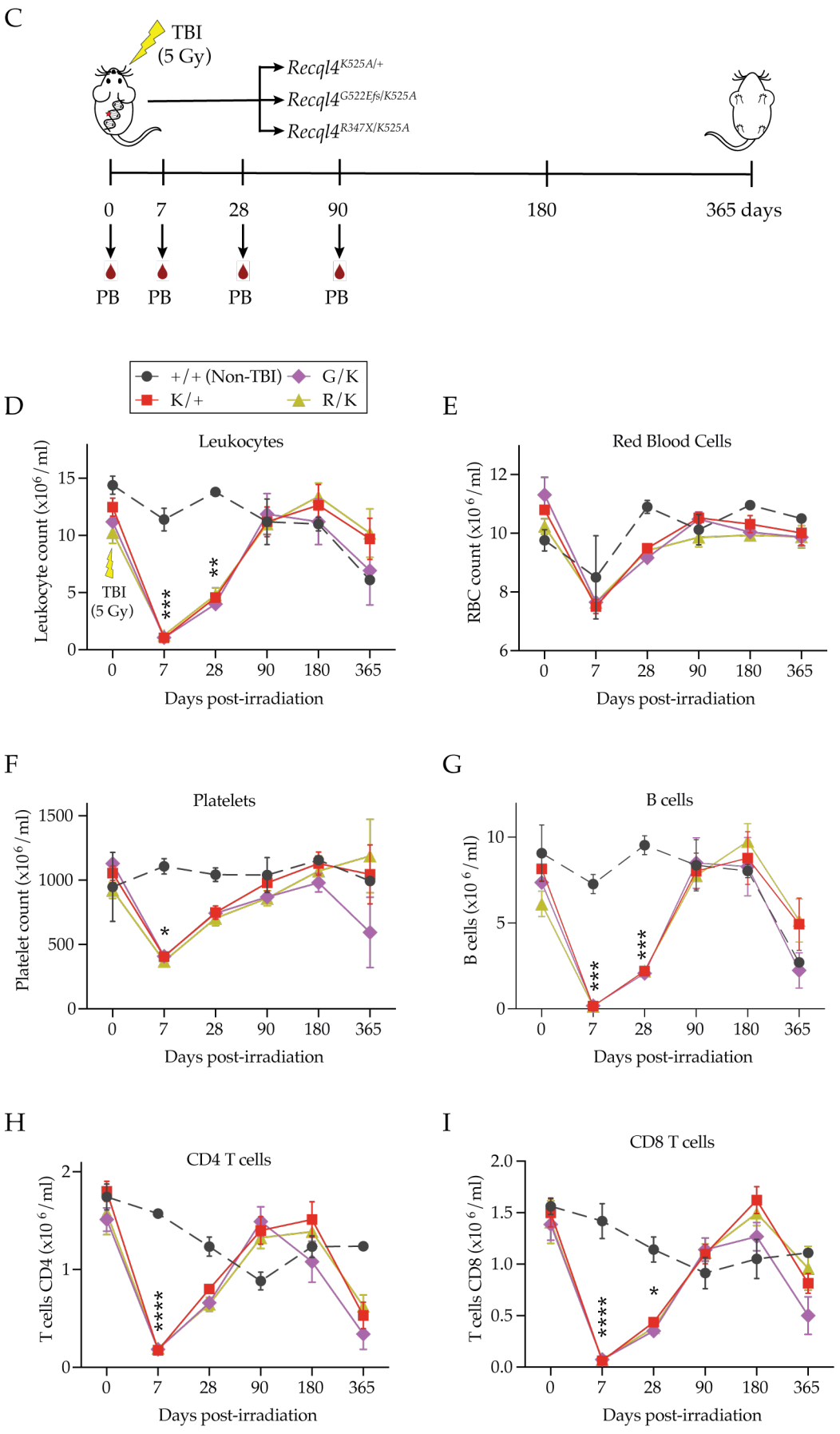
C
TBI
(5 Gy)
Recql4K525A/+
Recql4G522Efs/K525A
Recql4R347X/K525A
0
7
28
90
180
365 days
PB
PB
PB
PB
+/+ (Non-TBI)
K/+
G/K
R/K
D
Leukocytes
Leukocyte count (x10⁶/ml)
TBI
(5 Gy)
Days post-irradiation
E
Red Blood Cells
RBC count (x10⁶/ml)
Days post-irradiation
F
Platelets
Platelet count (x10⁶/ml)
Days post-irradiation
G
B cells
B cells (x10⁶/ml)
Days post-irradiation
H
CD4 T cells
T cells CD4 (x10⁶/ml)
Days post-irradiation
I
CD8 T cells
T cells CD8 (x10⁶/ml)
Days post-irradiation

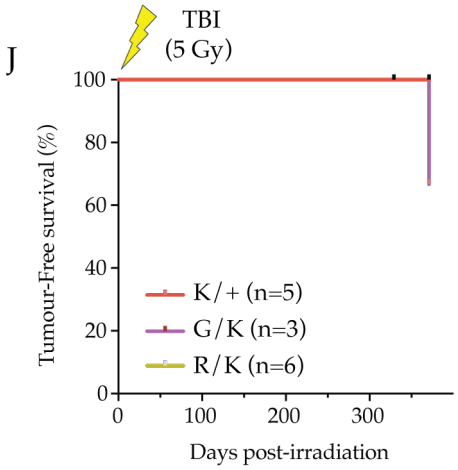

Figure 6.4: *Compound heterozygous Recql4 mutants tolerate a sublethal dose of ionising radiation and do not develop OS.* (A) Breeding data from 26 litters of *Recql4*$^{G522Efs/K525A}$ and 25 litters of *Recql4*$^{R347X/K525A}$ intercrosses. Observed and expected Mendelian rates of the indicated genotypes are shown. No statistical significance was achieved. (B) Kaplan-Meier tumour-free survival plots of the indicated genotypes. +/+, n=17; K/+, n=39; G/K, n=21; R/K, n=14. (C) Schematic representation of experimental setup. Compound heterozygous mutants received a single dose of 5 Gy γ-irradiation, and PB was assessed, and the animals monitored for tumour formation. Mice were euthanised at the last timepoint. PB cell counts following irradiation: (D) Leukocytes; (E) RBCs; (F) Platelets; (G) B cells; (H) CD4 T cells; (I) CD8 T cells. (J) Kaplan-Meier tumour-free survival plots of the irradiated mice. K/+, n=5; G/K, n=3; R/K, n=6. Data expressed as mean ± SEM, Ordinary one-way ANOVA. *P<0.05; **P<0.01; ***P<0.001; ****P<0.0001. TBI=Total body irradiation; K=K525A; G=G522Efs; R=R347X.

6.2.3.5 *Human mutations causing severe truncations fail to rescue Recql4 deletion recapitulating their murine homologs, while mutations that conserve the protein are better tolerated*

To analyse the effect of different human RECQL4 mutations, we utilised the Hoxb8 immortalised myeloid progenitor cells. This is a relevant cell type, given the requirement of RECQL4 for maintenance of this cell population *in vivo* [88]. First, we used this system to determine the effects of truncating murine *Recql4* mutations *in vitro*. Hoxb8 immortalised myeloid progenitor cell lines from *R26*-CreER^{T2} *Recql4*$^{fl/+}$, *R26*-CreER^{T2} *Recql4*$^{fl/K525A}$, *R26*-CreER^{T2} *Recql4*$^{fl/R347X}$, and *R26*-CreER^{T2} *Recql4*$^{fl/G522Efs}$ mice were treated with 400 nM/mL of 4-hydroxy-tamoxifen for 14 days to induce Cre recombinase activity and deletion of the floxed wild type *Recql4* allele, leaving only the mutant allele expressed. We achieved successful deletion by day

four, as confirmed by PCR for genomic recombination (Supp. Figure 6.5). The presence of a single *Recql4* wild type allele (fl/+ cells treated with 4-hydroxy-tamoxifen to become Δ/+) did not interfere with the proliferation rates (Figure 6.5 A), nor did the expression of a single helicase-inactive K525A allele (Figure 6.5 B). However, when the floxed allele was deleted in the cells carrying the truncating mutations G522Efs and R347X, a marked decrease of cell proliferation was observed, consistent with the *in vivo* phenotype [211] and demonstrating an essential requirement of the helicase and C-terminal domains deleted in these mutations (Figure 6.5 C, D).

Next, we used this cell line model to determine the capacity of different human *RECQL4* mutations to rescue HoxB8 *R26*-CreER^{T2} *Recql4*$^{\Delta/\Delta}$ myeloid cells, where both alleles of the endogenous murine *Recql4* were deleted. As expected, control fl/fl cells started dying at day four post-tamoxifen as they became *Recql4* null (Figure 6.5 E and Supp. Figure 6.6). Interestingly, when we expressed the wild type human RECQL4 protein, cell proliferation was not wholly restored, suggesting that overexpression of wild type RECQL4 can be detrimental (Figure 6.5 F). We further tested the ability of frequent human RTS associated *RECQL4* mutations, including the human equivalents to our murine germline mutations, to rescue Δ/Δ cell proliferation and viability. To do this, we used the same EGFP-fused human RECQL4 mutations: K508A, C525Afs, and R350Gfs (Figure 6.5 G, H), described previously and engineered the p.Arg807ProfsTer38 (R807Pfs), p.Gln757* (Q757X) and p.Leu638Pro (L638P) mutations based on recurrent mutations described in RTS patients [56]. The analysis showed that the helicase-inactive K508A mutant successfully rescued the Δ/Δ cells (Figure 6.5 G), while both the C525Afs and R350Gfs human mutants did not (Figure 6.5 H, I), similar to endogenous murine G522Efs and R347X (Figure 6.5 C, D). Both R807Pfs and Q757X mutations rescued the *Recql4* deletion (Figure 6.5 J, K), whereas the L638P achieved only partial rescue (Figure 6.5 L).

Finally, we visualised the EGFP-RECQL4 localisation in HoxB8 *R26*-CreER^{T2} *Recql4*$^{fl/fl}$. As it was seen in Kusa4b10 mesenchymal cells (Figure 6.1 I), the wild type human RECQL4 protein localised in the nucleus, as did K508A and R350Gfs. The C525Afs was poorly expressed (Figure 6.5 M). The R807Pfs and Q757Pfs mutants displayed both nuclear and cytoplasmic localisation, while the L638P mutant was located primarily in the cytoplasm. The sizes and expression levels of the predicted protein products were confirmed by

Western blotting (Supp. Figure 6.7). Collectively, these data demonstrate that not all mutations of RECQL4 are functionally equivalent. Mutations that result in severely truncated protein products, due to early stop codons or frameshifts, are more likely to affect transcript stability and localisation and are detrimental to both cellular and organismal health. In contrast, mutations that conserve most of the protein are largely tolerable.

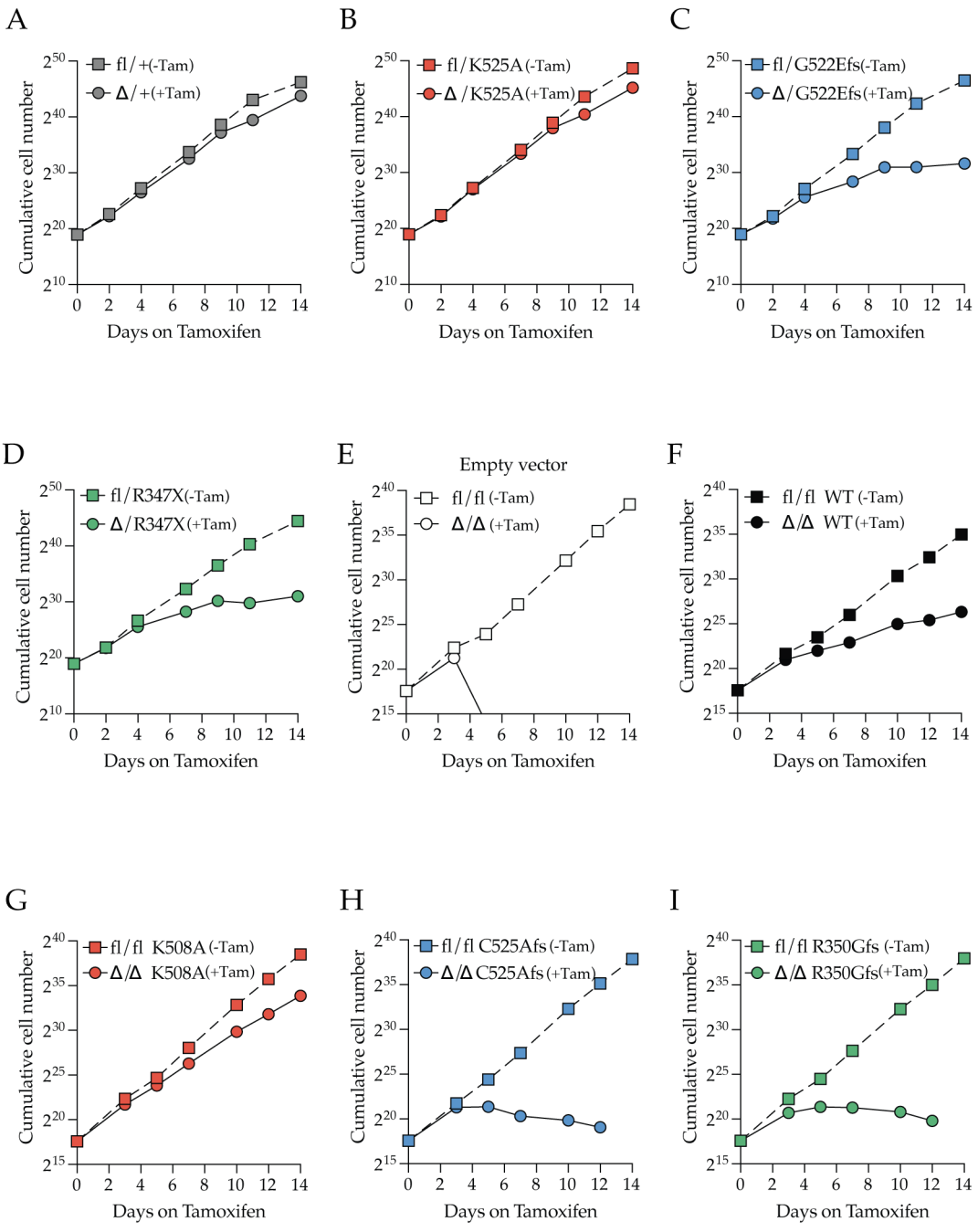

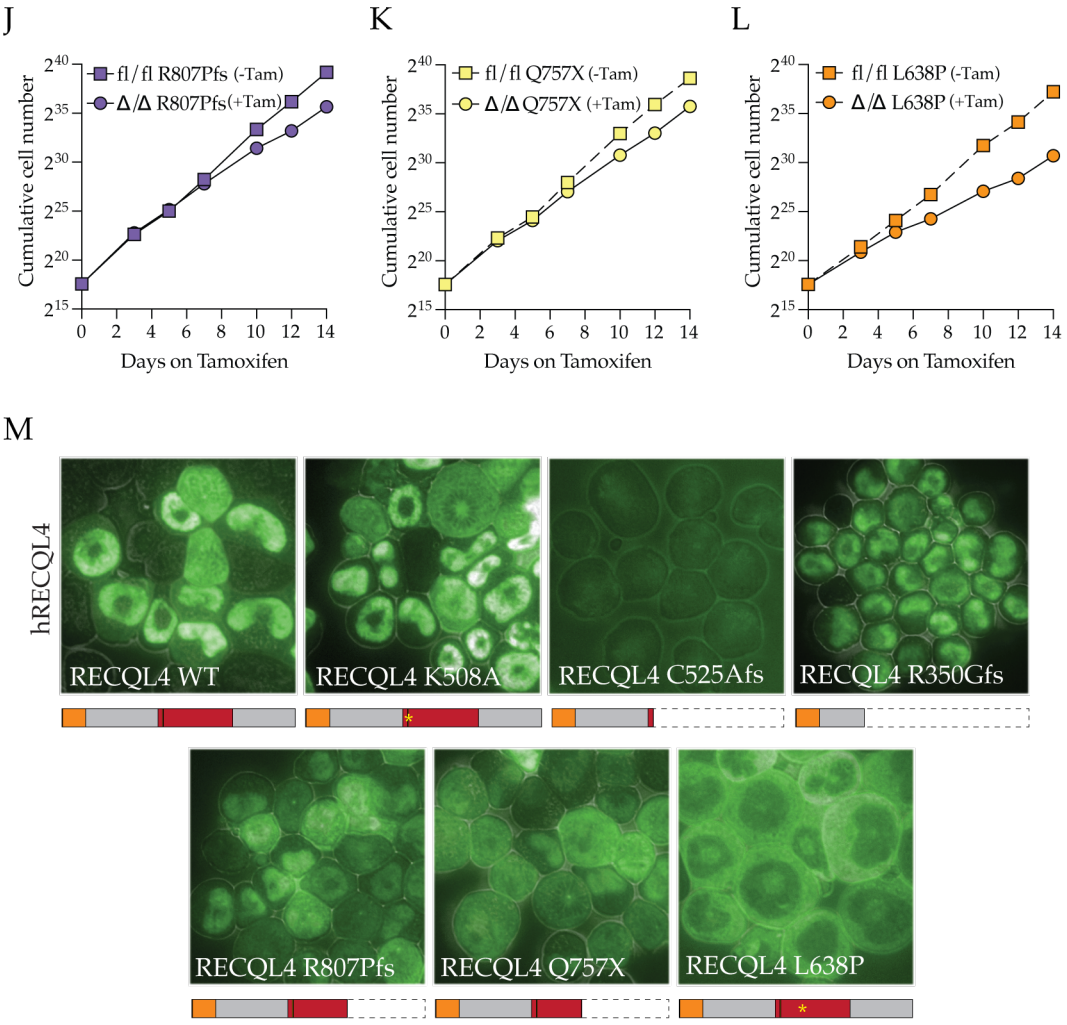

Figure 6.5: *Truncating human RECQL4 mutations C525Afs and R350Gfs fail to rescue Recql4 deletion and impede proliferation, similar to their murine homologs, while mutations that conserve the protein are better tolerated.* Proliferation curves of HoxB8 immortalised *R26*-CreER^{T2} myeloid cells without (fl) and with (Δ) tamoxifen-mediated *Recql4* deletion in the following cell lines: (A) fl/+; (B) fl/K525A; (C) fl/G522Efs; (D) fl/R347X. Proliferation curves of HoxB8 immortalised *R26*-CreER^{T2} *Recql4*$^{fl/fl}$ control myeloid cells (E) in the presence or absence of tamoxifen, and EGFP hRECQL4 over-expressing cells: (F) Wild type; (G) K508A; (H) C525Afs; (I) R350Gfs; (J) R807Pfs; (K) Q757X; and (L) L638P. Dotted lines represent individual controls not treated with tamoxifen. (M) Microscopy of EGFP-hRECQL4 expression in HoxB8 cells with WT, K508A, C525Afs, R350Gfs, R807Pfs, Q747X, L638P. A schematic illustration of the expected protein products is outlined below each figure. Orange box represents the Sld2-like region, red box the helicase region. Cell proliferation assays using murine mutations were repeated two times using independent cell lines. Retroviral complementation assays with human constructs were performed two times using the same parental cell line.

6.2.4 *Discussion*

Since Kitao *et al.* first cloned the *RECQL4* gene more than twenty years ago [113], some inroads have been made in the understanding of these mutations and their contribution to RTS. The majority of mutations reported in RTS patients are compound heterozygous mutations, containing at least one truncated allele and mainly impacting the helicase domain [56, 58]. This mutational spectrum implied that defects in the helicase region might be the main reason for the phenotypes of RTS. However, we recently showed that mice with a homozygous knock-in mutation that specifically inactivates RECQL4 ATP-dependent helicase activity were strikingly normal in terms of embryonic development, haematopoiesis, and DNA damage repair [211]. This led us to investigate the roles of truncating mutations.

Assessing the reported *RECQL4* mutations [56, 58, 64], RTS patients presenting with two severe truncating mutations are extremely rare. We identified several murine truncating mutations that closely map to mutations reported in RTS patients, affecting the helicase and C-terminal domain. With neither of these germline truncating mutants did we recover homozygous pups, suggestive of an essential developmental role for full-length RECQL4. Furthermore, in addition to lacking essential domains, there is the potential for these mutations to cause aberrant protein expression and localisation, further contributing to the phenotypes we observed. When we assessed protein levels of the truncating mutants, the G522Efs mutation was found to have undetectable protein. This could be either the consequence of nonsense-mediated mRNA decay or proteasomal degradation. The C525Afs human mutation, which maps closely to the murine G522Efs mutation, showed similar results. In contrast to the G522Efs mutation, the R347X mutation produced a short but stable protein that localised to the nucleus, albeit with reduced nucleolar intensity compared to WT or K508A protein. This protein retained the NTS1 (37-67 aa) nuclear localisation signal [123] but lacked one of the two predicted nucleolar localisation signals. The R350Gfs human mutation (mapping closely to the R347X) had a similar localisation and expression pattern. Taken together, we have shown that *Recql4* truncating mutations affect protein stability and subcellular localisation differently and that this phenotype is reproduced using comparable human mutations.

The skeletal system is impacted in the majority of RTS patients. A study of 28 RTS patients examined by radiologic survey found that up to 75% had some form of skeletal abnormality, including abnormal metaphyseal trabeculation, brachymesophalangy, thumb or radial agenesis or hypoplasia [74]. Several additional studies have associated loss of RECQL4 with a more systemic skeletal involvement with a high proportion of patients reporting low bone density [74, 75, 77–79]. However, to our knowledge, no studies have mapped skeletal defects to specific RECQL4 mutations. We found that heterozygous expression of the truncating alleles was sufficient to cause low trabecular bone mass, impaired growth of cortical bone, and narrower bones. Furthermore, we found that truncating mutations affect normal skeletal formation by causing defects in the osteoblast lineage. These findings were comparable to findings we previously reported in an osteoblast lineage restricted knock-out, which showed that complete deletion of *Recql4* in the osteoblast lineage led to reduced bone volume and defects in osteoblast proliferation and maturation [181]. This suggested that at least for bone development, having a truncated RECQL4 protein is equivalent to having no RECQL4 at all, which highlights the critical function of the deleted domains in bone homeostasis. Interestingly, an osteochondral-lineage-specific mouse model reported more severe findings than ours. Cao *et al.* used *Prx1*-Cre to delete *Recql4* in early mesenchymal progenitor cells of the limb buds and described a 50% reduction in bone volume and cortical bone area [75]. While RECQL4 is clearly needed in the earlier skeletal cell populations, it is important to consider that our models use truncating heterozygous mutations, instead of null alleles. Thereby, any remaining RECQL4 protein in the pre-osteoblast population of our mutants, might be sufficient for partial function at this stage and explain the phenotypic differences between models. Lastly, we observed that the R347X mutation, which produced a stable yet the shortest predicted protein, led to a more severe bone phenotype than the poorly expressed G522Efs mutation. This suggested that the severity of the defects was proportional to the severity of the truncation, irrespective of protein expression. Furthermore, the fact that the largest truncation caused the most severe bone phenotype suggests that RECQL4 gene dosage is a critical regulator of bone mass, something relatively unknown until now. Collectively, these results demonstrate that heterozygous truncating mutations of RECQL4 cause a haploinsufficient osteoporotic-like phenotype through defects in the osteoblast lineage. Although RTS patients generally present

with compound heterozygous mutations, these results highlight the importance of having a full-length protein for bone development. Furthermore, they raise concerns regarding the osteoporosis status of the parents of RTS patients, which warrants further investigation.

A characteristic feature of syndromes associated with mutations in RECQL4 is cancer predisposition, particularly OS, cutaneous epithelial tumours, and haematological malignancies [67, 100, 108]. A recent study analysed paediatric patients with cancer and identified significant enrichment of heterozygous *RECQL4* loss-of-function variants in those who presented with OS [99]. This has raised the question of whether the presence of compound heterozygous *Recql4* mutations in mice is sufficient to initiate tumorigenesis. We found no differences in tumour burden or spectrum in our compound heterozygous mutants compared with the wild type controls, even after exposure to γ-irradiation. Furthermore, although previous studies have reported ionising radiation as a risk factor for the development of sarcomas [216, 217], and truncated RECQL4 products have been associated with hypersensitivity to ionising radiation [218] and the development of phenotypes in other systems [56], we did not observe either haematopoietic failure, OS development, or additional phenotypes. It is possible that the non-truncating but helicase-inactive allele is sufficient to rescue the phenotypes and that truncating mutations in both alleles are necessary for tumour initiation or the involvement of other systems. However, this could not be addressed in this study given the developmental lethality seen in our homozygous truncating mice. It is also possible that more bone-specific carcinogens, such as Ca45, 32P, and 89Sr, are required to initiate OS development. These agents would deliver a significantly higher dose of DNA damage directly to the bone cells than could have been achieved with TBI. This remains unexplored in the context of RECQL4. Finally, it is possible that additional genes are involved in the development of these phenotypes. These are potential limitations of this thesis that should be addressed in future studies.

Lastly, we have established a tractable *in vitro* cell line model, allowing us to examine the cellular consequences of different *RECQL4* mutations. We found a proliferation defect in cells carrying murine truncating mutations, very similar to human mutations. This confirms that our murine mutations are useful surrogates for understanding the functions of human disease-associated *RECQL4* mutations. We used this system to analyse other human

mutations at a cellular level. Surprisingly, we found that cells overexpressing the wild type protein could not completely rescue *Recql4* deletion, potentially suggesting that overexpression of RECQL4 can also be pathogenic. In fact, several studies have correlated overexpression of *RECQL4* with the development of malignancies [118, 219–223]. We also found that the L638P mutation, which resulted in a stable full-length product with cytoplasmic localisation, could not fully rescue the *Recql4* deletion. This demonstrates that in order for RECQL4 to function effectively, it needs to be located within the nucleus. Finally, the R807Pfs and Q757X mutations, which have been found in RTS patients with OS and lymphomas [56], were able to rescue the *Recql4* deletion. This denotes that small C-terminal deletions do not severely affect viability, unlike larger deletions that include both the helicase and the C-terminal domains. However, their association with malignancies remains unknown. By comparing different mutations in the same genetic context, this system allowed us to conclude that the different mutations have distinct consequences on RECQL4. While some mutations create unstable proteins, some alter its localisation without grossly affecting protein stability. Furthermore, the level of the truncation directly correlates with the severity of the phenotype. Given the increasing number of somatic *RECQL4* mutations reported in sporadic cancers, this *in vitro* system can serve as a platform to assess the impact of *RECQL4* mutations at a cellular level.

In conclusion, truncating RECQL4 mutations affect protein stability and localisation, contributing to the development of an osteoporosis-like phenotype through defects in early osteoblast progenitors in mice. However, they are not sufficient to promote OS initiation or tumorigenesis, even after exposure to irradiation. Future studies should focus on the identification of genes that cooperate with RECQL4 in normal development and tumorigenesis. These could include functional genetic screens and the sequencing of patient tumour samples. Together, these will allow a better understanding of the genetic landscape of RTS that will permit the generation of more complete models.

6.2.5 *Supporting information*

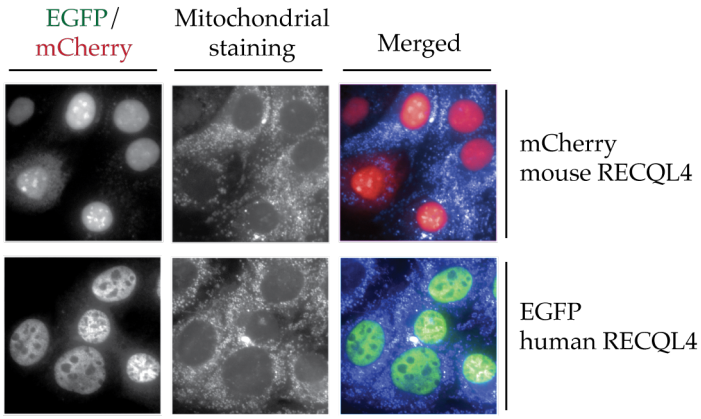

Supp. Figure 6.1: RECQL4 does not localise with mitochondria. Localisation of mCherry (red) fused mouse RECQL4 and EGFP (green) fused human RECQL4 in Kusa4b10 cells. In the same cell lines, mitochondrial localisation was determined by staining with Mitochondrial Staining Solution (MitoBlue, 1:500 diluted in HHBS). Images were colourised and merged.

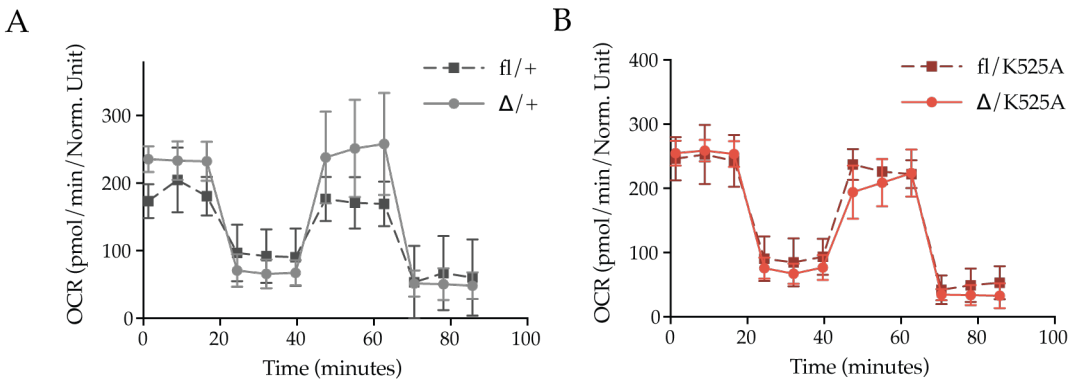

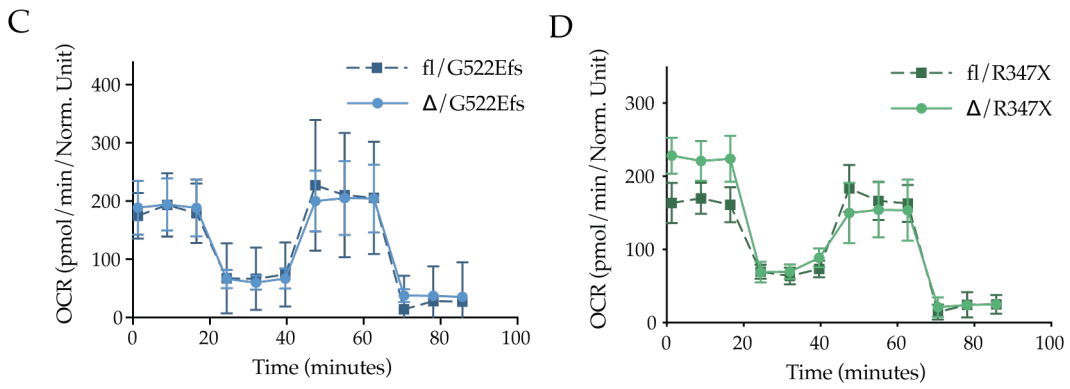

Supp. Figure 6.2: RECQL4 truncating mutants do not affect mitochondrial respiration. Seahorse XF24-3 instrument analysis of oxygen consumption rate (OCR) as a reflection of mitochondrial respiration in HoxB8 immortalised *R26*-CreER^{T2} myeloid cells after tamoxifen-mediated *Recql4* deletion (day 4 after tamoxifen addition) in the following cell lines: (A) Δ/+; (B) Δ/K525A; (C) Δ/G522Efs; (D) Δ/R347X. Dotted lines represent isogenic controls, not treated with tamoxifen. Data expressed as mean ± SEM. No statistical significance achieved between the tamoxifen-treated and non-treated groups. The experiment was performed using triplicate wells and was independently executed two times using the same cell lines.

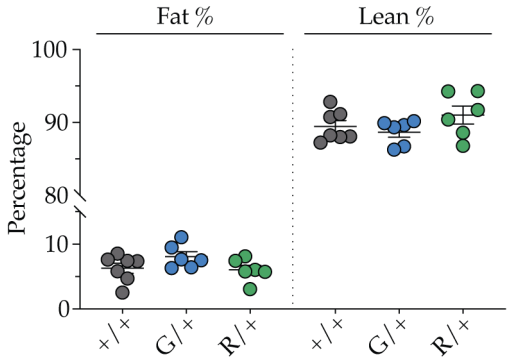

Supp. Figure 6.3: The reduced size of the heterozygous Recql4 mutants is not a result of a change in fat to lean mass ratio. Echo-MRI analysis of fat and lean percentage at ten weeks of age from males *Recql4*$^{+/+}$, *Recql4*$^{G522Efs/+}$, and *Recql4*$^{R347X/+}$ mice.

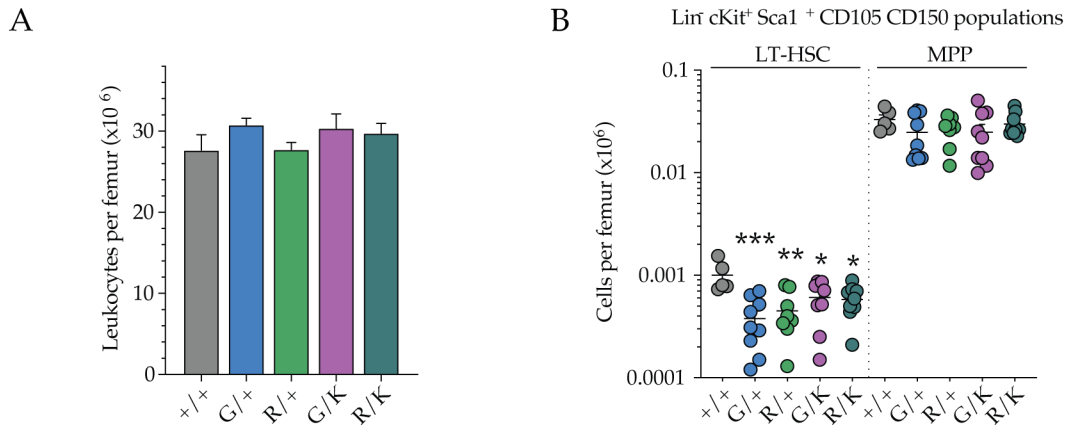

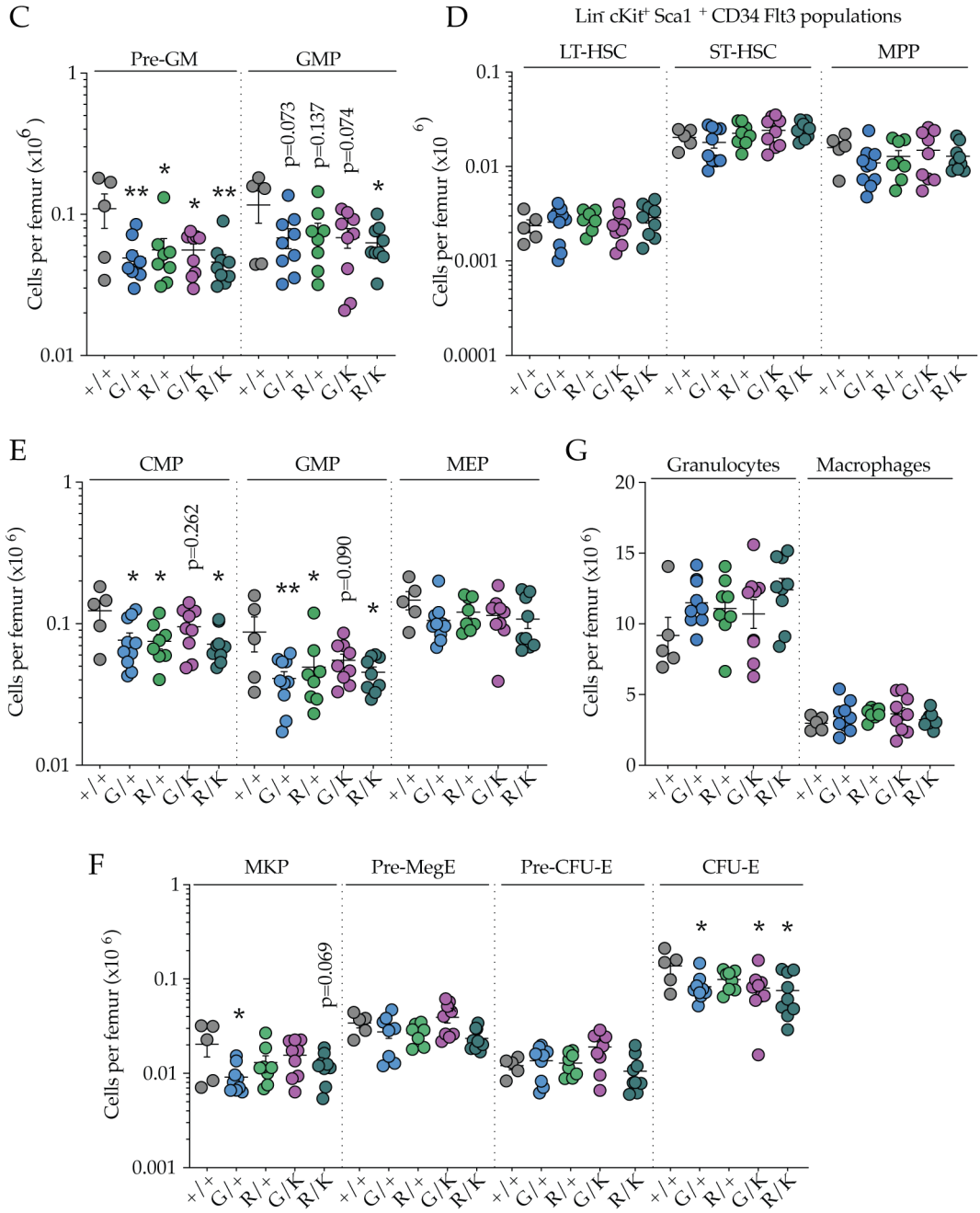

Supp. Figure 6.4: Heterozygous Recql4 truncating mutations mildly affect myeloid progenitor populations. (A) Total leukocyte counts. (B) Haematopoietic stem cells (HSC) and primitive progenitors based on Lin$^-$ c-kit$^+$ Sca-1$^+$ CD105/CD150 staining per femur. (C) Pre-GM and GMP populations per femur. (D) HSC and primitive progenitors based on Lin$^-$ c-kit$^+$ Sca-1$^+$ CD34/Flt3 staining per femur. (E) Numbers of myelo-erythroid progenitors (MEP) per femur. (F) Erythroid (Pre-CFU-E, CFU-E) and megakaryocyte progenitor (MkP) frequency in the BM and representative FACS plot. (G) Numbers of granulocytes and macrophages per femur. Data expressed as mean ± SEM, ordinary one-way ANOVA. *P<0.05; **P<0.01; ***P<0.001. Experiments were independently executed on separate cohorts, with results pooled for presentation. +/+=wild type, n=5; G=G522Efs, n=10; R=R347X, n=8; G/K=G522Efs/K525A, n=9; R/K=R347X/K525A, n=9.

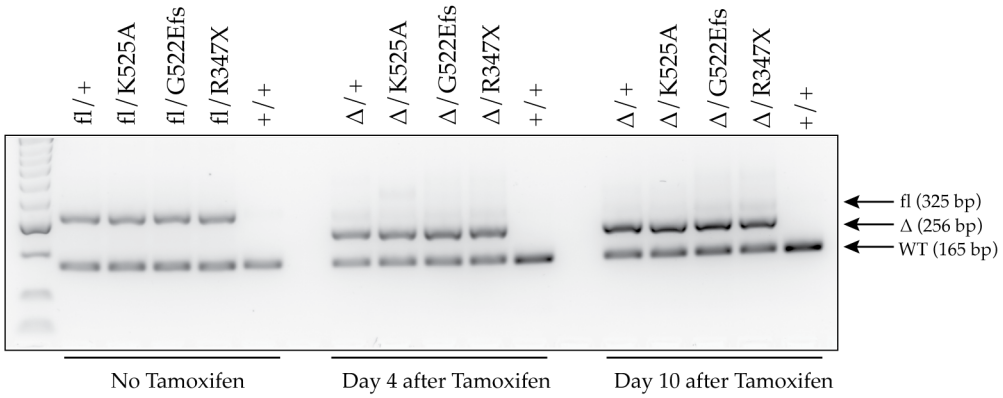

Supp. Figure 6.5: Effective deletion of Recql4 floxed allele in murine mutants. Genomic PCR from Hoxb8 immortalised *R26*-CreER^{T2} *Recql4*$^{fl/+}$, *R26*-CreER^{T2} *Recql4*$^{fl/K525A}$, *R26*-CreER^{T2} *Recql4*$^{fl/G522Efs}$, and *R26*-CreER^{T2} *Recql4*$^{fl/R347X}$ after addition of tamoxifen (400 nM/mL) for 14 days demonstrating efficient gene deletion. True wild type (+/+) was used as control.

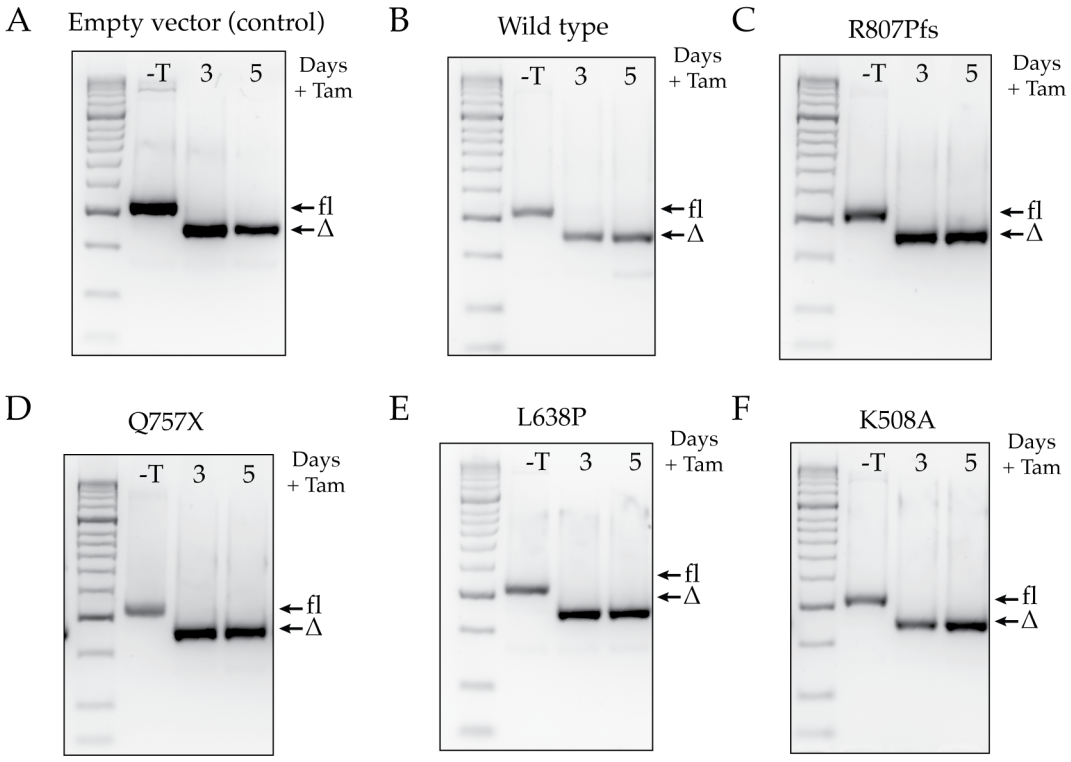

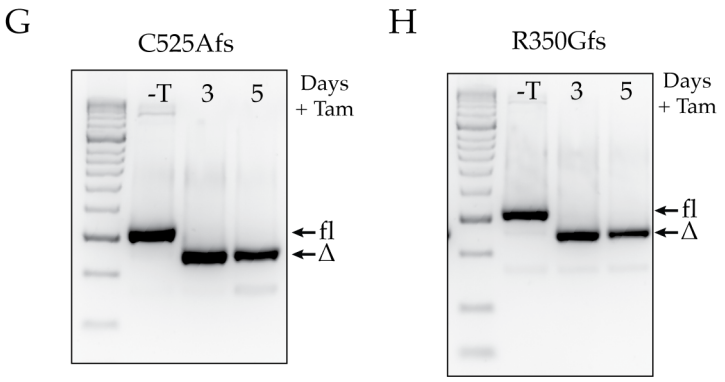

Supp. Figure 6.6: Effective deletion of Recql4 floxed alleles in cells expressing human constructs. Genomic PCR from Hoxb8 immortalised *R26*-CreER^{T2} *Recql4*$^{fl/fl}$ cells expressing: (A) empty vector (control); or EGFP fused (B) wild type RECQL4; (C) R807Pfs; (D) Q757X; (E) L638P; (F) K508A; (G) C525Afs; (H) R350Gfs. Efficient gene deletion was achieved after the addition of tamoxifen (400 nM/mL) for the indicated number of days.

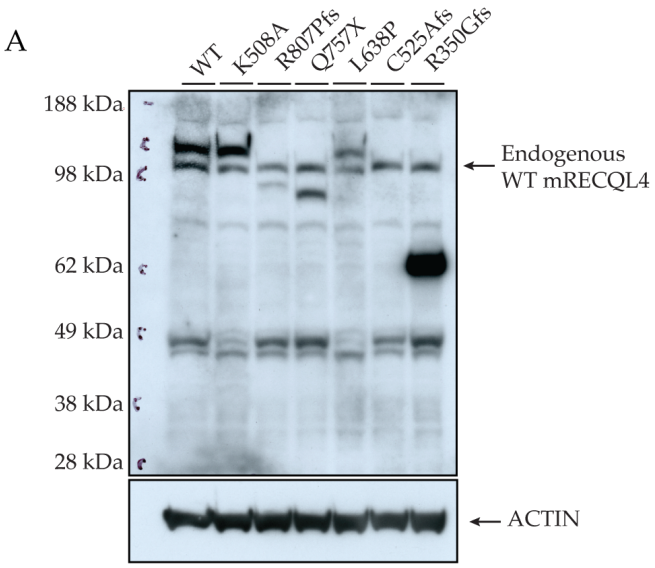

B

Human constructs	Expected protein size (kDa)
Endogenous mRECQL4 WT	135
EGFP hRECQL4 WT	161.8
EGFP hRECQL4 K508A	161.8
EGFP hRECQL4 R807Pfs	120.1
EGFP hRECQL4 Q757X	110.9
EGFP hRECQL4 L638P	161.8
EGFP hRECQL4 C525Afs	89.3
EGFP hRECQL4 R350Gfs	68.3

Supp. Figure 6.7: Protein expression of human constructs. (A) Western blot from Kusa4b10 cells expressing EGFP fused RECQL4 wild type, K508A, R807Pfs, Q757X, L638P, C525Afs, and R350Gfs. Cells probed with anti-human/mouse RECQL4 (clone 3B1; top). The same blot re-probed with anti-Actin (bottom). (B) Expected protein product sizes.

Supp. Table 6.1: Tumours observed in mutant mice. List of tumours found during autopsy.

TUMOUR TYPE	RECQL4$^{+/+}$	RECQL4$^{K525A/+}$	RECQL4$^{K525A/K525A}$	RECQL4$^{G522/K525A}$	RECQL4$^{R347X/K525A}$
Intestinal tumour	1	3	1	2	
Thymus tumour	2		2		1
Hepatic tumour	2	3	2	2	2
Lung tumour	1			1	
Spleen tumour				1	1
Mammary gland tumour			1		

Supp. Table 6.2: FACS Antibodies. List of antibodies used for flow cytometry in this study.

ANTIBODY (CLONE)	CONJUGATE	CATALOGUE #	COMPANY
Ter119 (TER-119)	PE	12-5921-83	Life Technologies Australia Pty Ltd/Thermo Fisher
CD71 (RI7 217.1.4)	APC	17-0711-82	Life Technologies Australia Pty Ltd/Thermo Fisher
B220/CD45R (RA3-6B2)	APC	17-0452-83	Life Technologies Australia Pty Ltd/Thermo Fisher
IgM (II/41)	Biotin	13-5790-82	Life Technologies Australia Pty Ltd/Thermo Fisher
CD43 (S7)	PE	553271	BD Pharmingen
CD19 (1D3)	PerCP-Cy5.5	45-0193-82	Life Technologies Australia Pty Ltd/Thermo Fisher
Mac1/CD11b (M1/70)	PE	12-0112-83	Life Technologies Australia Pty Ltd/Thermo Fisher

TABLE 6.2 – CONTINUED FROM PREVIOUS PAGE

ANTIBODY (CLONE)	CONJUGATE	CATALOGUE #	COMPANY
Gr-1/Ly6G (RB6-8C5)	PE-Cy7	25-5931-82	Life Technologies Australia Pty Ltd/Thermo Fisher
F4/80 (BM8.1)	APC	20-4801-U100	Tonbo Biosciences
CD4 (RM4-5)	eFluor-450	48-0042-82	Life Technologies Australia Pty Ltd/Thermo Fisher
CD8a/Ly-2 (53-6.7)	APC-eFluor 780	47-0081-82	Life Technologies Australia Pty Ltd/Thermo Fisher
TCRβ (H57-597)	PE	12-5961-83	Life Technologies Australia Pty Ltd/Thermo Fisher
CD25 (PC61.5)	PE	12-0251-83	Life Technologies Australia Pty Ltd/Thermo Fisher
CD44 (IM7)	APC	17-0441-83	Life Technologies Australia Pty Ltd/Thermo Fisher
Sca-1 (D7)	APC	17-5981-82	Life Technologies Australia Pty Ltd/Thermo Fisher
c-Kit/CD117 (2B8)	APC-eFluor-780	47-1171-82	Life Technologies Australia Pty Ltd/Thermo Fisher
CD34 (RAM34)	eFluor-660	50-0341-82	Life Technologies Australia Pty Ltd/Thermo Fisher
CD135/Flk2/Flt3 (A2F10)	PE	12-1351-82	Life Technologies Australia Pty Ltd/Thermo Fisher
FcgR/CD16/32 (93)	PerCP-Cy5.5	45-0161-82	Life Technologies Australia Pty Ltd/Thermo Fisher
CD41 (MWReg30)	eFluor-450	48-0411-82	Life Technologies Australia Pty Ltd/Thermo Fisher
CD105 (MJ7/18)	PE-Cy7	120409	Biolegend
CD150 (TC15-12F12.2)	PE	115904	Biolegend
Streptavidin	BV 605	563260	BD Pharmingen

6.3 RESEARCH IN CONTEXT

As mentioned in Chapter 2, previous murine models have contributed to the understanding of some of the functions of RECQL4, but they do not reflect the genetic status of RTS patients. As a result, the role and functions of truncating RECQL4 mutations in the pathogenesis of RTS have not been clearly differentiated from null alleles. To address this gap, in this chapter, I further characterised the long-term effects of a new series of truncating *Recql4* alleles that were introduced in Chapter 5, and that map closely to mutations reported in RTS patients.

The results of this chapter confirmed my hypothesis that truncating mutations of RECQL4 have deleterious effects on protein stability, cellular localisation, and bone homeostasis. Analysis of these mice demonstrated that while heterozygous animals were viable and fertile, homozygous mutants were developmentally lethal. Further analyses of heterozygous mice carrying two different RECQL4 truncating mutations demonstrated a haploinsufficient phenotype. In both cases, the germline heterozygous animals developed a low bone mass phenotype. Furthermore, I demonstrated that the skeletal defect was due to osteoblast lineage intrinsic defects. Analysis of the protein expression and localisation highlighted that amongst the mutations tested in detail the severity of the defect was related to the severity of truncation, irrespective of the protein expression, localisation and stability. I confirmed this using human RTS associated RECQL4 mutants in an *in vitro* complementation assay. This was unexpected and suggests that the degree of truncation is the primary determinant of the bone phenotype. However, these mutations did not result in elevated rates of tumour formation, not even after exposure to a sub-lethal dose of ionising radiation, which contradicts my hypothesis that tumour development is initiated by truncating mutations and accelerated by irradiation. These results point to the possibility that mutations in other genes, besides *Recql4*, might be contributing to the pathogenesis or tumorigenesis of RTS. The identification of additional genetic interactors of *Recql4* will be discussed in the following chapter.

CHAPTER 7

7

IDENTIFICATION OF NOVEL GENETIC INTERACTIONS WITH RECQL4 IN A GENOME-WIDE CRISPR/CAS9 RESCUE SCREEN

7.1 INTRODUCTION

Studies of familial cancer predisposition syndromes have yielded enormous insight into the pathogenesis of human cancer, both familial and sporadic. As one of them, RTS is associated with elevated rates of OS, epithelial tumours and haematological neoplasias [56, 64, 67]. However, the mechanisms involved in its pathogenesis or tumorigenesis remain mostly unknown.

In the previous chapters, I described several mouse models that resemble mutations seen in RTS patients and that have advanced our understanding of their *in vivo* effects. In Chapter 5, I generated a mouse model with an ATP-dependent helicase inactive mutation and showed that the ATP-dependent helicase activity of *Recql4* was not essential for its physiological functions. Then in Chapter 6, I generated mice carrying two distinct truncating mutations that deleted the helicase and the C-terminal domains, which altered the stability and subcellular localisation of RECQL4 and translated to a homozygous embryonic lethality and a haploinsufficient low bone mass phenotype. However, these mutations did not result in increased tumorigenesis, not even after exposure to a sub-lethal dose of ionising radiation. This might point to the possibility that mutations in other genes, besides *Recql4*, might be contributing to the development of these malignancies and to the phenotypes of RTS, an aspect of the disease that has been largely unexplored.

The literature regarding the molecular interactions of RECQL4 is limited. As previously described, a limited number of proteins have been demon-

strated to interact with RECQL4 in processes such as DNA replication, DNA repair, mitosis, and telomere maintenance (Table 2.2). Only recently, *ANAPC1* mutations were found in patients clinically diagnosed with RTS type 1 [59], which has many overlapping features with RTS type 2. This suggested that *RECQL4* and *ANAPC1* may share a common pathway. However, beyond these interacting proteins and the potential pathways involved, little is known about other factors that interact with RECQL4, both physically and genetically, and that contribute to the pathogenesis or tumorigenesis of the disease. Furthermore, as no treatments for RTS are available, we are unable to meaningfully improve the long-term outcomes of patients with RTS. This led me to investigate possible genetic interactions with mutant *Recql4* that may be able to improve the phenotypes associated with pathogenic *Recql4* mutations using a genome-wide genetic rescue screen. For this, I have chosen to utilise the recently developed Clustered Regularly Interspaced Short Palindrome Repeat-associated nuclease Cas9 (CRISPR/Cas9) technology with the mouse genome-wide Brie sgRNA KO library [190].

CRISPR/Cas9 was first discovered in archaea and bacteria as an immune mechanism to avoid viral DNA invasion [224]. It has recently demonstrated high efficiency in mammalian cells, and many reagents and tools have been rapidly developed and made available to the research community. For mammalian systems, it combines the Cas9 nuclease with a gene-specific targeted single guide RNA (sgRNA), which can be delivered into cells in several ways including via lentivirus or retrovirus, and serves as a molecular tag to achieve efficient genome editing at specific sites within DNA [225]. When Cas9 is guided to the target DNA, it creates DSBs as directed by the location of the sgRNA and PAM sequence that are then repaired via NHEJ [226]. This process can result in frameshift insertion/deletion (indel) mutations, which can be used to generate a specific gene knockout. Because of its high gene-editing efficacy and relative ease of use compared to transfected siRNA, genome-wide CRISPR/Cas9 knockout screens have been utilised to identify cooperating genes in several settings [227–230]. However, to my knowledge, it has not been applied to explore genes that cooperate with *RECQL4*.

In this chapter, I have performed a genome-wide loss-of-function rescue screen using CRISPR/Cas9 mediated gene disruption in murine Hoxb8 immortalised myeloid cells to better understand the genetic interactions

of mutant *Recql4*. The results revealed novel genes that potentially interact with mutant *Recql4*, particularly *Klhdc3*, which I further validated by sgRNA knockout and proliferation assays. This confirmed that *Klhdc3* mutation rescued the proliferation defect of *Recql4* mutant cell lines, suggesting a functional genetic relationship between these genes.

7.2 RESULTS

7.2.1 *Hoxb8 Recql4 myeloid cells stably express Cas9*

The screen was performed in Hoxb8 immortalised *R26*-CreER^{T2} *Recql4*$^{fl/+}$ (control) and *R26*-CreER^{T2} *Recql4*$^{fl/R347X}$ (mutant) myeloid cells. This cell type was chosen given the requirement of RECQL4 for maintenance of this cell population *in vivo* [88] and based on results from Chapter 5, which confirmed that restricted somatic expression of the R347X mutation causes loss of these populations [211]. Additionally, these cells divide rapidly (<24 hrs per cell cycle), and therefore, can be obtained in sufficient numbers for screening at a suitable copy number per sgRNA. Finally, they are non-adherent suspension cells, making cell culture significantly easier than for adherent cell lines. All these parameters combined made this cell line suitable for the screen. I then proceeded to infect these cell lines with pLentiCas9-blasticidin derived virus and to select with blasticidin for 14 days to generate stably expressing Cas9 cells (Figure 7.1 A).

To determine the activity of the Cas9 in the Hoxb8 *R26*-CreER^{T2} *Recql4*$^{fl/+}$ and *R26*-CreER^{T2} *Recql4*$^{fl/R347X}$ cell lines, these cells were transduced with a pLentiGuide expressing sgRNA targeting the cell surface marker CD44, which is highly expressed on the Hoxb8 cells, independent of genotype. Cells were kept in puromycin for five days to select for sgRNA expression and to allow gene editing to occur, then stained with a PE-Cy7 conjugated CD44 antibody and analysed by flow cytometry. The results showed a loss of CD44 expression in ~70% of the cells in both the control and the mutant cell lines (Figure 7.1 B), indicating effective gene editing by Cas9, and therefore, successful generation of Hoxb8 *Recql4* myeloid cells stably expressing Cas9.

I then determined if stable Cas9 expression had affected the cell proliferation phenotypes of the control and *Recql4* mutant cell lines. Hoxb8 *R26*-CreER^{T2} *Recql4*$^{fl/+}$ and *R26*-CreER^{T2} *Recql4*$^{fl/R347X}$ Cas9 cells were

treated with 4-hydroxy-tamoxifen for 14 days to induce CreER recombinase activity and deletion of the floxed allele, leaving only the mutant allele expressed. The mutant cell line showed a decrease in cell proliferation (Figure 7.1 C), consistent with what I previously observed *in vivo* (Figure 5.6) and in the parental non-Cas9 expressing cells of the same genotype (Figure 6.5). Similarly, successful deletion of the floxed *Recql4* allele was achieved by day four as confirmed by PCR for genomic recombination (Figure 7.1 D). In the mutant cells, a floxed band re-appeared at days 11 and 14, indicating a strong selection against loss of the WT allele favouring clonal outgrowth of non-recombined cells, even in the continuous presence of tamoxifen. Taken together, these results suggest that Cas9 Hoxb8 *Recql4* myeloid cells represent a robust platform for a short-term genome-wide CRISPR/Cas9 knockout screen.

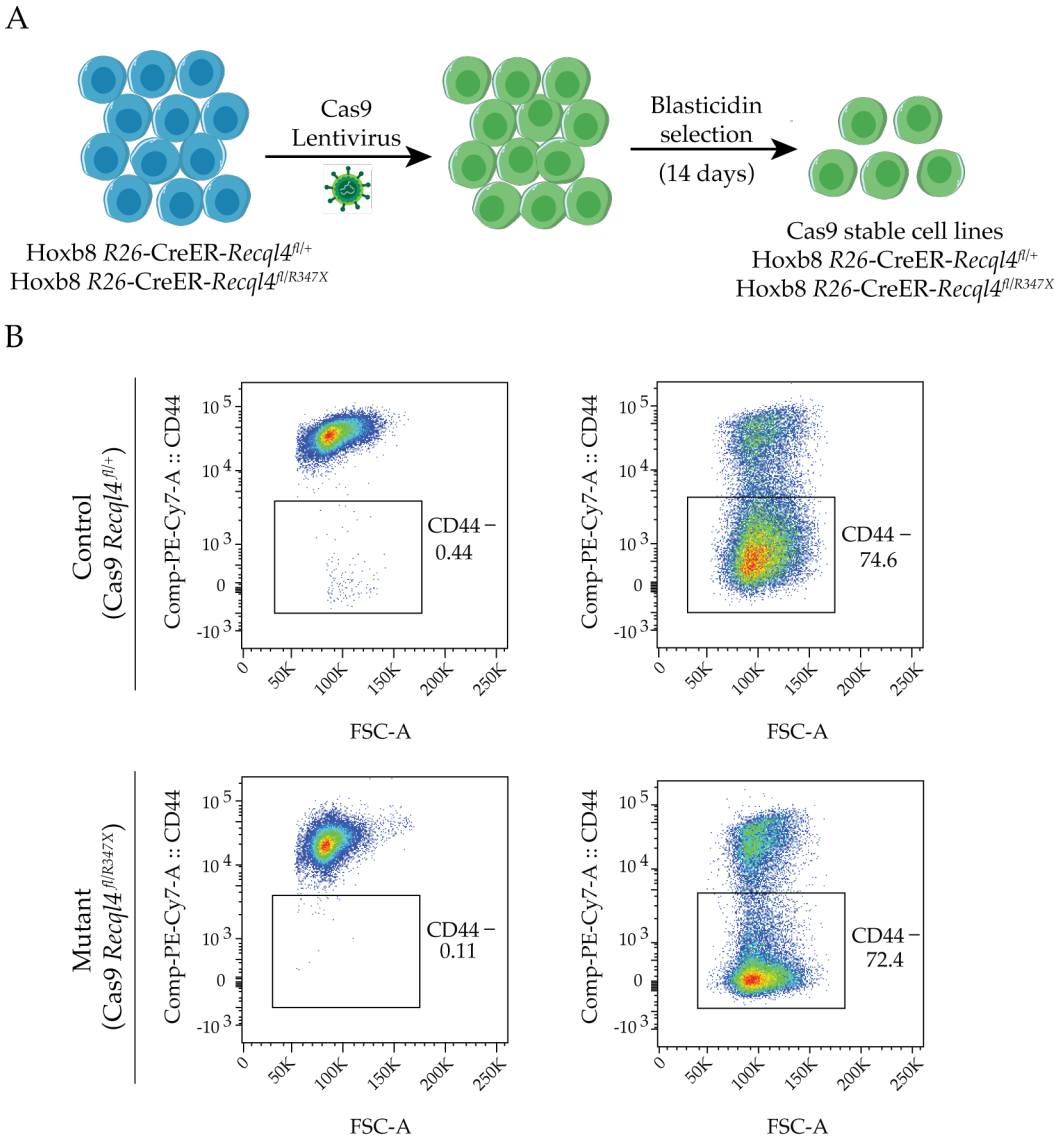

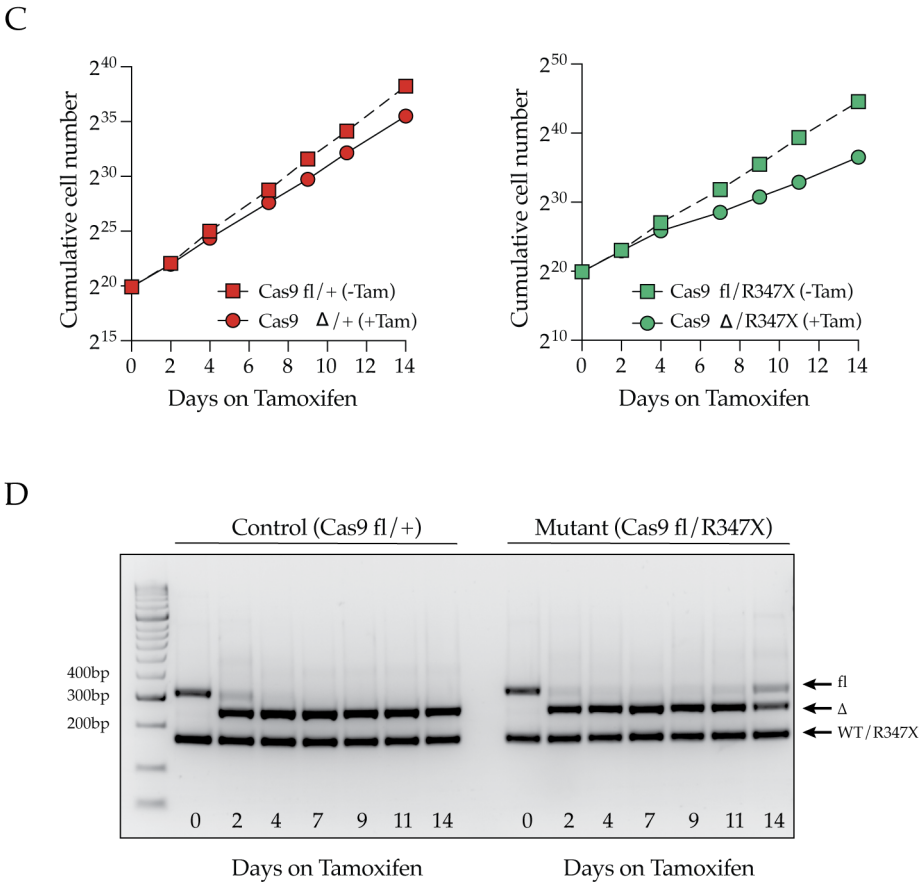

Figure 7.1: *Hoxb8 Recql4 myeloid cells stably expressing Cas9.* (A) Schematic representation of Cas9 transduction. Hoxb8 *R26*-CreER^{T2} *Recql4*$^{fl/+}$ and Hoxb8 *R26*-CreER^{T2} *Recql4*$^{fl/R347X}$ cells were transduced with pLentiCas9 virus and were subsequently selected with blasticidin for 14 days. (B) *In vitro* validation of Cas9 activity. Hoxb8 myeloid cells expressing Cas9 were transduced with sgRNA against *Cd44* to determine the gene-editing efficiency of Cas9. CD44 protein expression was measured by FACS after four days of puromycin selection showing efficient loss of expression. (C) Proliferation assay. *In vitro* validation of the phenotype caused by deletion of the floxed *Recql4* WT allele. Hoxb8 myeloid cells (control and mutant) expressing Cas9 received tamoxifen treatment for 14 days to delete the floxed allele. As expected, the mutant (R347X) cells showed slower proliferation than the controls after the addition of tamoxifen. (D) Analysis of recombination of Cas9 Hoxb8 myeloid cells. Genomic DNA PCR showing successful recombination and deletion of the floxed allele.

7.2.2 *Genome-wide CRISPR/Cas9 knockout screen identifies Klhdc3 as a candidate Recql4 interacting gene*

To uncover genes that interact with mutant *Recql4*, I conducted a pooled genome-wide CRISPR/Cas9 knockout screen in the Cas9 Hoxb8 *Recql4* myeloid cells. Control (Cas9 *R26*-CreER^{T2} *Recql4*$^{fl/+}$) and mutant (Cas9 *R26*-CreER^{T2} *Recql4*$^{fl/R347X}$) cells were infected with lentivirus containing

the Brie mouse genome-wide sgRNA library at a multiplicity of infection (MOI) of 0.3. This was chosen to reduce the probability of multiple sgRNA infecting a single cell. The library contained 78,637 sgRNAs targeting 19,674 genes (four sgRNAs per gene) [190]. Seven days after lentiviral transduction and puromycin selection, tamoxifen was added and maintained for 14 days to induce Cre-mediated recombination and delete the floxed wild type *Recql4* allele, leaving only the R347X allele (mutant) or the wild type (control) allele expressed. Cell pellets from the expanded surviving populations of both cell lines were collected at day 0 (the day the tamoxifen was added), and days 4 and 9 of tamoxifen treatment (Figure 7.2 A). By day 9, cells have undergone at least ten cell divisions allowing the identification of genes that, when deleted, restored the proliferation and viability of the mutant cells or those who were synthetic lethal with the R347X mutation. Next, gDNA was extracted from the cell pellets, and DNA libraries were prepared by PCR amplification of the integrated sgRNA constructs. The PCR products were pooled together to capture the full representation of the screen and then purified and analysed by Illumina HiSeq sequencing (sequencing performed by Novogene, SE150 bp).

The differences in sgRNAs levels between samples were computed using the CRISPR-Beta-Binomial package (CB^2) [191]. The analysis creates a normalised sgRNA read count for each of the four sgRNAs targeting a gene and calculates the fold change between the samples to generate a list of enriched or depleted sgRNAs. Before identifying candidate rescue genes, I evaluated the quality of the screen samples. First, I assessed the distribution of sgRNA frequencies across timepoints in the control and mutant samples. As shown in Figure 7.2 B, mapped sgRNA reads appeared to be uniformly distributed across samples. In Figure 7.2 C, the GINI index, a measure of evenness between samples, showed lower values at day 0 that mildly increased at day 4 and 9. This is expected in a positive selection screen where surviving clones with high counts for a few sgRNA can dominate the final pool. Next, I evaluated the sgRNA-levels across cell lines and timepoints. Predictably, the heatmap showed a high correlation between timepoints of the same cell lines and low correlation across different cell lines (Figure 7.2 D), which was explained by the proliferation defect seen in the mutant cell lines, but not in the control, after tamoxifen-induced deletion of the floxed *Recql4* allele. Similarly, the Principal Component Analysis (PCA) showed different read

count distributions across cell lines, which were sequentially increased at later timepoints (Figure 7.2 E). As a final validation of the performance of this screen, the $\log_2$ fold change (D9 vs D0) in sgRNA read counts of essential genes was assessed. These included universally essential genes such as *Polr2d*, *Sf3b1*, and *Tuba1a*; cell-type-specific genes such as *Hoxb8* (cell lines were immortalised with Hoxb8), *Csf2ra* (GM-CSF receptor, cell lines are dependent on GM-CSF for survival), and *Recql4*; and the top 10 human core essential genes, previously published by Hart *et al.* [194]. As anticipated, results showed a depletion of guides targeting essential genes (Figure 7.2 F), indicating a successful targeting approach and technical execution of the screen.

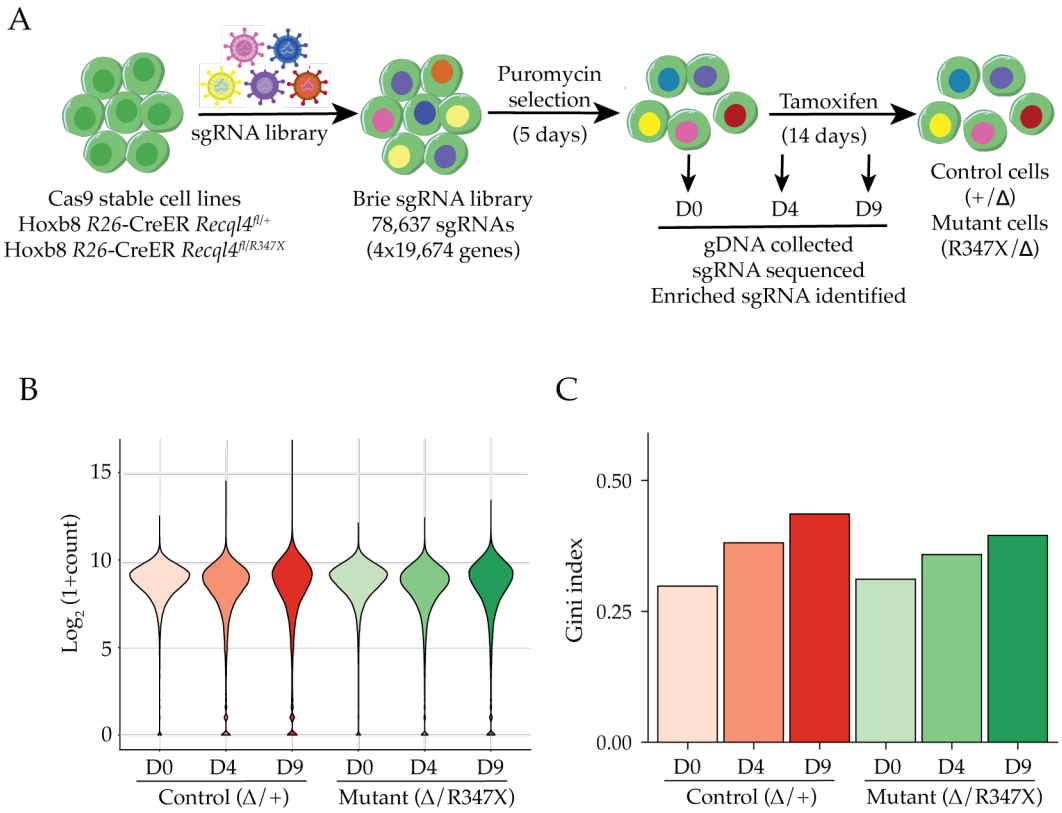

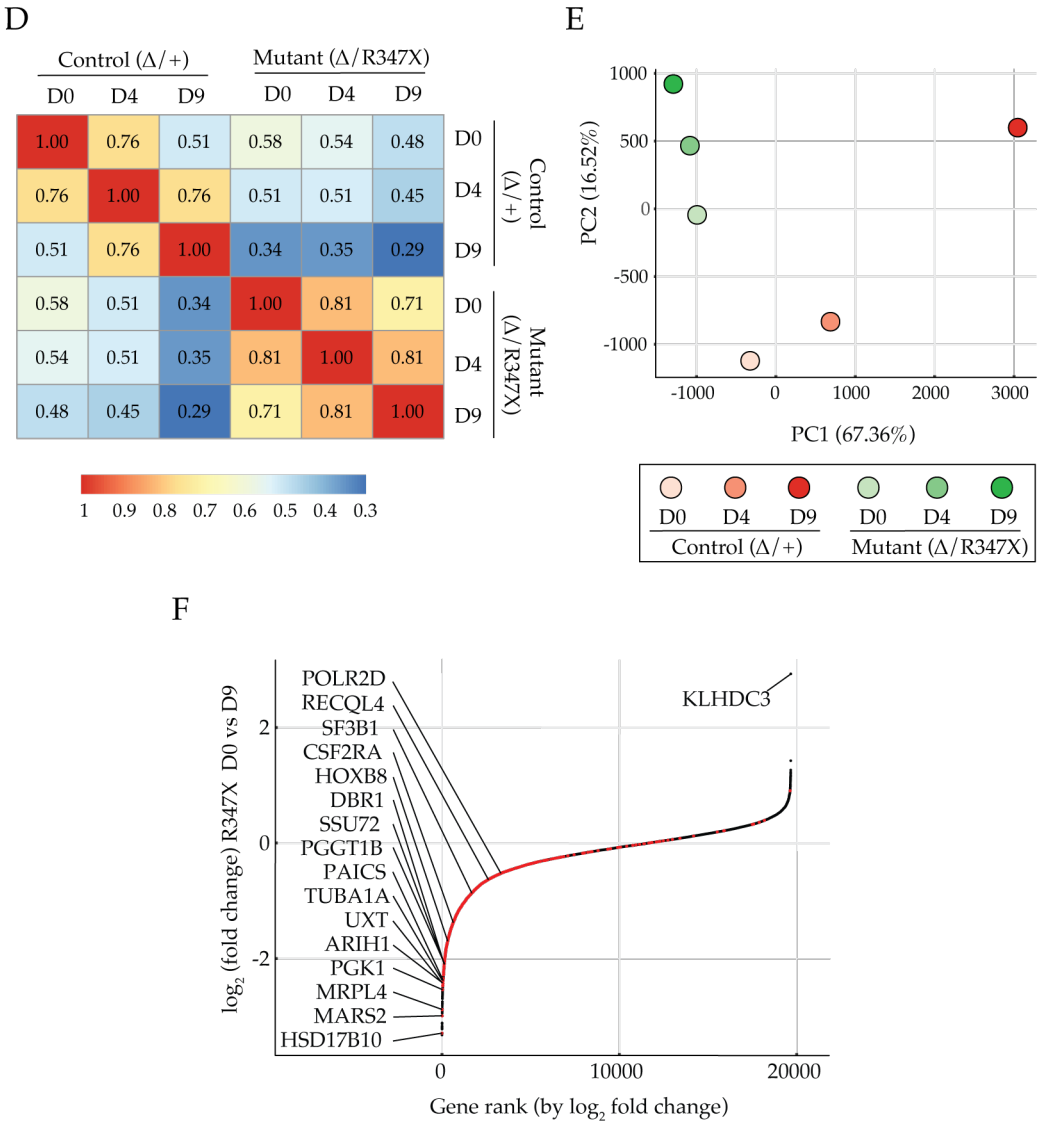

Figure 7.2: *CRISPR Screen design and quality control.* (A) Overview of CRISPR knock-out screening strategy. The Brie library containing 78,637 sgRNAs against 19,674 genes (~4 guides per gene) was packaged into lentiviral particles and transduced into stable Cas9 Hoxb8 *Recql4* myeloid cells. sgRNA transduced cells were then selected by puromycin for five days. sgRNA expressing cells were cultured in tamoxifen for 14 days and samples from days 0, 4 and 9 were collected for analysis. (B) sgRNA count distribution or mappability. Violin Plot showing sgRNA frequencies at day 0, 4, and 9 and control (fl/+) and mutant (fl/R347X) cell lines. (C) Gini index computed from normalised sgRNA counts for all cell line replicates. (D) Heatmap showing sgRNA-level correlation between timepoints of control and mutant cell lines. (E) Principle component analysis (PCA) of sgRNA-sequencing results from day 0, 4, and 9 of control and mutant cell lines. (F) Essential gene depletion. sgRNAs of R347 D9 vs D0 were ranked by $\log_2$ fold change, showing loss of representation of known and predicted essential genes.

Following quality control, the results were analysed and sgRNAs were ranked by $\log_2$ fold change ($\log_2$ FC), comparing D0 vs D4 and D9 and mutant vs control. The screen identified a list of sgRNAs that were enriched in the mutant (Δ/R347X) cells, which were not enriched in the control (Δ/+) cells (Figure 7.3 A). The most enriched rescue candidate was sgRNA against *Klhdc3* ($\log_2$ FC=2.93), followed by *Aqp9* ($\log_2$ FC=1.43), *Phf23* ($\log_2$ FC=1.26), *Sspo* ($\log_2$ FC=1.23), *Samd1* ($\log_2$ FC=1.21), *Hnrnph1* ($\log_2$ FC=1.20), *Glycam1* ($\log_2$ FC=1.17), *Ppp1r3f* ($\log_2$ FC=1.17), *Slc5a7* ($\log_2$ FC=1.17), and *Ralgapb* ($\log_2$ FC=1.16) (Figure 7.3 B). These top 10 sgRNAs in the mutant cells did not overlap with the top 10 sgRNAs of the control (Δ/+) cells, which revealed different enriched candidates (Figure 7.3 C). An expanded list of 25 rescue candidates, ranked by fold enrichment in the mutant cells, further specifies that all sgRNAs, except sg*Hnrnph1* and sg*Trp53*, were significantly more enriched in the mutant cells (Figure 7.3 D).

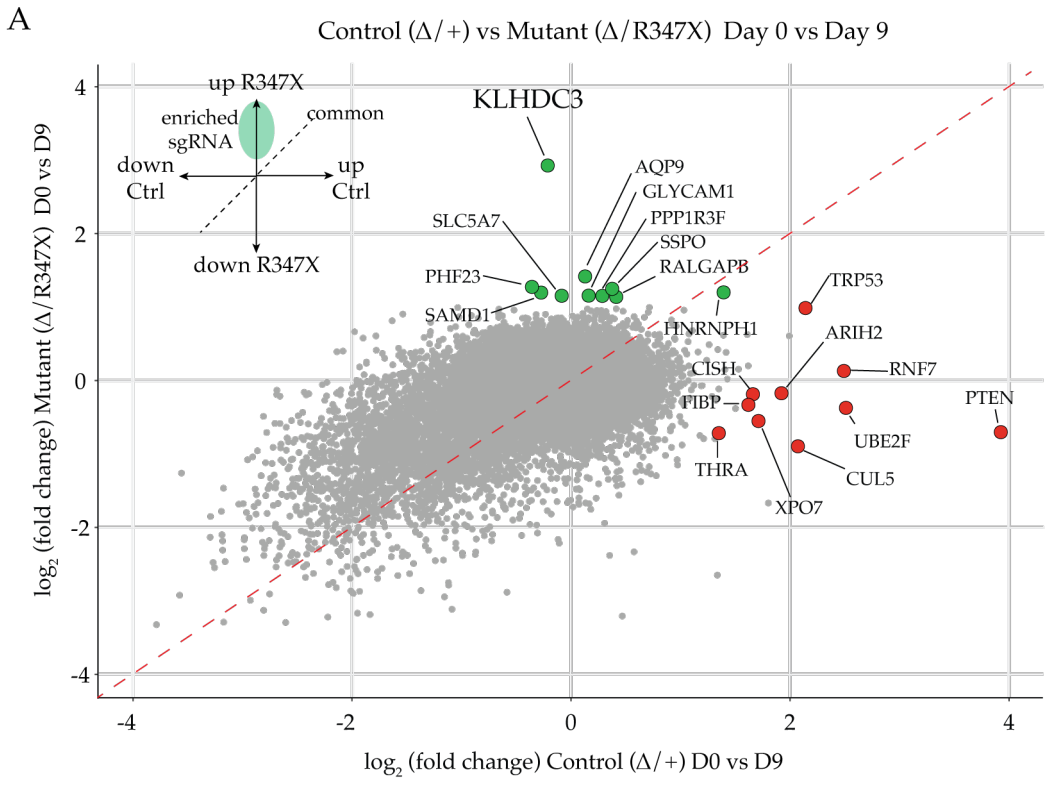

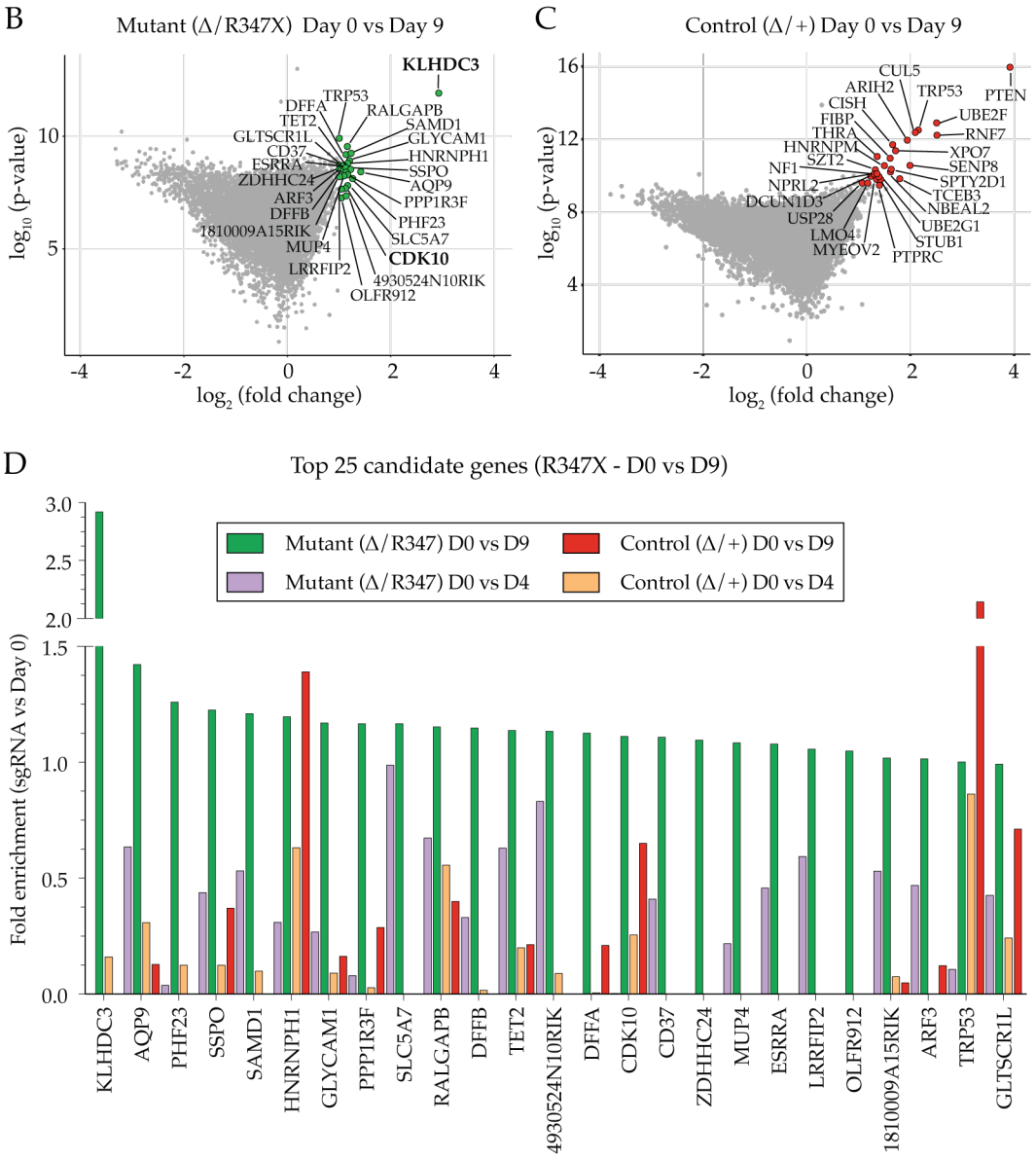

Figure 7.3: *Identification of top genetic hits in the CRISPR/Cas9 knockout screen.* (A) Scatterplot showing top 10 enriched genes in each of the mutant (Δ/R347X; green dots) and control (Δ/+; red dots) cell lines at day 9 post-tamoxifen compared to day 0. A schematic of the plot shows the area of interest shadowed in green. (B) Scatterplot showing top 10 enriched genes in the mutant (Δ/R347X) cell line at day 9 post-tamoxifen compared to day 0. (C) Scatterplot showing top 10 enriched genes in the control (Δ/+) cell line at day 9 post-tamoxifen compared to day 0. (D) List of top 25 enriched genes ranked according to fold enrichment in the mutant (Δ/R347X) cell line for day 9 post-tamoxifen versus day 0 (Green). The enrichment level of these genes in is also shown for D4 vs D0 and the control cells at the same timepoints: Mutant (Δ/R347X) day 4 versus day 0 (Purple); control (Δ/+) day 9 versus day 0 (Red); and control (Δ/+) day 4 versus day 0 (Orange).

Taken together, the results of this section show the successful application of a CRISPR/Cas9 knockout screen for positive selection using the Brie sgRNA library. From this screen I identified a variety of sgRNAs targeting genes that were significantly enriched in the mutant cell lines when compared to controls, indicating that deletion or inhibition of these genes might potentially rescue the proliferation defects seen in the mutants. One of the genes, *Klhdc3*, was identified as the top hit and will be validated in the next section.

7.2.3 *KLHDC3 mutation partially rescues the proliferation defect of cells expressing truncated mutant RECQL4*

Klhdc3 was the most enriched sgRNA in the mutant (Δ/R347X) cells. All four sgRNAs targeting *Klhdc3* in the library were increased in the RECQL4 mutant cells but not in control cells (Figure 7.4 A), implying that *Klhdc3* mutation might improve cell proliferation of $Recql4^{\Delta/R347X}$ cells only.

To validate these results, I generated *Klhdc3* knockout cells by infecting Hoxb8 Cas9 *R26*-$CreER^{T2}$ $Recql4^{fl/R347X}$ cells with two sgRNAs from the Brie library and two additional sgRNAs not represented in the screening library, with all sgRNA targeting different regions of the gene. As a control, mutant cells were also infected with a sgRNA targeting a non-essential cell surface marker (CD81) and sgRNA against a gene depleted in the R347X mutant but not in the control (*Zfp36l2*). One week after infection and five days after puromycin selection, tamoxifen was added to the cells for 14 days to delete the floxed allele and to determine if the loss of KLHDC3 could rescue the proliferation defect previously seen in the *Recql4* single mutant cells. The results were compared to non-tamoxifen treated cells, cells expressing sg*Cd81* and sg*Zfp36l2*, a non-targeting virus control (ZsGreen), and a non-infected control (mock). Results showed that mutation of *Klhdc3* using any of the four sgRNAs did not affect proliferation of the non-tamoxifen treated cells but was able to partially rescue the proliferation defect caused by deletion of the wild type *Recql4* allele in mutant cells (R347X). In contrast, cells transduced with sg*Cd81* and sg*Zfp36l2*, or a non-targeting virus did not show any rescue, similar to the non-infected control ((Figure 7.4 B).

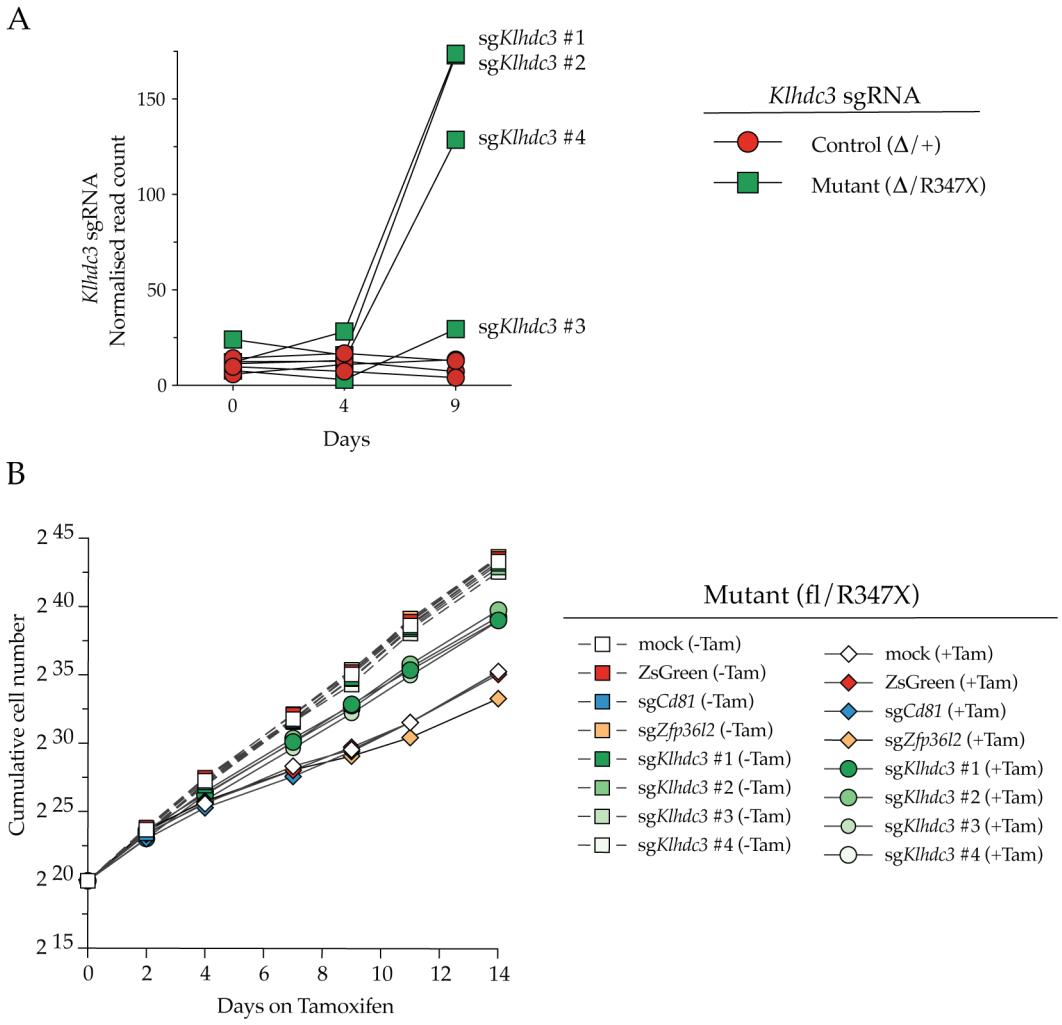

Figure 7.4: *Klhdc3 sgRNA knockout partially rescues proliferation defect in RECQL4 mutant cells.* (A) sgRNA read counts identifying *Klhdc3* as the gene target of the most significantly enriched sgRNAs in the library screening. The sgRNAs targeting *Klhdc3* were consistently enriched in tamoxifen-treated mutant (R347X) cells on day 9, in contrast to control cells. (B) Proliferation assay showing that sgRNAs against *Klhdc3* rescue RECQL4 R347X point mutant cells (circles). Results were compared to non-tamoxifen treated cells (squares), and sgRNA targeting *Cd81* (a non-essential cell surface marker), sg*Zfp36l2* (a guide depleted in the mutant but not in the control), ZsGreen (a non-targeting virus control), and a mock (non-infected) control (diamonds).

A variety of experiments were conducted to corroborate the validity of these findings. First, I performed PCR to confirm the efficiency of *Recql4* deletion. Effective deletion of the floxed allele was achieved by day four post-tamoxifen and was maintained for at least 14 days in the *Klhdc3* mutant cells, a time at which non-rescued control populations show significant outgrowth of non-deleted cells (Figure 7.5 A). Second, by Western blotting, I demonstrated stable loss of the wild type *Recql4* allele and stable expression

of the mutant protein nine days after tamoxifen treatment, which further confirmed the efficiency of *Recql4* deletion in the mutant cells (Figure 7.5 B). Finally, successful *Klhdc3* inactivation by sgRNA disruption was measured by quantitative RT-PCR and validated by the reduced RNA expression levels seen in the sg*Klhdc3* targeted Δ/R347X mutant cells (Figure 7.5 C). On the genomic DNA level, the editing efficiency of each sgRNA targeting *Klhdc3* was confirmed by T7 endonuclease assays (Figure 7.5 D) and Sanger sequence trace analyses by Tracking of Indels by Decomposition (TIDE) (Figure 7.5 E) [231], with both techniques showing 35-80% efficiency in mixed cell populations. Since no appropriate antibodies have been identified for KLHDC3, the loss of its expression at a protein level could not be determined by Western blotting at this time. Taken together, the experiments performed in this section confirm that the deletion of KLHDC3 can partially rescue the proliferation defect of $Recql4^{\Delta/R347X}$ mutant cells.

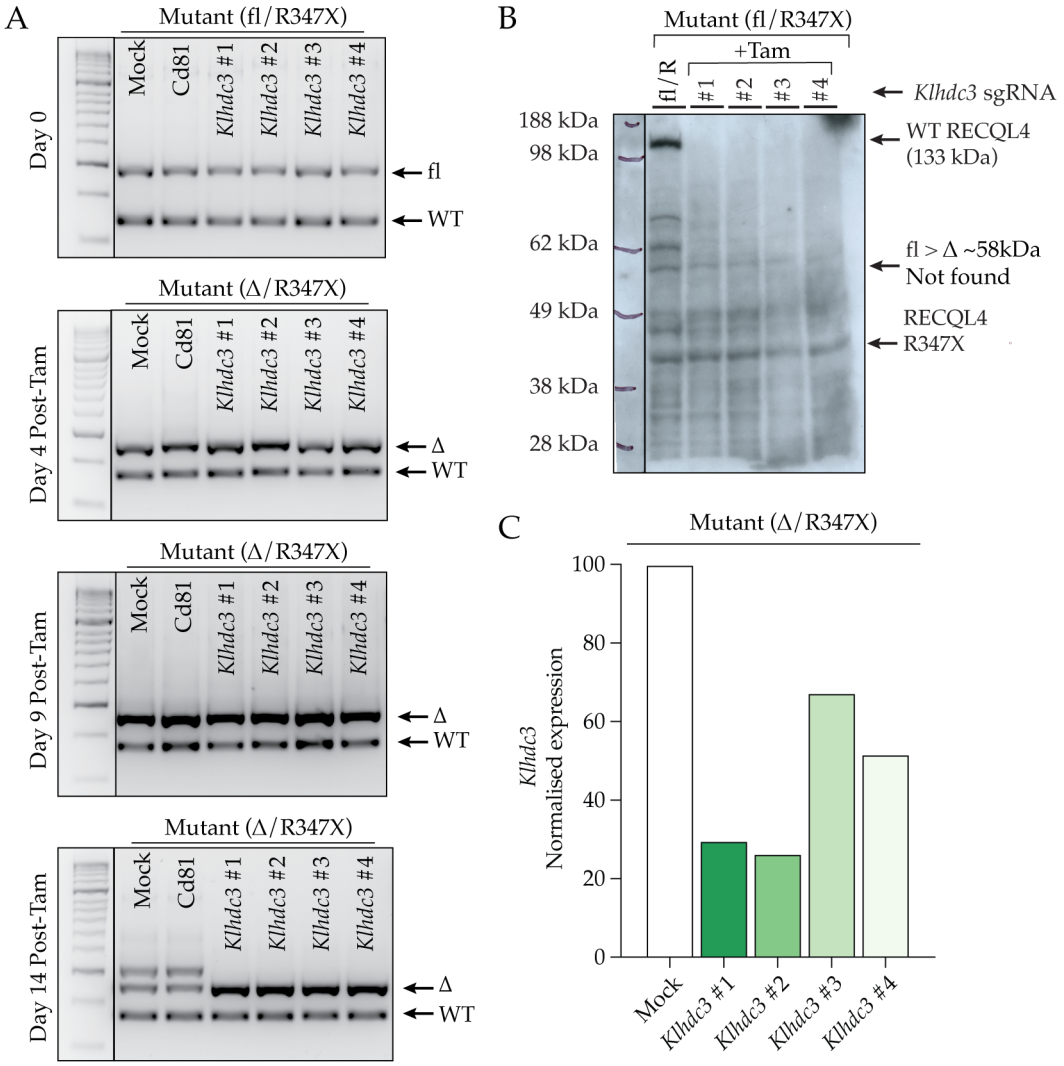

D

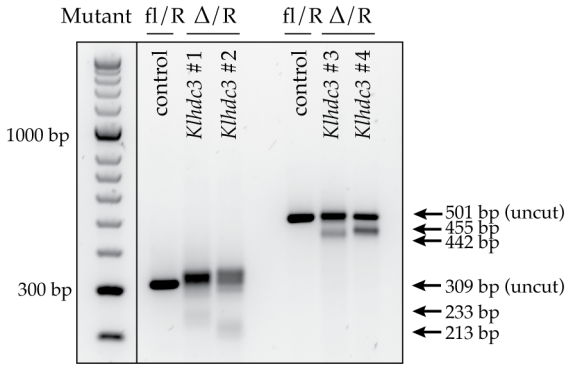
Mutant
fl/R
Δ/R
fl/R
Δ/R
control
Klhdc3 #1
Klhdc3 #2
control
Klhdc3 #3
Klhdc3 #4
1000 bp
300 bp
501 bp (uncut)
455 bp
442 bp
309 bp (uncut)
233 bp
213 bp

E

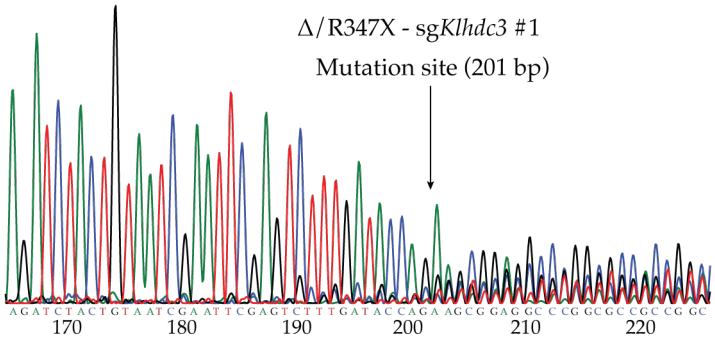
Δ/R347X - sgKlhdc3 #1
Mutation site (201 bp)
170
180
190
200
210
220

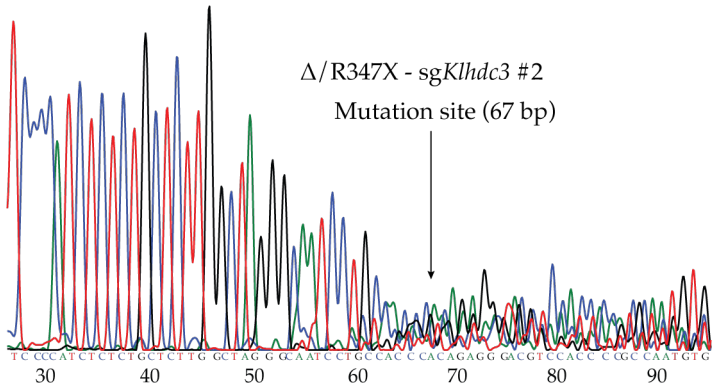
Δ/R347X - sgKlhdc3 #2
Mutation site (67 bp)
30
40
50
60
70
80
90

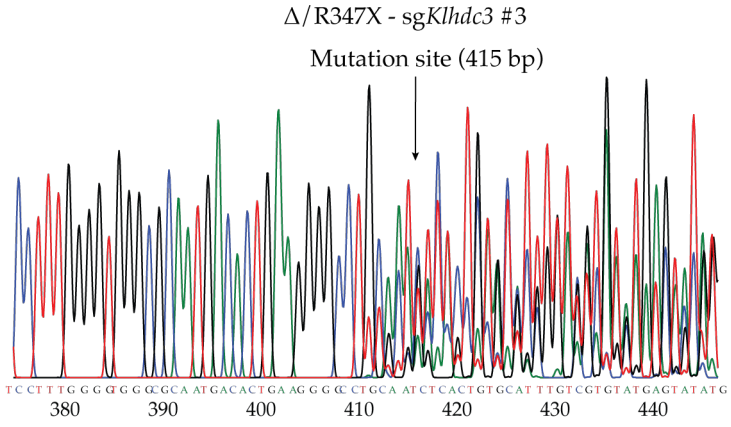
Δ/R347X - sgKlhdc3 #3
Mutation site (415 bp)
380
390
400
410
420
430
440

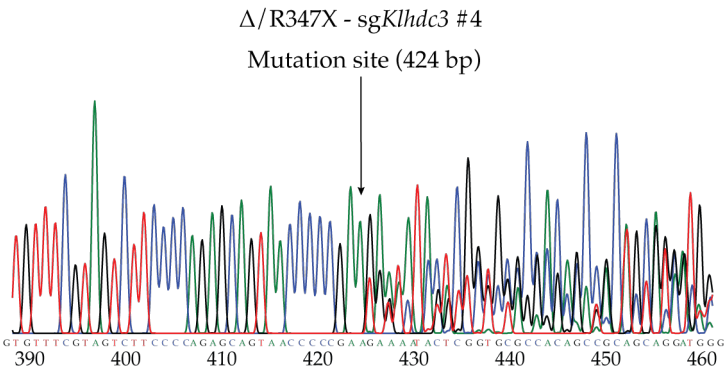

Figure 7.5: *Validation of stable Recql4 deletion and Klhdc3 mutation.* (A) Genomic PCR showing successful recombination and stable deletion of the floxed *Recql4* allele after addition of tamoxifen in *Klhdc3 Recql4* R347X double mutant cells. (B) Western blot of full-length WT and truncated R347X mutant RECQL4 protein in the non-tamoxifen treated control and tamoxifen-treated *Klhdc3* sgRNA mutant cells (Day 9 Post-Tam). (C) Quantitative real-time RT-PCR analysis of *Klhdc3* RNA expression in mock and tamoxifen-treated sg*Klhdc3 Recql4* R347X double mutant cells (Day 9 Post-Tam). (Expression relative to *Gapdh* and normalised to mock). (D) T7 endonuclease digestion of heteroduplex PCR products amplified from the genomic DNA surrounding the sgRNA target sites, showing cleavage of mismatched DNA at sites of indels $\geq$2 bases in a mixed population of *Klhdc3* sgRNA targeted mutant (R347X) cells (Day 9 Post-Tam). The sizes of the predicted cleavage products are labelled in the figure. (E) TIDE Quantitative Sanger sequence trace analysis of amplified genomic DNA regions surrounding the expected break site of individual *Klhdc3* sgRNAs in a mixed population of mutant (R347X) cells (Day 9 Post-Tam) [231].

7.3 DISCUSSION

In RTS, mutations predicted to result in a loss/truncation of RECQL4 are associated with deleterious effects, including an elevated risk of OS [58]. However, my results in Chapter 6 suggested that these inherited mutations are not sufficient to initiate tumorigenesis in mice. Additionally, there is still a subgroup of clinically diagnosed RTS patients that do not have mutations in *RECQL4* [232], which suggests that mutations in other genes might also be involved in the pathogenesis or tumorigenesis of RTS. Despite important discoveries regarding the role of *RECQL4* in RTS, its molecular interactions with other genes and the pathways in which it is involved remain relatively unknown. No genetic screen has directly addressed RECQL4 function, and only a few, more focused on DNA damage, have revealed putative pathways

in other RecQ helicase members [233–235]. For this reason, I performed a genome-wide CRISPR/Cas9 knockout rescue screen as an unbiased approach to identify genes that, when deleted, rescue the phenotypes associated with a truncating RECQL4 mutation.

For a successful CRISPR/Cas9 knockout rescue screen, several requirements need to be fulfilled. First, it is preferable that the cells present a distinct survival or proliferation phenotype, which allows for positive selection during a time-course [236]. In Chapter 6, the Hoxb8 *R26*-CreER^{T2} *Recql4*^{R347X} mutant cells showed such proliferation defect once tamoxifen was added and the wild type *Recql4* floxed allele was deleted. Furthermore, the R347X mutation produced a truncated but stable protein product, in contrast to the G522Efs mutation, which has no detectable protein. In addition, a similar mutation (p.Arg350GlyfsX21) has been commonly reported in patients with RTS [56], which provides extra validity to the selection of this cell line.

Another requirement of a successful CRISPR/Cas9 knockout screen is an efficient gene knockout across the cell lines of interest. This requires the assessment of Cas9 expression and subsequent DNA modification. While several methods, including confirmation of gDNA disruption and loss of RNA expression can be used for this purpose, the knockout of highly expressed surface proteins and its validation via flow cytometry is an attractive alternative. For this study, I used the latter method. I decided to knockout the cell surface marker CD44, highly expressed in the Hoxb8 cells, and found a ~70% decrease in its protein expression, which confirmed not only the validity of this technical approach but also the efficiency of gene editing in the Cas9 expressing cells used in this screen.

Lastly, the election of the method to analyse the data is a crucial step in a CRISPR/Cas9 screen. With several methods available, the web-based package CRISPR-Beta-Binomial (CB^2) was chosen for this study. This method has shown greater sensitivity to identify target genes and higher accuracy in the quantification of sgRNAs compared to other commonly used methods (RSA, RIGER, HiTSelect, PBNPA, MAGeCK, sgRSEA, PinAPL-Py, and ScreenBEAM) [191]. Furthermore, the quality control analysis performed in this study showed adequate sgRNA distribution and depletion of essential genes, parameters expected in CRISPR knockout screens. Together, these

findings confirm the robustness of this CRISPR/Cas9 screen and the veracity of the data analysis.

A discrete list of sgRNA enriched in the mutant (R347X) cells was revealed in our data analysis. All these rescue candidates were significantly enriched in the mutant cells and not in the control with the exception of sg*Hnrnph1* and sg*Trp53*, which were enriched in both cell lines. A possible explanation for this is that the knockout of *Trp53* by the guides allows cells to grow since there is no adequate DNA damage checkpoint control, normally regulated by P53 [237] in response to CRISPR-Cas9-induced DSBs [225]. As a result, these cells are positively selected and sg*Trp53* is enriched in both cell lines. Regarding sg*Hnrnph1*, it has been linked to DNA damage and apoptosis, and it has been shown to regulate P53 expression [238, 239]. Therefore, it is possible that its deletion also confers a growth advantage in the context of a Cas9 screen, and as a result, is enriched in both cell lines.

The results of the screen showed that the most enriched rescue candidate was sg*Klhdc3*, with no enrichment or depletion in control cells. This result was independently validated in the mutant cells by four different sgRNAs targeting *Klhdc3*, including two new ones. The validation confirmed that KLHDC3 mutation could partially rescue the proliferation defects caused by the deletion of the wild type *Recql4* allele in the R347X mutant cells. KLHDC3 is a Cullin2-RING E3 ubiquitin ligase (CRL2) complex adaptor. This complex contains a scaffold subunit (Cullin2), a catalytic subunit (RING), and an Elongin B/Elongin C adaptor (EloB/C) [240–242]. The complex binds to a group of proteins responsible for substrate recognition known as BC-box proteins [243]. The best-known BC-box protein is VHL (Von Hippel-Lindau), the loss of which causes Von Hippel-Lindau syndrome, characterised by the development of highly vascularised tumours [244]. These BC-box proteins select their substrates through recognition of specific short peptide motifs called “degrons” [245]. Once identified, the proteins containing these sequences are ubiquitinated by the CRL2 complex and thus tagged for degradation by the proteasome. Interestingly, KLHDC3 was recently identified as a BC-box protein that recognises specific substrates with an exposed C-terminal glycine residue [245, 246]. It was originally characterised by its targeted degradation of selenoproteins [247]; and later, it was found to play a broader role in protein degradation, not only of selenoproteins but also aberrant/truncated proteins. With this in mind,

a Western blot was performed to determine the potential targeting of a putative truncated translation product of the floxed recombined allele, which coincidentally ends in a canonical KLHDC3 degron. We extracted protein from lysates of *Klhdc3* mutant (Δ/R347X) cells and found no accumulation of protein products of the predicted size (~58 kDa), which confirmed that KLHDC3 did not target the potential protein product that may arise from the recombined floxed allele (Figure 7.5 B).

Regarding the expression pattern of KLHDC3, the Human Protein Atlas shows that KLHDC3 is broadly expressed in several tissues [248]. Furthermore, a study found KLHDC3 to be physiologically expressed in testis of mice [249]. On the other hand, although a previous study found that KLHDC3 is mutated in pancreatic cancer [250], the Catalogue of Somatic Mutations in Cancer (COSMIC) reports only 211 mutations from more than 38,000 samples tested [251], suggesting a relatively low frequency of mutations of KLHDC3 in human cancers. Finally, no other genetic interactions with KLHDC3 have been reported or listed in the publicly available Biological General Repository for Interaction Datasets (BioGRID) [252], making *Recql4* the first confirmed genetic interaction of *Klhdc3*, according to our findings.

More recently, it has been appreciated that KLHDC3 can also target other proteins in cells, more specifically naturally occurring isoforms that contain the requisite C-terminal degron motif. This expanded the role of KLHDC3 through sequence-specific regulation of a range of normal proteins containing a C-terminal residue with glycine, with PPP1R15A and USP49 being some of the physiological substrates in human cells [245, 246]. The finding that *Klhdc3* mutation improved the fitness and proliferation of *Recql4* mutant cells suggested that one or multiple physiological substrates, targeted by KLHDC3, can suppress the phenotypes associated with a pathogenic RECQL4 mutation. Therefore, these substrates are potential targets to improve the phenotypes associated with RTS. On the other hand, it suggests that proteins that are part of the ubiquitin-proteasome system might be involved in the pathogenesis of this disease. Interestingly, a previous study found that RECQL4 formed a stable complex with UBR1 and UBR2 [121]. Both of these proteins are important components of the ubiquitin-proteasome system.

The ubiquitin-proteasome system is an essential mechanism for protein degradation [253]. In cancer, it provides the survival advantage, typical of neoplastic cells, by regulating critical proteins involved in cell-cycle progression and apoptosis [254]. It contains multiple components, including the E3 ligases, which regulate widely diverse areas such as DNA repair, cell signalling, and cell trafficking [255]. The CRL2 complex, which works with KLHDC3, is an E3 ligase [240–242]. Furthermore, the APC1 protein, encoded by the *ANAPC1* gene and mutated in RTS type 1 patients, is the largest scaffold subunit of the APC/C E3 ligase [59, 60]. Therefore, the identification of both KLHDC3 and APC1 suggests that the $CRL2^{KLHDC3}$ and APC/C complexes, possibly by targeting specific common substrates, could play a vital role in the pathogenesis of RTS. However, more research is needed to confirm these findings and determine the specific mechanism.

Finally, the genome-wide screen also identified additional enriched candidates that have not been validated in this thesis. One promising candidate is CDK10 (See Figure 7.3 D). This has been linked to several cancers, both as a putative oncogene and tumour suppressor [256, 257] and has several clinically approved inhibitors that have shown potent and relatively specific inhibition [258]. Further validation of CDK10 could provide insight into its possible role in RTS and to the wider field of cancer development with potential for rapid translation.

While my studies arising from the genetic screen are not finalised due to available time, I have demonstrated that loss of KLHDC3 rescues the proliferation defect of a truncating RECQL4 mutation, which confirms my hypothesis that additional genes interact with *Recql4* to create the phenotypes of RTS. This finding has significant potential as a means to modify the lifetime trajectory and outcome for patients with inherited *RECQL4* mutations. In addition, to my knowledge, *Klhdc3* is the first confirmed genetic interaction associated with an improvement of the phenotypes caused by *Recql4* mutations. These results highlight the importance of identifying such modifiers for understanding RTS pathogenesis and the discovery of novel pathways for possible therapeutic intervention.

CHAPTER 8

8

CONCLUDING REMARKS

The study of *RECQL4* through murine models has been convoluted and complicated. Given that the majority of mutations in RTS involve the helicase domain, previous models have aimed to determine the functions of this domain by assessing the effects of its complete deletion. This has resulted in the generation of models carrying null alleles and elevated rates of perinatal lethality [139, 159, 177]. In addition, since the deletions of the exons that encode this domain also affect the C-terminal domain, the study of one of its presumed critical functions, the ATP-dependent helicase activity, has been challenging. On the other hand, the mutations introduced by these models do not reflect the mutation spectrum seen in RTS patients, which commonly present with truncating mutations that result in hypomorphic, rather than null alleles. Furthermore, these models, or the cells derived from them, have not been utilised to assess the effects of these mutations on the molecular interactions of *Recql4*, which is another area of the disease largely unexplored. To address all these gaps, in this thesis I generated murine models carrying mutations that inactivate specific functions or domains of RECQL4 and that resemble common mutations seen in RTS patients.

With the use of these models, this thesis is the first to look at the impact of murine *Recql4* mutations affecting different parts and functions of the protein on normal homeostasis, tumour development, and functional genetic interactions. This thesis has investigated the physiological requirements of the helicase activity, previously considered an essential function of RECQL4. The effects of the deletion of both the helicase and C-terminal domain, caused by truncating mutations that map closely to human mutations, were also investigated. Finally, given that the molecular landscape of RTS has not

been well established, this thesis has investigated novel functional genetic interactions in a genome-wide genetic rescue screen.

A prevailing theory in the field is that inactivation of the helicase function of RECQL4 is responsible for the phenotypes seen in RTS. This theory was contradicted by *in vitro* complementation studies, which showed in DT40 chicken cells [169], in *Drosophila* cells [174], and in primary murine haematopoietic cells [88] that an ATP-binding deficient RECQL4 mutation could restore the viability of RECQL4-depleted cells. This was the first glimpse that the ATP-dependent helicase function of RECQL4 was not essential for cell viability, at least *in vitro*. Assessing the physiological requirements of this function *in vivo* was the primary aim of the first component of this thesis, which was addressed in Chapter 5.

Using mice with a knock-in mutation that resulted in an inactive helicase function of RECQL4, I found that homozygous mice carrying this mutation were fertile and able to breed with no changes in survival. This suggests that, unlike the embryonic lethality seen in *Recql4* null alleles [88, 139], the helicase activity of RECQL4 is not required for fertility and normal physiological development of mice. With these results, I then proceeded to assess the requirements of the helicase domain in other cellular processes.

My host laboratory previously reported that somatic deletion of *Recql4* resulted in fully penetrant BM failure [88]. To determine whether the ATP-dependent helicase activity of RECQL4 was responsible for this phenotype, I assessed cohorts of homozygous and heterozygous mice carrying a helicase-inactive mutation and found that the majority of the haematopoietic cell types were unaffected. Additional experiments were performed to determine the role of the helicase domain in B and T cell development and DNA damage repair, and the results were the same; no changes observed in the homozygous mice, which were similar to the wild type controls. These findings demonstrated that, contrary to what was believed, the ATP-dependent helicase function of RECQL4 was not essential for haematopoiesis, B and T cell development or DNA damage repair. A similar observation was made in the human WRN helicase, another member of the RecQ helicases group. Biochemical analysis of a naturally occurring polymorphism showed that although this mutation caused a 90% reduction of the WRN helicase activity, the exonuclease activity of WRN was not affected and, as a result, none of

the heterozygous or homozygous carriers developed Werner Syndrome [208]. One interpretation of this and my findings is that there might be additional functions of the helicase besides the ATP-dependent helicase function. Another possibility is that given the structural similarity of these proteins, some functional redundancy may exist. However, given that the knockout of one RecQ helicase cannot be rescued by the remaining family members argues against this possibility. Instead, my interpretation is that defects in other domains or functions of RECQL4 might be responsible for the phenotypes seen in RTS. This theory was also explored in this chapter. Using a conditional deletion model that allowed the assessment of the effects of mutations after deleting the wild type *Recql4* allele, I found that mice carrying truncating, but not helicase-inactive, mutations developed BM failure. These findings confirm that the ATP-dependent helicase activity of RECQL4 is dispensable for haematopoiesis. Furthermore, they demonstrate that truncating mutations that delete both the helicase and C-terminal domains are pathogenic.

The identification of the dispensability of the ATP-dependent helicase function to the overall functions of RECQL4 has important implications in the field. First, it contradicts the theory that defects in this function are solely responsible for the phenotypes of RTS. Here I have homozygous mice with an inactive ATP-dependent helicase function and no apparent phenotypes. Second, it moves the attention to other domains and functions of RECQL4 like the C-terminal domain, which has been highly disregarded, and which is affected by truncating mutations in the majority of RTS patients. In fact, a recent study reported two RTS patients carrying homozygous mutations that affected the C-terminal domain only, and yet still developed the canonical, albeit milder features of RTS [110]. This highlights the contribution of this domain to the RTS phenotypes.

Based on these results, I decided to determine the impact of the deletion of the C-terminal and helicase domains in normal homeostasis and tumour development by using mice carrying *Recql4* truncating mutations. This was the aim of the second component of this thesis and was addressed in Chapter 6. For this chapter, I studied germline models carrying two distinct truncating mutations and observed that neither of these mutants produced homozygous pups. Reviewing the reported *RECQL4* mutations in the literature [56, 58, 64], RTS patients that present with two severe truncating mutations are extremely rare. Therefore, my results are consistent with the human data. Furthermore,

they suggest that having two severe truncating mutations of *RECQL4* is not tolerated and that there is an essential developmental role for the deleted domains. It is possible that the helicase domain has extra functions besides its ATP-dependent helicase activity or that the C-terminal domain has a supporting role in DNA replication. In fact, a study showed that two domains within the C-terminal section (R4ZBD and CTD) are responsible for interaction with more complex DNA structures, protein to protein interaction, and unwinding of dsDNA through translocation [23]. It is possible that perturbation of these processes, caused by the deletion of this domain, may have contributed to the developmental lethality seen in the homozygous mice. However, more research is needed to corroborate this theory.

Although I was not able to recover homozygous pups, the heterozygous mice were viable and fertile. Analysis of these mice demonstrated a haploinsufficient low bone mass phenotype, caused by intrinsic defects in the osteoblast lineage. These findings were comparable to what my host laboratory previously reported, which showed that complete deletion of *Recql4* in the osteoblast lineage led to reduced bone volume and defects in osteoblast proliferation and maturation [181]. Therefore, when it comes to bone development, having a truncated RECQL4 protein is equivalent to not having RECQL4 at all, which highlights the critical function of the deleted domains in bone homeostasis. Furthermore, the fact that heterozygous germline models presented with a low bone mass phenotype raises concerns regarding the osteoporosis status of the parents of RTS patients, something that to the best of my knowledge, has been unexplored. Future studies should focus on determining the bone density status of heterozygous carriers. These findings could not only help to further understand the role of *RECQL4* mutations in osteoporosis development, but could also encourage screening and implementation of preventive measures for those at risk.

In Chapter 6, I also explored the effects of truncating mutations at a cellular level. Through analysis of protein expression and localisation, I observed that the R347X mutation, which produced the most severe bone phenotype, had a truncated yet stable protein product with reduced nucleolar staining intensity. In contrast, the G522Efs mutation, whilst a longer predicted protein than the R347X mutation, had an essentially undetectable protein. These findings, together with the analysis of human *RECQL4* mutations in *in vitro* complementation assays, suggested that the severity of the defects was proportional

to the severity of the truncation, irrespective of the protein expression, localisation and stability. Furthermore, the fact that the largest truncation caused the most severe bone phenotype suggests that RECQL4 gene dosage is a critical regulator of bone mass, something relatively unknown until now.

Given the high predisposition to malignancies that RTS patients have [56, 64, 67] and the recent discovery of heterozygous *RECQL4* loss-of-function variants in OS samples [99], in Chapter 6, I presumed that tumour development was initiated by RECQL4 truncating mutations and accelerated by ionising radiation. However, under conditions of physiological ageing and carcinogen exposure, I did not observe elevated rates of tumour formation in the *Recql4* mutant mice. This result was unexpected as studies in RTS patients have shown that the presence of truncating mutations is associated with increased risk of OS [58]. One explanation for these findings is that truncating mutations in both alleles are necessary for tumours to develop. This was not possible in this thesis given the developmental lethality seen in our homozygous truncating mice. It would be interesting in future studies to generate models with truncating mutations at different levels of the protein as a way to avoid this lethality and to determine the tumorigenesis potential of compound heterozygous truncating mutations. Another explanation for the lack of tumours in these mice, is that additional genes are interacting with *Recql4* and contributing to the phenotypes of the disease. This led us to the final component of this thesis.

For this component, addressed in Chapter 7, the aim was to identify novel genetic interactions with *Recql4* that contribute to the improvement of the phenotypes associated with a pathogenic *Recql4* mutation using a genome-wide genetic screen. By using murine cells carrying a RECQL4 truncating mutation, I performed a CRISPR/Cas9 loss-of-function screen and identified several genes that, when deleted, rescued the phenotypes associated with a pathogenic RECQL4 mutation. However, by far the most enriched candidate was *Klhdc3*, for which further validation studies confirmed a similar rescue after its deletion. This finding is, to my knowledge, the first confirmed genetic interaction associated with an improvement of the cellular phenotypes caused by *Recql4* mutations. Moreover, this is one of the first physiologically relevant contexts where KLHDC3 has been specifically implicated.

KLHDC3 is a member of a subfamily of very recently described CRL2 adaptors that are part of the ubiquitin proteasome system. They were originally characterised to degrade selenoproteins and aberrant/truncated proteins containing unusual C-termini [247]. More recently however, KLHDC3 has been shown to specifically target physiological full-length protein substrates containing glycine at their C-terminal residue [245, 246]. Interestingly, RECQL4 has been shown to interact with UBR1 and UBR2, two components of the ubiquitin proteasome system [121]. These proteins are ubiquitin ligases that recognise destabilising N-terminal residues tagging them for degradation [259]. Based on the finding that loss of KLHDC3 improved the fitness and proliferation of RECQL4 truncating mutant cells, I propose that one or multiple substrates, that most likely contain glycine as their C-terminal residue, are suppressing the phenotypes caused by a truncating RECQL4 mutation. It is possible that these substrates are normally targeted by KLHDC3 and destroyed by the ubiquitin proteasome system, possibly through interaction of RECQL4 with URB1 and URB2. By deleting KLHDC3, these substrates are no longer degraded, allowing an increase in cell proliferation and suppressing the phenotypes caused by a pathogenic RECQL4 mutation. If this theory is correct, my findings hold significant potential to identify targets for disease modifying therapies for patients with *RECQL4* mutations, something currently non-existent in the management of RTS or for the majority of other inherited cancer predispositions.

As such, I believe that future studies should focus on the identification of functional interactions and pathways associated with RECQL4 as a way to alter the long-term disease trajectory of these patients. Firstly, it would be interesting to characterise the molecular basis of the rescue caused by the KLHDC3 deletion. This could unravel pathways, in which both KLHDC3 and RECQL4 are involved, that could contribute to a better understanding of the pathogenesis or tumorigenesis of RTS. Another important aspect would be to determine whether clinically relevant drugs that block the CRL2 pathway can replicate this rescue. An attractive drug is Pevonedistat. This drug, currently in phase II trials [260], has been shown to block the CRL2 pathway by inhibiting the NEDD8-activating enzyme, which is necessary for proteasomal degradation by CRL2 substrates [261]. If this drug shows a similar rescue of a truncating RECQL4 mutation, it could hold translational potential as a treatment for RTS patients. Secondly, since I only could validate

the top hit of the screen due to time constraints, future studies could include the validation of other hits. An interesting candidate is CDK10. This is a therapeutically actionable target with several potent inhibitors already available (SNS-032, riviciclib, flavopiridol, dinaciclib, AZD4573 and AT7519) [258]. Finally, since the knockout screen only identified genes that when deleted rescued the phenotypes of mutant cells, it would be worthwhile to look for genes that when overexpressed achieve a similar rescue. This can be now be done with a CRISPR/Cas9 mediated transcriptional activation (CRISPRa) gain-of-function screen, for which I already have validated cell lines ready to be used. The identification of these genes will give us a fuller picture of the genetic interactions of *Recql4*.

In summary, although it is clear that patients with RTS display a range of symptoms from skeletal dysplasias to increased cancer susceptibility, knowledge regarding the individual domains of RECQL4, the role of truncating mutations in cellular processes, and the functional molecular interactions with RECQL4 was limited. My thesis aimed to address all these gaps. Firstly, I demonstrated that the ATP-dependent helicase activity, thought the key feature of RECQL4 function, is not essential for normal development, homeostasis or ageing *in vivo*. Secondly, by using mice carrying truncating mutations that map closely to those reported in RTS patients, I discovered that truncating mutations affected stability and subcellular localisation of RECQL4 causing a haploinsufficient low bone mass phenotype and homozygous embryonic lethality. Furthermore, I found that RECQL4 gene dosage is an important regulator of bone mass, irrespective of protein expression, localisation and stability, and that truncating mutations are not sufficient to initiate tumorigenesis in mice. Finally, using an unbiased genome-wide screen, I identified that loss of *Klhdc3* rescued the proliferation defect caused by a truncating RECQL4 mutation. This not only provided evidence that additional genes interact with *Recql4* mutations, but also opened the door for future studies with the potential for clinical translation that could directly benefit patients with RTS.

APPENDIX

A

PUBLICATIONS ASSOCIATED WITH THIS THESIS

1. *Castillo-Tandazo W*, Smeets MF*, Murphy V, Liu R, Hodson C, Heierhorst J, Deans A, Walkley CR*. ATP-dependent helicase activity is dispensable for the physiological functions of Recql4. PLoS Genet. 2019;15(7):e1008266.
   DOI: https://doi.org/10.1371/journal.pgen.1008266
   * These authors contributed equally to this work.

PLOS GENETICS

RESEARCH ARTICLE

ATP-dependent helicase activity is dispensable for the physiological functions of Recql4

Wilson Castillo-Tandazo[1,2], Monique F. Smeets[1,2☯], Vincent Murphy[1], Rui Liu[1], Charlotte Hodson[1], Jörg Heierhorst[1,2], Andrew J. Deans[1,2], Carl R. Walkley[1,2,3☯]*

1 St. Vincent's Institute of Medical Research, Fitzroy, VIC, Australia, **2** Department of Medicine, St. Vincent's Hospital, The University of Melbourne, Fitzroy, VIC, Australia, **3** Mary MacKillop Institute for Health Research, Australian Catholic University, Melbourne, VIC, Australia

☯ These authors contributed equally to this work.
* cwalkley@svi.edu.au

Check for updates

OPEN ACCESS

Citation: Castillo-Tandazo W, Smeets MF, Murphy V, Liu R, Hodson C, Heierhorst J, et al. (2019) ATP-dependent helicase activity is dispensable for the physiological functions of Recql4. PLoS Genet 15 (7): e1008266. https://doi.org/10.1371/journal.pgen.1008266

Editor: Marshall S. Horwitz, University of Washington, UNITED STATES

Received: May 8, 2019

Accepted: June 21, 2019

Published: July 5, 2019

Copyright: © 2019 Castillo-Tandazo et al. This is an open access article distributed under the terms of the Creative Commons Attribution License, which permits unrestricted use, distribution, and reproduction in any medium, provided the original author and source are credited.

Data Availability Statement: All mouse lines are available from the Australian Phenome Bank (https://pb.apf.edu.au/). Strain identification numbers/names are: M789K (ID#7936); R347* (ID#7986); R26-CreER Recql4fl/fl (ID#7263); K525A (strain name: C57BL/6-Recql4<tm4Crw>) and G522Efs (strain name: C57BL/6-Recql4<tm5Crw>). All other relevant data are within the manuscript and its Supporting Information files.

Abstract

Rothmund-Thomson syndrome (RTS) is a rare autosomal recessive disorder characterized by skin rash (poikiloderma), skeletal dysplasia, small stature, juvenile cataracts, sparse or absent hair, and predisposition to specific malignancies such as osteosarcoma and hematological neoplasms. RTS is caused by germ-line mutations in *RECQL4*, a RecQ helicase family member. *In vitro* studies have identified functions for the ATP-dependent helicase of RECQL4. However, its specific role *in vivo* remains unclear. To determine the physiological requirement and the biological functions of Recql4 helicase activity, we generated mice with an ATP-binding-deficient knock-in mutation (*Recql4*^{K525A}). *Recql4*$^{K525A/K525A}$ mice were strikingly normal in terms of embryonic development, body weight, hematopoiesis, B and T cell development, and physiological DNA damage repair. However, mice bearing two distinct truncating mutations *Recql4*^{G522Efs} and *Recql4*^{R347*}, that abolished not only the helicase but also the C-terminal domain, developed a profound bone marrow failure and decrease in survival similar to a *Recql4* null allele. These results demonstrate that the ATP-dependent helicase activity of Recql4 is not essential for its physiological functions and that other domains might contribute to this phenotype. Future studies need to be performed to elucidate the complex interactions of RECQL4 domains and its contribution to the development of RTS.

Author summary

DNA helicases unwind double-stranded nucleic acids using energy from ATP to access genetic information during cell replication. In humans, several families of helicases have been described and one of particular importance is the RecQ family, where mutations in three of five members cause human disease. RECQL4 is a member of this family and its mutation results in Rothmund-Thomson syndrome (RTS). Prior studies have shown that defects in the helicase region of RECQL4 may contribute to the disease, but no studies have specifically assessed the biological effects of its absence in a whole animal model. In

PLOS GENETICS

Funding: This work was supported by the Office of the Assistant Secretary of Defense for Health Affairs through the Peer Reviewed Cancer Research under Award No. W81XWH-15-1-0315 (to CRW). Opinions, interpretations, conclusions and recommendations are those of the author and are not necessarily endorsed by the Department of Defense (USA); National Health and Medical Research Council Australia project grant (NHMRC; CRW and AJD, APP1102004); a Melbourne Research Scholarship (WCT, University of Melbourne); Victorian Cancer Agency Research Fellowship (CRW, MCRF15015; AJD, MCRF15024); This work was enabled by the Australian Phenomics Network and partly supported by funding from the Australian Government's National Collaborative Research Infrastructure Strategy and the Super Science Initiative through the Education Investment Fund (to Australian Phenomics Network); and in part by the Victorian State Government Operational Infrastructure Support (to St Vincent's Institute). The funders had no role in study design, data collection and analysis, decision to publish, or preparation of the manuscript.

Competing interests: The authors have declared that no competing interests exist.

this study, we generated a mouse model with a specific point mutation resulting in a helicase-inactive Recql4 protein. We found that an absence of ATP-dependent helicase activity does not perturb the physiological functions of Recql4 with the homozygous mutants being normal. In contrast, when we assessed point mutations that generate protein truncations these were pathogenic. Our results suggest that the helicase function of Recql4 is not essential for its physiological functions and that other domains of this protein might account for its functions in diseases such as RTS.

Introduction

Rothmund-Thomson syndrome (RTS) (OMIM #268400) is a rare autosomal recessive disorder characterized by skin rash (poikiloderma), skeletal dysplasia, small stature, sparse or absent hair, gastrointestinal complications, and high predisposition to specific malignancies such as osteosarcoma (OS) and hematological neoplasms [1, 2]. RTS and the related RAPADILINO and Baller-Gerold syndromes are associated with damaging germ-line mutations in *RECQL4* [3–5]. The majority of *RECQL4* mutations are located in its helicase domain, yet the physiological role of this domain remains unclear [6].

Helicases are enzymes that unwind double-stranded or more complex DNA and RNA structures using energy from ATP hydrolysis. The unwinding of double-stranded DNA (dsDNA) is necessary to allow access to the DNA during replication, repair, recombination and transcription [7]. In humans, five members of the RecQ helicase family have been identified: *RECQL1*, *RECQL4*, *RECQL5*, *BLM* and *WRN*. Mutations in three are associated with syndromes that present with premature aging and cancer-predisposition: *WRN* in Werner's syndrome, *BLM* in Bloom's syndrome, and *RECQL4* in RTS [8, 9]. RecQ-family helicases contain three highly conserved protein domains: an archetypal helicase domain, which contains seven conserved motifs that couple ATP hydrolysis to dsDNA strand separation [8, 9]; the RecQ C-terminal (RQC) domain, which features a beta-hairpin motif, a winged-helix domain and a zinc-binding motif, for intervention in the binding of G quadruplex DNA and stabilization of DNA structures [10]; and the Helicase-and-ribonuclease-D-like C-terminal (HRDC) domain, which promotes stable DNA binding [11]. RECQL4 differs from the other family members as it has no HRDC domain and lacks a structurally conserved RQC domain. Instead, it contains the structurally unique domain called RecQ4-Zn^{2+}-binding domain (R4ZBD) and, importantly, an N-terminal region of homology with the *S. cerevisiae* DNA replication initiation factor Sld2 [12, 13]. Sld2 is an essential protein required for activation of replication origins in yeast [14], and RECQL4 is the putative mammalian homologue.

The human *RECQL4* gene is located at the long arm of chromosome eight (8q24.3) and consists of 21 exons and 13 relatively short introns (<100 bp in length), yielding a full-length transcript of 3,627bp [3]. Mutations in the *RECQL4* gene have been found in the majority of RTS patients, and also in the related RAPADILINO and Baller-Gerold Syndromes [1, 6]. Most mutations are either nonsense or frameshift mutations and are predicted to create truncated proteins [6]. Over half of these impact the reading frame at exons 8–14 causing abnormal translation and or truncation of the RECQL4 protein with the presumed loss of DNA helicase function [6]. Very few mutations are located in the N-terminal Sld2 region, and those that are reported are primarily silent or missense [6]. This finding has led to the hypothesis that the N-terminal domain is critical for organismal viability, and that inactivation of the helicase function is a critical effect of the mutation spectrum that is found in RTS.

PLOS GENETICS

RECQL4 has been well characterized biochemically in terms of its single-stranded DNA (ssDNA) binding, ATP hydrolysis and DNA unwinding ability [15–17]. *In vitro*, RECQL4 ATPase and helicase activity is completely abolished by point mutations in the canonical Walker A and B motifs [18]. However, helicase-dead mutants can rescue cellular lethality in RECQL4-deficient DT40 chicken cells and murine hematopoietic cells *in vitro* [19, 20]. In addition, mutations that affect the helicase domain not only affect its activity but can also lead to protein truncation or unstable proteins, which does not allow the specific assessment of the physiological requirement of the ATP-dependent helicase RECQL4 in isolation. To understand the biological functions of RECQL4 helicase activity in a whole animal context, we generated a mouse model with a knock-in point mutation that specifically abolishes its ATP-dependent helicase activity (*Recql4*^{K525A}) and compared this to two different truncating mutations *Recql4*^{G522Efs} and *Recql4*$^{R347^*}$. Here we show that mice with a specific deficiency in Recql4 helicase activity are strikingly normal, in contrast to pathogenic effects of truncating mutations that remove the entire helicase domain and downstream part of the protein.

Results

The *Recql4*^{K525A} mutation lacks ATP-dependent helicase activity

We generated full-length wild-type mouse Recql4 protein, along with a K525A variant. The alanine substitution replaced a critical lysine, present in all Walker A motif-containing ATPases, that is necessary for ATP hydrolysis and corresponds to a previously analyzed human RECQL4 K508A mutation that lacks ATP-dependent helicase activity [15, 21] (Fig 1A). To biochemically characterize an ATPase deficient mutation in murine Recql4, we established *in vitro* assays for Recql4 function. Both WT and K525A proteins had equivalent affinity for ssDNA binding, using an electrophoretic-mobility shift assay (EMSA) (Fig 1B). In ATPase assays, the WT protein hydrolyzed ATP in a DNA-dependent manner whereas Recql4^{K525A} showed no activity above background levels (Fig 1C). Finally, we tested the ability of these recombinant proteins to unwind DNA, using a dsDNA substrate with a ssDNA loading site. If ATP-dependent helicase activity is present, the fluorophore-labeled strand is released from the quencher-labeled complementary strand providing a real-time fluorescent readout of unwinding activity (Fig 1D). Robust ATP-dependent unwinding of the substrate was observed when using WT-Recql4 protein, whereas no change in fluorescence was observed using the Recql4^{K525A} mutant consistent with an inability to unwind DNA (Fig 1E). Together, our results demonstrate that the Recql4^{K525A} protein is helicase and ATPase dead, despite equivalent protein stability and DNA binding properties.

Generation and validation of *Recql4* helicase-dead mutant mice

To understand the contribution of Recql4 helicase activity in the phenotypes of RTS, we generated an *in vivo* knock-in model of the K525A mutation. Sequencing of the *Recql4* locus in targeted mice confirmed the change in nucleotides encoding lysine (AAG) to alanine (GCA), and the resultant introduction of a unique *Msl*I restriction enzyme site in the mutant allele (Fig 2A). PCR amplification over the mutation site produces a 416 bp fragment in the wildtype that can cleaved to 361 bp (+55 bp) by *Msi*I when the mutation is present (Fig 2B). Finally, to determine the expression and stability of the mutant protein *in vivo* we generated a rat monoclonal antibody against the first 200aa from the N-terminal of murine Recql4 (clone 3B10). The K525A mutant protein has the same predicted molecular mass (~133kDa) as wild-type Recql4 and neither size nor abundance of the protein were affected by the mutation when assessed in thymocyte derived protein samples (Fig 2C). Taken together, these results demonstrate that the loss of helicase activity does not affect the expression or stability of the Recql4 protein *in vivo*.

PLOS GENETICS

RecQ helicase activity is not required for Recql4's physiological function

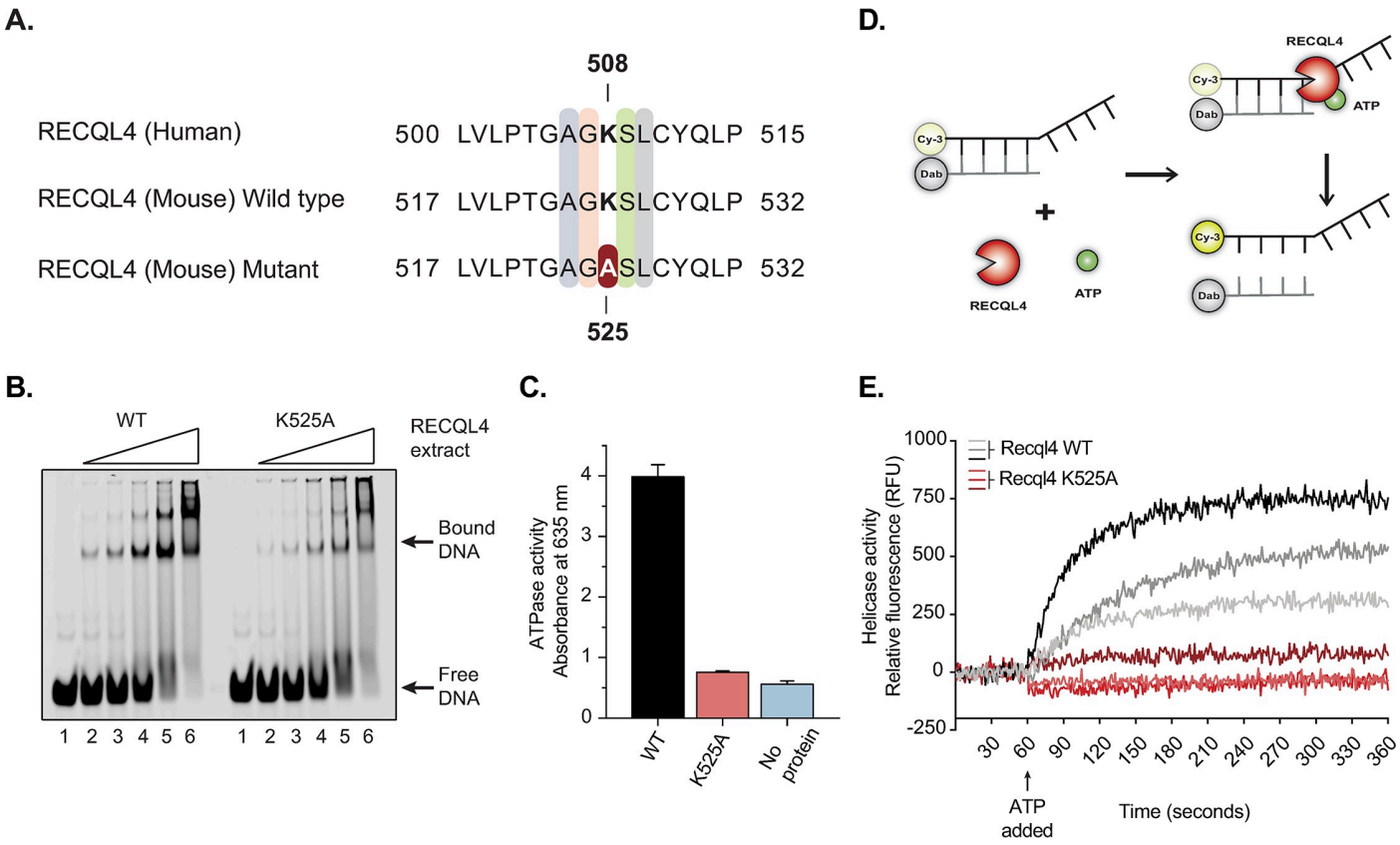

Fig 1. The *Recql4*^{K525A} mutation results in a biochemically inactive helicase protein. (A) Sequence homology between human and mouse RECQL4 showing the highly conserved amino acids between species. The helicase-dead mutation was achieved by replacing lysine by alanine in the 525 position in the mouse (508 in humans). (B) Electrophoretic-mobility shift assay (EMSA) comparing the DNA binding of WT versus K525A mutant Recql4. Lanes 1–6 show serial dilutions of Recql4 protein ranging from 19nM to 300nM bound to 25nM ssDNA oligo XOm1 conjugated to IRDye680. (C) *In vitro* ATPase assay of WT versus K525A mutant was obtained by measuring the absorbance at 635 nm. Proteins were assayed at 115nM in the presence of 1mM ATP and DNA in assay buffer. (D) Schematic representation of the fluorescence-based helicase assay. The dsDNA substrate with a ssDNA loading site is attached to a fluorescent donor (Cy-3) and a quencher acceptor (Dab). In the presence of ATP, the helicase (Recql4) is activated and separates the two complementary strands releasing the fluorescent probe. (E) Helicase assay of WT versus K525A mutant. After recording baseline fluorescence for 60 seconds, ATP was added, and helicase activity was measured in relative fluorescence units (RFU) for three different concentrations of Recql4 protein.

https://doi.org/10.1371/journal.pgen.1008266.g001

Recql4 helicase-dead mice are viable, have normal body weight and composition and normal long-term survival

We observed a slightly sub-Mendelian ratio of homozygous *Recql4*$^{K525A/K525A}$ animals at weaning from heterozygous breeding pairs, although this was not statistically significant by chi-squared test ($p = 0.6255$) (Fig 2D). Heterozygous and homozygous mice for the K525A mutation were viable and outwardly normal (Fig 2E). Further, we observed no difference across genotypes or sexes in 10-week old animals assessed for body weight and body composition (Fig 2F and 2G). Both male and female *Recql4*$^{K525A/K525A}$ animals were fertile and able to breed, and there was no difference in the survival when comparing the *Recql4*$^{K525A/K525A}$ and control genotypes using Kaplan Meier survival analysis (Fig 2H). Collectively these results show that, unlike the embryonic lethality of *Recql4* null alleles [20, 22], the Recql4^{K525A} protein supports normal development and adult homeostasis.

PLOS GENETICS

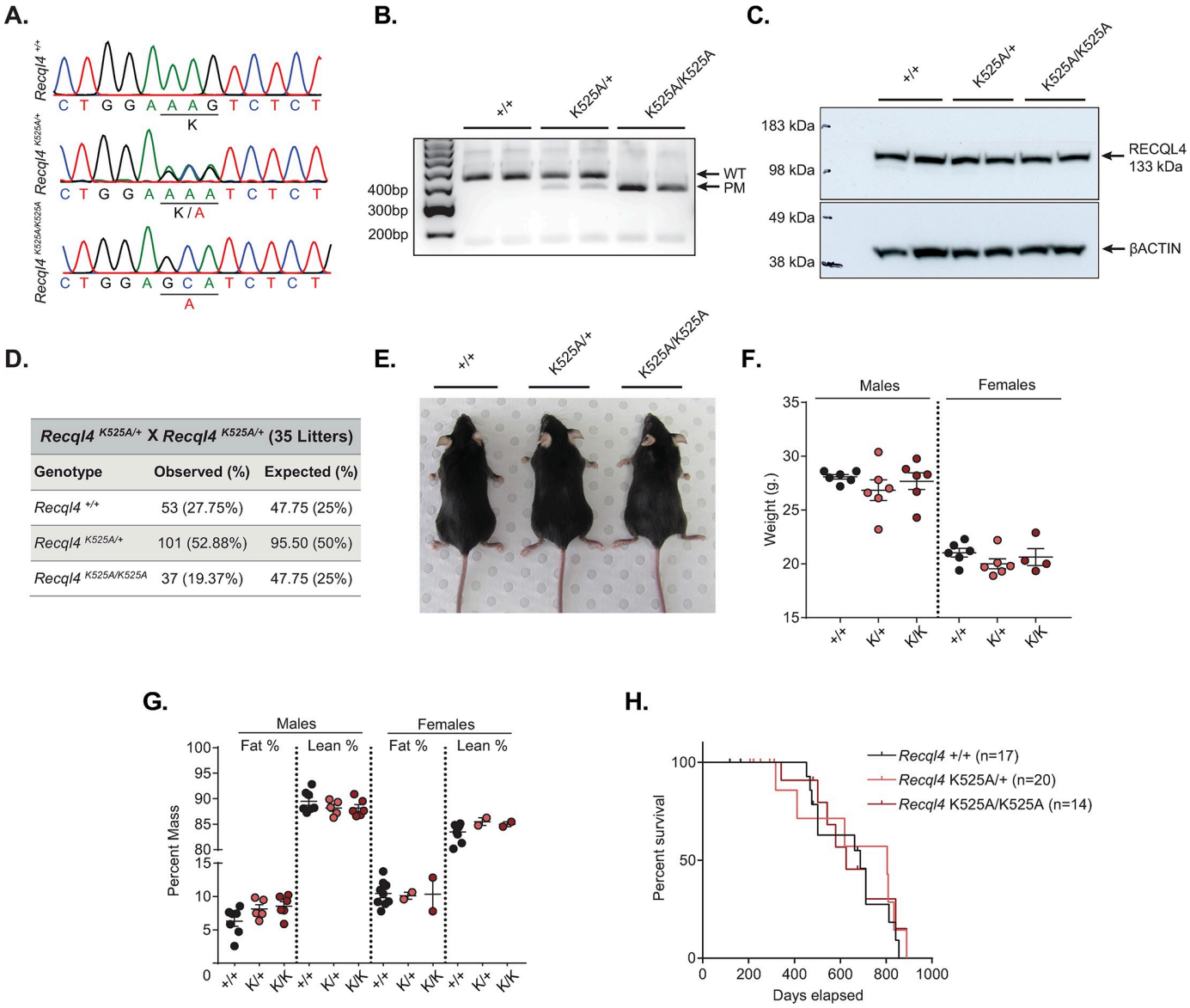

Fig 2. Homozygous and heterozygous helicase-dead mice are viable, have normal body weight and composition, and normal long-term survival. (A) Sequencing traces of the WT, heterozygous and homozygous K525A mutation. Altered nucleotide and amino acid changes are indicated above the sequence trace. (B) Genomic DNA PCR of *Recql4*$^{+/+}$, *Recql4*$^{K52A/+}$, *Recql4*$^{K525A/K525A}$. 2 different mice per genotype. (C) Western blot of thymocyte lysates from *Recql4*$^{+/+}$, *Recql4*$^{K52A/+}$, *Recql4*$^{K525A/K525A}$ 10 weeks old mice probed with anti-Recql4 (clone 3B10; top). The same blot re-probed with anti-β-Actin (bottom). (D) Breeding data from 35 litters of *Recql4*$^{K52A/+}$ intercrosses. Observed and expected mendelian rates of the indicated genotypes are shown. No statistical significance was achieved. (E) Representative photograph of male *Recql4*$^{+/+}$, *Recql4*$^{K52A/+}$, *Recql4*$^{K525A/K525A}$ mice. (F) Gross body weights of 10-week old male and female *Recql4*$^{+/+}$, *Recql4*$^{K52A/+}$, *Recql4*$^{K525A/K525A}$ mice. (G) Echo-MRI analysis of fat and lean percentage at 10 weeks of age from male and female *Recql4*$^{+/+}$, *Recql4*$^{K52A/+}$, *Recql4*$^{K525A/K525A}$ mice. (H) Kaplan-Meier survival plots of the indicated genotypes. K = K525A.

https://doi.org/10.1371/journal.pgen.1008266.g002

Recql4 helicase activity is not required for normal hematopoiesis

We previously reported that somatic deletion of *Recql4* resulted in a fully penetrant bone marrow (BM) failure [20]. To determine the role of helicase activity in hematopoiesis, we assessed cohorts of adult wild-type, *Recql4*$^{K525A/+}$ and *Recql4*$^{K525A/K525A}$ mice. Analysis of the peripheral blood (PB) revealed no changes in leukocyte or platelet numbers (Fig 3A and 3B). The absolute

PLOS GENETICS

RecQ helicase activity is not required for Recql4's physiological function

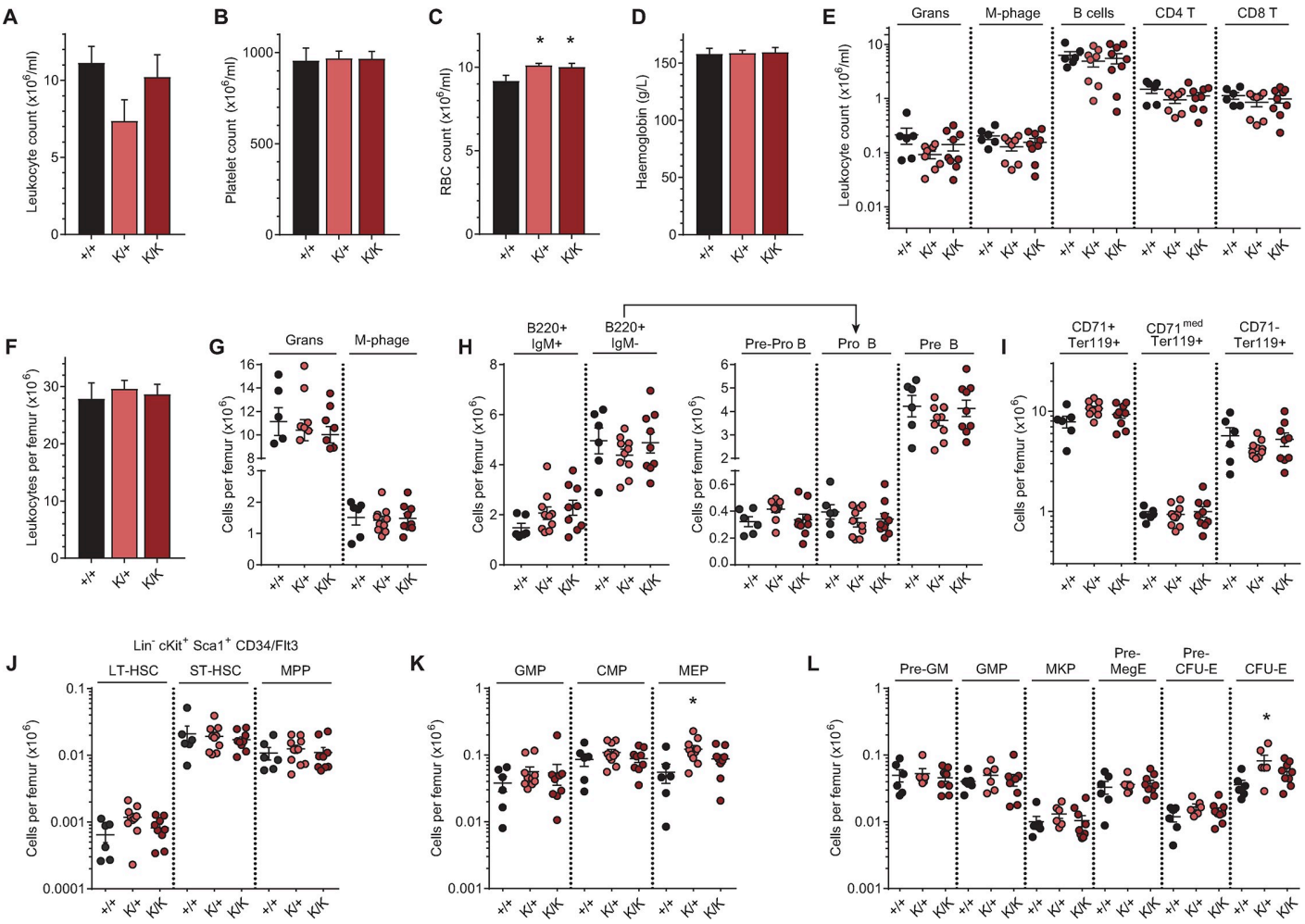

Fig 3. The ATP-dependent helicase function of Recql4 is not required for normal hematopoiesis *in vivo*. (A) Leukocyte counts in the PB of *Recql4*$^{+/+}$, *Recql4*$^{K525A/+}$, *Recql4*$^{K525A/K525A}$ 10-week old mice. (B) Platelet count. (C) Red blood cell count. (D) Hemoglobin. (E) Numbers of granulocytes, macrophages, B cells, CD4 T cells, and CD8 T cells in PB. (F) Leukocyte counts in BM. (G) Absolute numbers of granulocytes and macrophages in BM. (H) Mature (B220^{+}IgM^{+}), immature (B220^{+}IgM^{-}) B lymphocytes, and subsets of immature B lymphocytes per femur. (I) Erythroid fractions based on CD71/Ter119 staining per femur. (J) HSC and primitive progenitors based on Lin^{-}c-kit^{+}Sca-1^{+}CD34/Flt3 staining per femur. (K) Myeloid progenitor subpopulations in the BM. (L) Myeloid, erythroid and megakaryocyte progenitor frequency per femur. Data expressed as mean ± SEM, Student's t test. $^{*}P<0.05$; n≥6 per genotype. Experiments were independently executed on separate cohorts, with results pooled for presentation. K = K525A.

https://doi.org/10.1371/journal.pgen.1008266.g003

red blood cell counts were subtly increased in both the K525A/+ and K525A/K525A mutants, however, the hemoglobin levels were not changed compared to the WT (Fig 3C and 3D). Further analysis of the individual leukocyte subsets in the PB including granulocytes, macrophages, B lymphocytes, and CD4^{+} and CD8^{+} T lymphocytes revealed no significant differences in the proportions or absolute numbers of these populations (Fig 3E).

Within the BM, the total numbers of leukocytes were comparable across genotypes (Fig 3F). Similarly, granulocyte and macrophage numbers were similar (Fig 3G). Within the B-lymphoid populations (B220^{+}IgM^{-}), the Pre-B, Pro-B, and Pre-Pro-B subpopulations were all unaltered in *Recql4*$^{K525A/+}$ and *Recql4*$^{K52A/K525A}$ compared to WT littermates (Fig 3H), as were the erythroid subpopulations (Fig 3I). The frequencies and absolute numbers of the primitive hematopoietic stem cells (HSCs) and progenitors were also assessed. There were no major differences in the numbers of phenotypic long-term HSCs (LT-HSC), short-term HSCs

PLOS GENETICS

(ST-HSC) or multipotent progenitor (MPP (Lin^- c-kit^+ Sca-1^+ CD34/Flt3)) fractions, nor in their myeloid committed subpopulations (Fig 3J–3L). There was an elevation of the phenotypic myelo-erythroid progenitor (MEP, Lin^-c-kit^+Sca-1^-CD34/FcγRII) and colony forming unit-erythroid (CFU-E, $Lin^-LKS^-CD41^-FcγRII^-CD150^-CD105^+$) in the *Recql4*$^{K525A/+}$ animals, however the absolute change was very small and not statistically significant in the *Recql4*$^{K525A/K525A}$ mice. The basis for this mild elevation in RBC counts and committed erythroid progenitors is currently undefined. In summary, unlike for complete deletion of Recql4, the abrogation of Recql4 helicase activity does not substantively perturb hematopoiesis *in vivo*.

ATP-dependent helicase function is not required for B and T cell development

Our previous work demonstrated that the human helicase dead RECQL4 (K508A) was able to rescue *in vitro* B and T cell development from murine *Recql4*$^{\Delta/\Delta}$ hematopoietic cells [20]. To determine if this was also the case *in vivo*, T and B cell development was assessed from thymocytes and splenocytes respectively in 10-week-old mutant and WT mice. There was no difference in thymus cellularity or in the numbers of double positive $CD4^+/CD8^+$ nor the mature single positive $CD4^+$ and $CD8^+$ cells (Fig 4A and 4B). Analysis of early intra-thymic progenitor cells (double negative DN1-4) found no difference in the *Recql4*$^{K525A/K525A}$ compared to the WT littermates (Fig 4C). In the spleen there was no significant difference in the cellularity or number of mature B cells (Fig 4D and 4E). To determine the proportion of B cells in the follicular (FO) and marginal zone (MZ) of the white pulp of the spleen, we divided splenic cells with high expression of B220 and CD19 followed by analysis of CD21/CD23 expression (FO B cells: $CD21^{low}CD23^{high}$; MZ B cells: $CD21^{high}CD23^{low}$). No shift of B cells in the follicular or marginal zone compartments was apparent (Fig 4F). Therefore, consistent with the prior retroviral rescue data *in vitro*, the ATP-dependent helicase function of Recql4 is not required for B or T cell development and homeostasis in adult mice.

Given the role of RecQ helicases in repair of DNA damage [11], we sought to determine if there was a function for the ATP-dependent helicase activity of Recql4 during physiologically induced DNA damage occurring following B cell stimulation. We isolated mature B cells from WT, *Recql4*$^{+/K525A}$ and *Recql4*$^{K525A/K525A}$ spleens and stimulated them *in vitro* using bacterial lipopolysaccharide (LPS) and rmIL-4 to induce proliferation and immunoglobulin gene (*Ig*) class switch recombination. The proliferation of the cells in response to LPS was the same irrespective of Recql4 helicase status as measured by cell-trace violet dilution kinetics (Fig 4G and 4H). Additionally, the *Recql4*$^{K525A/K525A}$ cells underwent normal class switching to IgG1 (Fig 4I). Therefore maturation, physiological activation induced proliferation, DNA damage and immunoglobulin rearrangement of B cells do not require the helicase activity of Recql4.

The K525A mutation does not alter sensitivity to DNA damaging agents *in vitro*

To further test the requirement for RecQ helicase activity we compared the response to DNA damaging agents *in vitro*. For these studies, we established GM-CSF dependent myeloid progenitor cell lines from *R26*-CreER *Recql4*$^{fl/K525A}$ and *R26*-CreER *Recql4*$^{fl/+}$ (control genotype) by immortalization with HoxB8 [23]. To allow analysis of the requirement for RecQ helicase activity, the cells were treated with tamoxifen for 4 days to activate Cre-mediated deletion of the loxP flanked wild-type Recql4 (*Recql4*^{fl}) allele. This resulted in the cells either becoming Recql4 heterozygous (*Recql4*$^{\Delta/+}$) or expressing only the K525A mutant allele (*Recql4*$^{\Delta/K525A}$). Isogenic cells from each genotype (pre-treated with tamoxifen for 4 days or untreated) were seeded in 96-well plates and the response to four different genotoxic agents was assessed:

PLOS GENETICS

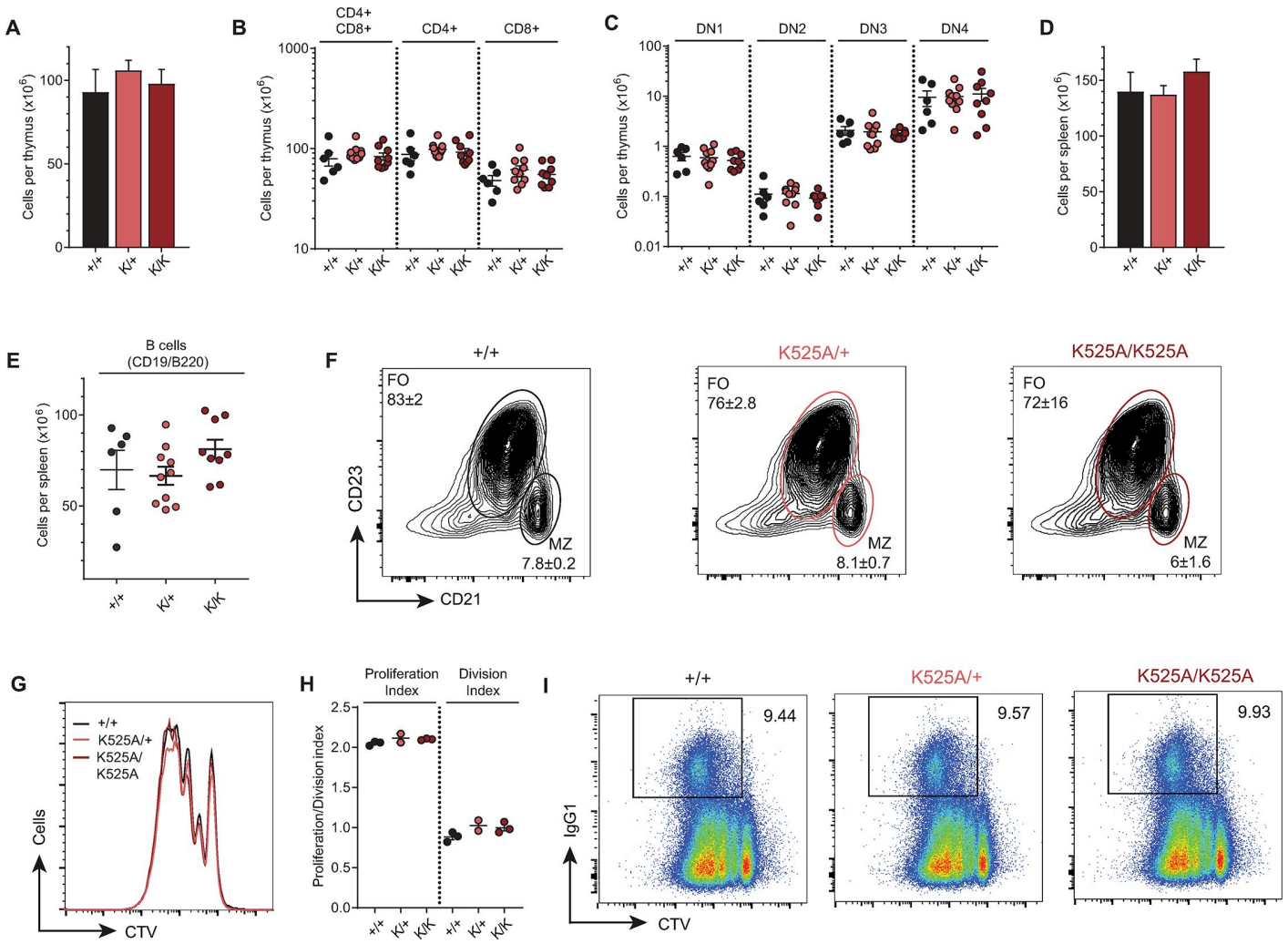

Fig 4. ATP-dependent helicase function of Recql4 is not required for B or T cell development. (A) Leukocyte counts in thymus. (B) Absolute numbers of double positive CD4/CD8, $CD4^+$, and $CD8^+$ T lymphocytes in thymus. (C) T cell progenitor populations (DN1-DN4). (D) Leukocyte counts in spleen. (E) B lymphocytes in spleen. (F) Representative (n = 2 mice per genotype) FACS plots of $B220^+CD19^+$ gated splenocytes stained for follicular (FO, $CD23^{hi}CD21^{low}$) and marginal zone (MZ, $CD21^{hi}CD23^{low}$) B cells. Numbers indicate cells x 10^6 per spleen. (G) CellTrace Violet (CTV) dilution in purified B cells treated for 96 hours with 15μg/ml LPS + 10ng/ml IL4. Representative examples of n = 3 mice per genotype. (H) Quantification of cell division (average division per cell in culture) and proliferation (average division/per dividing cell in culture) indices. n = 3 mice per genotype. (I) *In vitro* class-switch recombination to IgG1 in purified B cells treated as in panel B. Representative examples of n = 2 mice per genotype. Data expressed as mean ± SEM, Student's t test **(A-E)**. Experiments were independently executed on separate cohorts, with results pooled for presentation. K = K525A.

https://doi.org/10.1371/journal.pgen.1008266.g004

doxorubicin (topoisomerase II inhibitor), hydroxyurea (ribonucleotide reductase inhibitor), 4-nitroquinoline (oxidative DNA damage) and topotecan (topoisomerase I inhibitor). Cell viability was measured after 48 hours using the CellTiter-Glo Luminescent assay. As shown in Fig 5A–5D, *R26*-CreER *Recql4*$^{\Delta/K525A}$ had a comparable IC_{50} to Doxorubicin, Hydroxyurea, 4-Nitroquinoline, and Topotecan as the non-tamoxifen treated isogenic controls (Figs 5A–5D and S3). Additionally, *R26*-CreER *Recql4*$^{\Delta/+}$ showed a similar IC_{50} to Doxorubicin, Hydroxyurea, and Topotecan, except for 4-Nitroquinoline, which exhibited a mildly increased resistance in the tamoxifen-treated cells in comparison to the non-tamoxifen treated controls. These results indicate that the role of Recql4 in non-physiological, pharmacologically induced DNA repair does not depend on its helicase activity.

PLOS GENETICS

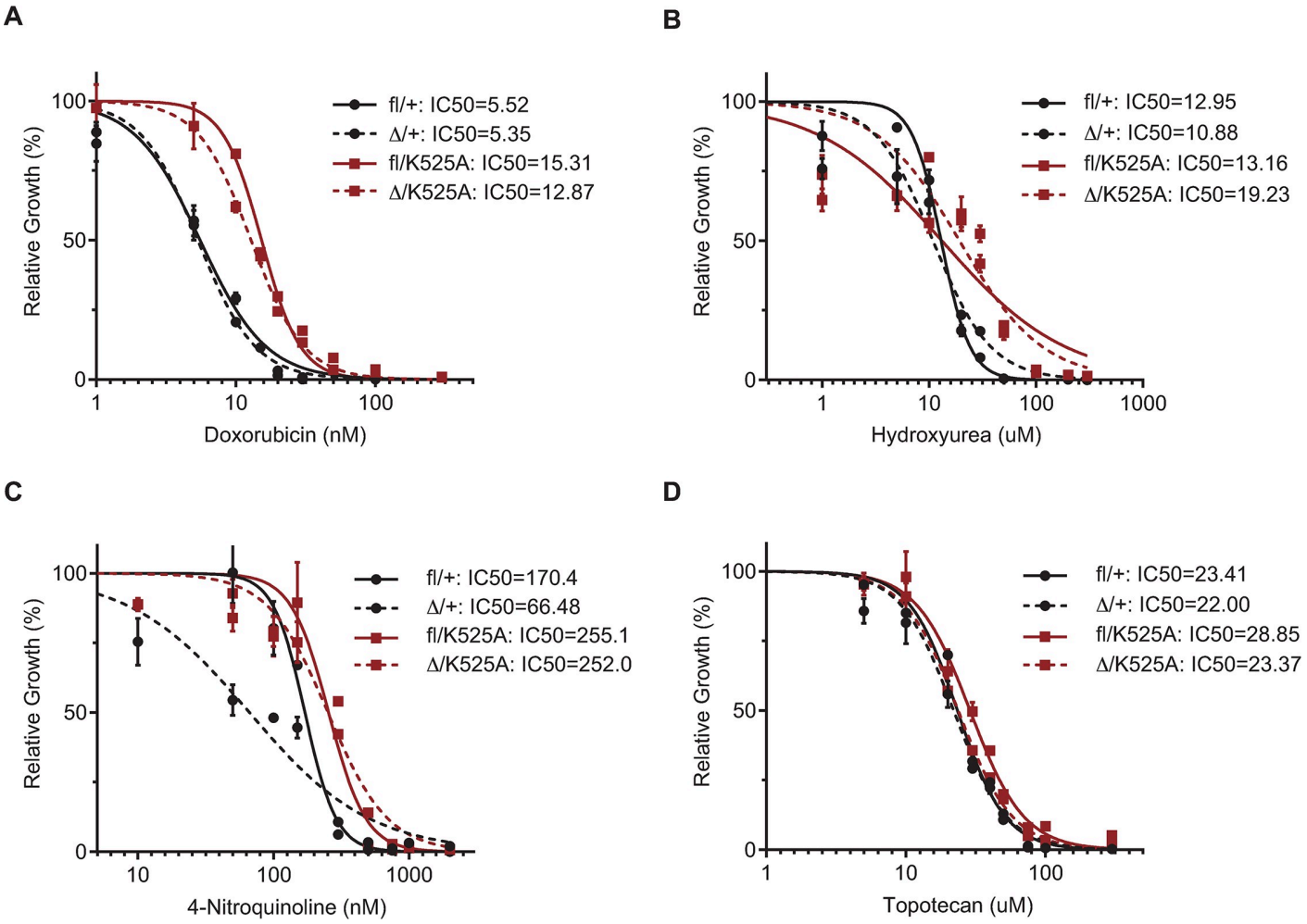

Fig 5. *In vitro* sensitivity to DNA damaging agents is not modified by helicase-dead mutation. Dose-response curves for relative growth rate of HoxB8 immortalized *R26*-CreER *Recql4*$^{fl/K525A}$ (red) and *R26*-CreER *Recql4*$^{fl/+}$ (black). Dotted lines represent cells expressing the K525 mutant only after the floxed allele was excised by tamoxifen addition. Cells were incubated for 48 hours with the following drugs: (A) Doxorubicin. (B) Hydroxyurea. (C) 4-Nitroquinoline. (D) Topotecan. The calculated IC_{50} values are stated for each genotype/treatment.

https://doi.org/10.1371/journal.pgen.1008266.g005

Truncating mutations, but not helicase inactivation, of Recql4 are pathogenic

The results so far establish that the ATP-dependent helicase activity of Recql4 is not essential *in vivo*. To directly compare the effects of having a protein truncating/hypomorphic allele compared to a helicase-dead full-length Recql4 protein, we established three additional point mutant alleles (Fig 6A). The G522EfsX43 truncated mutation was generated as a co-incidental mutation during the Crispr/Cas9 mediate generation of the K525A allele and maps closely to the relatively common RTS associated mutations in human *RECQL4*, S523TfsX35 and C525AfsX33 [6]. We also identified an *N*-ethyl-*N*-nitrosourea (ENU) mutagenesis induced truncated mutation R347* (R355 in humans). Three RTS patients have been reported with p. Arg350GlyfsX21 mutations, mapping closely to this allele [6] (S2 Fig). A second ENU induced mutation, M789K mutation (V767 in human), was identified and used as a control for mutations within the *Recql4* locus as this mutation was predicted to be benign. We crossed all the

PLOS GENETICS

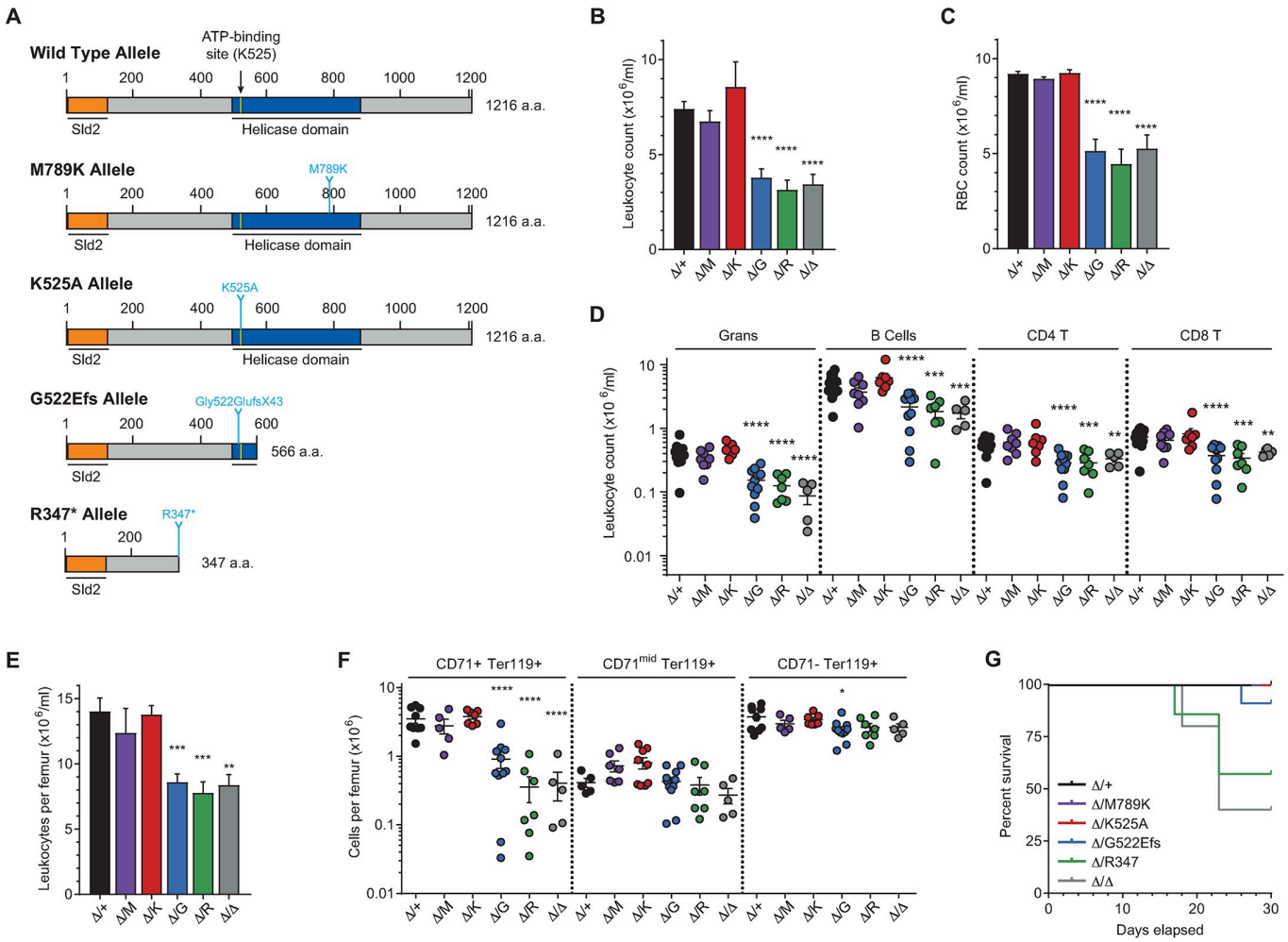

Fig 6. Truncating mutations, but not helicase inactivation, result in deleterious effects. (A) Schematic representation of the *R26*-CreER *Recql4*$^{fl/PM}$ murine alleles used in this study. (B) Leukocyte counts in PB. (C) Red Blood Cell counts in PB. (D) Absolute numbers of leukocyte subsets in PB. (E) Leukocyte counts in BM. (F) Erythroid fractions based on CD71/Ter119 staining per femur. (G) Kaplan-Meier survival plots of the indicated genotypes in days on Tamoxifen food. All data are from day of sacrifice and expressed as mean ± SEM, Student's t test. $^{*}P<0.05$; $^{**}P<0.01$; $^{***}P<0.001$; $^{****}P<0.0001$; n≥6 per genotype **(B-F)**. Experiments were independently executed on separate cohorts, with results pooled for presentation. M = M789K; K = K525A; G = G522Efs; R = R347*.

https://doi.org/10.1371/journal.pgen.1008266.g006

individual point mutant alleles (M789K, K525A, G522Efs and R347*) to the *R26*-CreER *Recql4*$^{fl/fl}$ line that we previously described and assessed the *R26*-CreER *Recql4*$^{fl/PM}$ in parallel with the *R26*-CreER *Recql4*$^{fl/+}$ and *R26*-CreER *Recql4*$^{fl/fl}$ allele. [20]. At 8–10 weeks of age, mice were fed tamoxifen containing chow for 30 days to activate the Cre mediated deletion of the wild-type *Recql4* floxed allele broadly throughout the body. Using this experimental design, the tamoxifen treated *R26*-CreER *Recql4*$^{fl/fl}$ animals (completely Recql4 deficient) developed fully penetrant BM failure [20]. The efficiency of *Recql4* deletion was confirmed by PCR for genomic recombination (S1 Fig).

Analysis of PB (Fig 6B) showed an approximately 50% reduction in leukocytes and erythrocytes in mice expressing the truncating mutations G522Efs and R347*, very similar to mice rendered null for Recql4 protein expression (*Recql4*$^{\Delta/\Delta}$). The K525A and M789K mutation, as well as the heterozygous (*Recql4*$^{fl/+}$) control, did not show any significant change in leukocyte or erythroid indices. In addition, analysis of individual lineages within the PB showed a similar

PLOS GENETICS

pattern across granulocytes, B lymphocytes, and $CD4^+$ and $CD8^+$ T lymphocytes in the truncating and null mutant (Fig 6B–6D). When the BM was analyzed, leukocytes and erythroid precursors ($CD71^+Ter119^+$) from *R26*-$CreER^{ki/+}$*Recql4*$^{\Delta/G522Efs}$ and *Recql4*$^{\Delta/R347^*}$ mice showed a dramatic decrease, consistent with the BM failure phenotype we had previously described in *Recql4*$^{\Delta/\Delta}$ (Fig 6E and 6F). The *Recql4*$^{\Delta/+}$ and K525A and M789K only expressing animals did not develop any phenotype after 30 days of treatment with tamoxifen and, whilst developing a pan-cytopenia in PB and BM, seven of eight G522Efs mice were still alive at the end of the treatment. In contrast, mice expressing the most severely truncating $R347^*$ allele developed a profound BM failure and three of five required euthanasia prior to 30 days of treatment, a phenotype similar to complete loss of Recql4 protein (Fig 6G). Collectively, these analyses establish that the ATP-dependent helicase is not required for the physiological functions of Recql4 *in vivo*, however mutations resulting in truncated protein products are deleterious.

Discussion

The N-terminal Sld2-domain of RECQL4 protein is unique among RecQ family members and has been shown to be critical for the initiation of DNA replication in chicken, Drosophila, Xenopus and human cells [12, 17, 19, 24, 25], mostly likely through Sld2-domain dependent recruitment of the MCM10 and CTF4 factors to origins of replication [26]. The importance of the Sld2-domain to cell viability is reflected in the mutation spectrum detected in RTS patients–it is rarely mutated and always intact in at least one allele [6]. These findings implied that RTS and related disorders were caused by the loss of activity of the canonical ATP-dependent helicase domain, whose role in the replication initiation function is less clear. While initial *in vitro* studies using purified full-length human RECQL4 protein did not detect any unwinding potential on long DNA substrates [27], it was later shown that RECQL4 could unwind shorter duplex regions if a single strand-loading region was provided [16, 18]. This activity, together with the single-stranded DNA dependent ATP hydrolyzing activity, was lost in human Walker motif mutants $RECQL4^{K508A}$ and ^{D605A}. We now demonstrate that the murine $Recql4^{K525A}$ mutant protein is able to bind DNA but cannot hydrolyze ATP nor unwind DNA substrates, confirming that the mutant is helicase-dead and the homologue of human $RECQL4^{K508A}$. Unexpectedly, however, we found that this protein behaved comparably to wild-type Recql4 in supporting viability, fertility and normal physiological development of mice. No phenotypes or symptoms consistent with RTS were observed. Perhaps more surprising, was the normal response of $Recql4^{K525A/K525A}$ cells in replication, and in their response to both physiologically or exogenously induced DNA damage.

The most highly conserved domain of the RecQ helicases is the ATPase core. By analogy to multiple other DNA helicases (reviewed in ref. [28]), it was assumed that the ATP-dependent helicase activity of RECQL4 is essential for normal cellular DNA metabolism. Several studies have reported findings consistent with this interpretation. Complementation experiments in *Drosophila* showed that the helicase-dead K898N mutant could not rescue the viability of RecQ4 null mutants [29]. Similarly, a helicase-inactive human D605A mutant could not restore replication of xRecql4 depleted cells in *Xenopus* egg extracts [12]. Murine studies to date have only assessed complete nulls or severe hypomorphic alleles. The deletion of the exons that precede the helicase domain (exons 5–8) resulted in embryonic lethality by day 3–6 and a significantly truncated protein with no helicase or C-terminal domain [22]. When the entire helicase domain was deleted (exons 9–13; in-frame deletion), mice were viable but showed high rates of perinatal lethality [30] and a truncated protein product of 480aa was predicted. With the aim to maintain an intact protein, a study replaced the last helicase coding exon (13) with a neomycin cassette. 95% of animals died within 2 weeks after birth and a

substantial number of short transcripts covering exon 1 to 12 were reported, encoding potentially truncated products [31]. Since all these models effectively create proteins that lack the helicase and C-terminal domain, it is unclear if the observed phenotype could be attributed to the absence of the helicase domain only. Our study demonstrates that mice carrying the K525A helicase-dead mutation, with a stable full-length Recql4 protein, were viable and fertile with no apparent phenotype. The *in vivo* studies reported herein support a conclusion that the ATP-dependent helicase activity of Recql4 is not essential for replication or viability and that other domains account for these functions.

A range of prior *in vitro* studies have pointed to the importance of the N-terminal Sld2-like region. Lethality of *RECQL4*-depleted chicken cells was rescued by expression of the N-terminal region only [19]. In addition, the N-terminal domain of RECQL4 was shown to physically interact with several proteins involved in DNA replication in *Xenopus laevis* and human cell extracts [32, 33]. In our *in vivo* experiments however, we have shown that one copy of the N-terminal region alone (R347* or G522Efs) is insufficient for viability, indicating that a certain level of expression or localization of full-length Recql4 protein is required even if it has no ATP-ase or unwinding capacity.

The high frequency of chromosome abnormalities found in cells from RTS patients and the increased cancer incidence rates, suggest that RECQL4 may have a role in maintaining genome stability through DNA repair [2]. Prior studies have attributed several DNA repair functions of RECQL4 to its ATP-dependent helicase region, but they also have noted participation of the N-terminal region. Lu et al. found that a helicase-dead K508M could not rescue the loss of DNA end resection and homologous recombination (HR) repair after RECQL4 siRNA knock down, suggesting that the ATP-dependent helicase function of RECQL4 is involved in HR [34]. However, they also showed that it is the N-terminus of RECQL4 that physically interacts with MRN and CtIP [35]. In a similar fashion, a role for RECQL4 in non-homologous end joining (NHEJ) was linked to its interaction with the Ku70-80 by the N-terminal domain [36]. RECQL4 deficiency has been associated with modulation of core proteins involved in base excision repair (BER) such as POLB, FEN1, and APE1. The latter has shown to specifically interact with the N-terminal region of RECQL4 [37]. Herein, we observed no differences in the sensitivity of helicase-dead mutant cells compared to WT cells in response to various kinds of DNA damage (NHEJ, MMEJ, and HR for doxorubicin, BER for hydroxyurea, NER and BER for 4-nitroquinoline, and BER/SSBR for topotecan). Taken together there was no evidence for a role for the ATP-dependent function of Recql4 in the repair of pathological environmentally induced DNA damage.

A recent study showed that RECQL4-depleted U2OS cells were also deficient in ATM dependent checkpoint activation in response to drug induced DNA DSBs. Complementation assays using helicase-inactive point mutants in Walker A (K508G) or Walker B motif (D605A and E606A) further indicated that this was the result of a lack of helicase activity [38]. The ATM pathway plays an equally important role in the physiological processes of DSB repair and recombination, such as V(D)J recombination in T cell development and class switch recombination in B cell activation [39–41]. In our *in vivo* analysis we did not detect any defect in T cell maturation at the $CD4^+/CD8^+$ double positive to $CD4^+$ and $CD8^+$ single positive transition or any earlier stage, nor did the mice develop any T cell lymphomas as a result of chromosomal anomalies. In addition, *in vitro* B cell activation and class switch recombination in helicase-dead splenic B lymphocytes was indistinguishable from that in WT cells, arguing that the helicase activity is not required for either physiological checkpoint activation or DNA damage repair.

RTS patients, however, usually present with compound heterozygous mutations. It was reported that in 46% of RTS patients compound heterozygous mutations were present in the

PLOS GENETICS

RECQL4 gene [6]. The majority of these mutations affect the helicase and C-terminal region and are predicted to create truncated proteins caused by an early stop codon, frameshift, or mis-splicing [6]. The phenotypes in RTS patients, although grossly similar, can vary widely in severity. The relatively common C525AfsX33 (12 alleles) for example, has been found in all three syndromes (RTS, RAPADILINO and Baller-Gerold) and no single mutation has been assigned to a specific set of clinical features. In our study we demonstrate that mice carrying a sole truncating mutation (G522Efs and R347*) presented with a BM failure reminiscent of the *Recql4* null. This was not seen in the helicase-dead K525A, the M789K or the WT heterozygous null mice. Furthermore, when we assessed BM, PB, thymus, and spleen from heterozygous and homozygous K525A helicase-dead mutants, we did not find any significant change. A similar observation was made for the human WRN helicase. A naturally occurring single nucleotide polymorphism (R834C) was shown to have less than 10% of the WT helicase activity, but normal exonuclease activity. None of the heterozygous or homozygous carriers of this mutation developed Werner Syndrome (as defined by the clinical phenotype), clearly separating the WRN helicase function from other WRN functions [42]. Our findings demonstrate that helicase activity of Recql4 is also not required *in vivo* in mammals.

Collectively, this study has demonstrated the ATP-dependent helicase activity of Recql4 is not physiologically essential for murine embryonic development or adult homeostasis, cellular replication and physiological DNA damage repair. However, mutations that create truncating proteins are not tolerated. Further studies will have to be performed to elucidate the complex interactions of Recql4 mutations, their role in RTS and the contribution of the individual Recql4 domains to its normal physiological function.

Materials and methods

Ethics statement

All animal experiments were approved by the Animal Ethics Committee, St. Vincent's Hospital, Melbourne, Australia (#007/14 and 011/15). Animals were euthanized by CO_2 asphyxiation or cervical dislocation.

Recql4 cloning, expression and purification

The full-length WT and K525A mutant codon optimized cDNA sequence of the mouse Recql4 containing 3xFLAG tag at the C-terminus were cloned into vector pFL-EGFP and transferred to the Multibac expression system to generate baculovirus [43]. Baculovirus infected High 5 cells were resuspended in TNG buffer (20mM TEA pH7.5, 150mM NaCl, 10% glycerol, 1mM EDTA, 1x mammalian protease inhibitors (Sigma-Aldrich) and 1mM DTT. Mixtures were sonicated three times for 30 seconds on ice. Lysates were clarified by centrifugation at 50K x *g* 30 minutes. Anti-Flag M2–Affinity Gel (Sigma-Aldrich) resin was added and incubated for 60 minutes. Resin was extensively washed with TNG (without PI or EDTA), then washed overnight in TNG containing Benzonase nuclease (Sigma-Aldrich). Further washes were performed to remove the nuclease. Subsequently Recql4 was eluted with 100ug/ml Flag peptide in TNG.

Recql4 helicase assay

Helicase assays were performed according to Kaiser et al [18]. 80μl reactions containing 0.5μM protein and 50nM of a 15nt 3'-overhang (OH) DNA substrate in assay buffer (20mM HEPES pH 8.0, 10mM NaCl, 5% Glycerol, 1mM $MgCl_2$, 0.5mM TCEP) were assayed in an EnSpire 2300 microplate reader (Perkin Elmer) at 25˚C. The DNA substrate (T3-Cy3 annealed to

PLOS GENETICS

RecQ helicase activity is not required for Recql4's physiological function

B1-Dab) contained a 3′-15nt polyT ssDNA loading site and a 15nt dsDNA part with a generic sequence. After recording baseline fluorescence for 60s (Excitation 530nm / Emission 580nm), the helicase reaction was initiated by adding ATP to a final concentration of 1.25mM and the increasing Cy3-fluorescence as the quencher-labelled bottom-DNA strand is separated from the Cy3-labelled top-DNA strand, was recorded for 5 min. Measurements using H_2O in place of ATP as well as reactions with buffer instead of protein served as blank and were subtracted from the ATP-data.

Recql4 ATPase assay

PiColorLock phosphate detection reagent (Expedeon) was used to measure the presence of inorganic phosphate (Pi) release from ATP as a measure Recql4 ATPase activity. The proteins were assayed at 115nM in the presence of 1mM ATP and DNA in assay buffer (20mM HEPES pH 8.0, 10mM NaCl, 5% Glycerol, 1mM $MgCl_2$, 0.5mM TCEP). Color change was measured at Abs_{650nm} in an EnSpire 2300 microplate reader (Perkin Elmer) at 25˚C.

Recql4 DNA binding assay

Electro-mobility shift assay (EMSA) was used to measure the relative binding of WT versus K525A mutant Recql4 to DNA binding. Protein was serially diluted from 300nM to 19nM and bound to 25nM single stranded DNA oligo XOm1 conjugated to IRDye680. Bound Protein-DNA complex was separated on a 6% TBE/Acrylamide gel. The gel was directly imaged on a Li-Cor Odyssey CLx near-infrared fluorescence imaging system (Millennium Science).

Mice

Recql4^{K525A} and *Recql4*^{G522Efs} mice were generated using Cripsr/Cas9 methods by the Mouse Engineering at Garvan/ABR (MEGA) services (Garvan Institute, Darlinghurst, Australia). Lysine 525 was mutated to Alanine (AAG>GCA) in single cell C57Bl/6 embryos via sgRNA-directed gene targeting and homologous recombination with a single stranded DNA oligonucleotide substrate. Viable pups were screened by DNA sequencing and one C57Bl/6 male carrying the K525A mutation on one allele and a 2bp insertion (GA) after the T521 codon (G522Efs) on the other allele was identified as a founder. The chemically (ENU) induced *Recql4*^{M789K} and *Recql4*^{R347X} mutations were obtained from the Australian Phenomics Facility (APF, Canberra, Australia: IGL01381 and IGL01809). *Recql4*$^{fl/fl}$ mice (C57BL/6-*Recql4*^{tm2272Arte}) have been previously described [20, 44]. *Rosa26*-CreER^{T2} mice on a C57Bl/6 background were purchased from The Jackson Laboratory (B6.129-*Gt(ROSA)26Sor*$^{tm1(cre/ERT2)Tyj}$/J, Stock Number: 008463) and have been previously described [20]. All lines were on a backcrossed C57Bl/6 background. ENU mutants were outcrossed at least 6 times and assessed across multiple generations to eliminate effects of any additional mutations. Tamoxifen containing food was prepared by Specialty Feeds (Perth, Australia) at 400mg/kg tamoxifen citrate (Sigma Aldrich) in a base of standard mouse chow.

Genotyping

Genotyping of the K525A mutants was performed by PCR using the following primers: mRecql4 K525A MO36-F9: 5'-TAGACCTTATGAAACCTCAAAGCC-3' and mRecql4 K525A MO36-R3: 5'- AGAACATTGGGCATTCGGC-3' to yield a 591bp product, which was then digested with MslI (NEB) restriction enzyme to generate two fragments of 416 and 175bp for the WT or three fragments of 361, 175 and 55bp for the K525A mutant. Primers for the M789K mutants are: mRecql4 M789K 1F: 5'- AATAGGTGGCAATGGGCAGG-3' and:

PLOS GENETICS

mRecql4 M789K 1R: 5'-GCACTCGGCGAAAGGATACA-3' yielding a 420bp PCR product, uncut by MslI when M789K mutant, but cut in two (277 and 143bp) when WT. The presence of the G522Efs and R347X mutations was determined by KASP (competitive allele specific PCR) technology (LGC) with custom designed (G522Efs) or facility provided (R347X primer: 5'- GAAGGTGACCAAGTTCATGCTAAAGCGTTTGTTTTTCATGTTGAGTCG-3', 5'-GAAGGTCGGAGTCAACGGATTCAAAGCGTTTGTTTTTCATGTTGAGTCA-3', reverse primer 5'-GCTTCCCTAGACAGAGGGAACTATA-3') sequences according to manufacturer instructions.

Protein extraction and western blotting

Thymocyte lysates were prepared in RIPA buffer (50mM Tris, 150mM NaCl, 1% NP-40, 0.5% sodium deoxycholate, 0.1% SDS, pH8.0) plus Complete protease inhibitor (Roche, 04693116001) and PhosStop (Roche, 4906837001) tablets. 25μg whole protein extracts were fractionated on pre-cast NuPAGE BOLT 8% Bis-Tris polyacrylamide gels (Invitrogen) and transferred onto Immobilon-P PVDF membranes (Merck Millipore). Membranes were blocked with 5% milk in TBST and incubated overnight with rat monoclonal anti-mouse Recql4 antibody (clone 3B10, WEHI Antibody Services, Walter and Eliza Hall Institute Biotechnology Centre) or mouse anti-β-Actin (Sigma Aldrich, A1978). Membranes were then probed with HRP-conjugated goat anti-rat (Thermo Fisher Scientific, 31470) or anti-mouse (Thermo Fisher Scientific, 31444) secondary antibodies and visualized using ECL Prime Substrate (Amersham).

Peripheral blood analysis

Peripheral blood was analyzed on a hematological analyzer (Sysmex KX-21N, Roche Diagnostics). For flow cytometric analysis, red blood cells were lysed using a red blood cell lysis buffer (150mM NH_4Cl, 10mM $KHCO_3$, 0.1mM Na_2EDTA, pH7.3).

Flow cytometry analysis

Bones were flushed, spleens and thymus crushed, and single cell suspensions were prepared in PBS containing 2% FBS. Antibodies against murine Ter119, CD71, B220, IgM, CD43, CD19, CD21, CD23, Mac-1, Gr1, F4/80, CD4, CD8, TCRβ, CD25, CD44, Sca-1, c-Kit, CD34, FLT3, FcγRII/III (CD16/32), CD41, CD105, CD150, either biotinylated or conjugated with phycoerythrin, phycoerythrin-Cy7, peridinin chlorophyll protein-Cy5.5, allophycocyanin, allophycocyanin eFluor780, eFluor660 or eFluor450 were all obtained from eBioscience, BioLegend or BD Pharmingen (S1 Table) [20, 45, 46]. Biotinylated antibodies were detected with streptavidin conjugated with Brilliant Violet-605. 30,000–500,000 cells were acquired on a BD LSRII-Fortessa and analyzed with FlowJo software Version 9 or 10.0 (Treestar).

In vitro class switch recombination assay

B cells were purified from single cell spleen suspensions using a B Cell Isolation kit (Miltenyi, 130-090-862); 10^6 cells per well were cultured in 6-well plates for 4 days in RPMI supplemented with 10% FCS, 100U/ml penicillin, 100ng/ml streptomycin, 2mM L-glutamine, 1 x MEM nonessential amino acids, 1mM sodium pyruvate, 50μM ß-mercaptoethanol, 15μg/ml LPS (Invivogen, tlrl-3pelps) and 10ng/ml recombinant murine IL-4 (Peprotech, 214–14), and stained with CellTrace Violet (Thermo Fisher Scientific, C34557) and rat anti-mouse IgG1-APC (BD Pharmingen, 550874) [47]. Stained cells were assessed using a LSRIIFortessa (BD) and data analysed using FACSDiva (BD) or FlowJo (Tree Star) software.

PLOS GENETICS

RecQ helicase activity is not required for Recql4's physiological function

In vitro DNA damage assay

Hoxb8 immortalized [23] *R26*-CreER^{T2} *Recql4*$^{fl/+}$ (control) and *R26*-CreER^{T2} *Recql4*$^{fl/K525A}$ cells were maintained in IMDM, 10% FBS (non-heat inactivated) and 1% GM-CSF containing media (BHK-HM5 cell conditioned media). The cells were treated for 4 days with 400nM 4-hydroxy tamoxifen (Merck Millipore) then genotyped to confirm complete recombination. Cells were then plated at 10,000 cells/well in 96 well plates (Corning, CLS3610) and incubated for 48 hours with the indicated concentration of drugs in triplicates per dose (dose range Doxorubicin: 0–0.5μM, Hydroxyurea: 0–0.5mM, 4-Nitroquinoline: 0–2μM and Topotecan: 0–0.5mM). Doxorubicin was obtained from St. Vincent's Hospital Pharmacy. Hydroxyurea was purchased from Selleck. 4-Nitroquinoline and Topotecan were purchased from Sigma-Aldrich. Cell viability was measured using ATP-Lite (Perkin Elmer) as directed by the manufacturer and measured on an EnSpire plate reader (Perkin Elmer). Data were plotted and the IC_{50} value calculated using Prism 7 software. The dose-response curve was plotted as mean ±SEM.

Supporting information

S1 Fig. Analysis of recombination and genotyping of point mutant alleles. Genomic PCR showing recombination of the floxed allele to produce the excised product of the expected size (left) and genotyping PCRs of the point mutants (right) of the following alleles: (A) M789K. (B) K525A. (C) G522Efs. (D) R347*.
(TIF)

S2 Fig. *RECQL4* mutations in COSMIC database (110 mutations; somatic mutations). Data from COSMIC database. Image generated using Protein painter (Pecan portal St Jude's).
(TIF)

S3 Fig. Drug assays—individual doses dataset. Data showing the response to each individual drug dose used to calculate the IC_{50} values in Fig 5 from *R26*-CreER *Recql4*$^{\Delta/K525A}$ and *R26*-CreER *Recql4*$^{\Delta/+}$ with the non-tamoxifen treated isogenic controls. The X axis shows the individual drug doses of (A) Doxorubicin, (B) Hydroxyurea, (C) 4-Nitroquinoline, (D) Topotecan.
(TIF)

S1 Table. FACS antibodies (anti-mouse). List of antibodies used for flow cytometry in this study.
(PDF)

Acknowledgments

We thank R. Brink and the Mouse Engineering Garvan/ABR (MEGA) Facility for generation of the K525A and G522EfsX41 alleles; the Australian Phenomics Facility for their technical expertise and provision of the Recql4R347* and M789K alleles; WEHI Antibody Facility for the generation of anti-Recql4 antibody.

Author Contributions

Conceptualization: Wilson Castillo-Tandazo, Monique F. Smeets, Jörg Heierhorst, Andrew J. Deans, Carl R. Walkley.

Formal analysis: Wilson Castillo-Tandazo, Monique F. Smeets, Carl R. Walkley.

Funding acquisition: Andrew J. Deans, Carl R. Walkley.

Investigation: Wilson Castillo-Tandazo, Monique F. Smeets, Vincent Murphy, Rui Liu, Charlotte Hodson, Carl R. Walkley.

Methodology: Wilson Castillo-Tandazo, Monique F. Smeets, Vincent Murphy, Rui Liu, Charlotte Hodson, Jörg Heierhorst, Andrew J. Deans, Carl R. Walkley.

Project administration: Monique F. Smeets, Carl R. Walkley.

Resources: Andrew J. Deans.

Supervision: Monique F. Smeets, Jörg Heierhorst, Andrew J. Deans, Carl R. Walkley.

Visualization: Wilson Castillo-Tandazo, Rui Liu, Carl R. Walkley.

Writing – original draft: Wilson Castillo-Tandazo, Monique F. Smeets, Carl R. Walkley.

Writing – review & editing: Wilson Castillo-Tandazo, Monique F. Smeets, Vincent Murphy, Rui Liu, Charlotte Hodson, Jörg Heierhorst, Andrew J. Deans, Carl R. Walkley.

References

1. Larizza L, Roversi G, Volpi L. Rothmund-Thomson syndrome. Orphanet J Rare Dis. 2010; 5:2. https://doi.org/10.1186/1750-1172-5-2 PMID: 20113479
2. Wang LL, Levy ML, Lewis RA, Chintagumpala MM, Lev D, Rogers M, et al. Clinical manifestations in a cohort of 41 Rothmund-Thomson syndrome patients. Am J Med Genet. 2001; 102(1):11–7. PMID: 11471165
3. Kitao S, Shimamoto A, Goto M, Miller RW, Smithson WA, Lindor NM, et al. Mutations in RECQL4 cause a subset of cases of Rothmund-Thomson syndrome. Nat Genet. 1999; 22(1):82–4. https://doi.org/10.1038/8788 PMID: 10319867
4. Siitonen HA, Kopra O, Kaariainen H, Haravuori H, Winter RM, Saamanen AM, et al. Molecular defect of RAPADILINO syndrome expands the phenotype spectrum of RECQL diseases. Hum Mol Genet. 2003; 12(21):2837–44. https://doi.org/10.1093/hmg/ddg306 PMID: 12952869
5. Van Maldergem L, Siitonen HA, Jalkh N, Chouery E, De Roy M, Delague V, et al. Revisiting the craniosynostosis-radial ray hypoplasia association: Baller-Gerold syndrome caused by mutations in the RECQL4 gene. J Med Genet. 2006; 43(2):148–52. https://doi.org/10.1136/jmg.2005.031781 PMID: 15964893
6. Siitonen HA, Sotkasiira J, Biervliet M, Benmansour A, Capri Y, Cormier-Daire V, et al. The mutation spectrum in RECQL4 diseases. Eur J Hum Genet. 2009; 17(2):151–8. https://doi.org/10.1038/ejhg.2008.154 PMID: 18716613
7. Delagoutte E, von Hippel PH. Helicase mechanisms and the coupling of helicases within macromolecular machines. Part I: Structures and properties of isolated helicases. Q Rev Biophys. 2002; 35(4):431–78. PMID: 12621862
8. Chu WK, Hickson ID. RecQ helicases: multifunctional genome caretakers. Nat Rev Cancer. 2009; 9(9):644–54. https://doi.org/10.1038/nrc2682 PMID: 19657341
9. Larsen NB, Hickson ID. RecQ Helicases: Conserved Guardians of Genomic Integrity. Adv Exp Med Biol. 2013; 767:161–84. https://doi.org/10.1007/978-1-4614-5037-5_8 PMID: 23161011
10. Pike AC, Shrestha B, Popuri V, Burgess-Brown N, Muzzolini L, Costantini S, et al. Structure of the human RECQ1 helicase reveals a putative strand-separation pin. Proc Natl Acad Sci U S A. 2009; 106(4):1039–44. https://doi.org/10.1073/pnas.0806908106 PMID: 19151156
11. Croteau DL, Popuri V, Opresko PL, Bohr VA. Human RecQ helicases in DNA repair, recombination, and replication. Annu Rev Biochem. 2014; 83:519–52. https://doi.org/10.1146/annurev-biochem-060713-035428 PMID: 24606147
12. Sangrithi MN, Bernal JA, Madine M, Philpott A, Lee J, Dunphy WG, et al. Initiation of DNA replication requires the RECQL4 protein mutated in Rothmund-Thomson syndrome. Cell. 2005; 121(6):887–98. https://doi.org/10.1016/j.cell.2005.05.015 PMID: 15960976
13. Marino F, Vindigni A, Onesti S. Bioinformatic analysis of RecQ4 helicases reveals the presence of a RQC domain and a Zn knuckle. Biophys Chem. 2013;177–178:34–9.
14. Kliszczak M, Sedlackova H, Pitchai GP, Streicher WW, Krejci L, Hickson ID. Interaction of RECQ4 and MCM10 is important for efficient DNA replication origin firing in human cells. Oncotarget. 2015; 6(38):40464–79. https://doi.org/10.18632/oncotarget.6342 PMID: 26588054

15. Rossi ML, Ghosh AK, Kulikowicz T, Croteau DL, Bohr VA. Conserved helicase domain of human RecQ4 is required for strand annealing-independent DNA unwinding. DNA Repair (Amst). 2010; 9 (7):796–804.

16. Suzuki T, Kohno T, Ishimi Y. DNA helicase activity in purified human RECQL4 protein. J Biochem. 2009; 146(3):327–35. https://doi.org/10.1093/jb/mvp074 PMID: 19451148

17. Xu X, Liu Y. Dual DNA unwinding activities of the Rothmund-Thomson syndrome protein, RECQ4. EMBO J. 2009; 28(5):568–77. https://doi.org/10.1038/emboj.2009.13 PMID: 19177149

18. Kaiser S, Sauer F, Kisker C. The structural and functional characterization of human RecQ4 reveals insights into its helicase mechanism. Nat Commun. 2017; 8:15907. https://doi.org/10.1038/ncomms15907 PMID: 28653661

19. Abe T, Yoshimura A, Hosono Y, Tada S, Seki M, Enomoto T. The N-terminal region of RECQL4 lacking the helicase domain is both essential and sufficient for the viability of vertebrate cells. Role of the N-terminal region of RECQL4 in cells. Biochim Biophys Acta. 2011; 1813(3):473–9. https://doi.org/10.1016/j.bbamcr.2011.01.001 PMID: 21256165

20. Smeets MF, DeLuca E, Wall M, Quach JM, Chalk AM, Deans AJ, et al. The Rothmund-Thomson syndrome helicase RECQL4 is essential for hematopoiesis. J Clin Invest. 2014; 124(8):3551–65. https://doi.org/10.1172/JCI75334 PMID: 24960165

21. Walker JE, Saraste M, Runswick MJ, Gay NJ. Distantly related sequences in the alpha- and beta-subunits of ATP synthase, myosin, kinases and other ATP-requiring enzymes and a common nucleotide binding fold. EMBO J. 1982; 1(8):945–51. PMID: 6329717

22. Ichikawa K, Noda T, Furuichi Y. [Preparation of the gene targeted knockout mice for human premature aging diseases, Werner syndrome, and Rothmund-Thomson syndrome caused by the mutation of DNA helicases]. Nihon Yakurigaku Zasshi. 2002; 119(4):219–26. PMID: 11979727

23. Wang GG, Calvo KR, Pasillas MP, Sykes DB, Häcker H, Kamps MP. Quantitative production of macrophages or neutrophils ex vivo using conditional Hoxb8. Nature Methods. 2006; 3(4):287–93. https://doi.org/10.1038/nmeth865 PMID: 16554834

24. Thangavel S, Mendoza-Maldonado R, Tissino E, Sidorova JM, Yin J, Wang W, et al. Human RECQ1 and RECQ4 helicases play distinct roles in DNA replication initiation. Mol Cell Biol. 2010; 30(6):1382–96. https://doi.org/10.1128/MCB.01290-09 PMID: 20065033

25. Wu J, Capp C, Feng L, Hsieh TS. Drosophila homologue of the Rothmund-Thomson syndrome gene: essential function in DNA replication during development. Dev Biol. 2008; 323(1):130–42. https://doi.org/10.1016/j.ydbio.2008.08.006 PMID: 18755177

26. Im JS, Ki SH, Farina A, Jung DS, Hurwitz J, Lee JK. Assembly of the Cdc45-Mcm2-7-GINS complex in human cells requires the Ctf4/And-1, RecQL4, and Mcm10 proteins. Proc Natl Acad Sci U S A. 2009; 106(37):15628–32. https://doi.org/10.1073/pnas.0908039106 PMID: 19805216

27. Macris MA, Krejci L, Bussen W, Shimamoto A, Sung P. Biochemical characterization of the RECQ4 protein, mutated in Rothmund-Thomson syndrome. DNA Repair (Amst). 2006; 5(2):172–80.

28. Wu Y, Brosh RM Jr. Helicase-inactivating mutations as a basis for dominant negative phenotypes. Cell Cycle. 2010; 9(20):4080–90. https://doi.org/10.4161/cc.9.20.13667 PMID: 20980836

29. Capp C, Wu J, Hsieh TS. Drosophila RecQ4 has a 3'-5' DNA helicase activity that is essential for viability. J Biol Chem. 2009; 284(45):30845–52. https://doi.org/10.1074/jbc.M109.008052 PMID: 19759018

30. Mann MB, Hodges CA, Barnes E, Vogel H, Hassold TJ, Luo G. Defective sister-chromatid cohesion, aneuploidy and cancer predisposition in a mouse model of type II Rothmund-Thomson syndrome. Hum Mol Genet. 2005; 14(6):813–25. https://doi.org/10.1093/hmg/ddi075 PMID: 15703196

31. Hoki Y, Araki R, Fujimori A, Ohhata T, Koseki H, Fukumura R, et al. Growth retardation and skin abnormalities of the Recql4-deficient mouse. Hum Mol Genet. 2003; 12(18):2293–9. https://doi.org/10.1093/hmg/ddg254 PMID: 12915449

32. Matsuno K, Kumano M, Kubota Y, Hashimoto Y, Takisawa H. The N-terminal noncatalytic region of Xenopus RecQ4 is required for chromatin binding of DNA polymerase alpha in the initiation of DNA replication. Mol Cell Biol. 2006; 26(13):4843–52. https://doi.org/10.1128/MCB.02267-05 PMID: 16782873

33. Xu X, Rochette PJ, Feyissa EA, Su TV, Liu Y. MCM10 mediates RECQ4 association with MCM2-7 helicase complex during DNA replication. EMBO J. 2009; 28(19):3005–14. https://doi.org/10.1038/emboj.2009.235 PMID: 19696745

34. Lu H, Shamanna RA, Keijzers G, Anand R, Rasmussen LJ, Cejka P, et al. RECQL4 Promotes DNA End Resection in Repair of DNA Double-Strand Breaks. Cell Rep. 2016; 16(1):161–73. https://doi.org/10.1016/j.celrep.2016.05.079 PMID: 27320928

35. Lu H, Shamanna RA, de Freitas JK, Okur M, Khadka P, Kulikowicz T, et al. Cell cycle-dependent phosphorylation regulates RECQL4 pathway choice and ubiquitination in DNA double-strand break repair. Nat Commun. 2017; 8(1):2039. https://doi.org/10.1038/s41467-017-02146-3 PMID: 29229926

36. Shamanna RA, Singh DK, Lu H, Mirey G, Keijzers G, Salles B, et al. RECQ helicase RECQL4 participates in non-homologous end joining and interacts with the Ku complex. Carcinogenesis. 2014; 35 (11):2415–24. https://doi.org/10.1093/carcin/bgu137 PMID: 24942867

37. Schurman SH, Hedayati M, Wang Z, Singh DK, Speina E, Zhang Y, et al. Direct and indirect roles of RECQL4 in modulating base excision repair capacity. Hum Mol Genet. 2009; 18(18):3470–83. https://doi.org/10.1093/hmg/ddp291 PMID: 19567405

38. Park SY, Kim H, Im JS, Lee JK. ATM activation is impaired in human cells defective in RecQL4 helicase activity. Biochem Biophys Res Commun. 2019; 509(2):379–83. https://doi.org/10.1016/j.bbrc.2018.12.151 PMID: 30594395

39. Bredemeyer AL, Sharma GG, Huang CY, Helmink BA, Walker LM, Khor KC, et al. ATM stabilizes DNA double-strand-break complexes during V(D)J recombination. Nature. 2006; 442(7101):466–70. https://doi.org/10.1038/nature04866 PMID: 16799570

40. Liao MJ, Van Dyke T. Critical role for Atm in suppressing V(D)J recombination-driven thymic lymphoma. Genes Dev. 1999; 13(10):1246–50. https://doi.org/10.1101/gad.13.10.1246 PMID: 10346813

41. Lumsden JM, McCarty T, Petiniot LK, Shen R, Barlow C, Wynn TA, et al. Immunoglobulin class switch recombination is impaired in Atm-deficient mice. J Exp Med. 2004; 200(9):1111–21. https://doi.org/10.1084/jem.20041074 PMID: 15504820

42. Kamath-Loeb AS, Zavala-van Rankin DG, Flores-Morales J, Emond MJ, Sidorova JM, Carnevale A, et al. Homozygosity for the WRN Helicase-Inactivating Variant, R834C, does not confer a Werner syndrome clinical phenotype. Sci Rep. 2017; 7:44081. https://doi.org/10.1038/srep44081 PMID: 28276523

43. van Twest S, Murphy VJ, Hodson C, Tan W, Swuec P, O'Rourke JJ, et al. Mechanism of Ubiquitination and Deubiquitination in the Fanconi Anemia Pathway. Mol Cell. 2017; 65(2):247–59. https://doi.org/10.1016/j.molcel.2016.11.005 PMID: 27986371

44. Ng AJ, Walia MK, Smeets MF, Mutsaers AJ, Sims NA, Purton LE, et al. The DNA helicase recql4 is required for normal osteoblast expansion and osteosarcoma formation. PLoS Genet. 2015; 11(4): e1005160. https://doi.org/10.1371/journal.pgen.1005160 PMID: 25859855

45. Liddicoat BJ, Piskol R, Chalk AM, Ramaswami G, Higuchi M, Hartner JC, et al. RNA editing by ADAR1 prevents MDA5 sensing of endogenous dsRNA as nonself. Science. 2015; 349(6252):1115–20. https://doi.org/10.1126/science.aac7049 PMID: 26275108

46. Singbrant S, Russell MR, Jovic T, Liddicoat B, Izon DJ, Purton LE, et al. Erythropoietin couples erythropoiesis, B-lymphopoiesis, and bone homeostasis within the bone marrow microenvironment. Blood. 2011; 117(21):5631–42. https://doi.org/10.1182/blood-2010-11-320564 PMID: 21421837

47. Becker JR, Cuella-Martin R, Barazas M, Liu R, Oliveira C, Oliver AW, et al. The ASCIZ-DYNLL1 axis promotes 53BP1-dependent non-homologous end joining and PARP inhibitor sensitivity. Nat Commun. 2018; 9(1):5406. https://doi.org/10.1038/s41467-018-07855-x PMID: 30559443

B

AFFILIATED PUBLISHED WORK

1. Walia MK**, *Castillo-Tandazo W***, Mutsaers AJ, Martin TJ, Walkley CR. Murine models of osteosarcoma: A piece of the translational puzzle. J Cell Biochem. 2018;119(6):4241-50.
   DOI: https://doi.org/10.1002/jcb.26601
   ** These authors are co-first authors.

2. *Castillo-Tandazo W*, Mutsaers AJ, Walkley CR. Osteosarcoma in the Post Genome Era: Preclinical Models and Approaches to Identify Tractable Therapeutic Targets. Curr Osteoporos Rep. 2019;17(5):343-52
   DOI: https://doi.org/10.1007/s11914-019-00534-w

3. Straszkowski L, Jovic T, *Castillo-Tandazo W*, Ritchie DS, Purton LE. Effects of chemotherapy agents used to treat pediatric acute lymphoblastic leukemia patients on bone parameters and longitudinal growth of juvenile mice. Exp Hematol. 2020;82:1-7
   DOI: https://doi.org/10.1016/j.exphem.2020.01.010

Received: 16 September 2017 | Accepted: 7 December 2017
DOI: 10.1002/jcb.26601

PROSPECTS

WILEY Journal of Cellular Biochemistry

Murine models of osteosarcoma: A piece of the translational puzzle

Mannu K. Walia[1] | **Wilson Castillo-Tandazo**[1,2] | **Anthony J. Mutsaers**[3] | **Thomas John Martin**[1,2] | **Carl R. Walkley**[1,2]

[1] St. Vincent's Institute, Fitzroy, Vic, Australia

[2] Department of Medicine, St. Vincent's Hospital, University of Melbourne, Fitzroy, Vic, Australia

[3] Departments of Biomedical Sciences and Clinical Studies, Ontario Veterinary College, University of Guelph, Guelph, Canada

Correspondence
Carl Walkley, St.Vincent's Institute, 9 Princes St, Fitzroy 3065 Victoria, Australia.
Email: cwalkley@svi.edu.au

Funding information
Ontario Research Fund; Ontario Veterinary College Pet Trust; National Health and Medical Research Council; Cancer Council Victoria; Victorian Cancer Agency; Melbourne Research Scholarship; Canadian Foundation for Innovation; Department of Health, State Government of Victoria

Abstract

Osteosarcoma (OS) is the most common cancer of bone in children and young adults. Despite extensive research efforts, there has been no significant improvement in patient outcome for many years. An improved understanding of the biology of this cancer and how genes frequently mutated contribute to OS may help improve outcomes for patients. While our knowledge of the mutational burden of OS is approaching saturation, our understanding of how these mutations contribute to OS initiation and maintenance is less clear. Murine models of OS have now been demonstrated to be highly valid recapitulations of human OS. These models were originally based on the frequent disruption of *p53* and *Rb* in familial OS syndromes, which are also common mutations in sporadic OS. They have been applied to significantly improve our understanding about the functions of recurrently mutated genes in disease. The murine models can be used as a platform for preclinical testing and identifying new therapeutic targets, in addition to testing the role of additional mutations in vivo. Most recently these models have begun to be used for discovery based approaches and screens, which hold significant promise in furthering our understanding of the genetic and therapeutic sensitivities of OS. In this review, we discuss the mouse models of OS that have been reported in the last 3-5 years and newly identified pathways from these studies. Finally, we discuss the preclinical utilization of the mouse models of OS for identifying and validating actionable targets to improve patient outcome.

KEYWORDS
mouse models, osteosarcoma, screening, translational oncology

1 | INTRODUCTION

Osteosarcoma (OS) is the most common cancer of bone, principally impacting teenagers and young adults. A second peak of OS incidence occurs later in life that can be associated with Paget's disease or where OS arises as a second cancer, however, how the OS that arises in these two populations compares to that in adolescence has not been defined.[1] For patients with localized disease 5-year survival rates have remained at 70% for greater than three decades.[2] Despite improvements in imaging and diagnostic technologies,

Mannu K. Walia and Wilson Castillo-Tandazo are co-first authors.

 © 2017 Wiley Periodicals, Inc.

patients with metastatic or relapsed OS presently have a 20-30% 5-year survival rate. Many subtypes and variants of OS have been described, however, osteoblastic OS is the most common OS subtype clinically (~60%), with fibroblastic and chondroblastic being approximately equally represented at ~15% each. There is no clear association between OS subtype at diagnosis and outcome. Despite being the most common primary cancer of bone, OS is classified as a rare cancer.

Research has so far led to only a limited number of clinically relevant biologic insights, with the improvements in patient outcome arising from the better application of existing therapies rather than from the introduction of new agents. Current management of OS utilizes combination chemotherapy—doxorubicin and cisplatin ± methotrexate—and surgery which has improved survival rates to ~70% at 5 years.[2,3] Given the age of the majority of patients, these treatment approaches are associated with a significant burden of side-effects, both short and long term. Pre-operative chemotherapy response is the strongest predictor of survival in patients with localized disease. There is an urgent need to discover new therapeutic targets in OS.

Improving outcomes in OS will rely on an improved understanding of both OS biology and the roles that recurrently mutated genes play in tumor initiation and maintenance. Over the last decade, a number of tractable murine models of OS have been established and validated, generated chiefly on the knowledge of human familial cancer syndromes that have elevated rates of OS.[4–9] Other reviews have covered this topic in greater detail than will be presented herein,[8,10–12] including alternative genes tested and models using orthotopic transplants. More recently knowledge of the mutational burden of OS has greatly expanded as a result of tumor sequencing.[13–15] Unfortunately, the detailed sequencing of the OS genome has not to date presented any immediately actionable pathways allowing direct translation. At the intersection of these approaches, coupled with the establishment of patient derived primary OS xenografts,[14] a platform of information and reagents has been developed that can be utilised in therapeutic advancement for OS. We will discuss recently developed murine models and how these have been applied and validated to highlight new methods to target OS.

2 | THE GENETICS OF HUMAN OS

Until recently our knowledge of the genetics of OS was largely derived from the study of familial cancer predisposition syndromes that had elevated rates of OS compared to other cancers and the general population. This has been highly informative, not just in OS, but in understanding genes involved in human cancer more generally. It was identified that patients with Li-Fraumeni syndrome,[16,17] hereditary retinoblastoma,[18,19] and RecQ helicase related disorders, primarily Rothmund-Thomson syndrome,[20,21] were all at greatly increased risk of OS. This led to the clear association of mutations in *TRP53* (*p53*), *RB1*, and *RECQL4* with OS, which for *TRP53* and *RB1* have been experimentally confirmed.

Most recently whole genome sequencing and exome capture have demarcated the mutational burden of conventional human OS.[13–15,22–24] These studies have transformed our understanding of the genetics of OS, with the very high to universal mutation of *TP53* accompanied by recurrent mutation of *RB1*, *ATRX* and *DLG2* in 29-53% of cases.[13–15,23] Mutations within the "p53 pathway" occur in all human cancers.[25] The most prevalent mutations in human cancers are point mutations resulting in p53 protein with altered function.[26] In contrast, unique genomic rearrangements and other mutation types in OS frequently result in null alleles of *TP53*.[14,23] The reason for this *TP53* mutational preference in osteoblastic cells, the lineage of origin of OS, is not clear. Additional mutations that occur recurrently at low frequency include mutations in the IGF signaling pathway.[13] Other features of OS have been revealed by these studies including a high mutation load as assessed by copy number, structure and nucleotide variants compared to other pediatric tumors,[27] the presence of chromothripsis—the generation through a single event of a randomly shattered and reconstructed chromosome[28]; and kataegis—a pattern of localized hypermutation.[29] The mutational and karyotypic changes reported reflect a fundamentally unstable genome that dramatically reshapes the OS genome and impacts the potential for therapeutic intervention.

Although we are now armed with a detailed list of the mutational burden of OS, this has yet to translate into meaningful clinical benefit. In part, this may reflect the lack of specificity of currently available therapies. However, the advent of new technologies such as Crispr or siRNA and the rapid improvements in immunotherapy may yield breakthroughs. In parallel, generating the fundamental knowledge of how the mutations that recurrently arise contribute to OS initiation and maintenance may identify key pathways and nodes that can be exploited to improve outcomes for OS patients. It is as a part of this later endeavor that murine models of human OS hold greatest promise.

3 | MURINE MODELS OF OS

The generation of murine models of human cancer is an attractive approach to further our understanding of how different mutations or changes in gene expression contribute to tumorigenesis. For osteosarcoma, murine models have been long established based on either the administration of mutagens such as radiation,[30] from the knock-out of

genes associated with familial predisposition to OS (such as $p53^{-/-}$[31]) or from phenotyping in mutant or transgenic mice.[32] However, not all cases of murine/rodent OS are useful in the pursuit of identifying and testing new therapeutic approaches for human OS. For example, the mutation of *Nf2* in mice led to a relatively high rate of OS, yet humans with neurofibromatosis 2 who have *NF2* mutations do not show elevated rates of OS,[33,34] indicating that not all murine models will be useful for this purpose. The generation of high fidelity models recapitulating the mutational pattern and specificity of human OS would be most useful in leveraging these murine cancers to ultimately improving outcomes for human OS.

This became possible with the increasing numbers of mesenchymal and osteoblast targeted Cre expressing mouse strains, coupled with conditional mutant alleles of the key genes implicated in familial OS, principally *p53* and *Rb1* (Figure 1 and Table 1). Several groups, including our own, were able to establish high/full penetrant OS models based on the deletion of *p53* and *Rb* in the osteoblast lineage.[4,5,7,9,35,36] The models described to date are summarized in Table 1. The genetic basis of these models has been confirmed to accurately reflect sporadic OS based on the subsequent sequencing of the human OS genome. These murine models reproduce the cardinal features of human OS, including histology, site of disease, metastatic preferences, transcriptional program, and karyotypic complexity.[7,36] Conceptually similar models have been established through the transgenic overexpression of SV40T antigen using the osteocalcin promoter, which acts to sequester p53 and Rb.[6] The murine models have established the dominance that loss of *p53* exerts on initiating OS, with the evidence indicating that loss of *Rb* co-operates with loss of *p53*. In contrast to the efficiency through which mutation of *p53* induces OS, we did not observe OS induction upon deletion of *Recql4* as is observed in patients with *RECQ4* mutation in Rothmund-Thomson syndrome.[52] This result has been confirmed with an independently generated null allele of *Recql4*.[38] Therefore, while RTS patients display an elevated rate of OS, the murine models established to date are not recapitulating this finding, suggesting that additional models may be needed to understand the OS predisposition in these patients.

These models have generated several important observations that inform our understanding of the human disease. Firstly, the cell of origin of OS has been a broadly discussed area, yet it has not reached a consensus. The murine models have utilized a range of Cre expressing lines that are active from multi-potential mesenchymal/skeletal progenitors through to late stage mature osteoblasts. The outcome of these studies is that the most efficient and high penetrant generation of OS occurs once $p53 \pm Rb$ are deleted in the early committed osteoblasts (*Osx*-Cre) onward (Figure 1 and Table 1). The demonstration that even cells considered mature osteoblasts, marked by expression of

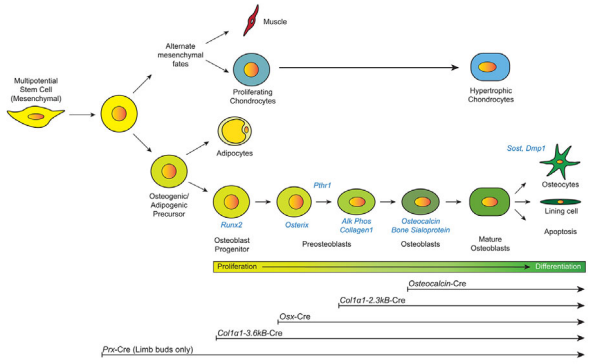

FIGURE 1 Outline of the cell populations targeted by different Cre expressing mouse models within the osteoblast lineage

Osteocalcin-Cre, with limited proliferative capacity could efficiently generate OS, strongly suggests that cells within the committed osteoblast lineage are the cell population from which OS arises.[9]

A second conclusion from these models is that the nature of the p53 mutation can influence the subtype of OS that evolves. Through comparing Cre:lox mediated *p53* deletion and shRNA mediated p53 knock-down, we were able to establish models of fibroblastic and osteoblastic OS, respectively.[36] This result suggested that the abrupt deletion of p53 immortalized cells rapidly, while in the shRNA model the pre-osteoblasts that express the shRNA were able to continue dividing and undergoing lineage differentiation until the levels of p53 were critically low and immortalization occurred at a more mature cell stage. The cell of origin may impact the clinical subtype observed, with more immature pre-osteoblasts favoring fibroblastic OS and more mature cells favoring osteoblastic OS. As a caveat, the use of *Osteocalcin*-Cre did not yield highly mineralized lesions,[9] cautioning a direct extrapolation of this observation.

Lastly, the deletion of *Recql4* did not result in the initiation of OS in murine models, including sensitized models with concurrent loss of *p53*. This was unexpected given the precedence from *p53* and *Rb* mutation in similar models, but multiple independent datasets support the failure to generate OS upon osteoblast restricted deletion of *Recql4*.[37,38] This raised several questions regarding the role of RECQ4 in OS and why RTS patients develop OS at high incidence. Complete null alleles of *Recql4* are not tumor suppressors but this is possibly a role of point mutation or truncating mutations where some protein expression is retained, an interpretation retrospectively consistent with the *RECQ4* mutation pattern in patients.[39] Another possibility is that Recql4 has distinct functional domains and roles, with the N-terminal region required for general DNA replication through its homology to Sld2, while the ATP-dependent helicase region and C-terminal parts of the protein are

TABLE 1 Outlines the results from genetically engineered OS models using these different Cre lines

Cell lineage	Cre	Gene	OS penetrance (%)	Metastatic disease	Median survival (weeks)	Mutation in human OS/familial cancer syndrome	Reference
Mesenchymal/skeletal progenitors	*Prx1*	$p53^{fl/fl}$	61	Yes (24%)	50	Yes/Li-Fraumeni syndrome	Lin et al[5]
		$Recql4^{fl/fl}$	0			No/Rothmund-Thomson syndrome	Lu et al[38]
		$p53^{fl/fl}$ $Rb^{fl/+}$	92		39	Yes/Li-Fraumeni syndrome, hereditary retinoblastoma	Calo et al
		$p53^{fl/fl}$ $Rb^{fl/fl}$	29		19	Yes/Li-Fraumeni syndrome, hereditary retinoblastoma	Lin et al[5]
Pre-osteoblasts	*Osx1*	$Rb^{fl/fl}$	0			Yes/hereditary retinoblastoma	Walkley et al[7]
		$p53^{fl/fl}$	100	Yes (40%)[a]	~42	Yes/Li-Fraumeni syndrome	Walkley et al[7]
		TRE-shp53.1224	100	Yes (83%)	~69	Yes/Li-Fraumeni syndrome	Mutsaers et al[36]
		$Recql4^{fl/fl}$	0			No/Rothmund-Thomson syndrome	Ng et al[37]
		$p53^{fl/fl}Rb^{fl/+}$	100	Yes (3.7%)	~23	Yes/Li-Fraumeni syndrome, hereditary retinoblastoma	Walkley et al[7]
		$p53^{fl/fl}$ $Rb^{fl/fl}$	100	Yes (37%)	~18	Yes/Li-Fraumeni syndrome, hereditary retinoblastoma	Walkley et al[7]
		TRE-shp53.1224 $pRb^{fl/fl}$	100	Yes (85%)	~57	Yes/Li-Fraumeni syndrome, hereditary retinoblastoma	Mutsaers et al[36]
		$p53^{R270H/+}$ SBmut	75	Yes (26.4%)	~86	Yes/Li-Fraumeni syndrome	Moriarity et al
		SBmut	24.4		~116	No/?	Moriarity et al
	Col1α1-3.6 kB	$p53^{fl/fl}$	60		~40	Yes/Li-Fraumeni syndrome	Lengner et al[35]
Osteoblasts	*Col1α1*-2.3 kB	$p53^{fl/fl}$	85		48	Yes/Li-Fraumeni syndrome	Lin et al[5]
	Col1α1-2.3 kB	Notch-ICD	100	Yes (40%)	~60	No	Tao et al[b,68]
	Osteocalcin	SV-40 T/t antigen	100	Yes (90%)	~30	Sequesters p53 and Rb	Molyneux et al[c,6]
		$p53^{fl/fl}$ $Rb^{fl/fl}$	44		~57	Yes/Li-Fraumeni syndrome, hereditary retinoblastoma	Quist et al[9]

[a]Small cohort of animals.
[b]Notch Intracellular domain.
[c]Tumors defined as "multi-ostotic bone tumors."

involved in the tumor suppressive function. This model is supported by data from analysis of hematopoietic cells where we could rescue *Recql4* deficient cells with a mutant form of full length RECQ4 that could not act as an ATP dependent DNA helicase.[40] It is apparent that more nuanced and refined models are required to understand the role of Recql4 in OS. A detailed analysis of the OS that arises in RTS patients would be highly valuable to determine whether this represents a genetically distinct entity of OS or is similar to sporadic OS, however, given the paucity of patients this may be very difficult.

3.1 | Newly identified pathways: Are all of them relevant to human OS?

The establishment of the high-fidelity models of OS has enabled recent studies testing the roles of specific genes and pathways in these models. These studies have identified several pathways of interest that may be relevant to human OS and progressing new treatment options as well as raising questions about how they relate to human OS.

3.2 | Newly identified pathways: Modulation of cAMP related pathways in OS

Genome wide association studies (GWAS) in OS have identified changes in cyclic AMP (cAMP) related processes as predisposing to OS. A GWAS defined two OS susceptibility loci in human: the metabotropic glutamate receptor *GRM4* and a region on chromosome 2p25.2 lacking annotated transcripts.[41] *GRM4* has a role in cAMP generation. A GWAS in dogs with OS identified variants of *GRIK4*, involved in cAMP pathways.[42] Using the murine OS model generated by an osteocalcin promoter-driven SV40T/t antigen (MOTO mouse), several tumors had inactivating mutations in a negative regulatory subunit of the cAMP-dependent protein kinase (PKA) complex, *Prkar1a*, which results in activation of the catalytic activity of PKA. One tumor had in this study exhibited amplification of *Prkaca*, the PKA catalytic component.[6]

Osteoblastic cells are highly responsive to cAMP, and major regulators of the osteoblast lineage, such as Parathyroid hormone (PTH) and PTHrP, increase cAMP and activate cAMP-dependent signaling.[43] PTHrP/PTH are key regulators of osteoblast and skeletal homeostasis.[44] PTHrP and PTH activate their shared receptor, PTHR1, on osteoblasts or OS cells, activating adenylyl cyclase and stimulating cAMP production,[45] followed by PKA activation, leading to the transcriptional changes associated with PTH/PTHrP treatment.[46,47] In normal osteoblasts, PTHrP is produced by osteoblastic lineage cells and acts in a paracrine manner upon other osteoblastic cells at different stages of differentiation.[48] Long-term treatment of rats with PTH(1-34) resulted in a high incidence of OS.[49] Elevated expression of PTHR1 is a feature of human and rodent OS.[30,50] PTHrP is expressed in murine OS subtypes where it acts in an autocrine/paracrine manner[51] to activate PTHR1 signaling. Collectively the evidence from multiple species implicates enhanced cAMP-PKA activity in OS.

Using the MOTO mouse, Khokha and coworkers demonstrated that loss of *Prkar1a* rapidly accelerated tumor formation in these mice.[6] Cells derived from the *Prkar1a* mutant mice exhibited continued signaling downstream of PKA. These mice develop many lesions across the skeleton at a very young age. Interestingly in humans, increased cAMP/PKA activity caused by the missense mutations to *GNAS1* causes fibrous dysplasia of bone.[52] Inactivating mutations of *PRKAR1A* are associated with Carney complex, an autosomal dominant multiple endocrine neoplasia syndrome,[53] where patients can develop osteochondromyxomas of the bone but are not noted to develop OS.[54] The sequencing of increasing numbers of human OS has not identified recurrent mutations in these specific genes, but has demonstrated an over-representation of mutations in the cAMP pathway, suggesting that the overall deregulation of this signaling cascade may be the critical requirement of mutations in this pathway.[55,56]

Consistent with a model that the increased activity of the cAMP pathway is required by OS are the results from our analysis of the role of PTHR1 and its ligand PTHrP. PTHR1 expression and responsiveness are a species-conserved feature of OS.[30,50] Primary cell cultures established from primary and metastatic lesions from the murine fibroblastic and osteoblastic OS models express PTHR1 and display robust induction of cAMP in response to both PTH and PTHrP.[51] The knock-down of PTHR1 caused a striking in vivo phenotype, with significantly impaired in vivo proliferation of the tumor and the acquisition of a mineralized state consistent with the cells having progressed in the differentiation cascade.[51] These studies indicate that active signaling through PTHR1 was required to maintain the immature state and proliferation of OS. Our subsequent studies have identified that OS cells require continuous expression of PTHrP, an autocrine ligand made by OS cells and able to act on PTHR1 in OS, with downstream activation of CREB1.[56] OS cells have basally elevated levels of cAMP that are maintained via autocrine PTHrP. Together with reduced expression of negative regulators of the cAMP pathway such as phosphodiesterases, this results in constitutive activation of cAMP in OS. The knock-down of either PTHrP or CREB1 had a major effect on the OS cells, with cells from the fibroblastic OS model demonstrating a significantly reduced proliferative capacity, while cells from the osteoblastic OS model were no longer viable upon knockdown of CREB1.[56] These studies suggested that activation of this signaling pathway is required for maintenance of established OS.

We then used a reductionist system to address the requirement for the cAMP pathway, centered on PTHrP and CREB1 during the initiation of OS. Using primary long bone osteoblasts that could be engineered to become p53 deficient, we observed that these cells reproducibly underwent a hyperproliferative transformation at approximately 12-14 days after deletion of p53.[37,56] The loss of p53 transcriptional activity was accompanied by activation of a cAMP gene signature. This suggested that deregulation of the cAMP pathway is an early event following loss of p53 in osteoblasts. To establish the requirement for this in the manifestations of the p53 deficient state, we knocked down expression of PTHrP or CREB1 immediately prior to deletion of p53. This demonstrated that expression of both PTHrP and CREB1 were necessary for the hyperproliferative transformation of primary osteoblasts in response to mutation of p53. These results, together with the prior related work in the MOTO model and GWAS based studies, establish that deregulation of the PTHrP-cAMP-PKA-CREB1 pathway is species conserved and required for both initiation and maintenance of OS. While yet to be demonstrated in primary human OS, murine studies demonstrated that osteoblastic OS is more sensitive to reductions in this pathway than fibroblastic OS. Such differential sensitivities between the OS subtypes would warrant further investigation.[56]

3.3 | Newly identified pathways: Is RANK-RANKL a good target?

Based on their analysis of the MOTO mouse, Khokha and coworkers identified RANK-RANKL signaling as a potential target in OS,[57,58] quite apart from its role in osteoclast formation. This pathway is critical in osteoclastogenesis and has been implicated in a number of different cancer types, most prominently breast cancers and cancer associated with bone resorption.[59] This latter action is the basis of a study targeting RANK signaling therapeutically in OS.[60] In the MOTO mouse model, the effects of RANK-RANKL deletion were compared between whole body deletion (MOTO-*Rankl*$^{-/-}$) and osteoblast vs osteoclast deletion of Rank (MOTO-*Rank*$^{\Delta/\Delta OB}$ and MOTO-*Rank*$^{\Delta/\Delta OC}$, respectively).[58] It was observed that whole body loss of RANKL potently suppressed tumor formation in the MOTO mice. In contrast, the deletion of RANK in osteoblasts using *Col1α1*-Cre did not modify tumor formation in these mice. Strikingly, the deletion of RANK in osteoclasts was proposed to inhibit OS formation in the MOTO background. This was a potentially highly interesting observation and one with translational potential given the development of RANKL inhibitors for clinical application. Unfortunately, the interpretation of the model used to achieve osteoclast specificity warrants caution. The authors used *Mx1*-Cre to undertake these studies and treated the mice with pIpC (for 13 weeks) to induce Cre activity to delete a conditional *Rank* allele. While a good model for broad somatic deletion in the adult mouse, it is difficult to reconcile existing data with the interpretation that the model achieved osteoclast specific RANK deletion. A large body of literature demonstrates the activity of *Mx1*-Cre broadly in hematopoietic cells including hematopoietic stem and progenitors, skeletal stem and progenitor cells (that give rise to osteoblasts and would be forming the OS in these models) and many other tissues in the mouse.[61–65] The model used and the effects are more consistent with a whole body somatic deletion of *Rank*, rather than the result of osteoclast specificity. Supportive of this is the lack of RANK expression in the tumor cells (mesenchymal derived osteoblast lineage cells) derived from the MOTO-*Rank*$^{\Delta/\Delta OC}$ mice. Additionally, there are conflicting data regarding the expression of RANK and RANKL in human OS.[66,67] Further work is required to clarify the requirement for RANK in OS cells.

3.4 | Newly identified pathways: Notch and OS?

Work from Lee and coworkers reported that activation of Notch1 could generate OS in mouse models.[68] Notch is a member of a family of transmembrane receptors that are important regulators in a range of developmental and tumor pathways. In humans, mutations in *NOTCH* generally target the intracellular domain (termed NICD) and lead to constitutive activity of this pathway. Activation of Notch1 or its ligands leads to alterations in bone homeostasis through proliferative and anti-differentiation mechanisms.[69,70] Lee and coworkers crossed the *R26*-LSL-NICD mice to *Col1α1*-2.3kB-Cre mice to generate osteoblast specific overexpression of Notch1 in this lineage.[68] They observed complete penetrance tumor induction by ~1 year of age. The concurrent deletion of *p53* led to a rapid acceleration of tumor formation and concomitant reduction in survival, in a manner comparable to the effect of loss of one or both *Rb* alleles on a *p53* null osteoblast background.[7] These studies demonstrate that in mice activation of Notch is a potent means to generate tumors of bone. However, the data from the increasingly large numbers of human OS that have been sequenced have not identified recurrent mutations in *NOTCH1*, nor in other components of this signaling cascade.[13–15,22–24] It is presently unclear to what extent this represents a finding that can be leveraged therapeutically against OS or if this represents a murine model of OS with limited translational potential to human OS.

3.5 | Newly identified pathways: Interrogating the genome

The use of the OS predisposed mice for unbiased gene discovery is a very attractive utilization of these models.

These models are potentially powerful discovery platforms and can be used to understand the in vivo mutational spectrum that leads to OS. Moriarity and coworkers have done just this, using in vivo transposon mediated mutagenesis to identify mutations that co-operate with a *p53* mutation to accelerate OS formation in mice.[48] Using an *Osx*-Cre LSL-*Trp53*^{R270H} background to mutagenize with a *Sleeping Beauty* transposon system, they analyzed the mutations that occurred in a large number of tumors and metastatic nodules.[71] A total of 232 recurrent transpositions were identified in the tumors, with the confirmation of the involvement of a number of known pathways including the PI3K-mTOR axis, *Myc* and *Pten*.[14,15,72] In addition to these, new pathways and targets were identified involving recurrent mutations in the *Sema4d* and *Sema6d*, genes involved in axonal guidance.[71] This approach, coupled with newly developed methods involving Crispr mediated genome modulation, provides significant new developments in understanding the genetics of OS. It would be interesting to determine in such a model if there were a fundamental difference between the effects of *p53* hot-spot mutation, as used by Moriarity et al and as commonly seen in many human cancers, and the impact of a null allele of p53 which is a common mutational preference in OS. It is apparent that the deletion of *p53* using *Osx*-Cre and the introduction of a heterozygous p53 point mutant have significantly different latency in vivo,[7,71] with the null allele more rapidly generating disease. Whether the same co-operative events emerged in vivo would be an interesting test of the role of how the different p53 mutations influence tumor evolution, in this case in a robust model of human cancer.

4 | PRECLINICAL UTILIZATION OF MURINE MODELS OF OS

The murine models established based on deletion of *p53* and *Rb1* in the committed osteoblast population demonstrate a high degree of conservation with human OS.[7,11,73] The demonstration that these models have conserved chemical/drug sensitivities and genetic vulnerabilities with primary human OS would greatly extend their application. Recent work has begun to provide evidence that this is indeed the case and that the murine OS cells share a similar therapeutic and genetic sensitivity to primary human OS.

Initial studies focused on the testing of specific agents or genetic vulnerabilities. As an example, it was demonstrated that OS cells, both murine and human, are sensitive to the bromodomain (BET) inhibitors.[74,75] The original rationale for testing these inhibitors arose from the observation in other settings that BRD4 inhibitors inhibited Myc function, and Myc has been strongly linked with OS.[76,77] A range of structurally diverse BET inhibitors, including JQ1 and I-BET151/I-BET762, demonstrate activity against murine primary fibroblastic and osteoblastic OS and a human PDX derived cell line. In our hands, we did not see an association between the activity of these compounds and a reduction in Myc protein levels, but we did observe reduction in FosL1 levels.[74] The activity of JQ1 was confirmed in vivo, where it showed potent activity against OS. When tested in vitro with standard of care chemotherapy, BET inhibition enhanced the activity of doxorubicin. We further added CDK9 inhibitors together with JQ1, based on the mechanism whereby BRD4 recruits the P-TEFb complex to promoters to alter gene expression.[78] The targeting of both BRD4 and CDK9, with either flavopiridol or dinaciclib, was synergistic and demonstrated efficacy against both murine and human OS.[74]

More recently multiple groups, including our own, have reported results from genome-wide genetic screens and drug/chemical library screens.[14,15,72] These initial screens have been conducted to identify drugs/chemicals or genetic susceptibilities in OS cells and, unexpectedly, converged on a common pathway. We conducted a whole genome siRNA and in parallel a selected small molecule inhibitor screen using primary OS cells derived from the *Osx*-Cre *p53*$^{fl/fl}$ *pRb*$^{fl/fl}$ model.[7,72] The siRNA screen was performed in the presence and absence of doxorubicin, with the aim of identifying loss of function alleles that killed OS or that modified the response to doxorubicin.[72] From the siRNA screen a number of hits were identified, the most directly interesting from a translational perspective being the PI3K-mTOR axis. We found an enrichment of hits in this pathway in the murine OS cells that was confirmed across independent samples and in human PDX derived OS cells. The same result was achieved using an independent, both technologically and biologically, shRNA loss of representation screen against murine OS derived cell lines.[15] Strikingly, the results from our chemical screen of predominantly kinase inhibitors identified activity from a group of PI3K-mTOR inhibitors, with those that inhibited both PI3Kα and mTOR most effective.[72] Further evidence for the tractability of this pathway was provided by Dyer and coworkers, who had been conducting a more extensive chemical screen of primary human OS cells maintained as PDXs.[14] In these cells, drugs that targeted the PI3K-mTOR axis were active against OS, and like the mouse, this activity showed a preference for combined inhibitors of PI3Kα and mTOR being most effective.[72] That the murine models and primary human OS demonstrate such a close conserved sensitivity to PI3Kα-mTOR inhibition demonstrated the validity of these models as tools for preclinical discovery and testing. Additional parameters, such as changes in miRNAs,[79] can also be demonstrated to show strong conservation between primary murine and primary human OS. These recent studies have further validated the genetically modified mouse models of OS as highly faithful recapitulations of human OS and

demonstrated that these can be applied for discovery and testing of new therapeutic approaches.

5 | CONCLUSIONS AND FUTURE DIRECTIONS

Valid murine models are an extremely valuable resource in advancing both our understanding of the genetics of cancer and in the development of new therapies. In the case of rare cancers, such as osteosarcoma, these models are of even greater importance as the ability to test numerous agents simultaneously in humans is limited. The development and validation of the murine models of OS, contributed to by numerous groups, has provided a new opportunity to explore the genetics and therapeutic targeting of OS. Coupled with the increasing sequence information available from primary human OS, the establishment of patient derived xenografts, and the development of naturally occurring OS and testing of investigational therapeutics in large breed dogs, we are now poised to be able to probe the OS genome at unprecedented depth. The murine models established to date provide a highly flexible and tractable system with which to identify and test new therapeutic approaches for OS.

ACKNOWLEDGMENTS

WC-T is supported by a Melbourne Research Scholarship (Melbourne University). Work in A.J.M's laboratory is supported by grants from the Canadian Foundation for Innovation, Ontario Research Fund, and OVC Pet Trust. Work in C.R.W's laboratory is supported by grants from the NHMRC, Cancer Council Victoria and Victorian Cancer Agency, in part by the Victorian State Government OIS (to St. Vincent's Institute).

ORCID

Carl R. Walkley http://orcid.org/0000-0002-4784-9031

REFERENCES

1. Mirabello L, Troisi RJ, Savage SA. Osteosarcoma incidence and survival rates from 1973 to 2004: data from the Surveillance, Epidemiology, and End Results Program. *Cancer*. 2009;115:1531–1543.
2. Janeway KA, Barkauskas DA, Krailo MD, et al. Outcome for adolescent and young adult patients with osteosarcoma: a report from the Children's Oncology Group. *Cancer*. 2012;118:4597–4605.
3. Janeway KA, Grier HE. Sequelae of osteosarcoma medical therapy: a review of rare acute toxicities and late effects. *Lancet Oncol*. 2010;11:670–678.
4. Berman SD, Calo E, Landman AS, et al. Metastatic osteosarcoma induced by inactivation of Rb and p53 in the osteoblast lineage. *Proc Natl Acad Sci USA*. 2008;105:11851–11856.
5. Lin PP, Pandey MK, Jin F, Raymond AK, Akiyama H, Lozano G. Targeted mutation of p53 and Rb in mesenchymal cells of the limb bud produces sarcomas in mice. *Carcinogenesis*. 2009;30:1789–1795.
6. Molyneux SD, Di Grappa MA, Beristain AG, et al. Prkar1a is an osteosarcoma tumor suppressor that defines a molecular subclass in mice. *J Clin Invest*. 2010;120:3310–3325.
7. Walkley CR, Qudsi R, Sankaran VG, et al. Conditional mouse osteosarcoma, dependent on p53 loss and potentiated by loss of Rb, mimics the human disease. *Genes Dev*. 2008;22:1662–1676.
8. Ng AJ, Mutsaers AJ, Baker EK, Walkley CR. Genetically engineered mouse models and human osteosarcoma. *Clin Sarcoma Res*. 2012;2:19.
9. Quist T, Jin H, Zhu JF, Smith-Fry K, Capecchi MR, Jones KB. The impact of osteoblastic differentiation on osteosarcomagenesis in the mouse. *Oncogene*. 2015;34:4278–4284.
10. Kansara M, Thomas DM. Molecular pathogenesis of osteosarcoma. *DNA Cell Biol*. 2007;26:1–18.
11. Mutsaers AJ, Walkley CR. Cells of origin in osteosarcoma: mesenchymal stem cells or osteoblast committed cells? *Bone*. 2014;62:56–63.
12. Uluckan O, Segaliny A, Botter S, Santiago JM, Mutsaers AJ. Preclinical mouse models of osteosarcoma. *Bonekey Rep*. 2015;4:670.
13. Behjati S, Tarpey PS, Haase K, et al. Recurrent mutation of IGF signalling genes and distinct patterns of genomic rearrangement in osteosarcoma. *Nat Commun*. 2017;8:15936.
14. Chen X, Bahrami A, Pappo A, et al. Recurrent somatic structural variations contribute to tumorigenesis in pediatric osteosarcoma. *Cell Rep*. 2014;7:104–112.
15. Perry JA, Kiezun A, Tonzi P, et al. Complementary genomic approaches highlight the PI3 K/mTOR pathway as a common vulnerability in osteosarcoma. *Proc Natl Acad Sci USA*. 2014;111:E5564–E5573.
16. Li FP, Fraumeni JF, Jr. Soft-tissue sarcomas, breast cancer, and other neoplasms. A familial syndrome? *Ann Intern Med*. 1969;71:747–752.
17. Malkin D, Li FP, Strong LC, et al. Germ line p53 mutations in a familial syndrome of breast cancer, sarcomas, and other neoplasms. *Science*. 1990;250:1233–1238.
18. Hansen MF, Koufos A, Gallie BL, et al. Osteosarcoma and retinoblastoma: a shared chromosomal mechanism revealing recessive predisposition. *Proc Natl Acad Sci USA*. 1985;82:6216–6220.
19. Friend SH, Bernards R, Rogelj S, et al. A human DNA segment with properties of the gene that predisposes to retinoblastoma and osteosarcoma. *Nature*. 1986;323:643–646.
20. Kitao S, Shimamoto A, Goto M, et al. Mutations in RECQL4 cause a subset of cases of Rothmund-Thomson syndrome. *Nat Genet*. 1999;22:82–84.
21. Wang LL, Gannavarapu A, Kozinetz CA, et al. Association between osteosarcoma and deleterious mutations in the RECQL4 gene in Rothmund-Thomson syndrome. *J Natl Cancer Inst*. 2003;95:669–674.
22. Kovac M, Blattmann C, Ribi S, et al. Exome sequencing of osteosarcoma reveals mutation signatures reminiscent of BRCA deficiency. *Nat Commun*. 2015;6:8940.

23. Ribi S, Baumhoer D, Lee K, et al. TP53 intron 1 hotspot rearrangements are specific to sporadic osteosarcoma and can cause Li-Fraumeni syndrome. *Oncotarget*. 2015;6:7727–7740.
24. Lorenz S, Baroy T, Sun J, et al. Unscrambling the genomic chaos of osteosarcoma reveals extensive transcript fusion, recurrent rearrangements and frequent novel TP53 aberrations. *Oncotarget*. 2016;7:5273–5288.
25. Hanahan D, Weinberg RA. Hallmarks of cancer: the next generation. *Cell* 2011;144:646–674.
26. Bieging KT, Mello SS, Attardi LD. Unravelling mechanisms of p53-mediated tumour suppression. *Nat Rev Cancer*. 2014;14: 359–370.
27. Chen X, Pappo A, Dyer MA. Pediatric solid tumor genomics and developmental pliancy. *Oncogene*. 2015;34:5207–5215.
28. Stephens PJ, Greenman CD, Fu B, et al. Massive genomic rearrangement acquired in a single catastrophic event during cancer development. *Cell*. 2011;144:27–40.
29. Nik-Zainal S, Alexandrov LB, Wedge DC, et al. Mutational processes molding the genomes of 21 breast cancers. *Cell*. 2012;149:979–993.
30. Martin TJ, Ingleton PM, Underwood JC, Michelangeli VP, Hunt NH, Melick RA. Parathyroid hormone-responsive adenylate cyclase in induced transplantable osteogenic rat sarcoma. *Nature*. 1976;260:436–438.
31. Jacks T, Remington L, Williams BO, et al. Tumor spectrum analysis in p53-mutant mice. *Curr Biol*. 1994;4:1–7.
32. Wang ZQ, Liang J, Schellander K, Wagner EF, Grigoriadis AE. C-fos-induced osteosarcoma formation in transgenic mice: cooperativity with c-jun and the role of endogenous c-fos. *Cancer Res*. 1995;55:6244–6251.
33. McClatchey AI, Saotome I, Mercer K, et al. Mice heterozygous for a mutation at the Nf2 tumor suppressor locus develop a range of highly metastatic tumors. *Genes Dev*. 1998;12:1121–1133.
34. Stemmer-Rachamimov AO, Nielsen GP, Rosenberg AE, et al. The NF2 gene and merlin protein in human osteosarcomas. *Neurogenetics*. 1998;2:73–74.
35. Lengner CJ, Steinman HA, Gagnon J, et al. Osteoblast differentiation and skeletal development are regulated by Mdm2-p53 signaling. *J Cell Biol*. 2006;172:909–921.
36. Mutsaers AJ, Ng AJ, Baker EK, et al. Modeling distinct osteosarcoma subtypes in vivo using Cre:lox and lineage-restricted transgenic shRNA. *Bone*. 2013;55:166–178.
37. Ng AJ, Walia MK, Smeets MF, et al. The DNA helicase Recql4 is required for normal osteoblast expansion and osteosarcoma formation. *PLoS Genet*. 2015;11:e1005160.
38. Lu L, Harutyunyan K, Jin W, et al. RECQL4 Regulates p53 Function In Vivo During Skeletogenesis. *J Bone Miner Res*. 2015;30:1077–1089.
39. Siitonen HA, Sotkasiira J, Biervliet M, et al. The mutation spectrum in RECQL4 diseases. *Eur J Hum Genet*. 2009;17:151–158.
40. Smeets MF, DeLuca E, Wall M, et al. The Rothmund-Thomson syndrome helicase RECQL4 is essential for hematopoiesis. *J Clin Invest*. 2014;124:3551–3565.
41. Savage SA, Mirabello L, Wang Z, et al. Genome-wide association study identifies two susceptibility loci for osteosarcoma. *Nat Genet*. 2013;45:799–803.
42. Karlsson EK, Sigurdsson S, Ivansson E, et al. Genome-wide analyses implicate 33 loci in heritable dog osteosarcoma, including regulatory variants near CDKN2A/B. *Genome Biol*. 2013;14:R132.
43. Suva LJ, Winslow GA, Wettenhall RE, et al. A parathyroid hormone-related protein implicated in malignant hypercalcemia: cloning and expression. *Science*. 1987;237:893–896.
44. McCauley LK, Martin TJ. Twenty-five years of PTHrP progress: from cancer hormone to multifunctional cytokine. *J Bone Miner Res*. 2012;27:1231–1239.
45. Juppner H, Abou-Samra AB, Freeman M, et al. A G protein-linked receptor for parathyroid hormone and parathyroid hormone-related peptide. *Science*. 1991;254:1024–1026.
46. Gardella TJ, Juppner H. Molecular properties of the PTH/PTHrP receptor. *Trends Endocrinol Metab*. 2001;12:210–217.
47. Pioszak AA, Xu HE. Molecular recognition of parathyroid hormone by its G protein-coupled receptor. *Proc Natl Acad Sci USA*. 2008; 105:5034–5039.
48. Martin TJ. Osteoblast-derived PTHrP is a physiological regulator of bone formation. *J Clin Invest*. 2005;115:2322–2324.
49. Vahle JL, Sato M, Long GG, et al. Skeletal changes in rats given daily subcutaneous injections of recombinant human parathyroid hormone (1-34) for 2 years and relevance to human safety. *Toxicol Pathol*. 2002;30:312–321.
50. Yang R, Hoang BH, Kubo T, et al. Over-expression of parathyroid hormone Type 1 receptor confers an aggressive phenotype in osteosarcoma. *Int J Cancer*. 2007;121:943–954.
51. Ho PW, Goradia A, Russell MR, et al. Knockdown of PTHR1 in osteosarcoma cells decreases invasion and growth and increases tumor differentiation in vivo. *Oncogene*. 2015;34:2922–2933.
52. Weinstein LS, Shenker A, Gejman PV, Merino MJ, Friedman E, Spiegel AM. Activating mutations of the stimulatory G protein in the McCune-Albright syndrome. *N Engl J Med*. 1991;325: 1688–1695.
53. Kirschner LS, Carney JA, Pack SD, et al. Mutations of the gene encoding the protein kinase A type I-alpha regulatory subunit in patients with the Carney complex. *Nat Genet*. 2000;26:89–92.
54. Carney JA, Boccon-Gibod L, Jarka DE, et al. Osteochondromyxoma of bone: a congenital tumor associated with lentigines and other unusual disorders. *Am J Surg Pathol*. 2001;25:164–176.
55. Walkley CR, Walia MK, Ho PW, Martin TJ. PTHrP, its receptor, and protein kinase A activation in osteosarcoma. *Mol Cell Oncol*. 2014;1:e965624.
56. Walia MK, Ho PM, Taylor S, et al. Activation of PTHrP-cAMP-CREB1 signaling following p53 loss is essential for osteosarcoma initiation and maintenance. *Elife*. 2016;5:e13446.
57. Beristain AG, Narala SR, Di Grappa MA, Khokha R. Homotypic RANK signaling differentially regulates proliferation, motility and cell survival in osteosarcoma and mammary epithelial cells. *J Cell Sci*. 2012;125:943–955.
58. Chen Y, Di Grappa MA, Molyneux SD, et al. RANKL blockade prevents and treats aggressive osteosarcomas. *Sci Transl Med*. 2015;7:317ra197.
59. Lacey DL, Boyle WJ, Simonet WS, et al. Bench to bedside: elucidation of the OPG-RANK-RANKL pathway and the development of denosumab. *Nat Rev Drug Discov*. 2012;11: 401–419.
60. Gorlick R, Janeway K, Lessnick S, Randall RL, Marina N, Committee COGBT. Children's Oncology Group's 2013 blueprint for research: bone tumors. *Pediatr Blood Cancer*. 2013;60:1009–1015.
61. Kuhn R, Schwenk F, Aguet M, Rajewsky K. Inducible gene targeting in mice. *Science*. 1995;269:1427–1429.

62. Roberts CW, Leroux MM, Fleming MD, Orkin SH. Highly penetrant, rapid tumorigenesis through conditional inversion of the tumor suppressor gene Snf5. *Cancer Cell*. 2002;2:415–425.
63. Park D, Spencer JA, Koh BI, et al. Endogenous bone marrow MSCs are dynamic, fate-restricted participants in bone maintenance and regeneration. *Cell Stem Cell*. 2012;10:259–272.
64. Yilmaz OH, Valdez R, Theisen BK, et al. Pten dependence distinguishes haematopoietic stem cells from leukaemia-initiating cells. *Nature*. 2006;441:475–482.
65. Walkley CR, Shea JM, Sims NA, Purton LE, Orkin SH. Rb regulates interactions between hematopoietic stem cells and their bone marrow microenvironment. *Cell*. 2007;129:1081–1095.
66. Lee JA, Jung JS, Kim DH, et al. RANKL expression is related to treatment outcome of patients with localized, high-grade osteosarcoma. *Pediatr Blood Cancer*. 2011;56:738–743.
67. Branstetter D, Rohrbach K, Huang LY, et al. RANK and RANK ligand expression in primary human osteosarcoma. *J Bone Oncol*. 2015;4:59–68.
68. Tao J, Jiang MM, Jiang L, et al. Notch activation as a driver of osteogenic sarcoma. *Cancer Cell*. 2014;26:390–401.
69. Engin F, Yao Z, Yang T, et al. Dimorphic effects of Notch signaling in bone homeostasis. *Nat Med*. 2008;14:299–305.
70. Hilton MJ, Tu X, Wu X, et al. Notch signaling maintains bone marrow mesenchymal progenitors by suppressing osteoblast differentiation. *Nat Med*. 2008;14:306–314.
71. Moriarity BS, Otto GM, Rahrmann EP, et al. A Sleeping Beauty forward genetic screen identifies new genes and pathways driving osteosarcoma development and metastasis. *Nat Genet*. 2015;47:615–624.
72. Gupte A, Baker EK, Wan SS, et al. Systematic screening identifies dual PI3K and mTOR inhibition as a conserved therapeutic vulnerability in osteosarcoma. *Clin Cancer Res*. 2015;21:3216–3229.
73. Janeway KA, Walkley CR. Modeling human osteosarcoma in the mouse: from bedside to bench. *Bone*. 2010;47:859–865.
74. Baker EK, Taylor S, Gupte A, et al. BET inhibitors induce apoptosis through a MYC independent mechanism and synergise with CDK inhibitors to kill osteosarcoma cells. *Sci Rep*. 2015;5:10120.
75. Lamoureux F, Baud'huin M, Rodriguez Calleja L, et al. Selective inhibition of BET bromodomain epigenetic signalling interferes with the bone-associated tumour vicious cycle. *Nat Commun* 2014;5:3511.
76. Shimizu T, Ishikawa T, Sugihara E, et al. C-MYC overexpression with loss of Ink4a/Arf transforms bone marrow stromal cells into osteosarcoma accompanied by loss of adipogenesis. *Oncogene*. 2010;29:5687–5699.
77. Delmore JE, Issa GC, Lemieux ME, et al. BET bromodomain inhibition as a therapeutic strategy to target c-Myc. *Cell*. 2011;146:904–917.
78. Zippo A, Serafini R, Rocchigiani M, Pennacchini S, Krepelova A, Oliviero S. Histone crosstalk between H3S10ph and H4K16ac generates a histone code that mediates transcription elongation. *Cell*. 2009;138:1122–1136.
79. Bhattacharya S, Chalk AM, Ng AJ, et al. Increased miR-155-5p and reduced miR-148a-3p contribute to the suppression of osteosarcoma cell death. *Oncogene*. 2016;35:5282–5294.

How to cite this article: Walia MK, Castillo-Tandazo W, Mutsaers AJ, Martin TJ, Walkley CR. Murine models of osteosarcoma: A piece of the translational puzzle. *J Cell Biochem*. 2018;119:4241–4250. https://doi.org/10.1002/jcb.26601

View publication stats

Current Osteoporosis Reports
https://doi.org/10.1007/s11914-019-00534-w

CANCER-INDUCED MUSCULOSKELETAL DISEASES (E KELLER AND J STERLING, SECTION EDITORS)

Osteosarcoma in the Post Genome Era: Preclinical Models and Approaches to Identify Tractable Therapeutic Targets

Wilson Castillo-Tandazo[1,2] · Anthony J. Mutsaers[3] · Carl R. Walkley[1,2,4]

© Springer Science+Business Media, LLC, part of Springer Nature 2019

Abstract

Purpose of Review Osteosarcoma (OS) is the most common cancer of bone, yet is classified as a rare cancer. Treatment and outcomes for OS have not substantively changed in several decades. While the decoding of the OS genome greatly advanced the understanding of the mutational landscape of OS, immediately actionable therapeutic targets were not apparent. Here we describe recent preclinical models that can be leveraged to identify, test, and prioritize therapeutic candidates.

Recent Findings The generation of multiple high fidelity murine models of OS, the spontaneous disease that arises in pet dogs, and the establishment of a diverse collection of patient-derived OS xenografts provide a robust preclinical platform for OS. These models enable evidence to be accumulated across multiple stages of preclinical evaluation. Chemical and genetic screening has identified therapeutic targets, often demonstrating cross species activity. Clinical trials in both PDX models and in canine OS have effectively tested new therapies for prioritization.

Summary Improving clinical outcomes in OS has proven elusive. The integrated target discovery and testing possible through a cross species platform provides validation of a putative target and may enable the rigorous evaluation of new therapies in models where endpoints can be rapidly assessed.

Keywords Osteosarcoma · Mouse models · Patient-derived xenograft · Canine OS, sarcoma

Introduction

Osteosarcoma (OS) is the most common primary malignant bone tumor in children and adolescents aged 10–20 years. It is commonly located in the metaphyseal growth plates of the long bones of the extremities [1]. Histologically, OS is characterized by the production of bone stroma by malignant osteoblastic lineage cells, which can be further classified into osteoblastic, chondroblastic, and fibroblastic subtypes [2]. While histological subtypes are described, current standard-of-care treatment and outcomes are independent of the subtype ascribed. Numerous risk factors for OS development have been determined including rapid bone turnover and growth, exposure to radiation, and genetic diseases such as Li-Fraumeni syndrome, hereditary retinoblastoma, Rothmund-Thomson syndrome (RTS), RAPADILINO syndrome, Werner's syndrome, and Bloom's syndrome [3]. The vast majority of OS occurs sporadically. OS is characterized by complex genomic structures and rearrangements as well as high interpatient heterogeneity, making the identification of broadly applicable therapeutically actionable pathways a challenge. Patients with non-metastatic OS have a 5-year survival rate of 60–70%, which is dramatically reduced to 20–30% when metastases develop [4]. Despite the stabilization of survival rates over the last 30 years, the treatment of OS still relies on surgery and combination chemotherapy, with very few

This article is part of the Topical Collection on *Cancer-induced Musculoskeletal Diseases*

✉ Carl R. Walkley
cwalkley@svi.edu.au

✉ Anthony J. Mutsaers
mutsaers@uoguelph.ca

[1] St. Vincent's Institute, 9 Princes St, Fitzroy, VIC 3065, Australia

[2] Department of Medicine, St. Vincent's Hospital, University of Melbourne, Fitzroy, VIC 3065, Australia

[3] Department of Biomedical Sciences, Ontario Veterinary College, Department of Clinical Studies, Ontario Veterinary College, University of Guelph, Guelph, Canada

[4] Mary MacKillop Institute for Health Research, Australian Catholic University, Melbourne, VIC 3000, Australia

Published online: 16 September 2019

modifications in several decades [5]. This has led to a plateau in survival rates, particularly in metastatic OS, but no significant improvements in therapeutic response have been achieved since the introduction and optimization of chemotherapy regimens.

Whole genome and exome sequencing (WGS/WES) studies have characterized the genomic landscape of OS, defining it as strikingly complex [6, 17, 18••, 19, 20]. OS tumors are aneuploid and have high rates of chromosomal aberrations, including chromothripsis [20] and the presence of hypermutable regions known as "kataegis" [17]. *TP53* is the most frequently mutated gene in OS and has a long-known association with OS due to the overrepresentation of OS in the spectrum of cancers affecting Li-Fraumeni syndrome patients. The sequencing of the OS genome reported > 90% TP53 mutations in one allele and > 80% in both alleles [17], a finding replicated across studies and cohorts [6, 21–24]. Interestingly, there is an apparent preference in OS for null or loss of protein expression mutations in *TP53* due to the inversion of intron 1. The reason for the preference for inactivating/null mutations, rather than the more prevalent hotspot point mutations seen in many cancers, has not been resolved. Other genes recurrently mutated in sporadic OS include *RB1*, *ATRX*, and *DLG2* [17, 18••]. In Rothmund-Thomson syndrome, a rare autosomal recessive disorder caused by mutations in the *RECQL4* gene, OS is reported in 32% of patients and remains among the top causes of mortality in these patients [25]. Despite the OS predisposition in RTS, mutations in *RECQL4* are not found in sporadic OS for at present unknown reasons.

Our understanding of the genomic landscape of OS is approaching saturation. This information has principally derived from a combination of exome, whole genome, and RNA sequencing studies, with some limited additional insight from genome-wide association studies. This has provided a comprehensive list of genes that can contribute to OS, but has not identified readily actionable therapeutic targets that would be broadly applicable. As a result, additional approaches are required to identify and test therapeutic vulnerabilities and then triage these to prioritize clinical testing. Three models using primary tumor material have been developed and applied: genetically engineered murine models, patient-derived primary tumor material (both in cell culture and as xenografts), and the spontaneous disease that arises in large breed dogs (Fig. 1). Here we will review how these models have been utilized to progress therapeutic target identification and development in OS. (Table 1).

Preclinical Models: Genetically Engineered Murine Models of OS

Initial high fidelity, autochthonous murine models of OS were generated over a decade ago, based on the known genetics of familial cancer syndromes predisposed to OS. These models utilized the loss of *p53* and *Rb* in cells of the osteoblastic lineage, allowing the development of OS with full penetrance and high metastatic rates [26–30]. Extensive characterization of these models at the histologic, transcriptomic, genomic, and most recently genetic/therapeutic vulnerabilities has established that these models are faithful representations of OS as it occurs in humans. The murine models demonstrated an absolute requirement for mutation of *p53*, a finding consistent with the near universal mutation of *TP53* in human OS. In the mouse models, the loss of *Rb1* alone was not sufficient to initiate OS, but when lost with *p53* was a potent accelerating event. Interestingly, the genetic cooperativity between p53/Rb loss at accelerating OS is apparent only within the committed osteoblast populations (as marked by *Osx1*-Cre expression), as when p53/Rb are concurrently deleted in more immature populations (marked by *Prx1*-Cre), the rate of OS drops and undifferentiated sarcomas predominate [27, 31]. Retrospectively, this may not be surprising given the shared mutational spectrum of the undifferentiated sarcoma genome and OS, suggestive of a significant contribution from the cell of origin to the ultimate tumor that arises [32].

Additional models have recently been described. Using a range of different Cre drivers, Quist et al. were able to demonstrate that OS can arise from across a differentiated spectrum of cells within the osteoblastic lineage. Strikingly, even cells within the committed osteoblast populations were able to efficiently initiate OS in vivo [29]. These findings, together with data generated in a range of other independent models using additional Cre drivers, are consistent with the cell of origin of OS coming from within the osteoblastic lineage [33]. Several models have recently been described using hot spot mutations of p53, rather than the null alleles used previously [34, 35]. One study found that while disease latency was comparable between the different p53 alleles, the metastatic frequency was higher in a p53R172H point mutant model (53% of animals with metastatic dissemination) compared with the *p53* null allele (25% of animals) [35]. We previously reported metastatic rates of 50% in *Osx1*-Cre $p53^{fl/fl}$ mice and up to > 80% in *Osx1*-Cre TRE-p53.1224 (an osteoblast-restricted shRNA directed against endogenous p53) [28], suggesting that there may be difference across cohorts (e.g., mouse strain, overall health status) and animal facilities. A separate study also applied a p53 point mutant allele and *Osx1*-Cre in a mutagenic model using sleeping beauty transposase [31, 34]. Given the mutational preference in human OS for null alleles, often as a result of inversions of the first intron which have been found in both sporadic OS and Li-Fraumeni patients, the use of genetically modified null alleles would appear to more closely mirror the human disease. A detailed comparison between murine OS tumors derived from null alleles to those harboring p53 point mutations would be warranted to resolve if there are fundamental differences generated by the p53 mutation type applied. This is particularly

Table 1 Summary of the most recent targeted therapeutics identified for osteosarcoma

Drug/molecule	Pathway involved	Mechanism/effect	Model tested	Evidence from multiple species?	Reference
Dual PI3K-mTOR inhibitor • GSK2126458 • PKI-587 • BEZ-235	PI3K pathway/mTOR pathway	Dual inhibition of PI3K and mTOR pathways was more potent than PI3K-selective agents on established OS cell lines	Murine primary/met cell lines; human primary cell lines (PDX derived)	Yes; currently in phase II clinical trial (MATCH study: Clinicaltrials.gov ID NCT03213678)	[6, 7]
BET bromodomain inhibitor • JQ1 • I-BET151 • I-BET762	BET proteins/chromatin	Inhibition of the bromodomain of the BET signaling pathway disrupted the vicious cycle between bone-associated tumors and bone resorption through transcriptional repression of *MYC*, *RUNX1*, or *FOSL1*	Human OS cell lines; mouse cell lines in vitro and in vivo	Yes; currently in phase I clinical trials	[8, 9]
IAP antagonists (SMAC mimetics) • SM-164 • GDC-0152 • LCL161	Apoptosis pathway	Activation of caspases through the inactivation of inhibitors of apoptosis molecules (XIAP and cIAPs)	Murine primary/met cell lines	Not for OS	[10•]
PI3K inhibitors MEK inhibitors	PI3K pathway/MEK pathway	Dual inhibition of PI3K and MEK pathways showed to be effective in solid tumor xenografts carrying KRAS mutations, HER2 amplifications, or PTEN deletions and mutations	Human primary OS cell lines (PDX derived); in vivo PDX	Yes; phase I clinical trials	[11]
HDAC inhibitors • Parabinostat • Romidepsin	Chromatin/transcription factors: Runx2/Wnt/B-catenin pathway	Induce maturation and differentiation of bone through the inhibition of transcription factor Runx2 and regulation of Wnt/B-catenin pathway. When combined with nucleoside analog gemcitabine or topoisomerase inhibitor, doxorubicin showed synergistic effects	Human OS cell lines	Not yet in OS—romidepsin used for soft tissue sarcomas	[11••, 12]
Listeria vaccine expressing *HER2* (ADXS31-164)	HER2 targeting; immune response	Anti-HER2 immune response, T lymphocyte activation, interferon responses; improved survival compared with historical control	Canine phase I clinical trial		[13]
Salmonella encoding IL2 (SalpIL2)	IL2 expression	Recombinant *Salmonella* expressing IL-2 vaccine; delivery of IL-2 to hypoxic tumor	Canine phase I clinical trial		[14]
Viral vector gene therapy e.g., Adenoviral FasL Oncolytic therapy (viral) e.g., (VSV-IFNβ-NIS)	Various FasL; interferon beta and sodium iodide symporter	Stimulators of immune response, tumor lysis; stimulation of inflammation and lymphocyte infiltration into the tumor	Canine clinical trials		[15, 16]

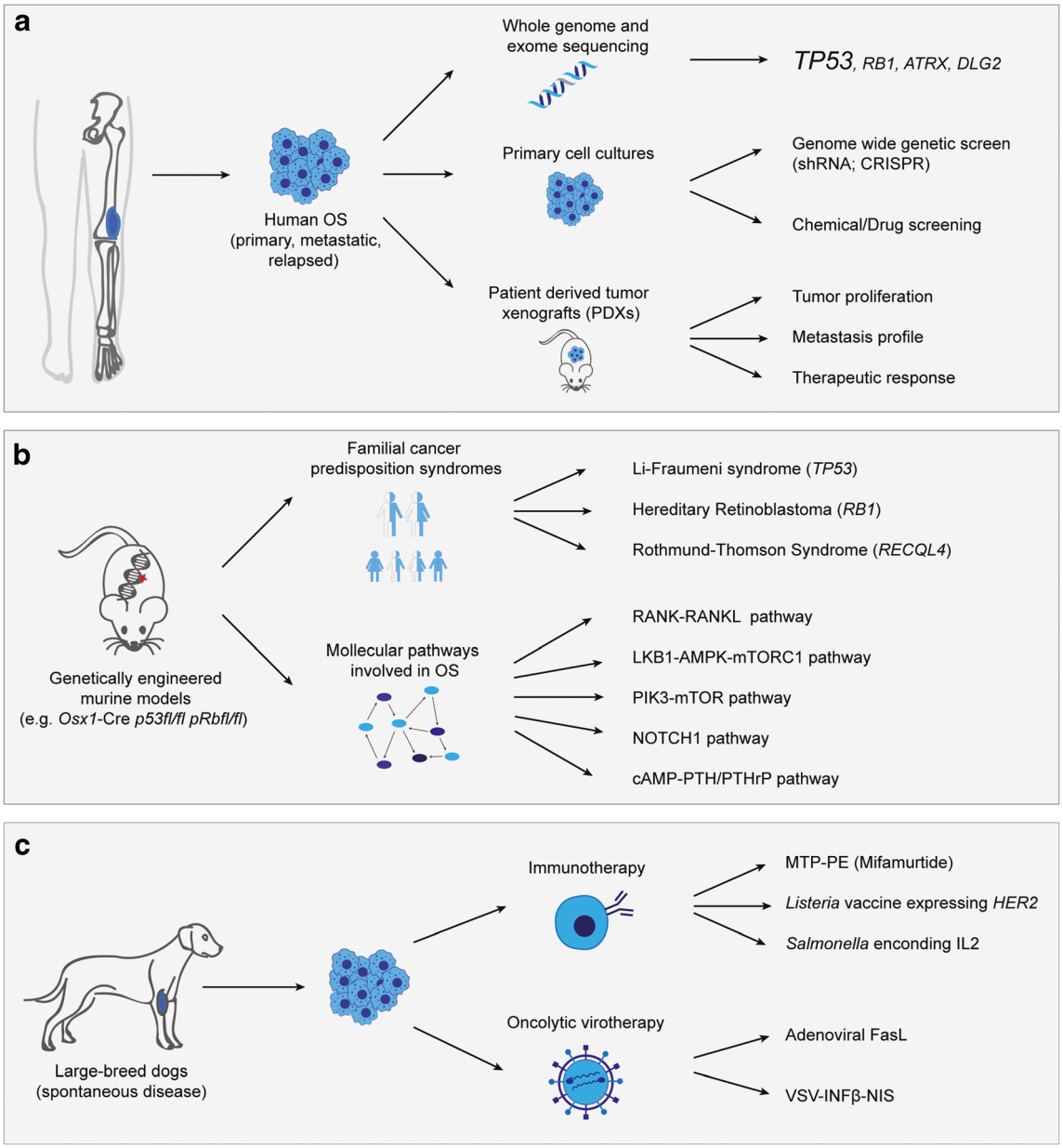

Fig. 1 Different preclinical models and approaches for progressing preclinical targets in osteosarcoma. **a** Human OS samples and primary cells derived from them have been applied to characterize the genomic landscape through both whole genome and exome sequencing. The use of these as primary samples and cell cultures has contributed to the identification of therapeutic vulnerabilities through chemical/drug and genome-wide genetic screens. Additionally, their engraftment in immunodeficient mice (patient-derived tumor xenografts (PDXs)) has been used to study the proliferation, metastatic profile, and therapeutic response of OS in experimental designs mimicking clinical trials. **b** Genetically engineered murine models have been used to understand the high prevalence of OS in several familial cancer predisposition syndromes: Li-Fraumeni syndrome (*TP53*), hereditary retinoblastoma (*RB1*), and Rothmund-Thomson syndrome (*RECQL4*). They have also been applied for target discovery and validation studies to identify and establish evidence for targeting novel molecular pathways, including RANK-RANKL, LKB1-AMPK-mTORC1, PIK3-mTOR, NOTCH1, and cAMP-PTH-PTHrP pathways. **c** Large breed dogs provide an attractive model for OS preclinical development due to their high resemblance to the human disease, the spontaneous development of OS (i.e., non-genetically modified animals), and the advantage of studying OS in an immunocompetent organism that shares the human environment. They have facilitated the development of current treatment approaches and in the testing of novel therapies including immunotherapy and oncolytic virotherapy

important if the gene expression and genetic signatures of these murine models are to be utilized in cross species comparisons and to validate their utility as preclinical platforms [7, 28, 30, 36].

More recently, a number of different models have been described to result in OS in vivo and have been applied to understand the roles of additional genes in OS initiation. In contrast to the OS predisposition in Rothmund-Thomson

Syndrome patients, we and others have failed to observe OS in models based on the deletion of *Recql4*, the described genetic cause of RTS [37, 38]. While the low bone mass of RTS patients can be recapitulated in the murine models, the mice do not develop OS suggesting either species differences or that pathogenic mutations in *RECQL4*, rather than null alleles, need to be assessed before a final conclusion can be drawn regarding the role of RECQL4 in OS initiation. One of the more confounding recent studies reported the development of OS following the expression of activated Notch in the osteoblastic populations [39]. While the analysis provides support for the conclusions reached, the relevance of this model to understanding human OS is questionable given the lack of mutations in *NOTCH1* or any of its ligands in human OS [6, 17, 18••]. Another pathway explored in vivo in murine models is the role of RANKL and its receptor (RANK), a signaling pathway essential for bone homeostasis through the differentiation and activation of osteoclasts [40]. The conditional deletions of RANK in either the osteoblast or osteoclast lineage were assessed using the osteocalcin-driven SV-40^{Tg} (MOTO) background. The authors proposed that deletion of RANK in osteoclasts inhibits OS formation [41]. It is important when interpreting the conclusions to consider that the study used *Mx1*-Cre to induce the conditional deletion of *Rank* allele, and numerous studies have demonstrated that *Mx1*-Cre is not specific to osteoclasts but able to activate gene recombination broadly, including efficiently in hematopoietic and skeletal stem and progenitor cells [42–45]. Han et al. generated a mouse model based on the conditional knockout of *Lkb1* (also known as Stk1) in periosteum-derived *Ctsk*-Cre-expressing cells. LKB1 is a serine/threonine kinase that phosphorylates AMPK, which inactivates mTORC1 in the LKB1-AMPK-mTORC1 pathway [46]. The authors found that loss of *Lkb1* in this model led to OS formation by increasing mTORC1 activity [47•]. Although mutations in *LKB1* are not commonly found in human OS, reduced LKB1 protein expression has been found in 41% of OS patients [48]. This may explain why this pathway is affected in OS and could also serve as a potential therapeutic target.

The development and validation of independent murine models of OS has cemented the central role of mutation of p53 in OS initiation. These models have now been utilized to explore the in vivo genetics of OS and in a range of preclinical target identification approaches. One advantage of the murine models is the ability to isolate and establish treatment-naïve paired primary and metastatic primary cell cultures, enabling a range of complementary experimental approaches. This has recently been matched by the establishment of a number of primary human OS-derived cell cultures. The murine cell lines derived from the *Osx1*-Cre $p53^{fl/fl}$ $pRb^{fl/fl}$ models have proven to be highly useful for pre-clinical screening, enabling both chemical/drug screens and genome scale loss of function studies using both siRNA and shRNA [6, 7]. Independent, orthogonal approaches converged to provide evidence that targeting of the PI3K-mTOR axis was a therapeutic vulnerability in OS [6, 7]. These studies were able to confirm that this was species conserved, utilizing primary early passage cell lines derived from patient-derived xenografts. Supporting the findings of these agnostic chemical-genetic screens, the PI3K-mTOR pathway was also targeted in a transposon-based mutagenesis model of OS [34]. Pathway-specific studies have also been reported. A number of preclinical studies have assessed the efficacy of new generation epigenetic-targeted therapy in OS models. These have demonstrated in vivo activity of small molecule inhibitors of the bromodomain and extra terminal repeat (BET) family [8, 9]. The activity of BET inhibitors was species conserved across both primary mouse and human OS; however, the mechanism of action remains unresolved with discrepancies between that observed in primary tumor-derived samples and from long established human OS cell lines [8, 9]. Small molecule inhibitors targeting cell death–related pathways have also demonstrated efficacy against murine OS-derived cell cultures [10•].

Another pathway that has become increasingly understood through application of the murine OS models is the role of cAMP and parathyroid hormone (PTH)/parathyroid hormone–related protein (PTHrP) and their shared cell surface receptor (PTHR1) in OS biology. These pathways are intimately involved in osteoblast biology and therapeutics targeting this pathway in clinical use for the treatment of low bone mass. The clinically applied agent, PTH [1–7, 17–43], was associated with a high incidence of OS in long-term toxicology studies in rats [49, 50], a finding not reported to date in primate studies of the same agent [51]. OS cells expressed PTHR1 and make autocrine PTHrP, leading to constitutive stimulation of the cAMP/CREB1 pathway [28, 52]. The knock-down of either PTHrP, the most likely ligand for this pathway in OS, or the transcriptional effector of this pathway CREB1, was able to prevent the hyperproliferative transformation of osteoblasts following loss of p53 in vitro, and significantly reduce OS proliferation in vivo [53]. Further studies demonstrated that murine osteoblastic cells do not normally tolerate constitutively elevated levels of cAMP, but can if they become p53 deficient [54••]. This provided a nexus between the near obligate loss of p53 in OS and the ability of these cells to tolerate the sustained early activation of the cAMP pathway. Targeting this pathway with chemical inhibitors of the interaction of Creb1 and its cofactor CBP demonstrated that this is a potentially actionable therapeutic pathway in OS [54••].

Collectively, murine models have provided experimental confirmation of the relative importance of the different genes recurrently mutated in OS. The roles of a number of these still remain to be discerned, such as *ATRX* and *DLG2*, while the murine models have yet to provide further insight into why patients with *RECQL4* mutations are predisposed to OS. The models have proven to be a vital source of primary tumor

material with paired metastatic samples and cell cultures, enabling testing of a range of targeted agents and agnostic screening for new vulnerabilities. The studies, contributed to by many groups, have demonstrated that the murine models are an effective platform for understanding OS genetics and biology and for identification of new therapeutic options. The murine models are complementary to two additional preclinical translational platforms: patient-derived xenografts and the spontaneous OS that arises in domestic large breed dogs.

Patient-Derived Tumor Material and Xenografts

As a tumor type, OS is highlighted by complex genomic changes resulting in intra- and inter-tumor heterogeneity. Coupled with the lack of obviously therapeutically actionable targets, such as recurrently mutated kinases, the primarily pediatric cohort impacted by OS, and the relatively small number of overall patients, the introduction of new therapeutic strategies has been gradual. An increasingly favored approach for preclinical therapeutic testing is through patient-derived tumor xenografts (PDX). This approach takes tumor tissue obtained at the time of diagnosis from patients and engrafts the tumor material into immunodeficient mice. One key aspect of this approach is that the source is primary human material, alleviating the concerns that have mounted regarding the use of long-established OS-derived cell lines, which are subject to selection and drift over many generations in tissue culture [55•]. PDXs can be used to understand a tumor's proliferation, metastasis, and therapeutic response both in vitro and in vivo. This can be particularly useful in patients with heterogeneous cancers and a limited therapeutic spectrum allowing a more personalized clinical and therapeutic approach. Several groups have generated OS PDXs achieving high rates of engraftment and recapitulating the human tumor biology [11••, 56–58]. Furthermore, these models have also been used to determine pathways affected and to test new drugs. By implanting primary and metastatic OS tumors into immunodeficient mice, Loh and colleagues recapitulated the key radiographic and histologic features of the original patient tumors and then utilized these xenografted samples to perform drug screening studies using PDX-expanded and previously established OS cell lines [11••]. The authors found that combination of PI3K/MEK and PI3K/mTOR inhibitors was more effective against OS cells than the individual drugs, consistent with the results from the screening of murine models [11••]. In addition, Histone deacetylase (HDAC) and mTOR inhibitors showed greater efficacy when combined with standard-of-care drugs doxorubicin and gemcitabine [11••]. Such approaches demonstrate the power of primary human PDX models for prioritization of agents for clinical testing. As noted by the authors, these models require a high level of technical and experimental skill to generate reproducible in vivo xenografts, due to the preference for orthotopic intratibial/intrafemoral transplant of the PDX. A separate group reported the establishment of 15 PDXs and characterized them using WGS and RNA sequencing. They found that the primary tumors were relatively stable to the corresponding PDXs. They also tested several drugs that blocked the pathways of known amplified genes. This "genome-matched" therapeutic approach had near 60% tumor growth inhibition in vivo, particularly with tumors presenting *MYC*, *CDK4*, *AURKB*, and *AKT1/2* amplifications [59••]. The discoveries made using PDX models are promising; however, they are still not widely utilized at present due to their recent derivation and a number of additional factors such as difficulties/expense associated with the highly immunocompromised murine models required and the relative difficulty in obtaining primary OS samples. A generic challenge of in vivo PDX models, not limited to OS, is the study of immune-based therapies or tumor-host interactions due to the use of highly immunodeficient mice required as recipients. This can be addressed, to a limited extent currently, by humanization of the hematopoietic system of the murine recipients; however, this remains a challenge and needs to be considered. Extensive ongoing work optimizing the ability of immunodeficient mice to support full human hematopoiesis will eventually overcome this hurdle.

Preclinical Studies: Canine OS

Similar to humans, OS is the most common primary bone tumor in domestic dogs. However, unlike people where OS is a rare cancer type, OS is much more common in large and giant dog breeds. There are ~ 75,000 new OS cases diagnosed in pet dogs per year in the USA, which is approximately 75-fold higher than in humans [60]. Beyond the high incidence, rapid translation of results is further facilitated by the fact that the normal canine lifespan is very condensed compared with humans, so clinical trials are more rapidly completed in dogs, and involve the same surgical, radiation, and imaging equipment (e.g., CT, MRI, PET) utilized in human oncology centers. Historically, dogs have proven to be a high value OS translational model in the development of modern limb salvage surgery methods, but also more recently in the areas of novel radiation, medical, and immunotherapeutic treatments [61–63]. As more is learnt about canine OS on a genomic level, canine models will be increasingly used in clinical trials of novel drugs proposed for targeted treatment of OS. The mutational profile of human and canine OS is similar, with mutations in *p53*, *Rb1*, *PTEN*, *MYC*, and *mTOR* found in both species [64]. More recently, the tumor suppressor Disks Large Homolog 2 (*DLG2*) was confirmed as a relevant tumor suppressor in OS using comparative genomics of humans and dogs [65••], and the histone methyltransferase *SETD2* was

identified as a potential driver of the canine disease using exome sequencing [66••]. The expression of known OS protein markers was measured by immunohistochemistry in canine OS and showed a similar profile to human OS [67]. Comparisons have also been made between human and canine OS cell lines on a proteomic level, revealing shared expression of several proteins considered important for hallmarks such as metastasis [68].

The primary tumors that develop spontaneously in dogs are primarily found in the metaphysis of long bones, an anatomical location similar to a large proportion of human OS [69, 70]. This anatomic propensity is in contrast to initial murine models, where high rates of tumor formation occurred on the jaw and snout, which we now believe was the result of both the expression pattern of the *Osx1*-Cre transgene used and species differences in tooth development between mice and humans [28, 30]. The predominant metastatic profile of canine OS is to the lungs, similar to humans. In addition, because dogs develop the disease spontaneously, they can be used to study OS in the context of an intact immune system which cannot be done in PDX models [71]. Dogs also share a common environment with humans, unlike experimental models based in mice, which may be increasingly important as we further understand environmental and microbiome effects on carcinogenesis, tumor behavior, and therapeutic response.

Immunotherapy has become a breakthrough approach in cancer treatment. The power of canine OS for therapy discovery and testing is historically evidenced by the efficacy of non-specific immunostimulant muramyl tripeptide phosphatidylethanolamine (MTP-PE), now approved in Europe as mifamurtide for treatment of human OS [72, 73]. Trials using numerous immune and biotherapy approaches are underway in pet dogs with cancer, including canine OS treatment [63]. *HER2* has been studied as a relevant target in OS, including the canine disease, and a recombinant vaccine has been developed using an attenuated *Listeria monocytogenes* vector expressing this target. This vaccine completed phase I clinical trial in 18 canine OS cases, with promising clinical results, as well as evidence of T lymphocyte infiltration, and interferon gamma-specific responses [13]. This treatment has now gone on to evaluation following chemotherapy in the adjuvant setting in a larger canine OS trial. A recombinant *Salmonella* expressing IL-2 vaccine was also tested in the OS adjuvant setting with doxorubicin chemotherapy in 19 dogs, with promising clinical results in an admittedly small study. The safety endpoints were met, permitting further evaluation of this novel therapeutic approach in larger future trials [14]. Another biotherapy currently being investigated in canine OS is the use of viruses as vectors for agent delivery, or mediators of cancer cell destruction (oncolytic virotherapy). Delivery of a replication-deficient adenoviral vector for intra-tumor activation of Fas ligand (FasL) was tested in a phase I trial in 56 dogs with OS, followed by standard adjuvant chemotherapy. Dogs treated with the Ad-FasL that had evidence of inflammation and high lymphocyte infiltration had significantly improved survival compared with historical controls. This result was particularly strong in tumors that expressed low FasL, which may be a marker of eligibility for this type of treatment [15]. Oncolytic virotherapy has been investigated using recombinant vesicular stomatitis virus (VSV), engineered to express interferon beta and the sodium-iodide symporter (NIS). Following preclinical studies in mice and purpose-bred laboratory dogs, a small cohort of 8 dogs with naturally occurring cancers, including OS, were evaluated for dose feasibility, pharmacokinetics, and biological activity. High VSV levels were detected in the blood, and viral shedding was not detectable [16]. Further development of these and other immune/virotherapy approaches are currently proceeding in veterinary oncology, the results of which may inform the successful design and implementation of similar trials in humans.

Conclusions

While our understanding of genetics and mutational spectrum of OS has never been better, the introduction of new therapies and improvements in clinical outcomes has not yet leveraged this knowledge. The development and validation of multiple complementary preclinical models of OS is a substantial step forward. The future improvements of outcomes for patients with OS, and metastatic OS in particular, are able to make use of the strengths of each of these models and the rapid advances in technologies allowing genome-wide screening, sequencing, and immunotherapy. The near real-time monitoring of the in vivo evolution and behavior of OS in human patients is also now possible [74], and concurrent developments in tumor monitoring such as circulating tumor DNA will allow a detailed understanding of the complexities of therapy response. The potential for personalized medicine has been a goal of the genomic area, and such approach has begun to be implemented in the management of canine OS. In a multi-institutional effort, genomic profiling of individual dog OS cases and development of a personalized medicine algorithm (termed Pmed) concluded that such an approach is feasible, with good quality data obtained in an average turnaround time of 5 business days [75]. Another recent study employed a gene expression model to predict sensitivity to doxorubicin and platinum chemotherapy using a retrospective comparison of clinical outcome in canine OS cases. Longer disease-free intervals were seen in cases where the bioinformatic predictions matched the drug received [76]. Equally importantly given the rare status of human OS and the limited numbers of patients eligible for clinical trials is the capacity to leverage these preclinical models for prioritization of agents for testing. A good example is the testing of the multi-targeted kinase

inhibitors sunitinib and its sister compound toceranib, which demonstrated efficacy in murine models but this was not able to be demonstrated in larger scale canine clinical trials [77•, 78•, 79•, 80•]. The full utilization of these preclinical platforms offers a means to prioritize agents for clinical trials and to improve OS outcome across multiple species.

Funding Information Work in CRW's laboratory is supported by National Health and Medical Research Council Australia project grant (NHMRC; APP1102004); a Melbourne Research Scholarship (W.C-T. University of Melbourne); Victorian Cancer Agency Research Fellowship (C.R.W. MCRF15015); the Office of the Assistant Secretary of Defense for Health Affairs through the Peer Reviewed Cancer Research under Award No. W81XWH-15-1-0315 (to C.R.W.). Opinions, interpretations, conclusions and recommendations are those of the author and are not necessarily endorsed by the Department of Defense (USA); Work in CRW's laboratory was enabled in part by the Victorian State Government Operational Infrastructure Support (to St Vincent's Institute). Work in AJM's laboratory is supported by the OVC Pet Trust Foundation and is enabled by infrastructure support from the Canada Foundation for Innovation.

Compliance with Ethical Standards

Conflict of Interest Carl Walkley reports grants from National Health and Medical Research Council, Australia, Victorian Cancer Agency Research Fellowship, and Victorian State Government Operational Infrastructure Support, during the conduct of the study.

Wilson Castillo-Tandazo reports grants from Melbourne Research Scholarship, University of Melbourne, during the conduct of the study.

Anthony Mutsaers reports grants from OVC Pet Trust Foundation and the Canada Foundation for Innovation, during the conduct of the study.

Human and Animal Rights and Informed Consent This article does not contain any studies with human or animal subjects performed by any of the authors.

References

Papers of particular interest, published recently, have been highlighted as:
- • Of importance
- •• Of major importance

1. Ottaviani G, Jaffe N. The epidemiology of osteosarcoma. Cancer Treat Res. 2009;152:3–13.
2. Klein MJ, Siegal GP. Osteosarcoma: anatomic and histologic variants. Am J Clin Pathol. 2006;125(4):555–81.
3. Kansara M, Teng MW, Smyth MJ, Thomas DM. Translational biology of osteosarcoma. Nat Rev Cancer. 2014;14(11):722–35.
4. Janeway KA, Barkauskas DA, Krailo MD, Meyers PA, Schwartz CL, Ebb DH, et al. Outcome for adolescent and young adult patients with osteosarcoma: a report from the Children's Oncology Group. Cancer. 2012;118(18):4597–605.
5. Bielack SS, Hecker-Nolting S, Blattmann C, Kager L. Advances in the management of osteosarcoma. F1000Res. 2016;5:2767.
6. Perry JA, Kiezun A, Tonzi P, Van Allen EM, Carter SL, Baca SC, et al. Complementary genomic approaches highlight the PI3K/mTOR pathway as a common vulnerability in osteosarcoma. Proc Natl Acad Sci U S A. 2014;111(51):E5564–73.
7. Gupte A, Baker EK, Wan SS, Stewart E, Loh A, Shelat AA, et al. Systematic screening identifies dual PI3K and mTOR inhibition as a conserved therapeutic vulnerability in osteosarcoma. Clin Cancer Res. 2015;21(14):3216–29.
8. Lamoureux F, Baud'huin M, Rodriguez Calleja L, Jacques C, Berreur M, Redini F, et al. Selective inhibition of BET bromodomain epigenetic signalling interferes with the bone-associated tumour vicious cycle. Nat Commun. 2014;5:3511.
9. Baker EK, Taylor S, Gupte A, Sharp PP, Walia M, Walsh NC, et al. BET inhibitors induce apoptosis through a MYC independent mechanism and synergise with CDK inhibitors to kill osteosarcoma cells. Sci Rep. 2015;5:10120.
10.• Shekhar TM, Miles MA, Gupte A, Taylor S, Tascone B, Walkley CR, et al. IAP antagonists sensitize murine osteosarcoma cells to killing by TNFalpha. Oncotarget. 2016;7(23):33866–86. **Demonstrated that OS cells are sensitive to non-genotosic agents such as SMAC mimetics**.
11.•• Loh AHP, Stewart E, Bradley CL, Chen X, Daryani V, Stewart CF, et al. Combinatorial screening using orthotopic patient derived xenograft-expanded early phase cultures of osteosarcoma identify novel therapeutic drug combinations. Cancer Lett. 2019;442:262–70. **A "clinical trial" using human primary OS PDXs. Demonstrated efficacy of novel therapeutic combinations**.
12. Cain JE, McCaw A, Jayasekara WS, Rossello FJ, Marini KD, Irving AT, et al. Sustained low-dose treatment with the histone deacetylase inhibitor LBH589 induces terminal differentiation of osteosarcoma cells. Sarcoma. 2013;2013:608964.
13. Mason NJ, Gnanandarajah JS, Engiles JB, Gray F, Laughlin D, Gaurnier-Hausser A, et al. Immunotherapy with a HER2-targeting Listeria induces HER2-specific immunity and demonstrates potential therapeutic effects in a phase I trial in canine osteosarcoma. Clin Cancer Res. 2016;22(17):4380–90.
14. Fritz SE, Henson MS, Greengard E, Winter AL, Stuebner KM, Yoon U, et al. A phase I clinical study to evaluate safety of orally administered, genetically engineered *Salmonella enterica* serovar *Typhimurium* for canine osteosarcoma. Vet Med Sci. 2016;2(3):179–90.
15. Modiano JF, Bellgrau D, Cutter GR, Lana SE, Ehrhart NP, Ehrhart E, et al. Inflammation, apoptosis, and necrosis induced by neoadjuvant fas ligand gene therapy improves survival of dogs with spontaneous bone cancer. Mol Ther. 2012;20(12):2234–43.
16. Naik S, Galyon GD, Jenks NJ, Steele MB, Miller AC, Allstadt SD, et al. Comparative oncology evaluation of intravenous recombinant oncolytic vesicular stomatitis virus therapy in spontaneous canine Cancer. Mol Cancer Ther. 2018;17(1):316–26.
17. Chen X, Bahrami A, Pappo A, Easton J, Dalton J, Hedlund E, et al. Recurrent somatic structural variations contribute to tumorigenesis in pediatric osteosarcoma. Cell Rep. 2014;7(1):104–12.
18.•• Behjati S, Tarpey PS, Haase K, Ye H, Young MD, Alexandrov LB, et al. Recurrent mutation of IGF signalling genes and distinct patterns of genomic rearrangement in osteosarcoma. Nat Commun. 2017;8:15936. **Detailed analysis of the genomic landscape of > 100 human OS demonstrates distinct rearrangement types and a recurrent process characterized by chromothripsis and genomic amplification**.
19. Lorenz S, Baroy T, Sun J, Nome T, Vodak D, Bryne JC, et al. Unscrambling the genomic chaos of osteosarcoma reveals extensive transcript fusion, recurrent rearrangements and frequent novel TP53 aberrations. Oncotarget. 2016;7(5):5273–88.
20. Stephens PJ, Greenman CD, Fu B, Yang F, Bignell GR, Mudie LJ, et al. Massive genomic rearrangement acquired in a single catastrophic event during cancer development. Cell. 2011;144(1):27–40.

21. Kovac M, Blattmann C, Ribi S, Smida J, Mueller NS, Engert F, et al. Exome sequencing of osteosarcoma reveals mutation signatures reminiscent of BRCA deficiency. Nat Commun. 2015;6:8940.
22. Mirabello L, Yeager M, Mai PL, Gastier-Foster JM, Gorlick R, Khanna C, et al. Germline TP53 variants and susceptibility to osteosarcoma. J Natl Cancer Inst. 2015;107(7).
23. Joseph CG, Hwang H, Jiao Y, Wood LD, Kinde I, Wu J, et al. Exomic analysis of myxoid liposarcomas, synovial sarcomas, and osteosarcomas. Genes Chromosom Cancer. 2014;53(1):15–24.
24. Bousquet M, Noirot C, Accadbled F, Sales de gauzy J, Castex MP, Brousset P, et al. Whole-exome sequencing in osteosarcoma reveals important heterogeneity of genetic alterations. Ann Oncol. 2016;27(4):738–44.
25. Wang LL, Levy ML, Lewis RA, Chintagumpala MM, Lev D, Rogers M, et al. Clinical manifestations in a cohort of 41 Rothmund-Thomson syndrome patients. Am J Med Genet. 2001;102(1):11–7.
26. Berman SD, Calo E, Landman AS, Danielian PS, Miller ES, West JC, et al. Metastatic osteosarcoma induced by inactivation of Rb and p53 in the osteoblast lineage. Proc Natl Acad Sci U S A. 2008;105(33):11851–6.
27. Lin PP, Pandey MK, Jin F, Raymond AK, Akiyama H, Lozano G. Targeted mutation of p53 and Rb in mesenchymal cells of the limb bud produces sarcomas in mice. Carcinogenesis. 2009;30(10):1789–95.
28. Mutsaers AJ, Ng AJ, Baker EK, Russell MR, Chalk AM, Wall M, et al. Modeling distinct osteosarcoma subtypes in vivo using Cre:lox and lineage-restricted transgenic shRNA. Bone. 2013;55(1):166–78.
29. Quist T, Jin H, Zhu JF, Smith-Fry K, Capecchi MR, Jones KB. The impact of osteoblastic differentiation on osteosarcomagenesis in the mouse. Oncogene. 2015;34(32):4278–84.
30. Walkley CR, Qudsi R, Sankaran VG, Perry JA, Gostissa M, Roth SI, et al. Conditional mouse osteosarcoma, dependent on p53 loss and potentiated by loss of Rb, mimics the human disease. Genes Dev. 2008;22(12):1662–76.
31. Walia MK, Castillo-Tandazo W, Mutsaers AJ, Martin TJ, Walkley CR. Murine models of osteosarcoma: a piece of the translational puzzle. J Cell Biochem. 2018;119(6):4241–50.
32. Steele CD, Tarabichi M, Oukrif D, Webster AP, Ye H, Fittall M, et al. Undifferentiated sarcomas develop through distinct evolutionary pathways. Cancer Cell. 2019;35(3):441–56 **e8**.
33. Mutsaers AJ, Walkley CR. Cells of origin in osteosarcoma: mesenchymal stem cells or osteoblast committed cells? Bone. 2014;62:56–63.
34. Moriarity BS, Otto GM, Rahrmann EP, Rathe SK, Wolf NK, Weg MT, et al. A sleeping beauty forward genetic screen identifies new genes and pathways driving osteosarcoma development and metastasis. Nat Genet. 2015;47(6):615–24.
35. Pourebrahim R, Zhang Y, Liu B, Gao R, Xiong S, Lin PP, et al. Integrative genome analysis of somatic p53 mutant osteosarcomas identifies Ets2-dependent regulation of small nucleolar RNAs by mutant p53 protein. Genes Dev. 2017;31(18):1847–57.
36. Scott MC, Temiz NA, Sarver AE, LaRue RS, Rathe SK, Varshney J, et al. Comparative transcriptome analysis quantifies immune cell transcript levels, metastatic progression, and survival in osteosarcoma. Cancer Res. 2018;78(2):326–37.
37. Lu L, Harutyunyan K, Jin W, Wu J, Yang T, Chen Y, et al. RECQL4 regulates p53 function in vivo during Skeletogenesis. J Bone Miner Res. 2015;30(6):1077–89.
38. Ng AJ, Walia MK, Smeets MF, Mutsaers AJ, Sims NA, Purton LE, et al. The DNA helicase Recql4 is required for normal osteoblast expansion and osteosarcoma formation. PLoS Genet. 2015;11(4):e1005160.
39. Tao J, Jiang MM, Jiang L, Salvo JS, Zeng HC, Dawson B, et al. Notch activation as a driver of osteogenic sarcoma. Cancer Cell. 2014;26(3):390–401.
40. Dougall WC. RANKL signaling in bone physiology and cancer. Curr Opin Support Palliat Care. 2007;1(4):317–22.
41. Chen Y, Di Grappa MA, Molyneux SD, McKee TD, Waterhouse P, Penninger JM, et al. RANKL blockade prevents and treats aggressive osteosarcomas. Sci Transl Med. 2015;7(317):317ra197.
42. Walkley CR, Shea JM, Sims NA, Purton LE, Orkin SH. Rb regulates interactions between hematopoietic stem cells and their bone marrow microenvironment. Cell. 2007;129(6):1081–95.
43. Roberts CW, Leroux MM, Fleming MD, Orkin SH. Highly penetrant, rapid tumorigenesis through conditional inversion of the tumor suppressor gene Snf5. Cancer Cell. 2002;2(5):415–25.
44. Park D, Spencer JA, Koh BI, Kobayashi T, Fujisaki J, Clemens TL, et al. Endogenous bone marrow MSCs are dynamic, fate-restricted participants in bone maintenance and regeneration. Cell Stem Cell. 2012;10(3):259–72.
45. Kuhn R, Schwenk F, Aguet M, Rajewsky K. Inducible gene targeting in mice. Science. 1995;269(5229):1427–9.
46. Shaw RJ, Bardeesy N, Manning BD, Lopez L, Kosmatka M, DePinho RA, et al. The LKB1 tumor suppressor negatively regulates mTOR signaling. Cancer Cell. 2004;6(1):91–9.
47.• Han Y, Feng H, Sun J, Liang X, Wang Z, Xing W, et al. Lkb1 deletion in periosteal mesenchymal progenitors induces osteogenic tumors through mTORC1 activation. J Clin Invest. 2019;130. **Evidence that loss of Lkb1 can lead to osteosarcoma-like tumors in vivo.**
48. Presneau N, Duhamel LA, Ye H, Tirabosco R, Flanagan AM, Eskandarpour M. Post-translational regulation contributes to the loss of LKB1 expression through SIRT1 deacetylase in osteosarcomas. Br J Cancer. 2017;117(3):398–408.
49. Watanabe A, Yoneyama S, Nakajima M, Sato N, Takao-Kawabata R, Isogai Y, et al. Osteosarcoma in Sprague-Dawley rats after long-term treatment with teriparatide (human parathyroid hormone (1-34)). J Toxicol Sci. 2012;37(3):617–29.
50. Jolette J, Attalla B, Varela A, Long GG, Mellal N, Trimm S, et al. Comparing the incidence of bone tumors in rats chronically exposed to the selective PTH type 1 receptor agonist abaloparatide or PTH(1-34). Regul Toxicol Pharmacol. 2017;86:356–65.
51. Vahle JL, Zuehlke U, Schmidt A, Westmore M, Chen P, Sato M. Lack of bone neoplasms and persistence of bone efficacy in cynomolgus macaques after long-term treatment with teriparatide [rhPTH(1-34)]. J Bone Miner Res. 2008;23(12):2033–9.
52. Ho PW, Goradia A, Russell MR, Chalk AM, Milley KM, Baker EK, et al. Knockdown of PTHR1 in osteosarcoma cells decreases invasion and growth and increases tumor differentiation in vivo. Oncogene. 2015;34(22):2922–33.
53. Walia MK, Ho PM, Taylor S, Ng AJ, Gupte A, Chalk AM, et al. Activation of PTHrP-cAMP-CREB1 signaling following p53 loss is essential for osteosarcoma initiation and maintenance. Elife. 2016;5.
54.•• Walia MK, Taylor S, Ho PWM, Martin TJ, Walkley CR. Tolerance to sustained activation of the cAMP/Creb pathway activity in osteoblastic cells is enabled by loss of p53. Cell Death Dis. 2018;9(9):844. **Provided evidence linking tolerance to elevated cAMP in osteoblasts with loss of p53. Demonstrated that inhibition of the transcriptional activity of CREB1 could be effective in OS**.
55.• Stewart E, Federico S, Karlstrom A, Shelat A, Sablauer A, Pappo A, et al. The childhood solid tumor network: a new resource for the developmental biology and oncology research communities. Dev Biol. 2016;411(2):287–930. **Description of a significant human OS tumor resource**.
56. Blattmann C, Thiemann M, Stenzinger A, Roth EK, Dittmar A, Witt H, et al. Establishment of a patient-derived orthotopic osteosarcoma mouse model. J Transl Med. 2015;13:136.

57. Kito F, Oyama R, Sakumoto M, Takahashi M, Shiozawa K, Qiao Z, et al. Establishment and characterization of novel patient-derived osteosarcoma xenograft and cell line. In Vitro Cell Dev Biol Anim. 2018;54(7):528–36.
58. Meohas W, Granato RA, Guimaraes JAM, Dias RB, Fortuna-Costa A, Duarte MEL. Patient-derived xenografts as a preclinical model for bone sarcomas. Acta Ortop Bras. 2018;26(2):98–102.
59.•• Sayles LC, Breese MR, Koehne AL, Leung SG, Lee AG, Liu HY, et al. Genome-informed targeted therapy for osteosarcoma. Cancer Discov. 2019;9(1):46–63. **Describes a genome informed approach to selection of targeted agents for OS therapy**.
60. Schiffman JD, Breen M. Comparative oncology: what dogs and other species can teach us about humans with cancer. Philos Trans R Soc Lond B Biol Sci. 2015;370(1673).
61. Withrow SJ, Wilkins RM. Cross talk from pets to people: translational osteosarcoma treatments. ILAR J. 2010;51(3):208–13.
62. Fan TM, Selting KA. Exploring the potential utility of pet dogs with cancer for studying radiation-induced immunogenic cell death strategies. Front Oncol. 2018;8:680.
63. Tarone L, Barutello G, Iussich S, Giacobino D, Quaglino E, Buracco P, et al. Naturally occurring cancers in pet dogs as preclinical models for cancer immunotherapy. Cancer Immunol Immunother. 2019.
64. Fenger JM, London CA, Kisseberth WC. Canine osteosarcoma: a naturally occurring disease to inform pediatric oncology. ILAR J. 2014;55(1):69–85.
65.•• Shao YW, Wood GA, Lu J, Tang QL, Liu J, Molyneux S, et al. Cross-species genomics identifies DLG2 as a tumor suppressor in osteosarcoma. Oncogene. 2019;38(2):291–8. **Evidence of the utility of canine OS for target and genetic discovery**.
66.•• Sakthikumar S, Elvers I, Kim J, Arendt ML, Thomas R, Turner-Maier J, et al. SETD2 is recurrently mutated in whole-exome sequenced canine osteosarcoma. Cancer Res. 2018;78(13):3421–31. **Evidence of the utility of canine OS for target and genetic discovery**.
67. Al-Khan AA, Gunn HJ, Day MJ, Tayebi M, Ryan SD, Kuntz CA, et al. Immunohistochemical validation of spontaneously arising canine osteosarcoma as a model for human osteosarcoma. J Comp Pathol. 2017;157(4):256–65.
68. Roy J, Wycislo KL, Pondenis H, Fan TM, Das A. Comparative proteomic investigation of metastatic and non-metastatic osteosarcoma cells of human and canine origin. PLoS One. 2017;12(9):e0183930.
69. Heyman SJ, Diefenderfer DL, Goldschmidt MH, Newton CD. Canine axial skeletal osteosarcoma. A retrospective study of 116 cases (1986 to 1989). Vet Surg. 1992;21(4):304–10.
70. Mirabello L, Troisi RJ, Savage SA. Osteosarcoma incidence and survival rates from 1973 to 2004: data from the surveillance, epidemiology, and end results program. Cancer. 2009;115(7):1531–43.
71. Wycislo KL, Fan TM. The immunotherapy of canine osteosarcoma: a historical and systematic review. J Vet Intern Med. 2015;29(3):759–69.
72. MacEwen EG, Kurzman ID, Rosenthal RC, Smith BW, Manley PA, Roush JK, et al. Therapy for osteosarcoma in dogs with intravenous injection of liposome-encapsulated muramyl tripeptide. J Natl Cancer Inst. 1989;81(12):935–8.
73. Meyers PA, Schwartz CL, Krailo MD, Healey JH, Bernstein ML, Betcher D, et al. Osteosarcoma: the addition of muramyl tripeptide to chemotherapy improves overall survival–a report from the Children's Oncology Group. J Clin Oncol. 2008;26(4):633–8.
74. Brady SW, Ma X, Bahrami A, Satas G, Wu G, Newman S, et al. The clonal evolution of metastatic osteosarcoma as shaped by cisplatin treatment. Mol Cancer Res. 2019;17(4):895–906.
75. Monks NR, Cherba DM, Kamerling SG, Simpson H, Rusk AW, Carter D, et al. A multi-site feasibility study for personalized medicine in canines with osteosarcoma. J Transl Med. 2013;11:158.
76. Fowles JS, Brown KC, Hess AM, Duval DL, Gustafson DL. Intra- and interspecies gene expression models for predicting drug response in canine osteosarcoma. BMC Bioinformatics. 2016;17:93.
77.• Kumar RM, Arlt MJ, Kuzmanov A, Born W, Fuchs B. Sunitinib malate (SU-11248) reduces tumour burden and lung metastasis in an intratibial human xenograft osteosarcoma mouse model. Am J Cancer Res. 2015;5(7):2156–68.
78.• Kim C, Matsuyama A, Mutsaers AJ, Woods JP. Retrospective evaluation of toceranib (palladia) treatment for canine metastatic appendicular osteosarcoma. Can Vet J. 2017;58(10):1059–64.
79.• Laver T, London CA, Vail DM, Biller BJ, Coy J, Thamm DH. Prospective evaluation of toceranib phosphate in metastatic canine osteosarcoma. Vet Comp Oncol. 2018;16(1):E23–E9.
80.• London CA, Gardner HL, Mathie T, Stingle N, Portela R, Pennell ML, et al. Impact of toceranib/piroxicam/cyclophosphamide maintenance therapy on outcome of dogs with appendicular osteosarcoma following amputation and carboplatin chemotherapy: a multi-institutional study. PLoS One. 2015;10(4):e0124889. **Collectively, reference entries [77–80] demonstrate the strength of combining mutliple species to test new agents prior to prioritisation for human clinial trial**.

Publisher's Note Springer Nature remains neutral with regard to jurisdictional claims in published maps and institutional affiliations.

ELSEVIER

Experimental Hematology

Experimental Hematology 2020;82:1–7

BRIEF COMMUNICATION

Effects of chemotherapy agents used to treat pediatric acute lymphoblastic leukemia patients on bone parameters and longitudinal growth of juvenile mice

Lenny Straszkowski[a], Tanja Jovic[a], Wilson Castillo-Tandazo[a,b], David S. Ritchie[b,c,d,e], and Louise E. Purton[a,b]

[a]*St. Vincent's Institute of Medical Research, Fitzroy, VIC, Australia;* [b]*Department of Medicine, University of Melbourne, Parkville, VIC, Australia;* [c]*Peter MacCallum Cancer Centre, Parkville, VIC, Australia;* [d]*Victorian Comprehensive Cancer Centre, Parkville, VIC, Australia;* [e]*Royal Melbourne Hospital, Parkville, VIC, Australia*

(Received 13 November 2019; revised 20 January 2020; accepted 21 January 2020)

Acute lymphoblastic leukemia (ALL) is the most common childhood cancer. Therapies for pediatric ALL have improved such that more than 80% of patients survive to 5 years post-therapy, and most survive to adulthood. These ALL patients experience long-term side effects that permanently affect their quality of life, with bone loss and reduced longitudinal growth being the most common skeletal complications. To determine the effects of the chemotherapeutic agents used in ALL induction therapy on bone density and longitudinal growth in mice, we treated juvenile mice with doxorubicin, dexamethasone, vincristine, L-asparaginase, or combination therapy. At adulthood, mice were culled and bones collected and scanned by micro-computed tomography (micro-CT). Mice that received doxorubicin and combination therapy exhibited reduced longitudinal growth and significant reductions in trabecular bone volume, trabecular thickness, and trabecular number, with increased trabecular separation. Mean cortical thickness, cortical area, marrow area, endocortical perimeter, and polar moment of inertia were significantly reduced by doxorubicin and combination therapy. Vincristine treatment significantly decreased trabecular bone volume, trabecular number, and increased trabecular separation but had no effects on cortical bone. Dexamethasone treatment increased trabecular bone separation, cortical marrow area, and cortical bone periosteal perimeter. Mice treated with L-asparaginase did not have any bone phenotypes. In conclusion, these data indicate that the majority of the chemotherapy agents used in induction therapy for pediatric ALL have long-term effects on bone in mice. A single dose of doxorubicin in juvenile mice was sufficient to cause the majority of the bone phenotypes, with combination therapy intensifying these effects. **© 2020 ISEH – Society for Hematology and Stem Cells. Published by Elsevier Inc. All rights reserved.**

The most common form of childhood malignancy is acute lymphoblastic leukemia (ALL) [1]. The discovery of effective therapeutic options has improved its cure rate dramatically [2]; however, patients experience significant late complications across multiple systems, including bone [3–5]. A study found that many patients had decreased longitudinal bone growth (short stature) at adulthood [6]. Furthermore, decreased bone mineral density (BMD) is another common musculoskeletal side effect, with 39% of patients experiencing fractures throughout the course of their treatment, and approximately half of these not initiated by trauma [1,4,7,8]. Although irradiation was considered to be a major contributor to these bone complications, similar complications have been reported to occur in long-term survivors who were not treated with irradiation [9,10].

Offprint requests to: Louise E. Purton, St. Vincent's Institute of Medical Research, 9 Princes Street, Fitzroy, VIC 3065, Australia; E-mail: lpurton@svi.edu.au

0301-472X/© 2020 ISEH – Society for Hematology and Stem Cells. Published by Elsevier Inc. All rights reserved.
https://doi.org/10.1016/j.exphem.2020.01.010

The cause of the bone loss in pediatric ALL patients remains unclear, although it has been speculated that it is due to the leukemia itself or to the corticosteroids that are used to reduce inflammation in the patients [11]. A study that assessed BMD of ALL patients at diagnosis revealed a decrease in BMD in the lumbar spine region accompanied by reduced bone formation markers. However, when patients started receiving treatment, the total BMD decreased significantly and bone resorption markers increased, increasing the fracture rate by six times in ALL patients compared with healthy controls [2].

There is a discrepancy in whether the bone loss in ALL patients is due to the therapy or the disease itself [11]. Recent studies have reported that the leukemia significantly contributes to the bone loss. A morphometry study of trephine bone marrow sections obtained from ALL patients at diagnosis revealed significantly reduced trabecular bone, accompanied by reduced numbers of osteoblasts and osteoclasts [12]. A recent study in mice found that T-cell ALL destroyed mature osteoblasts [13]. In addition, another study in mice found that pre-B-cell ALL caused loss of osteoblasts and a significant reduction in bone, because of, at least in part, increased osteoclast activity [14]. In this study, we investigated the bone phenotypes in mice treated with doxorubicin, L-asparaginase, vincristine, and dexamethasone, because all of these chemotherapy agents are used in induction therapies for pediatric ALL patients [9].

Methods

Mice

All experiments were approved by the St. Vincent's Health (Melbourne) Animal Ethics Committee and conducted in strict compliance with the regulatory standards of the Australian Code of Practice for the Care and Use of Animals for Scientific Purposes. Four-week-old C57BL/6 male mice were treated with 10 mg/kg doxorubicin, given once intravenously on day 1 of treatment, or the following agents administered 5 days per week for 2 weeks intraperitoneally: 5 mg/kg dexamethasone, 0.15 mg/kg vincristine, or 1000 IU/kg L-asparaginase (all chemotherapy agents from Sigma-Aldrich, St. Louis, MO) [15,16]. For combination therapy, mice were treated with all chemotherapeutic agents as specified above. Control mice were injected with saline at all time points. The mice were culled at 12 weeks of age via CO_2 inhalation.

Growth plate measurements

The tibias were harvested, cleaned of all tissue, fixed in 2% paraformaldehyde (PFA, Sigma) at 4°C overnight, and then decalcified by replacing the EDTA solution twice over 2 weeks. Samples were processed and embedded in paraffin. The growth plate width was assessed on 5 μm sections stained with Safranin-O and Fast Green as previously described [17].

Micro-computed tomography

The femurs were harvested and cleaned of all tissue, fixed in 2% PFA at 4°C overnight, and stored in 70% ethanol until analysis. The femurs were scanned at an x-ray potential of 50 kV, with a current of 100 μA and at an isotropic voxel size of 9 μm using the Skyscan1076 (Bruker-MicroCT, Kontich, Belgium), in accordance with standard guidelines [18]. NRecon software (Version 1.6.8, SkyScan) was used with the following parameters to reconstruct serial tomograms: a beam hardening correction of 35%, ring artifact reduction of 6, and smoothing of 1. A trabecular region 2.1 mm distal from the femur apex extending 2 mm was analyzed in CTAn (Version 1.12.0, SkyScan). An adaptive threshold of 40 −255 was used to demarcate the trabecular bone from the endocortical border.

Statistics

All data were analyzed using one-way analysis of variance with Dunnett's multiple comparisons (GraphPad Prism 8.0.2).

Results

Four-week-old C57BL/6 male mice were treated with 10mg/kg doxorubicin, given once intravenously on day 1 of treatment, or the following administered 5 days per week for 2 weeks intraperitoneally: 5 mg/kg dexamethasone, 0.15 mg/kg vincristine, or 1000 IU/kg L-asparaginase. Mice receiving combination therapy were treated with all drugs. Controls were treated with saline. Bone parameters were assessed when mice reached 12 weeks of age.

The effects of individual chemotherapeutic agents and combination therapy on the femoral length of the mice were determined by micro-computed tomography (micro-CT) at adulthood (12 weeks of age). A single dose of doxorubicin significantly decreased the femoral length of the mice compared with saline-treated controls and all other chemotherapeutic agents, and this was further reduced by combination therapy (Figure 1A). Interestingly, we found no significant effects between the growth plates of mice treated with different drugs and saline-treated controls, although dexamethasone treatment caused an increase in the tibial growth plate compared with doxorubicin-treated mice (Figure 1B).

In accordance with our results, previous studies have reported reduced longitudinal bone growth in pediatric ALL survivors [19,20], which was thought to result from the effects of glucocorticoids or irradiation [21–23]. Our results suggest that doxorubicin contributes to the reduced longitudinal growth observed in adult survivors of ALL and that other drugs synergize to further affect this phenotype. Furthermore, our data suggest that these effects are independent of changes to the growth plate.

The effects of the chemotherapy agents on bone parameters were assessed by micro-CT (Figure 2A). A single dose of doxorubicin caused significant reductions in trabecular bone volume, trabecular bone number, and trabecular thickness, which were further reduced by combination therapy (Figure 2B–D). Doxorubicin,

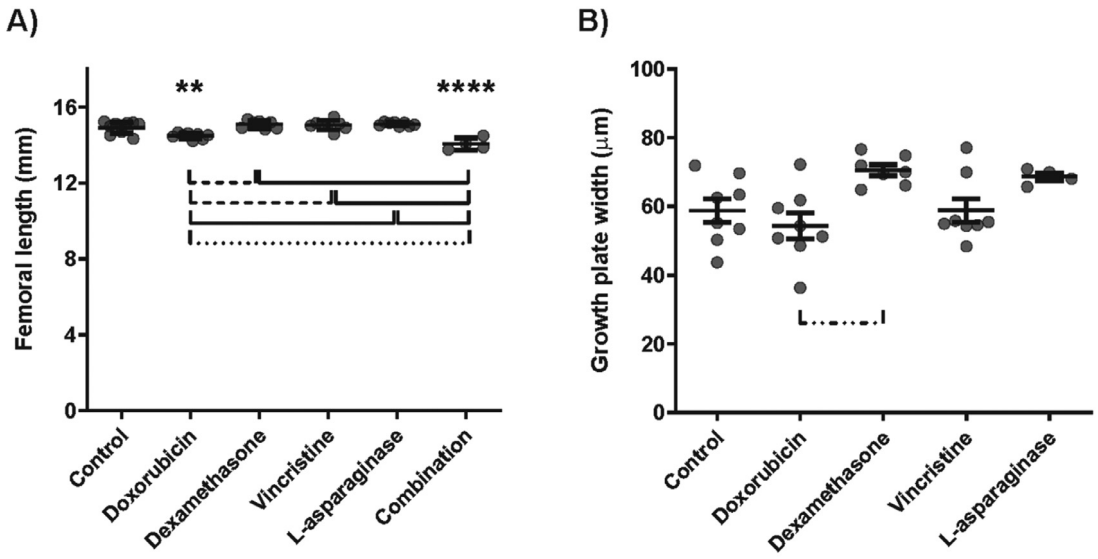

Figure 1. Effects of single chemotherapy agents and combination therapy on longitudinal growth. The data show the femoral length and growth plate width. Given here are individual mouse values with bars representing the mean ± SD ($n = 4–12$). $^{**}p < 0.01$, $^{****}p < 0.0001$ compared with saline-treated controls. Significant differences between the different chemotherapy treatments are represented by horizontal bars: ⌙⋯⌝, $p < 0.05$; ⌙-⋯-⌝, $p < 0.01$; ⌙--⌝, $p < 0.001$; ⌙—⌝, $p < 0.0001$.

dexamethasone, and vincristine all individually increased trabecular bone separation, which was further increased by combination therapy (Figure 2E). Vincristine treatment also caused significantly decreased trabecular bone volume (Figure 2B) and trabecular number (Figure 2C). L-Asparaginase treatment had no effects.

Trabecular bone forms by endochondral ossification, which occurs during embryogenesis [24]. Trabecular bone is an active site of bone remodeling, which involves a coupling between osteoclasts and osteoblasts. We previously reported that single doses of other chemotherapy agents or whole-body irradiation cause significant, irreversible trabecular bone loss in wild-type mice [25]. This was due to inflammation occurring early posttherapy, causing a transient increase in osteoclastogenesis and subsequent bone loss [25]. A single dose of the bisphosphonate zoledronic acid, administered before therapy, was sufficient to prevent the trabecular bone loss [25]. Trabecular bone loss occurs in ALL patients within the first month of chemotherapy [9], accompanied by increased markers of bone resorption and vitamin D deficiency [9]. A subsequent report indicated that vitamin D deficiency did not contribute to the bone loss [26].

A single dose of doxorubicin significantly decreased cortical thickness, cortical marrow area, cortical area, endocortical perimeter, periosteal perimeter, and mean polar moment of inertia compared with saline-treated controls and mice treated with other single chemotherapeutic agents (Figure 3A–G). Collectively, these changes contributed to the increased fragility of the bone. Combination therapy further reduced all of these parameters with the exception of cortical marrow area (Figure 3A–G). Interestingly, dexamethasone treatment significantly increased the marrow area and the periosteal perimeter in comparison with all other therapies and saline treatment (Figure 3C,F), indicating that the bones were wider. L-Asparaginase treatment had no effects.

Cortical bone formation occurs in early postnatal life and involves the coalescence of trabecular bone at the metaphyseal cortex (a process called corticalization) [27]. This process is most active during bone growth and is the last stage of longitudinal bone growth [27]. The significant reductions in cortical bone observed in mice treated with doxorubicin or combination therapy (Figure 3A–G) were consistent with reduced femoral length (Figure 1A). Given that effects on growth plate width were not detected (Figure 1B), our data suggest that the reduced longitudinal growth of the mice was caused by reduced bone corticalization. These results are consistent with other findings that showed that reduced longitudinal growth observed in mice that did not have growth plate abnormalities associated with defective osteoblasts [27]. Although we did not investigate osteoblast function here, it is noteworthy that doxorubicin has been reported to decrease osteoblast survival, differentiation, and trabecular bone volume in mice when administered once weekly for 4 weeks [28].

Our study was conducted on healthy juvenile mice, whereas it has been reported that patients diagnosed with ALL have a decreased bone mineral density before commencing treatment [2]. Recent studies in mice have confirmed that ALL has detrimental effects on osteoblasts

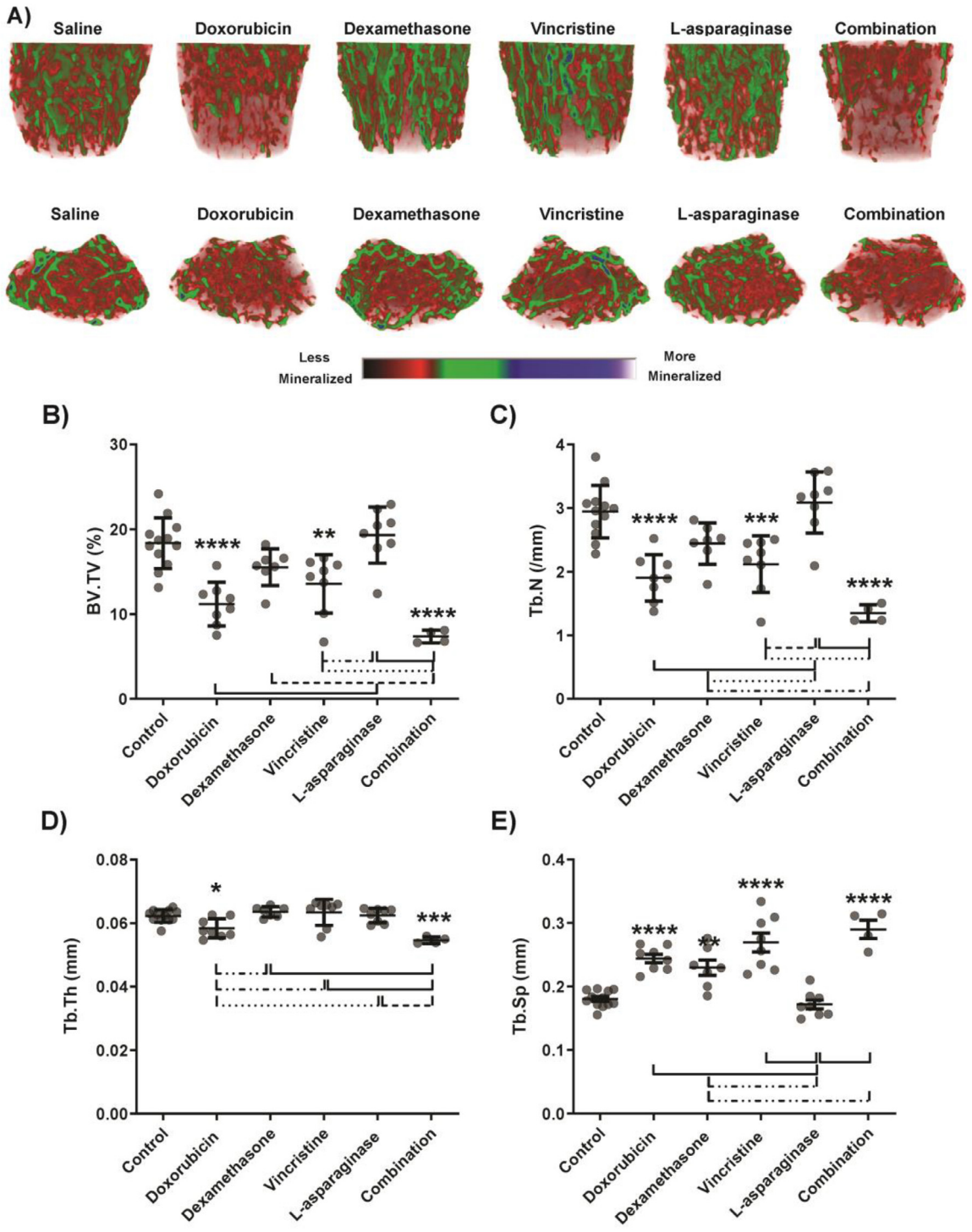

Figure 2. Effects of individual chemotherapy agents and combination therapy on trabecular bone parameters of the femurs of adult mice. (A) Representative micro-computed tomography images of trabecular bone regions: the coronal plane (top) and axial plane (bottom) of femurs treated with saline, doxorubicin, dexamethasone, vincristine, L-asparaginase, and combination therapy. (B) Trabecular bone volume (BV/TV). (C) Trabecular number (Tb.N). (D) Trabecular thickness (Tb.Th). (E) Trabecular separation (Tb.Sp). Shown are individual mouse values with bars representing the mean ± SD ($n = 4–12$).Significant differences between the different chemotherapy treatments are represented by horizontal bars: ⌊.....⌋, $p < 0.05$; ⌊.-.-.⌋, $p < 0.01$; ⌊-----⌋, $p < 0.001$; ⌊——⌋, $p < 0.0001$.

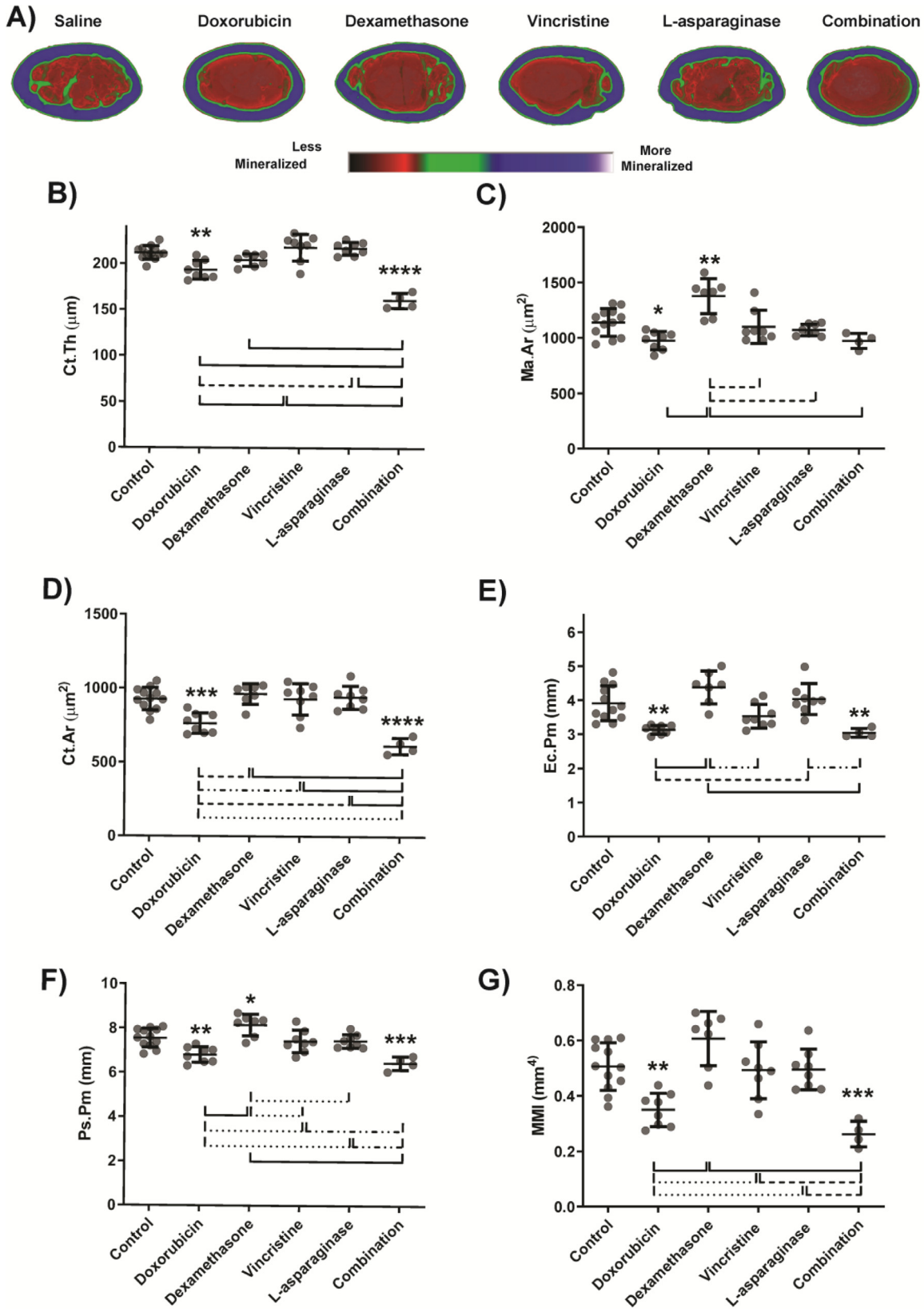

Figure 3. Effects of individual chemotherapy agents and combination therapy on the cortical bone parameters of the femurs of adult mice. (A) Representative micro-computed tomography axial plane images of the cortical bone of femurs treated with saline, doxorubicin, dexamethasone, vincristine, L-asparaginase, and combination therapy. (B) Cortical thickness (Ct.Th). (C) Marrow area (Ma.Ar). (D) Cortical area (Ct.Ar). (E) Endocortical perimeter (EC.Pm). (F) Periosteal perimeter (Ps.Pm). (G) Mean polar moment of inertia (MMI). Shown are individual mouse values with bars representing the mean ± SD ($n = 4–12$). Significant differences between the different chemotherapy treatments are represented by horizontal bars: ⌊.....⌋, $p < 0.05$; ⌊.-.-.⌋, $p < 0.01$; ⌊-----⌋, $p < 0.001$; ⌊——⌋, $p < 0.0001$.

[13,14] and trabecular bone parameters [14]. The latter study also reported that the bone loss was associated with increased osteoclasts and that bisphosphonate treatment reduced tumor burden and improved bone mass and survival of the mice [14]. To date, few clinical trials have investigated the effectiveness of bisphosphonates in improving bone mass in children with ALL, and further trials are warranted [29].

Collectively, our data reveal that chemotherapy may contribute to the bone phenotypes commonly observed in long-term pediatric ALL survivors. With the exception of L-asparaginase, all chemotherapy agents used in the treatment of pediatric ALL cause significant late effects in wild-type mice. The most severe bone phenotypes were observed after a single dose of doxorubicin or combination therapy. Our findings may also be relevant to other types of cancer that are treated with these chemotherapy agents.

Acknowledgments

This research was supported by a grant from the National Health and Medical Research Council of Australia (GNT1006485 to LEP) and by the Operational Infrastructure Support Program from the Victorian Government (to St. Vincent's Institute). WCT was supported by a Melbourne Research Scholarship awarded by the University of Melbourne. We thank the staff at St. Vincent's BioResource Centre for caring for the animals used in this study.

References

1. Brennan BM, Rahim A, Adams JA, Eden OB, Shalet SM. Reduced bone mineral density in young adults following cure of acute lymphoblastic leukaemia in childhood. Br J Cancer. 1999;79:1859–1863.
2. van der Sluis IM, van den Heuvel-Eibrink MM, Hahlen K, Krenning EP, de Muinck Keizer-Schrama SM. Altered bone mineral density and body composition, and increased fracture risk in childhood acute lymphoblastic leukemia. J Pediatr. 2002;141:204–210.
3. Schmiegelow K, Muller K, Mogensen SS, et al. Non-infectious chemotherapy-associated acute toxicities during childhood acute lymphoblastic leukemia therapy. F1000Res. 2017;6:444.
4. Arikoski P, Komulainen J, Voutilainen R, et al. Reduced bone mineral density in long-term survivors of childhood acute lymphoblastic leukemia. J Pediatr Hematol Oncol. 1998;20:234–240.
5. Veerman AJ, Hahlen K, Kamps WA, et al. High cure rate with a moderately intensive treatment regimen in non-high-risk childhood acute lymphoblastic leukemia: Results of protocol ALL VI from the Dutch Childhood Leukemia Study Group. J Clin Oncol. 1996;14:911–918.
6. Vandecruys E, Dhooge C, Craen M, Benoit Y, De Schepper J. Longitudinal linear growth and final height is impaired in childhood acute lymphoblastic leukemia survivors after treatment without cranial irradiation. J Pediatr. 2013;163:268–273.
7. Rohani F, Arjmandi Rafsanjani K, Bahoush G, Sabzehparvar M, Ahmadi M. Bone mineral density in survivors of childhood acute lymphoblastic leukemia. Asian Pac J Cancer Prev. 2017;18:535–540.
8. Haddy TB, Mosher RB, Reaman GH. Osteoporosis in survivors of acute lymphoblastic leukemia. Oncologist. 2001;6:278–285.
9. Orgel E, Mueske NM, Wren TA, et al. Early injury to cortical and cancellous bone from induction chemotherapy for adolescents and young adults treated for acute lymphoblastic leukemia. Bone. 2016;85:131–137.
10. Browne EK, Zhou Y, Chemaitilly W, et al. Changes in body mass index, height, and weight in children during and after therapy for acute lymphoblastic leukemia. Cancer. 2018;124:4248–4259.
11. Davies JH, Evans BA, Jenney ME, Gregory JW. Skeletal morbidity in childhood acute lymphoblastic leukaemia. Clin Endocrinol (Oxf). 2005;63:1–9.
12. Nguyen TV, Melville A, Nath S, et al. Bone marrow recovery by morphometry during induction chemotherapy for acute lymphoblastic leukemia in children. PLoS One. 2015;10:e0126233.
13. Hawkins ED, Duarte D, Akinduro O, et al. T-cell acute leukaemia exhibits dynamic interactions with bone marrow microenvironments. Nature. 2016;538:518–522.
14. Cheung LC, Tickner J, Hughes AM, et al. New therapeutic opportunities from dissecting the pre-B leukemia bone marrow microenvironment. Leukemia. 2018;32:2326–2338.
15. Kang MH, Kang YH, Szymanska B, et al. Activity of vincristine, L-ASP, and dexamethasone against acute lymphoblastic leukemia is enhanced by the BH3-mimetic ABT-737 in vitro and in vivo. Blood. 2007;110:2057–2066.
16. Jansson J, Hsu YC, Kuzin II, Campbell A, Mullen CA. Acute lymphoblastic leukemia cells that survive combination chemotherapy in vivo remain sensitive to allogeneic immune effects. Leuk Res. 2011;35:800–807.
17. Green AC, Rudolph-Stringer V, Straszkowski L, et al. Retinoic acid receptor gamma activity in mesenchymal stem cells regulates endochondral bone, angiogenesis, and B lymphopoiesis. J Bone Miner Res. 2018;33:2202–2213.
18. Bouxsein ML, Boyd SK, Christiansen BA, Guldberg RE, Jepsen KJ, Muller R. Guidelines for assessment of bone microstructure in rodents using micro-computed tomography. J Bone Miner Res. 2010;25:1468–1486.
19. van der Sluis IM, van den Heuvel-Eibrink MM, Hahlen K, Krenning EP, de Muinck Keizer-Schrama SM. Bone mineral density, body composition, and height in long-term survivors of acute lymphoblastic leukemia in childhood. Med Pediatr Oncol. 2000;35:415–420.
20. Chow EJ, Friedman DL, Yasui Y, et al. Decreased adult height in survivors of childhood acute lymphoblastic leukemia: a report from the Childhood Cancer Survivor Study. J Pediatr. 2007;150:370–375.
21. Chrysis D, Ritzen EM, Savendahl L. Growth retardation induced by dexamethasone is associated with increased apoptosis of the growth plate chondrocytes. J Endocrinol. 2003;176:331–337.
22. Lethaby C, Wiernikowski J, Sala A, Naronha M, Webber C, Barr RD. Bisphosphonate therapy for reduced bone mineral density during treatment of acute lymphoblastic leukemia in childhood and adolescence: a report of preliminary experience. J Pediatr Hematol Oncol. 2007;29:613–616.
23. Mushtaq T, Ahmed SF. The impact of corticosteroids on growth and bone health. Arch Dis Child. 2002;87:93–96.
24. Maes C. Signaling pathways effecting crosstalk between cartilage and adjacent tissues: Seminars in cell and developmental biology: The biology and pathology of cartilage. Semin Cell Dev Biol. 2017;62:16–33.
25. Quach JM, Askmyr M, Jovic T, et al. Myelosuppressive therapies significantly increase pro-inflammatory cytokines and directly cause bone loss. J Bone Miner Res. 2015;30:886–897.

26. Orgel E, Mueske NM, Sposto R, et al. A randomized controlled trial testing an adherence-optimized Vitamin D regimen to mitigate bone change in adolescents being treated for acute lymphoblastic leukemia. Leuk Lymphoma. 2017;58:2370–2378.
27. Moon YJ, Yun CY, Choi H, Kim JR, Park BH, Cho ES. Osterix regulates corticalization for longitudinal bone growth via integrin beta3 expression. Exp Mol Med. 2018;50:80.
28. Rana T, Chakrabarti A, Freeman M, Biswas S. Doxorubicin-mediated bone loss in breast cancer bone metastases is driven by an interplay between oxidative stress and induction of TGFbeta. PLoS One. 2013;8:e78043.
29. Harris AM, Lee AR, Wong SC. Systematic review of the effects of bisphosphonates on bone density and fracture incidence in childhood acute lymphoblastic leukaemia. Osteoporos Int. 2020;31:59–66.

C

LIST OF AWARDS ARISING DURING THIS CANDIDATURE

1. *Young Investigator Award*; American Society of Bone and Mineral Research (ASBMR) 2019 Annual Meeting. Orlando, USA. The award recognises young investigators who submit top ranking abstracts to an ASBMR Meeting.

2. *International Student of the Year – Research*; Victorian International Education Awards 2018. Award given to international postgraduate students who have demonstrated outstanding academic achievement and have contributed to the internationalisation of the institution and to the Victorian community.

3. *"International Meeting on RECQ Helicases & Related Diseases" Travel Award.* Tokyo, Japan. Award given to the best abstract submission.

4. *SVI Top-Up Award*; St. Vincent's Institute of Medical Research. Award given to commencing PhD students with the most competitive CVs.

5. *Melbourne Research Scholarship*; University of Melbourne. Scholarship given to high achieving international students undertaking a Doctoral degree.

D

LIST OF MEETINGS ATTENDED TO PRESENT RESEARCH ARISING FROM THIS THESIS

1. *American Society of Bone and Mineral Research (ASBMR) 2019 Annual Meeting*. Orlando, USA. Oral Poster Presentation and Plenary Poster Presentation.

2. *Victorian Comprehensive Cancer Centre (VCCC) Research Conference 2019*. Melbourne, Australia. Poster Presentation.

3. *International Meeting on RECQ Helicases and Related Diseases 2018*. Tokyo, Japan. Poster and Oral Presentation.

BIBLIOGRAPHY

[1] Wu Y. Unwinding and rewinding: double faces of helicase? J Nucleic Acids. 2012;2012:140601.

[2] Mojumdar A. Mutations in conserved functional domains of human RecQ helicases are associated with diseases and cancer: A review. Biophysical Chemistry. 2020;265:106433.

[3] Gorbalenya AE, Koonin EV. Helicases: amino acid sequence comparisons and structure-function relationships. Current Opinion in Structural Biology. 1993;3(3):419–29.

[4] Brosh RM, Matson SW. History of DNA Helicases. Genes. 2020;11(3):255.

[5] Singleton MR, Dillingham MS, Wigley DB. Structure and mechanism of helicases and nucleic acid translocases. Annu Rev Biochem. 2007;76:23–50.

[6] Story RM, Weber IT, Steitz TA. The structure of the E. coli recA protein monomer and polymer. Nature. 1992;355(6358):318–25.

[7] Scheffzek K, Ahmadian MR, Kabsch W, Wiesmuller L, Lautwein A, Schmitz F, et al. The Ras-RasGAP complex: structural basis for GTPase activation and its loss in oncogenic Ras mutants. Science. 1997;277(5324):333–8.

[8] Walker JE, Saraste M, Runswick MJ, Gay NJ. Distantly related sequences in the alpha- and beta-subunits of ATP synthase, myosin, kinases and other ATP-requiring enzymes and a common nucleotide binding fold. EMBO J. 1982;1(8):945–51.

[9] Trakselis MA. Structural Mechanisms of Hexameric Helicase Loading, Assembly, and Unwinding. F1000Res. 2016;5.

[10] Byrd AK, Raney KD. Superfamily 2 helicases. Front Biosci (Landmark Ed). 2012;17:2070–88.

[11] Nakayama H, Nakayama K, Nakayama R, Irino N, Nakayama Y, Hanawalt PC. Isolation and genetic characterization of a thymineless death-resistant mutant of Escherichia coli K12: identification of a new mutation (recQ1) that blocks the RecF recombination pathway. Mol Gen Genet. 1984;195(3):474–80.

[12] Gangloff S, McDonald JP, Bendixen C, Arthur L, Rothstein R. The yeast type I topoisomerase Top3 interacts with Sgs1, a DNA helicase homolog: a potential eukaryotic reverse gyrase. Mol Cell Biol. 1994;14(12):8391–8.

[13] Gupta SV, Schmidt KH. Maintenance of Yeast Genome Integrity by RecQ Family DNA Helicases. Genes (Basel). 2020;11(2):205.

[14] Murray JM, Lindsay HD, Munday CA, Carr AM. Role of Schizosaccharomyces pombe RecQ homolog, recombination, and checkpoint genes in UV damage tolerance. Mol Cell Biol. 1997;17(12):6868–75.

[15] Hickson ID. RecQ helicases: caretakers of the genome. Nat Rev Cancer. 2003;3(3):169–78.

[16] Vindigni A, Hickson ID. RecQ helicases: multiple structures for multiple functions? HFSP J. 2009;3(3):153–64.

[17] Cui S, Arosio D, Doherty KM, Brosh J R M, Falaschi A, Vindigni A. Analysis of the unwinding activity of the dimeric RECQ1 helicase in the presence of human replication protein A. Nucleic Acids Res. 2004;32(7):2158–70.

[18] Yu CE, Oshima J, Wijsman EM, Nakura J, Miki T, Piussan C, et al. Mutations in the consensus helicase domains of the Werner syndrome gene. Werner's Syndrome Collaborative Group. Am J Hum Genet. 1997;60(2):330–41.

[19] Lohman TM, Bjornson KP. Mechanisms of helicase-catalyzed DNA unwinding. Annu Rev Biochem. 1996;65:169–214.

[20] Iyer LM, Leipe DD, Koonin EV, Aravind L. Evolutionary history and higher order classification of AAA+ ATPases. J Struct Biol. 2004;146(1-2):11–31.

[21] Bernstein DA, Zittel MC, Keck JL. High-resolution structure of the E.coli RecQ helicase catalytic core. EMBO J. 2003;22(19):4910–21.

[22] Liu JL, Rigolet P, Dou SX, Wang PY, Xi XG. The zinc finger motif of Escherichia coli RecQ is implicated in both DNA binding and protein folding. J Biol Chem. 2004;279(41):42794–802.

[23] Kaiser S, Sauer F, Kisker C. The structural and functional characterization of human RecQ4 reveals insights into its helicase mechanism. Nat Commun. 2017;8:15907.

[24] Wu L, Chan KL, Ralf C, Bernstein DA, Garcia PL, Bohr VA, et al. The HRDC domain of BLM is required for the dissolution of double Holliday junctions. EMBO J. 2005;24(14):2679–87.

[25] Kitano K, Yoshihara N, Hakoshima T. Crystal structure of the HRDC domain of human Werner syndrome protein, WRN. J Biol Chem. 2007;282(4):2717–28.

[26] Larsen NB, Hickson ID. RecQ Helicases: Conserved Guardians of Genomic Integrity. Adv Exp Med Biol. 2013;767:161–84.

[27] Singh DK, Popuri V, Kulikowicz T, Shevelev I, Ghosh AK, Ramamoorthy M, et al. The human RecQ helicases BLM and RECQL4 cooperate to preserve genome stability. Nucleic Acids Res. 2012;40(14):6632–48.

[28] Ghosh AK, Rossi ML, Singh DK, Dunn C, Ramamoorthy M, Croteau DL, et al. RECQL4, the protein mutated in Rothmund-Thomson syndrome, functions in telomere maintenance. J Biol Chem. 2012;287(1):196–209.

[29] Brosh J R M. DNA helicases involved in DNA repair and their roles in cancer. Nat Rev Cancer. 2013;13(8):542–58.

[30] German J. Bloom syndrome: a mendelian prototype of somatic mutational disease. Medicine (Baltimore). 1993;72(6):393–406.

[31] Chaganti RS, Schonberg S, German J. A manyfold increase in sister chromatid exchanges in Bloom's syndrome lymphocytes. Proc Natl Acad Sci U S A. 1974;71(11):4508–12.

[32] Oshima J, Sidorova JM, Monnat J R J. Werner syndrome: Clinical features, pathogenesis and potential therapeutic interventions. Ageing Res Rev. 2017;33:105–114.

[33] Yokote K, Chanprasert S, Lee L, Eirich K, Takemoto M, Watanabe A, et al. WRN Mutation Update: Mutation Spectrum, Patient Registries, and Translational Prospects. Hum Mutat. 2017;38(1):7–15.

[34] Gebhart E, Bauer R, Raub U, Schinzel M, Ruprecht KW, Jonas JB. Spontaneous and induced chromosomal instability in Werner syndrome. Hum Genet. 1988;80(2):135–9.

[35] Schulz VP, Zakian VA, Ogburn CE, McKay J, Jarzebowicz AA, Edland SD, et al. Accelerated loss of telomeric repeats may not explain accelerated replicative decline of Werner syndrome cells. Hum Genet. 1996;97(6):750–4.

[36] Murfuni I, De Santis A, Federico M, Bignami M, Pichierri P, Franchitto A. Perturbed replication induced genome wide or at common fragile sites is differently managed in the absence of WRN. Carcinogenesis. 2012;33(9):1655–63.

[37] Li D, Frazier M, Evans DB, Hess KR, Crane CH, Jiao L, et al. Single nucleotide polymorphisms of RecQ1, RAD54L, and ATM genes are associated with reduced survival of pancreatic cancer. J Clin Oncol. 2006;24(11):1720–8.

[38] Arora A, Parvathaneni S, Aleskandarany MA, Agarwal D, Ali R, Abdel-Fatah T, et al. Clinicopathological and Functional Significance of RECQL1 Helicase in Sporadic Breast Cancers. Mol Cancer Ther. 2017;16(1):239–50.

[39] Arora A, Abdel-Fatah TM, Agarwal D, Doherty R, Croteau DL, Moseley PM, et al. Clinicopathological and prognostic significance of RECQL5 helicase expression in breast cancers. Carcinogenesis. 2016;37(1):63–71.

[40] Patterson K, Arya L, Bottomley S, Morgan S, Cox A, Catto J, et al. Altered RECQL5 expression in urothelial bladder carcinoma increases cellular proliferation and makes RECQL5 helicase activity a novel target for chemotherapy. Oncotarget. 2016;7(46):76140–50.

[41] Sharma S, Sommers JA, Choudhary S, Faulkner JK, Cui S, Andreoli L, et al. Biochemical analysis of the DNA unwinding and strand annealing activities catalyzed by human RECQ1. J Biol Chem. 2005;280(30):28072–84.

[42] Debnath S, Sharma S. RECQ1 Helicase in Genomic Stability and Cancer. Genes (Basel). 2020;11(6):622.

[43] Popuri V, Tadokoro T, Croteau DL, Bohr VA. Human RECQL5: guarding the crossroads of DNA replication and transcription and providing backup capability. Crit Rev Biochem Mol Biol. 2013;48(3):289–99.

[44] Hamadeh Z, Lansdorp P. RECQL5 at the Intersection of Replication and Transcription. Front Cell Dev Biol. 2020;8:324.

[45] Kaariainen H, Ryoppy S, Norio R. RAPADILINO syndrome with radial and patellar aplasia/hypoplasia as main manifestations. Am J Med Genet. 1989;33(3):346–51.

[46] Siitonen HA, Kopra O, Kaariainen H, Haravuori H, Winter RM, Saamanen AM, et al. Molecular defect of RAPADILINO syndrome expands the phenotype spectrum of RECQL diseases. Hum Mol Genet. 2003;12(21):2837–44.

[47] Kellermayer R, Siitonen HA, Hadzsiev K, Kestila M, Kosztolanyi G. A patient with Rothmund-Thomson syndrome and all features of RAPADILINO. Arch Dermatol. 2005;141(5):617–20.

[48] Baller F. Radiusaplasie und Inzucht. Z Menschl Vererb Konstitutionsl. 1950;29:782–90.

[49] Gerold M. [Healing of a fracture in an unusual case of congenital anomaly of the upper extremities]. Zentralbl Chir. 1959;84(21):831–4.

[50] Kohlhase J, Schubert L, Liebers M, Rauch A, Becker K, Mohammed SN, et al. Mutations at the SALL4 locus on chromosome 20 result in a range of clinically overlapping phenotypes, including Okihiro syndrome, Holt-Oram syndrome, acro-renal-ocular syndrome, and patients previously reported to represent thalidomide embryopathy. J Med Genet. 2003;40(7):473–8.

[51] Bukowska-Olech E, Popiel D, Koczyk G, Sowinska-Seidler A, Socha M, Wojciechowicz B, et al. Adapting SureSelect enrichment protocol to the Ion Torrent S5 platform in molecular diagnostics of craniosynostosis. Sci Rep. 2020;10(1):4159.

[52] Van Maldergem L, Siitonen HA, Jalkh N, Chouery E, De Roy M, Delague V, et al. Revisiting the craniosynostosis-radial ray hypoplasia association: Baller-Gerold syndrome caused by mutations in the RECQL4 gene. J Med Genet. 2006;43(2):148–52.

[53] Rothmund A. Über Cataracten in Verbindung mit einer eigenthümlichen Hautdegeneration. Archiv für Ophthalmologie. 1868;14(1):159–82.

[54] Thomson MS. Poikiloderma congexitale. British Journal of Dermatology. 1936;48(5):221–34.

[55] Taylor WB. Rothmund's Syndrome—Thomson's Syndrome: Congenital Poikiloderma With or Without Juvenile Cataracts A Review of the Literature, Report of a Case, and Discussion of the Relationship of the Two Syndromes. AMA archives of dermatology. 1957;75(2):236–44.

[56] Siitonen HA, Sotkasiira J, Biervliet M, Benmansour A, Capri Y, Cormier-Daire V, et al. The mutation spectrum in RECQL4 diseases. Eur J Hum Genet. 2009;17(2):151–8.

[57] Wang LL, Plon SE. Rothmund-Thomson Syndrome. In: GeneReviews®. Seattle (WA): University of Washington, Seattle; 1993-2020. Available from: https://www.ncbi.nlm.nih.gov/books/NBK1237/.

[58] Wang LL, Gannavarapu A, Kozinetz CA, Levy ML, Lewis RA, Chintagumpala MM, et al. Association between osteosarcoma and deleterious mutations in the RECQL4 gene in Rothmund-Thomson syndrome. J Natl Cancer Inst. 2003;95(9):669–74.

[59] Ajeawung NF, Nguyen TTM, Lu L, Kucharski TJ, Rousseau J, Molidperee S, et al. Mutations in ANAPC1, Encoding a Scaffold Subunit of the Anaphase-Promoting Complex, Cause Rothmund-Thomson Syndrome Type 1. Am J Hum Genet. 2019;105(3):625–30.

[60] Eguren M, Manchado E, Malumbres M. Non-mitotic functions of the Anaphase-Promoting Complex. Semin Cell Dev Biol. 2011;22(6):572–8.

[61] Alfieri C, Zhang S, Barford D. Visualizing the complex functions and mechanisms of the anaphase promoting complex/cyclosome (APC/C). Open Biol. 2017;7(11):170204.

[62] Imai F, Yoshizawa A, Fujimori-Tonou N, Kawakami K, Masai I. The ubiquitin proteasome system is required for cell proliferation of the lens epithelium and for differentiation of lens fiber cells in zebrafish. Development. 2010;137(19):3257–68.

[63] Dickinson ME, Flenniken AM, Ji X, Teboul L, Wong MD, White JK, et al. High-throughput discovery of novel developmental phenotypes. Nature. 2016;537(7621):508–14.

[64] Larizza L, Roversi G, Volpi L. Rothmund-Thomson syndrome. Orphanet J Rare Dis. 2010;5:2.

[65] Ahn JW, Inkeles M, Hristov A, Eshaq M. Histopathologic features of Rothmund-Thomson syndrome. JAAD Case Rep. 2019;5(8):726–28.

[66] Yang JY, Sohn YB, Lee JS, Jang JH, Lee ES. Rare presentation of Rothmund-Thomson syndrome with predominantly cutaneous findings. JAAD Case Rep. 2017;3(3):172–4.

[67] Wang LL, Levy ML, Lewis RA, Chintagumpala MM, Lev D, Rogers M, et al. Clinical manifestations in a cohort of 41 Rothmund-Thomson syndrome patients. Am J Med Genet. 2001;102(1):11–7.

[68] Bottomley WK, Box JM. Dental anomalies in the Rothmund-Thomson syndrome. Report of a case. Oral Surg Oral Med Oral Pathol. 1976;41(3):321–6.

[69] Canger EM, Celenk P, Devrim I, Avsar A. Oral findings of rothmund-thomson syndrome. Case Rep Dent. 2013;2013:935716.

[70] Haytac MC, Oztunc H, Mete UO, Kaya M. Rothmund-Thomson syndrome: a case report. Oral Surg Oral Med Oral Pathol Oral Radiol Endod. 2002;94(4):479–84.

[71] Kraus BS, Gottlieb MA, Meliton HR. The dentition in Rothmund's syndrome. J Am Dent Assoc. 1970;81(4):895–915.

[72] Rathi NV, Bhattad MS, Thosar N, Baliga S. Dental management of Rothmund-Thomson syndrome with partial anodontia. BMJ Case Rep. 2015;2015:bcr2015209994.

[73] Vennos EM, Collins M, James WD. Rothmund-Thomson syndrome: review of the world literature. J Am Acad Dermatol. 1992;27(5 Pt 1):750–62.

[74] Mehollin-Ray AR, Kozinetz CA, Schlesinger AE, Guillerman RP, Wang LL. Radiographic abnormalities in Rothmund-Thomson syndrome and genotype-phenotype correlation with RECQL4 mutation status. AJR Am J Roentgenol. 2008;191(2):W62–6.

[75] Cao F, Lu L, Abrams SA, Hawthorne KM, Tam A, Jin W, et al. Generalized metabolic bone disease and fracture risk in Rothmund-Thomson syndrome. Hum Mol Genet. 2017;26(16):3046–55.

[76] Leslie WD, Tsang JF, Caetano PA, Lix LM, Manitoba Bone Density P. Effectiveness of bone density measurement for predicting osteoporotic fractures in clinical practice. J Clin Endocrinol Metab. 2007;92(1):77–81.

[77] Carlson AM, Thomas KB, Kirmani S, Lindor NM. Chronic tibial nonunion in a Rothmund-Thomson syndrome patient. Am J Med Genet A. 2012;158A(9):2250–3.

[78] Beckmann N. Multiple Low Energy Long Bone Fractures in the Setting of Rothmund-Thomson Syndrome. Case Rep Med. 2015;2015:495164.

[79] Barisonek KL, Protzman NM, Wobst GM, Brigido SA. Delayed Union of a Jones Fracture in a Patient With Rothmund-Thomson Syndrome: A Case Report and Review of the Literature. J Foot Ankle Surg. 2016;55(2):291–3.

[80] Yadav S, Thakur S, Kohlhase J, Bhari N, Kabra M, Gupta N. Report of Two Novel Mutations in Indian Patients with Rothmund-Thomson Syndrome. J Pediatr Genet. 2019;8(3):163–7.

[81] Blaustein HS, Stevens AW, Stevens PD, Grossman ME. Rothmund-Thomson syndrome associated with annular pancreas and duodenal stenosis: a case report. Pediatr Dermatol. 1993;10(2):159–63.

[82] Zhang X, Geng S, Zheng Y. Rare presentation of Rothmund-Thomson syndrome with novel compound heterozygous mutations of the RECQL4 gene. An Bras Dermatol. 2020;95(4):538–40.

[83] Kubota M, Yasunaga M, Hashimoto H, Kimata H, Mikawa H, Shinya A, et al. IgG4 deficiency with Rothmund-Thomson syndrome: a case report. Eur J Pediatr. 1993;152(5):406–8.

[84] Ito T, Tokura Y, Moriwaki S, Yasuda K, Ohnishi A, Furukawa F, et al. Rothmund-Thomson syndrome with herpes encephalitis. Eur J Dermatol. 1999;9(5):354–6.

[85] Broom MA, Wang LL, Otta SK, Knutsen AP, Siegfried E, Batanian JR, et al. Successful umbilical cord blood stem cell transplantation in a patient with Rothmund-Thomson syndrome and combined immunodeficiency. Clin Genet. 2006;69(4):337–43.

[86] De Somer L, Wouters C, Morren MA, De Vos R, Van Den Oord J, Devriendt K, et al. Granulomatous skin lesions complicating Varicella infection in a patient with Rothmund-Thomson syndrome and immune deficiency: case report. Orphanet J Rare Dis. 2010;5:1–5.

[87] Rudilla F, Franco-Jarava C, Martinez-Gallo M, Garcia-Prat M, Martin-Nalda A, Riviere J, et al. Expanding the Clinical and Genetic Spectra of Primary Immunodeficiency-Related Disorders With Clinical Exome Sequencing: Expected and Unexpected Findings. Front Immunol. 2019;10:2325.

[88] Smeets MF, DeLuca E, Wall M, Quach JM, Chalk AM, Deans AJ, et al. The Rothmund-Thomson syndrome helicase RECQL4 is essential for hematopoiesis. J Clin Invest. 2014;124(8):3551–65.

[89] Parsa N. Environmental factors inducing human cancers. Iran J Public Health. 2012;41(11):1–9.

[90] Brodeur GM, Nichols KE, Plon SE, Schiffman JD, Malkin D. Pediatric Cancer Predisposition and Surveillance: An Overview, and a Tribute to Alfred G. Knudson Jr. Clin Cancer Res. 2017;23(11):e1–e5.

[91] Ottaviani G, Jaffe N. The epidemiology of osteosarcoma. Cancer Treat Res. 2009;152:3–13.

[92] Janeway KA, Barkauskas DA, Krailo MD, Meyers PA, Schwartz CL, Ebb DH, et al. Outcome for adolescent and young adult patients with osteosarcoma: a report from the Children's Oncology Group. Cancer. 2012;118(18):4597–605.

[93] Ferrari S, Smeland S, Mercuri M, Bertoni F, Longhi A, Ruggieri P, et al. Neoadjuvant chemotherapy with high-dose Ifosfamide, high-dose methotrexate, cisplatin, and doxorubicin for patients with localized osteosarcoma of the extremity: a joint study by the Italian and Scandinavian Sarcoma Groups. J Clin Oncol. 2005;23(34):8845–52.

[94] Hicks MJ, Roth JR, Kozinetz CA, Wang LL. Clinicopathologic features of osteosarcoma in patients with Rothmund-Thomson syndrome. J Clin Oncol. 2007;25(4):370–5.

[95] Nishijo K, Nakayama T, Aoyama T, Okamoto T, Ishibe T, Yasura K, et al. Mutation analysis of the RECQL4 gene in sporadic osteosarcomas. Int J Cancer. 2004;111(3):367–72.

[96] Chen X, Bahrami A, Pappo A, Easton J, Dalton J, Hedlund E, et al. Recurrent somatic structural variations contribute to tumorigenesis in pediatric osteosarcoma. Cell Rep. 2014;7(1):104–12.

[97] Kovac M, Blattmann C, Ribi S, Smida J, Mueller NS, Engert F, et al. Exome sequencing of osteosarcoma reveals mutation signatures reminiscent of BRCA deficiency. Nat Commun. 2015;6:8940.

[98] Mirabello L, Zhu B, Koster R, Karlins E, Dean M, Yeager M, et al. Frequency of Pathogenic Germline Variants in Cancer-Susceptibility Genes in Patients With Osteosarcoma. JAMA Oncol. 2020;6(5):724–34.

[99] Maciaszek JL, Oak N, Chen W, Hamilton KV, McGee RB, Nuccio R, et al. Enrichment of heterozygous germline RECQL4 loss-of-function variants in pediatric osteosarcoma. Cold Spring Harb Mol Case Stud. 2019;5(5):a004218.

[100] Stinco G, Governatori G, Mattighello P, Patrone P. Multiple cutaneous neoplasms in a patient with Rothmund-Thomson syndrome: case report and published work review. J Dermatol. 2008;35(3):154–61.

[101] Borg MF, Olver IN, Hill MP. Rothmund-Thomson syndrome and tolerance of chemoradiotherapy. Australas Radiol. 1998;42(3):216–8.

[102] Howell SM, Bray DW. Amelanotic melanoma in a patient with Rothmund-Thomson syndrome. Arch Dermatol. 2008;144(3):416–7.

[103] Piquero-Casals J, Okubo AY, Nico MM. Rothmund-thomson syndrome in three siblings and development of cutaneous squamous cell carcinoma. Pediatr Dermatol. 2002;19(4):312–6.

[104] Ilhan I, Arikan U, Buyukpamukcu M. Myelodysplastic syndromes and RTS. Pediatr Hematol Oncol. 1996;13(2):197.

[105] Narayan S, Fleming C, Trainer AH, Craig JA. Rothmund-Thomson syndrome with myelodysplasia. Pediatr Dermatol. 2001;18(3):210–2.

[106] Porter WM, Hardman CM, Abdalla SH, Powles AV. Haematological disease in siblings with Rothmund-Thomson syndrome. Clin Exp Dermatol. 1999;24(6):452–4.

[107] Rizzari C, Bacchiocchi D, Rovelli A, Biondi A, Cantu'-Rajnoldi A, Uderzo C, et al. Myelodysplastic syndrome in a child with Rothmund-Thomson syndrome: a case report. J Pediatr Hematol Oncol. 1996;18(1):96–7.

[108] Simon T, Kohlhase J, Wilhelm C, Kochanek M, De Carolis B, Berthold F. Multiple malignant diseases in a patient with Rothmund-Thomson syndrome with RECQL4 mutations: Case report and literature review. Am J Med Genet A. 2010;152A(6):1575–9.

[109] Spurney C, Gorlick R, Meyers PA, Healey JH, Huvos AG. Multicentric osteosarcoma, Rothmund-Thomson syndrome, and secondary nasopharyngeal non-Hodgkin's lymphoma: a case report and review of the literature. J Pediatr Hematol Oncol. 1998;20(5):494–7.

[110] Colombo EA, Locatelli A, Cubells Sanchez L, Romeo S, Elcioglu NH, Maystadt I, et al. Rothmund-Thomson Syndrome: Insights from New Patients on the Genetic Variability Underpinning Clinical Presentation and Cancer Outcome. Int J Mol Sci. 2018;19(4):1103.

[111] Kitao S, Shimamoto A, Goto M, Miller RW, Smithson WA, Lindor NM, et al. Mutations in RECQL4 cause a subset of cases of Rothmund-Thomson syndrome. Nat Genet. 1999;22(1):82–4.

[112] Wang LL, Worley K, Gannavarapu A, Chintagumpala MM, Levy ML, Plon SE. Intron-size constraint as a mutational mechanism in Rothmund-Thomson syndrome. Am J Hum Genet. 2002;71(1):165–7.

[113] Kitao S, Ohsugi I, Ichikawa K, Goto M, Furuichi Y, Shimamoto A. Cloning of two new human helicase genes of the RecQ family: biological significance of multiple species in higher eukaryotes. Genomics. 1998;54(3):443–52.

[114] Thangavel S, Mendoza-Maldonado R, Tissino E, Sidorova JM, Yin J, Wang W, et al. Human RECQ1 and RECQ4 helicases play distinct roles in DNA replication initiation. Mol Cell Biol. 2010;30(6):1382–96.

[115] Xu X, Rochette PJ, Feyissa EA, Su TV, Liu Y. MCM10 mediates RECQ4 association with MCM2-7 helicase complex during DNA replication. EMBO J. 2009;28(19):3005–14.

[116] Uhlen M, Fagerberg L, Hallstrom BM, Lindskog C, Oksvold P, Mardinoglu A, et al. Proteomics. Tissue-based map of the human proteome. Science. 2015;347(6220):1260419. Available from: https://www.proteinatlas.org/ENSG00000160957-RECQL4/tissue.

[117] Anwar T, Rufail ML, Djomehri SI, Gonzalez ME, Lazo de la Vega L, Tomlins SA, et al. Next-generation sequencing identifies recurrent copy number variations in invasive breast carcinomas from Ghana. Mod Pathol. 2020;Mar(9):1–9.

[118] Chen H, Yuan K, Wang X, Wang H, Wu Q, Wu X, et al. Overexpression of RECQL4 is associated with poor prognosis in patients with gastric cancer. Oncol Lett. 2018;16(4):5419–25.

[119] Su Y, Meador JA, Calaf GM, Proietti De-Santis L, Zhao Y, Bohr VA, et al. Human RecQL4 helicase plays critical roles in prostate carcinogenesis. Cancer Res. 2010;70(22):9207–17.

[120] Kitao S, Lindor NM, Shiratori M, Furuichi Y, Shimamoto A. Rothmund-thomson syndrome responsible gene, RECQL4: genomic structure and products. Genomics. 1999;61(3):268–76.

[121] Yin J, Kwon YT, Varshavsky A, Wang W. RECQL4, mutated in the Rothmund-Thomson and RAPADILINO syndromes, interacts with

ubiquitin ligases UBR1 and UBR2 of the N-end rule pathway. Hum Mol Genet. 2004;13(20):2421–30.

[122] Petkovic M, Dietschy T, Freire R, Jiao R, Stagljar I. The human Rothmund-Thomson syndrome gene product, RECQL4, localizes to distinct nuclear foci that coincide with proteins involved in the maintenance of genome stability. J Cell Sci. 2005;118(Pt 18):4261–9.

[123] Burks LM, Yin J, Plon SE. Nuclear import and retention domains in the amino terminus of RECQL4. Gene. 2007;391(1-2):26–38.

[124] Dietschy T, Shevelev I, Pena-Diaz J, Huhn D, Kuenzle S, Mak R, et al. p300-mediated acetylation of the Rothmund-Thomson-syndrome gene product RECQL4 regulates its subcellular localization. J Cell Sci. 2009;122(Pt 8):1258–67.

[125] Chi Z, Nie L, Peng Z, Yang Q, Yang K, Tao J, et al. RecQL4 cytoplasmic localization: implications in mitochondrial DNA oxidative damage repair. Int J Biochem Cell Biol. 2012;44(11):1942–51.

[126] Woo LL, Futami K, Shimamoto A, Furuichi Y, Frank KM. The Rothmund-Thomson gene product RECQL4 localizes to the nucleolus in response to oxidative stress. Exp Cell Res. 2006;312(17):3443–57.

[127] Croteau DL, Rossi ML, Canugovi C, Tian J, Sykora P, Ramamoorthy M, et al. RECQL4 localizes to mitochondria and preserves mitochondrial DNA integrity. Aging Cell. 2012;11(3):456–66.

[128] Fragkos M, Ganier O, Coulombe P, Mechali M. DNA replication origin activation in space and time. Nat Rev Mol Cell Biol. 2015;16(6):360–74.

[129] Tanaka S, Araki H. Multiple regulatory mechanisms to inhibit untimely initiation of DNA replication are important for stable genome maintenance. PLoS Genet. 2011;7(6):e1002136.

[130] Moiseeva TN, Bakkenist CJ. Regulation of the initiation of DNA replication in human cells. DNA Repair (Amst). 2018;72:99–106.

[131] Kanemaki M, Labib K. Distinct roles for Sld3 and GINS during establishment and progression of eukaryotic DNA replication forks. EMBO J. 2006;25(8):1753–63.

[132] Kubota Y, Takase Y, Komori Y, Hashimoto Y, Arata T, Kamimura Y, et al. A novel ring-like complex of Xenopus proteins essential for the initiation of DNA replication. Genes Dev. 2003;17(9):1141–52.

[133] Labib K. How do Cdc7 and cyclin-dependent kinases trigger the initiation of chromosome replication in eukaryotic cells? Genes Dev. 2010;24(12):1208–19.

[134] Ohlenschlager O, Kuhnert A, Schneider A, Haumann S, Bellstedt P, Keller H, et al. The N-terminus of the human RecQL4 helicase is a homeodomain-like DNA interaction motif. Nucleic Acids Res. 2012;40(17):8309–24.

[135] Im JS, Park SY, Cho WH, Bae SH, Hurwitz J, Lee JK. RecQL4 is required for the association of Mcm10 and Ctf4 with replication origins in human cells. Cell Cycle. 2015;14(7):1001–9.

[136] Shin G, Jeong D, Kim H, Im JS, Lee JK. RecQL4 tethering on the pre-replicative complex induces unscheduled origin activation and replication stress in human cells. J Biol Chem. 2019;294(44):16255–65.

[137] Rivera-Mulia JC, Desprat R, Trevilla-Garcia C, Cornacchia D, Schwerer H, Sasaki T, et al. DNA replication timing alterations identify common markers between distinct progeroid diseases. Proc Natl Acad Sci U S A. 2017;114(51):E10972–80.

[138] Rossi ML, Ghosh AK, Kulikowicz T, Croteau DL, Bohr VA. Conserved helicase domain of human RecQ4 is required for strand annealing-independent DNA unwinding. DNA Repair (Amst). 2010;9(7):796–804.

[139] Ichikawa K, Noda T, Furuichi Y. [Preparation of the gene targeted knockout mice for human premature aging diseases, Werner syndrome, and Rothmund-Thomson syndrome caused by the mutation of DNA helicases]. Nihon Yakurigaku Zasshi. 2002;119(4):219–26.

[140] Kelley MR, Fishel ML. In: Kelley MR, Fishel ML, editors. Chapter 1 - Overview of DNA repair pathways, current targets, and clinical trials bench to clinic. Boston: Academic Press; 2016. p. 1–54.

[141] Wilson r D M, Bohr VA. The mechanics of base excision repair, and its relationship to aging and disease. DNA Repair (Amst). 2007;6(4):544–59.

[142] Schurman SH, Hedayati M, Wang Z, Singh DK, Speina E, Zhang Y, et al. Direct and indirect roles of RECQL4 in modulating base excision repair capacity. Hum Mol Genet. 2009;18(18):3470–83.

[143] Duan S, Han X, Akbari M, Croteau DL, Rasmussen LJ, Bohr VA. Interaction between RECQL4 and OGG1 promotes repair of oxidative base lesion 8-oxoG and is regulated by SIRT1 deacetylase. Nucleic Acids Res. 2020;48(12):6530–46.

[144] Fan W, Luo J. RecQ4 facilitates UV light-induced DNA damage repair through interaction with nucleotide excision repair factor xeroderma pigmentosum group A (XPA). J Biol Chem. 2008;283(43):29037–44.

[145] Song L, Yuan F, Zhang Y. Does a helicase activity help mismatch repair in eukaryotes? IUBMB Life. 2010;62(7):548–53.

[146] Lu H, Shamanna RA, Keijzers G, Anand R, Rasmussen LJ, Cejka P, et al. RECQL4 Promotes DNA End Resection in Repair of DNA Double-Strand Breaks. Cell Rep. 2016;16(1):161–73.

[147] Park SY, Kim H, Im JS, Lee JK. ATM activation is impaired in human cells defective in RecQL4 helicase activity. Biochem Biophys Res Commun. 2019;509(2):379–83.

[148] Shamanna RA, Singh DK, Lu H, Mirey G, Keijzers G, Salles B, et al. RECQ helicase RECQL4 participates in non-homologous end joining and interacts with the Ku complex. Carcinogenesis. 2014;35(11):2415–24.

[149] Grant SG, Wenger SL, Latimer JJ, Thull D, Burke LW. Analysis of genomic instability using multiple assays in a patient with Rothmund-Thomson syndrome. Clin Genet. 2000;58(3):209–15.

[150] Jin W, Liu H, Zhang Y, Otta SK, Plon SE, Wang LL. Sensitivity of RECQL4-deficient fibroblasts from Rothmund-Thomson syndrome patients to genotoxic agents. Hum Genet. 2008;123(6):643–53.

[151] Miozzo M, Castorina P, Riva P, Dalpra L, Fuhrman Conti AM, Volpi L, et al. Chromosomal instability in fibroblasts and mesenchymal tumors from 2 sibs with Rothmund-Thomson syndrome. Int J Cancer. 1998;77(4):504–10.

[152] Werner SR, Prahalad AK, Yang J, Hock JM. RECQL4-deficient cells are hypersensitive to oxidative stress/damage: Insights for osteosarcoma prevalence and heterogeneity in Rothmund-Thomson syndrome. Biochem Biophys Res Commun. 2006;345(1):403–9.

[153] Hasty P, Campisi J, Hoeijmakers J, van Steeg H, Vijg J. Aging and genome maintenance: lessons from the mouse? Science. 2003;299(5611):1355–9.

[154] Palm W, de Lange T. How shelterin protects mammalian telomeres. Annu Rev Genet. 2008;42:301–34.

[155] Gilson E, Geli V. How telomeres are replicated. Nat Rev Mol Cell Biol. 2007;8(10):825–38.

[156] Ferrarelli LK, Popuri V, Ghosh AK, Tadokoro T, Canugovi C, Hsu JK, et al. The RECQL4 protein, deficient in Rothmund-Thomson syndrome is active on telomeric D-loops containing DNA metabolism blocking lesions. DNA Repair (Amst). 2013;12(7):518–28.

[157] Tornaletti S, Maeda LS, Lloyd DR, Reines D, Hanawalt PC. Effect of thymine glycol on transcription elongation by T7 RNA polymerase and mammalian RNA polymerase II. J Biol Chem. 2001;276(48):45367–71.

[158] Vogel C, Hager C, Bastians H. Mechanisms of mitotic cell death induced by chemotherapy-mediated G2 checkpoint abrogation. Cancer Res. 2007;67(1):339–45.

[159] Mann MB, Hodges CA, Barnes E, Vogel H, Hassold TJ, Luo G. Defective sister-chromatid cohesion, aneuploidy and cancer predisposition in a mouse model of type II Rothmund-Thomson syndrome. Hum Mol Genet. 2005;14(6):813–25.

[160] Yokoyama H, Moreno-Andres D, Astrinidis SA, Hao Y, Weberruss M, Schellhaus AK, et al. Chromosome alignment maintenance requires the MAP RECQL4, mutated in the Rothmund-Thomson syndrome. Life Sci Alliance. 2019;2(1):e201800120.

[161] Maiato H, Gomes AM, Sousa F, Barisic M. Mechanisms of Chromosome Congression during Mitosis. Biology (Basel). 2017;6(1):13.

[162] Fang H, Niu K, Mo D, Zhu Y, Tan Q, Wei D, et al. RecQL4-Aurora B kinase axis is essential for cellular proliferation, cell cycle progression, and mitotic integrity. Oncogenesis. 2018;7(9):1–2.

[163] Willems E, Dedobbeleer M, Digregorio M, Lombard A, Lumapat PN, Rogister B. The functional diversity of Aurora kinases: a comprehensive review. Cell Div. 2018;13(1):1–7.

[164] Croteau DL, Singh DK, Hoh Ferrarelli L, Lu H, Bohr VA. RECQL4 in genomic instability and aging. Trends Genet. 2012;28(12):624–31.

[165] De S, Kumari J, Mudgal R, Modi P, Gupta S, Futami K, et al. RECQL4 is essential for the transport of p53 to mitochondria in normal human cells in the absence of exogenous stress. J Cell Sci. 2012;125(10):2509–22.

[166] Macris MA, Krejci L, Bussen W, Shimamoto A, Sung P. Biochemical characterization of the RECQ4 protein, mutated in Rothmund-Thomson syndrome. DNA Repair (Amst). 2006;5(2):172–80.

[167] Xu X, Liu Y. Dual DNA unwinding activities of the Rothmund-Thomson syndrome protein, RECQ4. EMBO J. 2009;28(5):568–77.

[168] Suzuki T, Kohno T, Ishimi Y. DNA helicase activity in purified human RECQL4 protein. J Biochem. 2009;146(3):327–35.

[169] Abe T, Yoshimura A, Hosono Y, Tada S, Seki M, Enomoto T. The N-terminal region of RECQL4 lacking the helicase domain is both essential and sufficient for the viability of vertebrate cells. Role of the N-terminal region of RECQL4 in cells. Biochim Biophys Acta. 2011;1813(3):473–9.

[170] Sangrithi MN, Bernal JA, Madine M, Philpott A, Lee J, Dunphy WG, et al. Initiation of DNA replication requires the RECQL4 protein mutated in Rothmund-Thomson syndrome. Cell. 2005;121(6):887–98.

[171] Masumoto H, Muramatsu S, Kamimura Y, Araki H. S-Cdk-dependent phosphorylation of Sld2 essential for chromosomal DNA replication in budding yeast. Nature. 2002;415(6872):651–5.

[172] Muramatsu S, Hirai K, Tak YS, Kamimura Y, Araki H. CDK-dependent complex formation between replication proteins Dpb11, Sld2, Pol (epsilon), and GINS in budding yeast. Genes Dev. 2010;24(6):602–12.

[173] Keller H, Kiosze K, Sachsenweger J, Haumann S, Ohlenschlager O, Nuutinen T, et al. The intrinsically disordered amino-terminal region of human RecQL4: multiple DNA-binding domains confer annealing, strand exchange and G4 DNA binding. Nucleic Acids Res. 2014;42(20):12614–27.

[174] Capp C, Wu J, Hsieh TS. Drosophila RecQ4 has a 3'-5' DNA helicase activity that is essential for viability. J Biol Chem. 2009;284(45):30845–52.

[175] Marino F, Vindigni A, Onesti S. Bioinformatic analysis of RecQ4 helicases reveals the presence of a RQC domain and a Zn knuckle. Biophys Chem. 2013;177:34–9.

[176] Mojumdar A, De March M, Marino F, Onesti S. The Human RecQ4 Helicase Contains a Functional RecQ C-terminal Region (RQC) That Is Essential for Activity. J Biol Chem. 2017;292(10):4176–84.

[177] Hoki Y, Araki R, Fujimori A, Ohhata T, Koseki H, Fukumura R, et al. Growth retardation and skin abnormalities of the Recql4-deficient mouse. Hum Mol Genet. 2003;12(18):2293–9.

[178] Lu H, Fang EF, Sykora P, Kulikowicz T, Zhang Y, Becker KG, et al. Senescence induced by RECQL4 dysfunction contributes to Rothmund-Thomson syndrome features in mice. Cell Death Dis. 2014;5(5):e1226.

[179] Rodda SJ, McMahon AP. Distinct roles for Hedgehog and canonical Wnt signaling in specification, differentiation and maintenance of osteoblast progenitors. Development. 2006;133(16):3231–44.

[180] Lu Y, Xie Y, Zhang S, Dusevich V, Bonewald LF, Feng JQ. DMP1-targeted Cre expression in odontoblasts and osteocytes. J Dent Res. 2007;86(4):320–5.

[181] Ng AJ, Walia MK, Smeets MF, Mutsaers AJ, Sims NA, Purton LE, et al. The DNA helicase recql4 is required for normal osteoblast expansion and osteosarcoma formation. PLoS Genet. 2015;11(4):e1005160.

[182] Logan M, Martin JF, Nagy A, Lobe C, Olson EN, Tabin CJ. Expression of Cre Recombinase in the developing mouse limb bud driven by a Prxl enhancer. Genesis. 2002;33(2):77–80.

[183] Lu L, Harutyunyan K, Jin W, Wu J, Yang T, Chen Y, et al. RECQL4 Regulates p53 Function In Vivo During Skeletogenesis. J Bone Miner Res. 2015;30(6):1077–89.

[184] Liddicoat BJ, Piskol R, Chalk AM, Ramaswami G, Higuchi M, Hartner JC, et al. RNA editing by ADAR1 prevents MDA5 sensing of endogenous dsRNA as nonself. Science. 2015;349(6252):1115–20.

[185] Singbrant S, Russell MR, Jovic T, Liddicoat B, Izon DJ, Purton LE, et al. Erythropoietin couples erythropoiesis, B-lymphopoiesis, and bone homeostasis within the bone marrow microenvironment. Blood. 2011;117(21):5631–42.

[186] Becker JR, Cuella-Martin R, Barazas M, Liu R, Oliveira C, Oliver AW, et al. The ASCIZ-DYNLL1 axis promotes 53BP1-dependent non-homologous end joining and PARP inhibitor sensitivity. Nat Commun. 2018;9(1):1–12.

[187] Wang GG, Calvo KR, Pasillas MP, Sykes DB, Häcker H, Kamps MP. Quantitative production of macrophages or neutrophils ex vivo using conditional Hoxb8. Nature Methods. 2006;3(4):287–93.

[188] van Twest S, Murphy VJ, Hodson C, Tan W, Swuec P, O'Rourke JJ, et al. Mechanism of Ubiquitination and Deubiquitination in the Fanconi Anemia Pathway. Mol Cell. 2017;65(2):247–59.

[189] Sanjana NE, Shalem O, Zhang F. Improved vectors and genome-wide libraries for CRISPR screening. Nat Methods. 2014;11(8):783–84.

[190] Doench JG, Fusi N, Sullender M, Hegde M, Vaimberg EW, Donovan KF, et al. Optimized sgRNA design to maximize activity and minimize off-target effects of CRISPR-Cas9. Nat Biotechnol. 2016;34(2):184–191.

[191] Jeong HH, Kim SY, Rousseaux MWC, Zoghbi HY, Liu Z. Beta-binomial modeling of CRISPR pooled screen data identifies target genes with greater sensitivity and fewer false negatives. Genome Res. 2019;29(6):999–1008.

[192] Durinck S, Spellman PT, Birney E, Huber W. Mapping identifiers for the integration of genomic datasets with the R/Bioconductor package biomaRt. Nat Protoc. 2009;4(8):1184–91.

[193] Wickham H. ggplot2: elegant graphics for data analysis. Springer; 2016.

[194] Hart T, Tong AHY, Chan K, Van Leeuwen J, Seetharaman A, Aregger M, et al. Evaluation and Design of Genome-Wide CRISPR/SpCas9 Knockout Screens. G3 (Bethesda). 2017;7(8):2719–27.

[195] Delagoutte E, von Hippel PH. Helicase mechanisms and the coupling of helicases within macromolecular machines. Part I: Structures and properties of isolated helicases. Q Rev Biophys. 2002;35(4):431–78.

[196] Chu WK, Hickson ID. RecQ helicases: multifunctional genome caretakers. Nat Rev Cancer. 2009;9(9):644–54.

[197] Pike AC, Shrestha B, Popuri V, Burgess-Brown N, Muzzolini L, Costantini S, et al. Structure of the human RECQ1 helicase reveals a putative strand-separation pin. Proc Natl Acad Sci U S A. 2009;106(4):1039–44.

[198] Croteau DL, Popuri V, Opresko PL, Bohr VA. Human RecQ helicases in DNA repair, recombination, and replication. Annu Rev Biochem. 2014;83:519–52.

[199] Kliszczak M, Sedlackova H, Pitchai GP, Streicher WW, Krejci L, Hickson ID. Interaction of RECQ4 and MCM10 is important for efficient DNA replication origin firing in human cells. Oncotarget. 2015;6(38):40464–79.

[200] Wu J, Capp C, Feng L, Hsieh TS. Drosophila homologue of the Rothmund-Thomson syndrome gene: essential function in DNA replication during development. Dev Biol. 2008;323(1):130–42.

[201] Im JS, Ki SH, Farina A, Jung DS, Hurwitz J, Lee JK. Assembly of the Cdc45-Mcm2-7-GINS complex in human cells requires the Ctf4/And-1, RecQL4, and Mcm10 proteins. Proc Natl Acad Sci U S A. 2009;106(37):15628–32.

[202] Wu Y, Brosh J R M. Helicase-inactivating mutations as a basis for dominant negative phenotypes. Cell Cycle. 2010;9(20):4080–90.

[203] Matsuno K, Kumano M, Kubota Y, Hashimoto Y, Takisawa H. The N-terminal noncatalytic region of Xenopus RecQ4 is required for chromatin binding of DNA polymerase alpha in the initiation of DNA replication. Mol Cell Biol. 2006;26(13):4843–52.

[204] Lu H, Shamanna RA, de Freitas JK, Okur M, Khadka P, Kulikowicz T, et al. Cell cycle-dependent phosphorylation regulates RECQL4 pathway choice and ubiquitination in DNA double-strand break repair. Nat Commun. 2017;8(1):1–4.

[205] Bredemeyer AL, Sharma GG, Huang CY, Helmink BA, Walker LM, Khor KC, et al. ATM stabilizes DNA double-strand-break complexes during V(D)J recombination. Nature. 2006;442(7101):466–70.

[206] Liao MJ, Van Dyke T. Critical role for Atm in suppressing V(D)J recombination-driven thymic lymphoma. Genes Dev. 1999;13(10):1246–50.

[207] Lumsden JM, McCarty T, Petiniot LK, Shen R, Barlow C, Wynn TA, et al. Immunoglobulin class switch recombination is impaired in Atm-deficient mice. J Exp Med. 2004;200(9):1111–21.

[208] Kamath-Loeb AS, Zavala-van Rankin DG, Flores-Morales J, Emond MJ, Sidorova JM, Carnevale A, et al. Homozygosity for the WRN Helicase-Inactivating Variant, R834C, does not confer a Werner syndrome clinical phenotype. Sci Rep. 2017;7:44081.

[209] Gaggioli V, Zeiser E, Rivers D, Bradshaw CR, Ahringer J, Zegerman P. CDK phosphorylation of SLD-2 is required for replication initiation and germline development in C. elegans. J Cell Biol. 2014;204(4):507–22.

[210] Fairman-Williams ME, Guenther UP, Jankowsky E. SF1 and SF2 helicases: family matters. Curr Opin Struct Biol. 2010;20(3):313–24.

[211] Castillo-Tandazo W, Smeets MF, Murphy V, Liu R, Hodson C, Heierhorst J, et al. ATP-dependent helicase activity is dispensable for the physiological functions of Recql4. PLoS Genet. 2019;15(7):e1008266.

[212] Mirabello L, Troisi RJ, Savage SA. Osteosarcoma incidence and survival rates from 1973 to 2004: data from the Surveillance, Epidemiology, and End Results Program. Cancer. 2009;115(7):1531–43.

[213] Davey RA, Clarke MV, Sastra S, Skinner JP, Chiang C, Anderson PH, et al. Decreased body weight in young Osterix-Cre transgenic mice results in delayed cortical bone expansion and accrual. Transgenic Res. 2012;21(4):885–93.

[214] Huang W, Olsen BR. Skeletal defects in Osterix-Cre transgenic mice. Transgenic Res. 2015;24(1):167–72.

[215] Kohzaki M, Ootsuyama A, Sun L, Moritake T, Okazaki R. Human RECQL4 represses the RAD52-mediated single-strand annealing pathway after ionizing radiation or cisplatin treatment. Int J Cancer. 2020;146(11):3098–3113.

[216] Huvos AG, Woodard HQ. Postradiation sarcomas of bone. Health Phys. 1988;55(4):631–6.

[217] Virtanen A, Pukkala E, Auvinen A. Incidence of bone and soft tissue sarcoma after radiotherapy: a cohort study of 295,712 Finnish cancer patients. Int J Cancer. 2006;118(4):1017–21.

[218] Kohzaki M, Chiourea M, Versini G, Adachi N, Takeda S, Gagos S, et al. The helicase domain and C-terminus of human RecQL4 facilitate replication elongation on DNA templates damaged by ionizing radiation. Carcinogenesis. 2012;33(6):1203–10.

[219] Buffart TE, Coffa J, Hermsen MA, Carvalho B, van der Sijp JR, Ylstra B, et al. DNA copy number changes at 8q11-24 in metastasized colorectal cancer. Cell Oncol. 2005;27(1):57–65.

[220] Maire G, Yoshimoto M, Chilton-MacNeill S, Thorner PS, Zielenska M, Squire JA. Recurrent RECQL4 imbalance and increased gene expression levels are associated with structural chromosomal instability in sporadic osteosarcoma. Neoplasia. 2009;11(3):260–8.

[221] Narayan G, Bourdon V, Chaganti S, Arias-Pulido H, Nandula SV, Rao PH, et al. Gene dosage alterations revealed by cDNA microarray analysis in cervical cancer: identification of candidate amplified and overexpressed genes. Genes Chromosomes Cancer. 2007;46(4):373–84.

[222] Saglam O, Shah V, Worsham MJ. Molecular differentiation of early and late stage laryngeal squamous cell carcinoma: an exploratory analysis. Diagn Mol Pathol. 2007;16(4):218–21.

[223] Thomassen M, Tan Q, Kruse TA. Gene expression meta-analysis identifies chromosomal regions and candidate genes involved in breast cancer metastasis. Breast Cancer Res Treat. 2009;113(2):239–49.

[224] Barrangou R, Fremaux C, Deveau H, Richards M, Boyaval P, Moineau S, et al. CRISPR provides acquired resistance against viruses in prokaryotes. Science. 2007;315(5819):1709–12.

[225] Jinek M, Chylinski K, Fonfara I, Hauer M, Doudna JA, Charpentier E. A programmable dual-RNA-guided DNA endonuclease in adaptive bacterial immunity. Science. 2012;337(6096):816–21.

[226] Rouet P, Smih F, Jasin M. Introduction of double-strand breaks into the genome of mouse cells by expression of a rare-cutting endonuclease. Mol Cell Biol. 1994;14(12):8096–106.

[227] Chen S, Sanjana NE, Zheng K, Shalem O, Lee K, Shi X, et al. Genome-wide CRISPR screen in a mouse model of tumor growth and metastasis. Cell. 2015;160(6):1246–60.

[228] Huang J, Chen M, Xu ES, Luo L, Ma Y, Huang W, et al. Genome-wide CRISPR Screen to Identify Genes that Suppress Transformation in the Presence of Endogenous Kras(G12D). Sci Rep. 2019;9(1):1–10.

[229] Sanson KR, Hanna RE, Hegde M, Donovan KF, Strand C, Sullender ME, et al. Optimized libraries for CRISPR-Cas9 genetic screens with multiple modalities. Nat Commun. 2018;9(1):1–5.

[230] Shalem O, Sanjana NE, Hartenian E, Shi X, Scott DA, Mikkelson T, et al. Genome-scale CRISPR-Cas9 knockout screening in human cells. Science. 2014;343(6166):84–7.

[231] Brinkman EK, van Steensel B. Rapid Quantitative Evaluation of CRISPR Genome Editing by TIDE and TIDER. Methods Mol Biol. 2019;1961:29–44.

[232] Suter AA, Itin P, Heinimann K, Ahmed M, Ashraf T, Fryssira H, et al. Rothmund-Thomson Syndrome: novel pathogenic mutations and frequencies of variants in the RECQL4 and USB1 (C16orf57) gene. Mol Genet Genomic Med. 2016;4(3):359–66.

[233] Behan FM, Iorio F, Picco G, Goncalves E, Beaver CM, Migliardi G, et al. Prioritization of cancer therapeutic targets using CRISPR-Cas9 screens. Nature. 2019;568(7753):511–6.

[234] Chan EM, Shibue T, McFarland JM, Gaeta B, Ghandi M, Dumont N, et al. WRN helicase is a synthetic lethal target in microsatellite unstable cancers. Nature. 2019;568(7753):551–6.

[235] Yeo NC, Chavez A, Lance-Byrne A, Chan Y, Menn D, Milanova D, et al. An enhanced CRISPR repressor for targeted mammalian gene regulation. Nat Methods. 2018;15(8):611–6.

[236] Sharma S, Petsalaki E. Application of CRISPR-Cas9 Based Genome-Wide Screening Approaches to Study Cellular Signalling Mechanisms. Int J Mol Sci. 2018;19(4):933.

[237] Di Leonardo A, Linke SP, Clarkin K, Wahl GM. DNA damage triggers a prolonged p53-dependent G1 arrest and long-term induction of Cip1 in normal human fibroblasts. Genes Dev. 1994;8(21):2540–51.

[238] Decorsiere A, Cayrel A, Vagner S, Millevoi S. Essential role for the interaction between hnRNP H/F and a G quadruplex in maintaining p53 pre-mRNA 3'-end processing and function during DNA damage. Genes Dev. 2011;25(3):220–5.

[239] Li Y, Bakke J, Finkelstein D, Zeng H, Wu J, Chen T. HNRNPH1 is required for rhabdomyosarcoma cell growth and survival. Oncogenesis. 2018;7(1):1–3.

[240] Kamura T, Maenaka K, Kotoshiba S, Matsumoto M, Kohda D, Conaway RC, et al. VHL-box and SOCS-box domains determine binding specificity for Cul2-Rbx1 and Cul5-Rbx2 modules of ubiquitin ligases. Genes Dev. 2004;18(24):3055–65.

[241] Mahrour N, Redwine WB, Florens L, Swanson SK, Martin-Brown S, Bradford WD, et al. Characterization of Cullin-box sequences that direct recruitment of Cul2-Rbx1 and Cul5-Rbx2 modules to Elongin BC-based ubiquitin ligases. J Biol Chem. 2008;283(12):8005–13.

[242] Petroski MD, Deshaies RJ. Function and regulation of cullin-RING ubiquitin ligases. Nat Rev Mol Cell Biol. 2005;6(1):9–20.

[243] Cai W, Yang H. The structure and regulation of Cullin 2 based E3 ubiquitin ligases and their biological functions. Cell Div. 2016;11(1):1–11.

[244] Pozzebon ME, Varadaraj A, Mattoscio D, Jaffray EG, Miccolo C, Galimberti V, et al. BC-box protein domain-related mechanism for VHL protein degradation. Proc Natl Acad Sci U S A. 2013;110(45):18168–73.

[245] Koren I, Timms RT, Kula T, Xu Q, Li MZ, Elledge SJ. The Eukaryotic Proteome Is Shaped by E3 Ubiquitin Ligases Targeting C-Terminal Degrons. Cell. 2018;173(7):1622–35.

[246] Lin HC, Yeh CW, Chen YF, Lee TT, Hsieh PY, Rusnac DV, et al. C-Terminal End-Directed Protein Elimination by CRL2 Ubiquitin Ligases. Mol Cell. 2018;70(4):602–13.

[247] Lin HC, Ho SC, Chen YY, Khoo KH, Hsu PH, Yen HC. SELENOPROTEINS. CRL2 aids elimination of truncated selenoproteins produced by failed UGA/Sec decoding. Science. 2015;349(6243):91–5.

[248] Uhlen M, Fagerberg L, Hallstrom BM, Lindskog C, Oksvold P, Mardinoglu A, et al. Proteomics. Tissue-based map of the human proteome. Science. 2015;347(6220):1260419. Available from: https://www.proteinatlas.org/ENSG00000124702-KLHDC3/tissue.

[249] Ohinata Y, Sutou S, Mitsui Y. A novel testis-specific RAG2-like protein, Peas: its expression in pachytene spermatocyte cytoplasm and meiotic chromatin. FEBS Lett. 2003;537(1-3):1–5.

[250] Murphy SJ, Hart SN, Lima JF, Kipp BR, Klebig M, Winters JL, et al. Genetic alterations associated with progression from pancreatic intraepithelial neoplasia to invasive pancreatic tumor. Gastroenterology. 2013;145(5):1098–1109 e1.

[251] Tate JG, Bamford S, Jubb HC, Sondka Z, Beare DM, Bindal N, et al. COSMIC: the Catalogue Of Somatic Mutations In Cancer. Nucleic Acids Res. 2019;47(D1):D941–D947. Available from: https://cancer.sanger.ac.uk/cosmic/gene/analysis?ln=KLHDC3.

[252] Oughtred R, Stark C, Breitkreutz BJ, Rust J, Boucher L, Chang C, et al. The BioGRID interaction database: 2019 update. Nucleic Acids Res. 2019;47(D1):D529–D541. Available from: https://orcs.thebiogrid.org/Search?searchType=key&search=KLHDC3&organism=all.

[253] Ciechanover A. The ubiquitin-proteasome proteolytic pathway. Cell. 1994;79(1):13–21.

[254] Shen M, Schmitt S, Buac D, Dou QP. Targeting the ubiquitin-proteasome system for cancer therapy. Expert Opin Ther Targets. 2013;17(9):1091–108.

[255] Teixeira LK, Reed SI. Ubiquitin ligases and cell cycle control. Annu Rev Biochem. 2013;82:387–414.

[256] Yu JH, Zhong XY, Zhang WG, Wang ZD, Dong Q, Tai S, et al. CDK10 functions as a tumor suppressor gene and regulates survivability of biliary tract cancer cells. Oncol Rep. 2012;27(4):1266–76.

[257] Zhao BW, Chen S, Li YF, Xiang J, Zhou ZW, Peng JS, et al. Low Expression of CDK10 Correlates with Adverse Prognosis in Gastric Carcinoma. J Cancer. 2017;8(15):2907–14.

[258] Robert T, Johnson JL, Guichaoua R, Yaron TM, Bach S, Cantley LC, et al. Development of a CDK10/CycM in vitro Kinase Screening Assay and Identification of First Small-Molecule Inhibitors. Front Chem. 2020;8:147.

[259] Kwon YT, Xia Z, An JY, Tasaki T, Davydov IV, Seo JW, et al. Female lethality and apoptosis of spermatocytes in mice lacking the UBR2 ubiquitin ligase of the N-end rule pathway. Mol Cell Biol. 2003;23(22):8255–71.

[260] Moyo TK, Watts JM, Skikne BS, Mendler JH, Klimek VM, Chen SC, et al. Preliminary Results from a Phase II Study of the Combination of Pevonedistat and Azacitidine in the Treatment of MDS and MDS/MPN after Failure of DNA Methyltransferase Inhibition. Blood. 2019;134:4236–4236.

[261] Swords RT, Coutre S, Maris MB, Zeidner JF, Foran JM, Cruz J, et al. Pevonedistat, a first-in-class NEDD8-activating enzyme inhibitor, combined with azacitidine in patients with AML. Blood. 2018;131(13):1415–24.

COLOPHON

This document was created in Overleaf v2 using the typographical look-and-feel `classicthesis` developed by André Miede and Ivo Pletikosić. The style was modified to conform to the University of Melbourne thesis guidelines.

Final Version as of December 16, 2020 (classicthesis v4.6).